Biophysical Approaches for the Development of Stable, Long-Lived, Multi-Functional, and Potent Antibody Therapeutics

Dennis Ryan Goulet

A dissertation

submitted in partial fulfillment of the

requirements for the degree of

Doctor of Philosophy

University of Washington

2018

Reading Committee:

William M. Atkins, Chair

Abhinav Nath

Kelly K. Lee

Program Authorized to Offer Degree:

Pharmacy – Medicinal Chemistry

University of Washington

Abstract

Biophysical Approaches for the Development of
Stable, Long-Lived, Multi-Functional, and Potent Antibody Therapeutics

Dennis Ryan Goulet

Chair of the Supervisory Committee:
William M. Atkins
Department of Medicinal Chemistry

Antibody-based proteins have become an important class of biologic therapeutics, due in large part to the stability, specificity, and adaptability of the antibody framework. Indeed, antibodies not only have the inherent ability to bind both antigens and endogenous immune receptors, but they have also proven extremely amenable to protein engineering. Thus, several derivatives of the monoclonal antibody format, including bispecific and multispecific antibodies, antibody-drug conjugates, and antibody fragments, have demonstrated efficacy for treating human disease, particularly in the fields of immunology and oncology.

Presented here is a thorough examination of the design of antibody-based therapeutics, and a description of four projects that each use different combinations of biophysical methods to characterize clinically relevant properties of antibodies. Chapter 1 reviews several aspects of therapeutic antibody design, including therapeutic mechanisms, isotype selection, and engineering strategies. Chapter 2 explores the behavior of soluble antibody oligomers, using fluorescence correlation spectroscopy to monitor diffusion properties in buffer and serum. This work revealed

that antibody aggregation is dependent not only on oligomer size, but also on environment. In Chapter 3, a multiple regression method to predict antibody pharmacokinetic parameters is investigated. It was determined that combinations of neonatal Fc receptor binding parameters determined by biolayer interferometry and thermal stability parameters measured by differential scanning calorimetry allow for improved prediction of half-life and clearance. The kinetic mechanism of controlled Fab-arm exchange is presented in Chapter 4. A Förster resonance energy transfer method allowed for real-time monitoring of bispecific antibody formation and revealed conditions that accelerate the reaction. Finally, Chapter 5 explores the effect of Fc multimerization on Fc receptor binding and functionality. A novel antibody construct containing two Fc domains was generated and shown to exhibit multivalent binding to Fc gamma receptors and the neonatal Fc receptor. Collectively, this work demonstrates the utility of biophysical techniques in developing antibody therapeutics with increased conformational stability, longer half-life, multiple antigen-binding functionality, and higher-avidity Fc receptor binding.

TABLE OF CONTENTS

Page

List of figures iv
List of tables vi
Chapter 1: Considerations for the design of antibody-based therapeutics 1
1.1 Introduction to therapeutic antibodies 1
1.2 Antibody structure and function 2
1.3 Antigen specificity 10
1.4 Class, subclass, and allotype 17
1.5 Identification of variable regions 29
1.6 Expression system 35
1.7 Post-translational modifications 37
1.8 Fragmentation 42
1.9 Multimerization 46
1.10 Conjugation 48
1.11 Multispecificity 57
1.12 Protein engineering 64
1.13 Biophysical properties 67
1.14 Summary 75
1.15 References 82
Chapter 2: Diffusion of soluble aggregates of antibodies in serum 97
2.1 Introduction 97
2.2 Experimental procedures 99
2.2.1 Proteins and other materials 99
2.2.2 Generation of disulfide cross-linked THIOMAB 99
2.2.3 Generation of glutaraldehyde cross-linked Abs 100
2.2.4 Purification and characterization of antibody oligomers 101
2.2.5 Preparation of viscosity-matched buffers 101
2.2.6 Fluorescence correlation spectroscopy 102
2.3 Results 103
2.3.1 Generation of oligomeric standards 103
2.3.2 Benchmarks of viscosity 106
2.3.3 Diffusion of Ab oligomers in buffer and serum 106

2.4 Discussion 109
2.5 References 124
Chapter 3: A combinatorial approach to the prediction of antibody pharmacokinetics 127
3.1 Introduction 127
3.2 Experimental procedures 129
3.2.1 Proteins and other materials 129
3.2.2 Biolayer interferometry 129
3.2.3 Differential scanning calorimetry 130
3.2.4 Literature reports of antibody pharmacokinetics 131
3.2.5 Regression analysis 131
3.3 Results 132
3.3.1 Review of literature on antibody pharmacokinetics 132
3.3.2 Antibody binding to the neonatal Fc receptor at endosomal pH 132
3.3.3 Antibody binding to the neonatal Fc receptor at physiological pH 133
3.3.4 Antibody thermal stability 133
3.3.5 Multiple regression to identify combinations of PK predictors 134
3.3.6 Testing the predictive power of the model 136
3.4 Discussion 137
3.5 References 160
Chapter 4: Mechanism of controlled Fab-arm exchange to form bispecific antibodies 164
4.1 Introduction 164
4.2 Experimental procedures 167
4.2.1 Proteins and other materials 167
4.2.2 Hydrophobic interaction chromatography 167
4.2.3 Fluorescent labeling 167
4.2.4 IgG cleavage to generate Fc fragments 168
4.2.5 Förster resonance energy transfer 168
4.2.6 Fluorescence correlation spectroscopy 169
4.2.7 Disulfide redox kinetics 171
4.2.8 Simulation 171
4.3 Results 172
4.3.1 Characterization of IgG hinge mutants 172
4.3.2 Kinetics of controlled Fab-arm exchange 172

4.3.3 Effect of antibody concentration 173
4.3.4 Effect of reducing agent 173
4.3.5 Effects of pH and ionic strength 174
4.3.6 Kinetics with different pairs of parental Abs 176
4.3.7 Equilibrium dissociation constants 176
4.3.8 Kinetics of hinge redox reactions 177
4.3.9 Mechanistic model of controlled Fab-arm exchange 178
4.4 Discussion 180
4.5 References 209
Chapter 5: Designing a dual Fc antibody with enhanced avidity for Fc receptors 212
5.1 Introduction 212
5.2 Experimental procedures 213
5.2.1 Proteins and other materials 213
5.2.2 Fc receptor binding kinetics to mono- and dual-Fc antibodies 215
5.2.3 Effect of Fc receptor density on complex dissociation rate 215
5.2.4 Stoichiometry of Fc receptor binding 216
5.2.5 ADCC reporter bioassay 217
5.3 Results 218
5.3.1 Design of dual Fc antibody 218
5.3.2 Purification and biochemical characterization 218
5.3.3 Functional characterization 219
5.3.4 Affinity for Fc receptors 219
5.3.5 Confirmation of bivalent binding 220
5.3.6 Stoichiometry of Fc receptor binding 221
5.3.7 Antibody-dependent cellular cytotoxicity 221
5.3.8 Mouse pharmacokinetics 223
5.4 Discussion 223
5.5 References 237

LIST OF FIGURES

1.1 Considerations for the design of IgG-based therapeutics 77
1.2 Antibody frameworks based on fragmentation or multimerization 78
1.3 Post-translational modifications of IgG antibodies 79
2.1 Preparation of covalent Ab oligomers 115
2.2 Sensorgrams for capped/uncapped THIOMAB binding to protein A 116
2.3 Demonstration of bsAb formation by HIC 117
2.4 SDS-PAGE showing the chemical nature of inter-Ab linkages 118
2.5 Purification of covalent Ab oligomers 119
2.6 Estimation of oligomer size by size-exclusion chromatography 120
2.7 FCS autocorrelations of free dye and cross-linked THIOMABs 121
2.8 Fitted diffusion times of free dye and Ab oligomers 122
3.1 Sensorgrams of bevacizumab binding to immobilized human FcRn 142
3.2 Sensorgrams of therapeutic mAbs binding to immobilized FcRn at pH 6.0 143
3.3 Correlations between mAb PK outcomes and biophysical parameters 144
3.4 Sensorgrams of therapeutic mAbs binding to immobilized FcRn at pH 7.0 145
3.5 Sensorgrams of a single concentration of mAbs binding to FcRn at pH 6.0 146
3.6 Sensorgrams of a single concentration of mAbs binding to FcRn at pH 7.0 147
3.7 Comparison of FcRn-IgG binding trends from independent experiments 148
3.8 Thermograms showing the unfolding of bevacizumab at pH 7.2 149
3.9 Thermograms for the eight clinical mAbs at pH 7.2 150
3.10 mAb thermograms fit to a 3-component, non-2-state model 151
3.11 Unsubtracted thermograms for calculations of ΔC_P for each mAb 152
3.12 LASSO analysis to determine the most important PK predictors 153
3.13 LASSO analysis using FcRn response at pH 6.0 154
3.14 Prediction of PK parameters using FcRn response at pH 7.0 and ΔC_P 155
3.15 Effect of IgG1 allotype and framework on mAb pharmacokinetics 156
3.16 Comparison of ΔC_P and GRAVY score 157
4.1 SDS-PAGE of parental Abs and purified Fc fragments 189
4.2 Kinetics of cFAE for Abs containing different extents of labeling 190

4.3 Comparison of wild-type Abs to hinge mutants 191
4.4 SDS-PAGE of Abs that were used to characterize cFAE kinetics 192
4.5 Size-exclusion chromatograms of wild-type Abs and hinge mutants..... 193
4.6 HIC of wild-type Abs and hinge mutants before and after cFAE..... 194
4.7 Kinetics of cFAE for two pairs of IgG1 Abs targeting different antigens..... 195
4.8 Kinetics of cFAE for IgG1 or IgG4PAA Abs..... 196
4.9 Effect of Ab concentration on the rate of cFAE 197
4.10 Kinetics of cFAE with varying concentrations of reductant..... 198
4.11 Fitted rates of cFAE with varying concentrations of reductant 199
4.12 Kinetics of cFAE at varying pH..... 200
4.13 Kinetics of cFAE at varying ionic strength..... 201
4.14 Fitted rates of cFAE at different pH and ionic strength..... 202
4.15 Half-Ab dissociation rates and dimerization affinities 203
4.16 SDS-PAGE to monitor the hinge disulfide redox during cFAE at 25 ºC 204
4.17 SDS-PAGE to monitor the hinge disulfide redox during cFAE at 31 ºC 205
4.18 Kinetic scheme for the mechanism of cFAE including measured rates 206
4.19 Comparison of half-Ab dissociation rates and dimerization affinities 207
5.1 Design of 1Fc and 2Fc antibodies..... 226
5.2 Biochemical characterization of 1Fc and 2Fc antibodies 227
5.3 Sensorgrams of 1Fc and 2Fc binding to FcγRI, FcγRIIIa, FcRn..... 228
5.4 Effect of Fc receptor density on FcR:mAb dissociation rate..... 229
5.5 Two-point FcR:mAb dissociation rates at varying FcR densities 230
5.6 Sensorgrams of soluble FcRs binding to Fab-captured 1Fc and 2Fc mAbs..... 231
5.7 Stoichiometry of FcR binding to 1Fc and 2Fc antibodies 232
5.8 ADCC reporter bioassay..... 233
5.9 ADCC assay based on LDH release 234
5.10 Pharmacokinetic profiles of 1Fc and 2 Fc mAbs in mice..... 235

LIST OF TABLES

1.1 Types of antigens and the indications for which they are appropriate 80
1.2 Properties of antibody subclasses 81
2.1 Purity of oligomer fractions assessed by SDS-PAGE densitometry 123
2.2 Average diffusion times of Ab oligomers reported by FCS 123
3.1 Literature pharmacokinetics and biophysical parameters for clinical mAbs..... 158
3.2 Prediction of mAb half-life and clearance using leave-one-out regression..... 159
4.1 Experimental kinetic parameters of cFAE..... 208
5.1 Kinetic parameters for 1Fc and 2Fc mAbs binding to captured Fc receptors 236
5.2 Stoichiometry and affinity of 1Fc and 2Fc mAbs for soluble Fc receptors..... 236
5.3 Parameters from ADCC assay measured by LDH release..... 236

ACKNOWLEDGEMENTS

I was fortunate to have several mentors in graduate school who contributed to my growth as a scientist and a person. One is Bill Atkins, whose constant encouragement helped me to pursue interesting ideas and seek understanding for its own sake, and whose discussions allowed me to think more deeply about important questions. Another is Abhi Nath, who taught me the value of tackling problems from multiple angles, and applying both experimental and computational techniques to test hypotheses. Mark Chiu instilled me with an appreciation for the complexity of therapeutic antibody design and showed me that the industry setting has ample opportunities for interesting mechanistic research. Committee members Kelly Lee and Champak Chatterjee provided helpful feedback that shaped my thesis into a more coherent package. In the lab, Adam Zwolak patiently explained biological and biochemical concepts, and taught me that often the only way to resolve a doubt is just to do the experiment.

I also want to thank everyone in the Atkins Lab – Mike Dabrowski, John Sumida, Hyewon Kwon, Nick Treuheit, Wynton McClary, Mavis Li, Michelle Redhair, Amanda Clouser, Lorela Paço, and Hayli Larsen – for teaching me so much, and making the lab such an enjoyable place to work and learn. Likewise, I am grateful to the Biologics Research group at Janssen – Matt Bunce, Mehabaw Derebe, Catherine Leettola, Tim McCabe, Steve McCarthy, Steve Orcutt, Steve Pomerantz, Susan Tam, and Di Zhang – for challenging me to grow immensely and gain confidence in the lab setting.

Thanks to all the faculty, staff, and students in Medicinal Chemistry who made graduate school a positive and productive endeavor. Thanks to David Baggett, Eric Evangelista, and Hannah Baughman, who shared in the struggles and triumphs associated with classes, exams, and presentations. Thanks to those who contributed directly with data in this thesis – James Williams with electron micrographs, David Plotnik with ADCC plots, and Mike Watson for helping collect DSC data.

Finally, I want to thank my family – BJ, MJ, DJ, and RJ – who were steadfast supporters through the whole process, and who have taught me many things in life that are even more important than therapeutic antibodies.

CHAPTER 1

Considerations for the Design of Antibody-Based Therapeutics

1.1 Introduction to therapeutic antibodies

The first therapeutic monoclonal antibody (mAb), muromonab-CD3 (OKT3), was approved by the Food and Drug Administration (FDA) in 1985 to prevent rejection of kidney, heart, and liver transplants.[1] In a typical mechanism for Ab-based therapeutics, OKT3 binds to and inhibits CD3 on the T cell receptor complex to prevent host T cells from being activated against foreign antigens on the transplanted tissue. Although OKT3 proved effective for preventing host-versus-graft disease, the mAb itself elicits an immune response resulting in its accelerated clearance. The origin of this immune reaction has been traced to non-human sequences on OKT3, a murine mAb. Subsequent generations of therapeutic Abs have humanized the amino acid sequence of mouse antibodies to chimeric, humanized, and fully human. This humanization of sequence to prevent immunogenicity is just one example of how mAb-based therapeutics have been improved through the decades. In fact, each part of the mAb structure has been strategically modified to alter biological effects and improve clinical outcomes.

Ab therapeutics represent the fastest growing class of drugs on the market, due in large part to naturally favorable attributes such as specificity, potency, and metabolic stability. Knowledge of humoral immunology and advances in protein engineering have further contributed to the development of these important drugs. Currently 60 mAb-based therapeutics are used in the clinic, with nearly as many in late stages of clinical trials.[2] The most fruitful applications of Abs lie in the fields of oncology (where built-in effector functions help to eliminate tumor cells) and immunology (where inhibition of inflammatory pathways is useful in treating autoimmunity). Over time, increasingly innovative Ab derivatives have replaced the standard naked mAb to

address the complex pathobiology of disease and improve upon existing therapies.

When designing mAb-based therapeutics, numerous factors must be considered, with each factor having a direct impact on protein structure and consequent impacts on biological and therapeutic function (**Figure 1.1**). For example, the choice of targeted antigen and Ab generation strategy affects the primary and tertiary structure of the Ab variable regions. Differences in this domain of the protein impact the nature of the antibody-antigen interaction, including specificity, affinity, and whether the binding event is activating or inhibitory. These biological properties, in turn, determine clinical properties like potency and therapeutic index. In the same vein, factors like antibody subclass and allotype affect the structure of the constant regions, which in turn influences binding to Fc receptors important for effector function and serum half-life. Thus, several determinants must be considered when creating new Ab-based therapeutics. Although distinct structural features have overlapping functional consequences, there exists the idea that Abs can be designed in a piecewise fashion to combine all desired features into a single optimized molecule. In this chapter, various design elements of therapeutic Abs are discussed, along with their impacts on structure and biological and clinical function. The aim is to cover the wide extent of design strategies and engineering options available, rather than to exhaustively discuss the literature on any given topic. Thus, more focused reviews have been cited for thorough discussion of individual design elements.

1.2 Antibody structure and function

1.2.1 Antibody domains

Structurally, each mAb molecule is composed of two identical heavy chains and two identical light chains assembled into three discrete functional domains. While the two antigen-binding fragments (Fabs) are responsible for binding to the specific molecular target with high

avidity, the crystallizable fragment (Fc) binds to immune receptors to elicit effector functions. The N-terminal half of the Fab arms contains the variable sequences, which differ between mAbs to confer them distinct specificities. In particular, three complementarity-determining region (CDR) loops on each chain contain hypervariable sequences that are situated at the antigen-binding interface. The remainder of the amino acid sequence contains constant regions that are identical for mAbs of a given subclass. Within each of the immunoglobulin (Ig) domains of an Ab (of which there are 12 in the IgG class), there is one intrachain disulfide bond. There are also interchain disulfide bonds linking heavy chains to each other (two pairs for IgG1) within the flexible hinge region; and linking each heavy chain to its light chain. Finally, Abs are decorated with glycan molecules that finetune Fc receptor interactions. While the site and number of glycosylation sites varies between Abs of different classes, the IgG Abs contain a well-conserved Asn-297 residue for attachment of N-linked glycans.

1.2.2 Classifications

Abs are divided into five structurally and functionally distinct classes (isotypes), each of which may contain additional subclasses (subtypes). This classification is defined by the type of heavy chain so that α, δ, ε, γ, or μ chains create IgA, IgD, IgE, IgG, or IgM Abs, respectively. In humans, IgA Abs are further divided into IgA1 and IgA2, while IgG Abs may be of the IgG1, IgG2, IgG3, or IgG4 subclasses. Structural differences between classes include the number of Ig-like domains (four per α, δ, or γ chain versus five per ε or μ chain), the oligomeric states (IgA dimers and IgM pentamers/hexamers), and diverse patterns of hinge disulfide bonds and glycosylation (**Table 1.2**). While each class of Ab uses a defining heavy chain, they share common light chains which may be of the κ or λ class. About two-thirds of endogenous Abs contain κ light chains, and the majority of clinical Abs also utilize light chains with the κ framework.[3] The

structural differences listed here allow B lymphocytes to generate adaptable immune responses that can be tailored over time via class-switch recombination.

1.2.3 Fc gamma receptors

Binding to class-specific Fc receptors (FcRs) expressed on leukocytes is one mechanism by which Abs elicit an adaptive immune response for elimination of infected or malignant cells. FcγRs, which bind to Abs of the IgG isotype via the lower hinge region, are the best described class of FcRs and the most important for existing Ab therapeutics. In humans, there are six FcγRs (FcγRI/CD64, FcγRIIa/CD32a, FcγRIIb/CD32b, FcγRIIc/CD32c, FcγIIIa/CD16a, and FcγRIIIb/CD16b) that differ based on the affinity of IgG binding and the downstream response of binding.[4,5] While most FcγRs have a low affinity for IgG and thus bind only to oligomeric immune complexes, FcγRI binds with high affinity to physiological concentrations of monomeric IgG1, IgG3, and IgG4. Thus, FcγRI is thought to be continuously occupied by monomeric IgG, which is displaced in the event of higher-avidity immune complex formation. FcγRI contains an additional extracellular Ig-like domain compared to the low affinity FcγRs (three instead of two), but the extra domain is not the primary determinant of its tight IgG affinity.[6] FcγRIIb is the only immunoinhibitory FcγR as it contains an intracellular immunotyrosine-based inhibitory motif (ITIM) used for downstream signaling. Conversely, the activating FcγRs generally contain (or are associated with a subunit that contains) an immunotyrosine-based activating motif (ITAM). The exception is FcγRIIIb, which instead signals through a glycosyl-phosphatidylinositol domain.

Expression of each FcγR is restricted to specific subsets of immune cells, which allows the cells to elicit clinically important effector functions. For example, FcγIIIa is highly expressed on natural killer (NK) cells and is responsible for antibody-dependent cell-mediated cytotoxicity (ADCC).[5] Through this mechanism, NK cells are directed to antibody-coated target cells, which

they lyse through delivery of cytotoxic granules. Similarly, myeloid cells like macrophages, monocytes, and dendritic cells express FcγRI and FcγRIIa. These receptors are involved in antibody-dependent cellular phagocytosis (ADCP), another immune mechanism for disposal of tumors or infected cells. In these contexts, activation of effector cells and subsequent cytotoxic mechanisms are dependent on clustering of FcγRs on the cell surface.

Clinically relevant FcγR polymorphisms exist that affect the strength of the IgG-Fc interaction and the potency of the immune response. FcγIIa H131 (versus R131) and FcγRIIIa V158 (versus F158) have been shown to bind more tightly to certain subtypes of IgG Abs. Although the differences in IgG1-FcγR affinity are less than two-fold in both cases, cancer patients treated with IgG1 mAbs such as rituximab and trastuzumab (for which ADCC is an important mechanism of tumor killing) show significantly better responses if they express the high affinity FcγR variants.[7-9] While this finding revealed the importance of FcγR-IgG affinity for tumor killing efficacy, the drug industry has focused on engineering the IgG component of the interaction to confer more potent effector function regardless of the patient's receptor genotype.

1.2.4 Neonatal Fc receptor

The neonatal Fc receptor (FcRn) also binds Abs exclusively of the IgG subclass, but is structurally similar to major histocompatibility complex (MHC) class I rather than the FcγRs. As the name suggests, FcRn is important for maternal-to-fetal transfer of IgG via the placenta; but it is also involved in IgG homeostasis in adults.[10] In fact, the exceptionally long half-lives of IgG and human albumin in the blood are attributed to FcRn-dependent salvage mechanisms. When proteins are endocytosed by endothelial cells en route to lysosomal degradation, IgG and albumin bind to FcRn at the acidic pH (<6.5) of the endosome. The bound proteins then get trafficked back to the cell surface and are released upon reaching physiological pH (7.4) due to the low affinity of

the interaction at this pH. Like MHC, the FcRn α chain is associated with the β2-microglobulin protein to create a transmembrane heterodimer. Both chains contribute contacts to the FcRn-IgG interface, which is located at the Cγ2/Cγ3 domains of the IgG molecule.[11] Expression of FcRn occurs in syncytiotrophoblasts (for fetal transport) and throughout the vascular endothelium (for systemic homeostasis).[10] Additionally, expression in professional antigen-presenting cells allows for trafficking of immune complexes to the lysosome, where antigens can be processed for peptide presentation on MHC.[12]

1.2.5 Other subclass-specific receptors

There are other classes of FcRs that will become therapeutically important as Abs of non-IgG classes are explored as drugs. IgA Abs bind to FcαRI (CD89) on neutrophils and other myeloid cells to elicit either anti- or proinflammatory pathways, depending on the extent of IgA oligomerization.[13,14] Before binding of IgA to FcαRI can occur, the receptor must be primed via "inside-out signaling" originating from inflammatory cytokines. Then, one of two extracellular Ig-like domains of FcαRI becomes capable of binding the Cα2/Cα3 region of IgA to elicit downstream signaling via two intracellular ITAM-containing FcR γ chains.[15] Binding of monomeric or dimeric IgA is anti-inflammatory by preventing immune activation via other effector FcRs. On the other hand, binding of immune complexed IgA activates pro-inflammatory pathways such as phagocytosis, antigen presentation, cytokine release, and ADCC.[13,15]

The receptor for IgM Abs, FcμR, is the most recently described subclass-specific receptor. It is expressed primarily on B lymphocytes and plays roles in their maturation and differentiation while also preventing survival of autoreactive B cells.[16] Binding of the IgM Fc to the single extracellular Ig-like domain of FcμR results in signal transduction through the intracellular tail and may work in conjunction with B cell receptor signaling. [17] Additionally, the receptor may mediate

antimicrobial functions by inducing pro-inflammatory cytokines and supporting the development of inflammatory dendritic cells.

Fcα/μR (CD351) binds to IgA and IgM Abs and is expressed in both hematopoietic (marginal zone B cells) and non-hematopoietic (follicular dendritic cells) tissues.[18] Endocytosis of IgM immune complexes via Fcα/μR negatively regulates the humoral immune response specifically for T-independent antigens.[18] Structurally, the receptor contains one extracellular Ig-like domain that binds to the Cα3 region of IgA and to the Cμ3/Cμ4 regions of IgM; and a cytoplasmic domain that may be involved in heterodimerization. Fcα/μR may also be important for proinflammatory IL-6 production when challenged with bacterial pathogens by associating with Toll-like receptor (TLR) 4.[19] However, this process does not appear to be Ig dependent. Fcα/μR may also play a role in the endocytosis of IgM-coated pathogens, thus granting IgM Abs opsonization potential that is independent of the complement pathway.[20]

The polymeric Ig receptor (pIgR) also binds to polymeric forms of both IgA and IgM to concentrate them into mucosal environments.[21] Soluble dimeric IgA binds pIgR on the basolateral side of intestinal epithelial cells to be transcytosed into the intestinal lumen. Proteolytic cleavage on the apical side releases IgA with the secretory component of pIgR bound to the IgA J chain. This secretory component serves to localize secreted IgA to the mucus layer of the intestine and prevent its degradation by digestive proteases.[22] Structurally, pIgR contains five extracellular Ig-like domains that become the secretory component after cleavage, while its cytoplasmic tail is necessary for intracellular sorting and transcytosis.[21]

FcεRI binds to immune complexes containing IgE Abs to elicit the degranulation of mast cells and basophils that is characteristic of type I hypersensitivity.[23] The full receptor complex is tetrameric, containing the Cε3-binding α chain and the TAM-containing $\beta\gamma_2$ chains.[24] IgE binding

capacity of FcεRI is confined to the two extracellular Ig-like domains of the α chain, creating a very high-affinity interaction. Although all four chains are present in mast cells and basophils, a trimeric variant lacking the β chain exists in myeloid cells and is involved in immune signaling and antigen presentation. IgE also binds via its Cε3-4 domain to the low affinity FcεRII (CD23), which is actually a C-type lectin that regulates levels of serum IgE.[24] FcεRII actually exists as two forms that differ in the sequence of the N-terminal intracellular domain. The A form is constitutively expressed on B cells and contributes to endocytosis of IgE complexes for antigen presentation, while the B form is inducibly expressed on myeloid cells and may play a role in the phagocytosis of microbes.[25]

1.2.6 Complement

Besides cell-surface receptors, IgG and IgM Abs also bind to bloodborne elements of the classical complement pathway. In the same way that the low-affinity FcγRs do not bind to monomeric IgG, C1q (the first component of the cascade) requires Ab oligomerization to form a stable, high-avidity interaction. In particular, IgG molecules hexamerize via the lower Fc into a C1q-binding conformation when bound to immobilized antigen on the surface of a target cell.[26] C1q itself is a hexamer of trimers, containing six globular head domains that contribute to the strong avidity effect. IgM, which naturally exists as pentamers and hexamers, does not need to further oligomerize to bind C1q; however, deposition onto a surface allows the formation of a more active C1q-binding conformation.[27] After surface-bound Abs capture C1q, a cascade of chemotactic, inflammatory molecules are generated for recruitment of other immune components. The complement pathway terminates in formation of a membrane attack complex (MAC) in the target cell membrane, causing osmolysis. Thus, the ability to elicit complement-dependent cytotoxicity (CDC) for targeted destruction of specific cells is another attribute of IgG and IgM

Abs that makes them attractive therapeutic options.

1.2.7 Bacterial Ig-binding proteins

So far, the Ab binding partners discussed have been mainly human proteins that direct immune mechanisms against invading pathogens. However, there is a bacterial family of proteins that have been adapted to evade the humoral response by binding Abs and inhibiting their interaction with endogenous receptors. The most well-studied of these cell wall-associated molecules are proteins A and G, which are expressed in *Staphylococcus aureus* and *Streptococcus*, respectively. Both proteins bind the Ab Fc region at the C_H2/C_H3 elbow, and thus bind competitively with FcRn.[28] However, they may also bind more weakly to the Fab domains: protein A to the V_H region of human V_H3 family Abs and protein G to the Cγ1 domain of human IgG Abs.[29] Subtle differences in the primary Fc binding site cause unique specificities for Ab species and subclasses. For example, while protein A binds strongly to most mouse and human Abs, it binds weakly to human IgG3 and mouse IgG1 (both of which are bound strongly by protein G). Another notable Ab-binding bacterial factor is protein L (from *Peptostreptococcus magnus*), which binds light chains of the κ class that are potentially present on Abs of all subclasses.[28] Recently, protein M from *Mycoplasma genitalium* was found to bind Abs even more universally with its well-conserved binding site in the V_L region that is present in both λ and κ light chains.[30]

Due to the ability of these proteins to bind a wide array of Abs with high specificity, they have become convenient tools for affinity-based Ab purification. Recombinant forms of proteins A, G, and L have been developed to further hone their Ab-binding specificities. For example, while native protein G binds to serum albumin in addition to Abs, the albumin-binding domain was removed from recombinant protein G to prevent binding of this common contaminant.[28] Additionally, the high affinity Fc-binding B-domain of protein A was engineered for increased

chemical stability to be used in commercial affinity resins. The properties of distinct bacterial proteins have also been combined into recombinant fusion proteins such as protein A/G. This derivative contains four Fc-binding domains from protein A and two from protein G to allow for capture of Abs of diverse species and classes.

1.2.8 Other receptors

While it is tempting to focus on the effector mechanisms that have been directly implicated in therapeutic success, one should also consider the possible effects of therapeutic Abs binding to less studied receptors. Eight Fc receptor-like (FcRL) proteins have been identified, some of which bind to aggregated Igs. Primarily expressed in B cells and sometimes containing ITAMs and/or ITIMs, FcRLs are thought to be involved in regulation of B cell activation. [31] Tripartite motif (TRIM) 21 is a ubiquitously expressed Fc-binding protein that elicits antibody-mediated proteolysis of intracellular antigens.[32] TRIM21 has been used to target specific intracellular proteins for Ab-mediated degradation via the proteasome. Sialylated IgG Abs can bind to lectins including some I-type Siglecs (e.g. Siglec-2/CD22) and C-type lectins (e.g. dendritic cell-specific ICAM-3 grabbing non-integrin, DC-SIGN/CD209; dendritic cell immunoreceptor, DCIR). Many of these receptors contain ITIM signaling motifs which may be involved in the favorable immunomodulatory effects of IVIg therapy.[7,33]

1.3 Antigen specificity

1.3.1 Mechanisms of action

Perhaps the most impactful decision in therapeutic Ab design is the choice of molecular target, which determines the mechanism by which the drug combats disease (**Table 1.1**). When treating cancer with cytotoxic mechanisms such as ADCC and CDC, the ideal antigen would be confined specifically to the tumor for minimization of damage to healthy tissue. For example, cell-

differentiating proteins CD19 and CD20 are favorable targets due to their expression almost exclusively on B lymphocytes.[34,35] Of course, this strategy is only appropriate when the malignant tissue expresses a defining antigen, and when the entire cell population can be safely eliminated. For B cell leukemias and lymphomas in particular, both of these conditions are satisfied due to the abundance of lymphocyte-defining antigens and the ability to deplete B cells without causing severe immunodeficiency or other negative effects. But for many tumors, either cell-specific antigens have not been identified, or the depletion of the entire (healthy and malignant) tissue population would cause loss of essential organ function.

In the cases where no tumor-specific antigens exist, the next best approach is to target antigens that are significantly overexpressed on tumor cells compared to normal tissues. Growth factor receptors such as epidermal growth factor receptor (EGFR) and human epidermal growth factor receptor 2 (HER) and adhesion molecules such as epithelial cell adhesion molecule (EpCAM) and carcinoembryonic antigen (CEA) are upregulated in many types of cancer and have been successfully targeted in cancer therapy or diagnosis.[35] Besides inhibiting cell proliferation, Abs against these targets also work to actively destroy overexpressing cells through signaling-induced cell death, ADCC, and CDC. Although such Abs have proven efficacious when used as monotherapies, they are susceptible to resistance mechanisms that might be overcome using multispecific antibodies that have additional mechanisms of action.

An alternative strategy in oncology is to inhibit immunomodulatory receptors that tumors use to evade the immune response. As cancer cells grow, they acquire mutations and neoantigens that would normally be recognized by T lymphocytes. In order to prevent immune recognition, many tumors express immunoinhibitory proteins such as programmed death ligand 1 (PDL1/CD274), which binds to PD1 on T cells to prevent their activation. A therapeutic approach

has been to inhibit PD1 (CD279), PDL1, and other inhibitory receptors like cytotoxic T lymphocyte-associated protein 4 (CTLA4/CD152), which increases the chances of a functional anti-tumor immune response.[35,36] Similarly, OX40 (CD134) is a costimulatory receptor on T cells that has been targeted with agonistic antibodies in the hopes of strengthening the T cell response.[37] Although immunostimulatory Abs such as anti-PD1 and anti-CTLA4 have been efficacious in the clinic, their autoimmune toxicities are a challenge that remains to be fully addressed.

For systemic inflammatory indications, it is often feasible to target soluble antigens rather than cell-surface receptors. Cytokines such as tumor necrosis factor α (TNFα) and interleukins (IL) 5, 12, 17A, and 23 have all been successfully targeted by inhibitory Abs for treatment of asthma, rheumatoid arthritis, Crohn's disease, psoriasis, and other inflammatory conditions.[38] Blocking the binding of these proinflammatory cytokines to their receptors helps to dampen systemic inflammation associated with chronic autoimmune disease.

In addition to human proteins, exogenous antigens can be targeted for prevention or treatment of infection. Anti-microbe Abs work by conferring passive immunity to the patient via pathogen neutralization and Fc-dependent immune mechanisms.[39] For example, Abs targeting respiratory syncytial virus protein F and *Clostridium difficile* enterotoxin B have been approved for prevention of the corresponding infections. Likewise, Ab binding to antigens on human target cells can also inhibit viral infection, as with CD4 and human immunodeficiency virus.[39] When designing therapeutic agents for treatment of infection, one should consider passive immunization in addition active vaccination strategies.

1.3.2 Antibody-antigen affinity

Intuitively, stronger antibody-antigen affinity can translate directly to higher potency and clinical efficacy. This trend has been observed commonly for antagonistic Abs that bind to

pathogenic epitopes, where binding affinity correlates with neutralization efficacy and reduction of infectivity.[40,41] By increasing the strength of the interaction, therapeutic doses can be reduced without sacrificing antagonistic potential. Generation of strongly binding Ab variants can be performed using a diverse array of methods. Besides carrying out affinity maturation in B lymphocytes, several *in vitro* display technologies and even *in silico* mutagenesis approaches have developed for this purpose.[42]

However, it must be emphasized that higher antigen-binding potency does not always create a more efficacious therapeutic. For Abs targeting solid tumors, it appears that there is an ideal range in antigen affinity that causes the most favorable properties.[43] If the K_D value is too low, the Ab may suffer from poor selectivity of tumor cells versus healthy tissue. Additionally, the slow dissociation rate of tight-binding Abs may cause them to cluster at the tumor periphery or be internalized before diffusing deeper into the malignant tissue.[44] Thus, the optimal antigen affinity varies on a case-by-case basis and must be optimized based on factors such as tumor size, antigen concentration, and the kinetics of receptor internalization.

1.3.3 Epitope

Abs targeting the same antigen may elicit different mechanisms of action by binding to distinct molecular features or conformations. For instance, anti-CD20 Abs can be binned into two groups based on differences in epitope and the types of effector functions induced. While type I Abs elicit the concentration of CD20 into lipid rafts and cause more efficient deposition of complement, type II Abs do not re-distribute CD20 in the membrane but cause more potent signaling-induced cell death.[45,46] Trastuzumab and pertuzumab, which target separate epitopes in the extracellular domain of HER2, have distinct modes of action including the inhibition of different types of HER2 heterodimerization.[47] The improved efficacy of trastuzumab/pertuzumab

combination therapy indicates that the mechanisms are synergistic.[48]

In extreme cases, Abs targeting different epitopes on the same antigen will produce the opposite effect. CD28 and CD40 are costimulatory molecules expressed on T cells and antigen presenting cells, respectively. Binding to these receptors in an activating manner enhances the immune response and is useful for cancer applications; meanwhile, inhibitory binding to prevent lymphocyte activation may be useful for treatment of autoimmunity. Interestingly, the epitope on these receptors determines their signaling output based on whether Ab binding mimics the interaction with the native receptor. For CD28, Abs that bind near the native B7-1/CD86 or B7-2/CD86 binding site cause a co-stimulatory output that is dependent upon concomitant T cell receptor signaling; but superagonistic Abs that bind at a distal site of CD28 cause T cell activation even in the absence of T cell receptor ligation.[49] For CD40, the situation is more complicated because activation of antigen presenting cells is dependent upon FcγRIIb-mediated receptor crosslinking. However, it appears that two distinct epitopes defined by CD40L/CD154 competitivity lead to an agonistic or antagonistic response at physiological concentrations of FcγR.[50] Thus, mapping the precise site of antibody-antigen binding can help to define the elicited response.

1.3.4 Advantages of multispecificity

Combining Ab specificities to simultaneously interact with two distinct antigens allows novel mechanisms to be explored. Bispecific Abs (bsAbs) targeting two tumor-associated antigens may have increased potency and decreased susceptibility to resistance mechanisms. For example, several bsAbs in clinical trials inhibit combinations of receptor tyrosine kinases including EGFR, HER2, HER3, and insulin-like growth factor 1 receptor (IGFR).[51,52] While monospecific Abs such as anti-EGFR and anti-IGFR may be prone to tumor resistance mechanisms such as compensatory

upregulation of alternate survival pathways, bsAbs targeting both receptors are less likely to be resisted due to the inhibition of orthogonal receptors.[52] Another benefit is that monovalent binding to each antigen may prevent toxicities that result from high-avidity binding or cross-linking.[53] Optimization of the affinity and valency of each Ab-binding domain may allow for increased tumor-targeting selectivity.[54] Thus, bsAbs targeting multiple antigens on the same type of target cell may increase the therapeutic window of anti-cancer drugs by increasing potency and decreasing off-target effects.

BsAbs may also be used for mechanisms that require co-localization of distinct cell types. The most prevalent of these mechanisms is T cell redirection, wherein Abs targeting both tumor antigens and CD3 on T cells allow for formation of an immunological synapse, activation and proliferation of the T cells, and potent ADCC. Receptors besides CD3 have been used to target other immune cells to the tumor site; for example, FcγIIIa for recruitment of NK cells.[51,52] Full-length IgG bsAbs may elicit trifunctional effects: in addition to binding tumor and T cells, they engage accessory cells like macrophages via the Fc domain to add phagocytosis to the tumor-killing repertoire.[51] It is thought that memory $CD4^+$ and especially $CD8^+$ lymphocytes dominate the immune response of T cell redirecting bsAbs, since these cells do not require the costimulatory signals that naïve T cells need for activation.[55] Future therapeutics may benefit from optimization of the geometry of the elicited cytolytic synapse, as well as the addition of costimulatory agonists or checkpoint inhibitors for generation of a more robust T cell response.[55]

While traditional mAbs are restricted to the circulatory and lymphatic systems, bsAbs can facilitate delivery into otherwise unreachable compartments. A number of neurological targets, such as beta-secretase 1 (BACE1) for Alzheimer's disease and leucine-rich repeat and immunoglobulin-like domain-containing protein 1 (LINGO1) for multiple sclerosis, are guarded

by the tight junctions of the blood-brain barrier.[56] However, endogenous carrier proteins expressed on the systemic side of the blood-brain barrier can be targeted by one arm of bsAbs for delivery to the brain, while also leaving one arm free to bind the therapeutic target. Using the function of transporters like the transferrin receptor (CD71) and insulin receptor, antibody concentrations within the brain can be significantly increased.[56,57] The antibody's precise affinity and epitope for the transporting receptor are both important parameters that must be optimized. Antibodies with weak transporter affinities may be advantageous, since they allow for efficient release on the brain side of the blood-brain barrier while also minimizing interference of the transporter's native function.[57] Inclusion of the Fc domain is another critical factor, since FcRn mediates antibody export from brain back into systemic circulation.[56] Outside of brain delivery, bsAbs may be useful for localization to other intractable but therapeutically relevant environments such as the intracellular cytosol.[58]

1.3.5 Delivery of cytotoxic agents

When inhibition and humoral immune mechanisms are insufficient to eliminate tumor cells, conjugation of cytotoxic moieties can be used to potentiate anti-cancer Abs while retaining their specificity. Although antibody-drug conjugates (ADCs) and other Ab conjugates have been widely used for cancer indications, they have also been investigated for immunosuppression and treatment of infection.[59,60] In each case, the Ab is used to deliver potent drugs or toxins to select cell types while minimizing off-target effects of the unconjugated drug. Since specificity of antigen expression is a favorable attribute of both naked Abs and ADCs, it is possible for the same Ab to be therapeutically useful with and without conjugation. An example is trastuzumab, which has been approved for treatment of breast cancer both as the naked Ab and as a conjugate to the cytotoxic agent emtansine. However, drug conjugation may potentiate the antitumor activity of a

naked Ab, as with brentuximab and brentuxuimab vedotin.[59]

An additional consideration for ADC antigens is their ability to internalize, and thus transfer the Ab and payload into the targeted cell.[61] Ideally, the rate of receptor-mediated internalization (clathrin- or caveolin-mediated) should surpass that of receptor-independent endocytosis, so that ADCs are concentrated into antigen-bearing cells. Rates of internalization of naked and conjugated Abs are often similar, but in some cases drug attachment alters these kinetics.[61] Affinity of the Ab for the receptor antigen may also affect the rate of ADC internalization, with one study showing faster internalization for ADCs with tighter Ag affinity.[62] While ADC-targeted receptors should internalize efficiently, they should also display minimal shedding from the membrane. Such antigen shedding may lead to accumulation of extracellular ADC-antigen immune complexes and an increase in systemic toxicity.[63] In summary, Ab conjugates offer targeted cytotoxicity, but must be designed to target antigens that are both specifically expressed and favorably localized after binding.

1.4 Class, subclass, and allotype

1.4.1 IgG1

The isotype of an antibody is a critical effector of its therapeutic properties, since the structural differences between frameworks determine biological function. Due to factors like long half-life, potent effector function, structural homogeneity, and thorough characterization, IgG1 Abs dominate the pool of biologics. Human IgG1 Abs are approximately 146 kDa in size, with 15 amino acids in the hinge region containing two pairs of inter-HC disulfide bonds. In contrast to other IgG subclasses in which the HC-LC disulfide bond occurs at the third cysteine of the heavy chain, IgG1 Abs contain this linkage at the fifth cysteine of the heavy chain. The paired cysteine occurs as the ultimate (κ) or penultimate (λ) residue of the light chain. IgG1 is not known to have

variation in quaternary structure, but is monomeric so that its two Fab arms bind antigen bivalently. Immunologically, an IgG1 response is typically elicited for protein antigens, and IgG1 is a common viral responder.[7] IgG1 is the predominant subtype in the blood, making up roughly half of the total Ig pool (or 67% of IgG Abs).[14]

All the FcγRs are bound by monomeric IgG1. Compared to IgG3, IgG1 binds more tightly to FcγRIIa but less tightly to FcγIIIa and FcγIIIb.[7] Thus, IgG1 is capable of mediating clinically useful mechanisms like ADCC and ADCP. Furthermore, IgG1 assembles into hexamers on the surface of target cells, allowing it to fix complement and mediate CDC. An intermediate hinge length and flexibility allow IgG1 to efficiently utilize both Fab arms for bivalent antigen binding and immune complex formation. While IgG1 is less prone to aggregation than IgG2 and IgG4, it is more susceptible to chemical degradation, possibly due to its longer hinge region.[64]

Polymorphisms in Ig constant regions exist for certain subclasses, including IgG1. Of these amino acid variants, those that elicit a serologic response in non-carriers are referred to as allotypes. It is possible for a heavy chain to have amino acid substitutions that are not true allotypes; for example, if the sequence of interest is found in the heavy chain of another subtype. These variants that are unique within a subclass, but redundant in other subclasses, are referred to as isoallotypes. Allotypes are referred to by either alphabetical or numeric labels, coupled with the subclass and the letter m (marker). For example, an allotype within IgG1 is G1m1, which is the same as G1m(a). The heavy chain protein expressed by an individual may contain multiple allotypes, which are often inherited together as a haplotype due to their close genetic proximity and low frequency of crossover. Although allotypes are, by definition, immunogenic, their ability to cause a robust response *in vivo* is less apparent. In fact, it appears that therapeutic Abs of a given allotype do not elicit more anti-drug Abs in individuals lacking that allotype.[65,66] Nevertheless, the

risk of immunogenicity of biologics may be lowered by using frameworks that lack allelic determinants.

For IgG1, four allotypes have been identified with the designations G1m1 [G1m(a)], G1m2 [G1m(x)], G1m3 [G1m(f)], and G1m17 [G1m(z)].[67] Each allotype involves substitution of one to two amino acids in the C_H1 or C_H3 domains. The four most common combinations of allotypes include the haplotypes G1m3; G1m3,1; G1m17,1; and G1m17,1,2.[67] As for marketed Abs, the preferred frameworks seem to be G1m3 and G1m17,1.[68] Interestingly, G1m17, which is not a naturally abundant haplotype, is also found in biologics, where the m1 substitution was removed to reduce immunogenicity.[68] The interplay between the allotypes of patients and therapeutics was highlighted in one study demonstrating that the half-life of infliximab (G1m17,1) is longer in patients with the G1m3 haplotype than those with the G1m17,1 allotype.[69] Apparently, the affinity of G1m17,1 mAbs for FcRn is higher than that of G1m3 Abs, allowing the administered infliximab to out-compete endogenous G1m3 Abs for access to endosomal recycling. The same report suggested that G1m3,1 Abs may have even slower clearance due to their superior FcRn binding.

1.4.2 IgG2

IgG2 is also about 146 kDa and is the second most prevalent IgG Ab in serum, representing 22% of IgG and 16% of total antibody.[14] It has a shorter hinge than IgG1, containing 12 amino acids, but actually contains more disulfide bonds in this region for four total HC-HC linkages. An IgG2 response is commonly produced by carbohydrate antigens found on encapsulated bacteria. Since peptide-MHC presentation is impossible for such antigens, the IgG2 response is often T-independent.

Three isomers of IgG2 exist. IgG2A, which is common when the molecule contains λ light chain, has paired hinge disulfides and the typical HC-LC disulfide linkage; IgG2B, common when

the molecule contains κ light chain, has shuffled disulfide bonds with the HC-LC disulfide bonds using a set of hinge cysteines; and IgG2A/B contains one of each of these disulfide configurations.[70] The IgG2A isomer is thought to confer more flexibility to the Fab arms relative to IgG2B, which can have functional consequences. For example, an IgG2 mAb was found to interact either agonistically or antagonistically with its antigen depending on whether its hinge disulfides were locked in the A or B configuration.[71] Heterogeneity in the hinge can also cause intermolecular disulfide linkages. Covalent dimers of IgG2 have been observed in recombinant systems as well as the serum, and the mAbs comprising these dimers could feasibly have the same or distinct specificities.[70,72] It has been postulated that mAb dimerization could provide an immunological advantage by increasing avidity for the low-affinity but regularly repeated carbohydrate antigens that are commonly targeted by endogenous IgG2 Abs.[72] Although the hinge isomers of IgG2 confer it with interesting properties, including the ability to form tetravalent dimers, this heterogeneity can be a problem when creating well-defined therapeutics.

IgG2 has weak effector functions compared to IgG1 and IgG3 due to its weaker affinity for FcγRs. Although monomeric IgG2 displays low micromolar affinity for most of the low-affinity FcγRs, it does not bind significantly to FcγRI or FcγRIIIb.[7] Complement fixation for IgG2 occurs only when the antigen is present on the target cell at high density.[7] Thus, IgG2 is a more immunologically silent isotype that may be useful for therapeutic applications that requires a strict blocking mechanism.

Only one serologically determined allotype of IgG2 has been found, denoted G2m23 [G2m(n)], as opposed to G2m.. which lacks antigenic determinants.[67] The G2m23 allotype contains the V282M substitution in the CH2 domain, as well as the P189T substitution in the CH3 domain. Functionally, the G2m23 allotype seems to confer an advantage against bacterial

infections, but the mechanism behind this, and its utility for IgG2 therapeutics, has not been studied.[73]

1.4.3 IgG3

As the third most abundant IgG subtype in the serum, making up 7% of IgG mAbs and 5% of mAbs overall, IgG3 offers strong effector function at the cost of proteolytic and pharmacokinetic instability.[14] Due to the extended hinge containing on average over 60 residues of which 11 are disulfide-forming cysteines, IgG3 mAbs are slightly larger than those of other subtypes at around 170 kDa. Although this long hinge allows for tight binding of Fc binding partners and flexibility of the Fabs, it renders the protein susceptible to cleavage. The IgG3 hinge is also notable for containing threonine residues that can be O-glycosylated.[74] Immunologically, the γ3 chain is the first of the class-switched constant regions, which causes IgG3 mAbs to appear early in the humoral response to viral protein antigens.[7] No prevalent deviations in quaternary structure have been observed for IgG3 mAbs, which exist mostly as monomers.

Compared to mAbs of other IgG subclasses, most IgG3 mAbs have a significantly reduced half-life in serum (one week as opposed to three weeks). This difference has been traced to R435 at the FcRn binding interface, which for all other IgG mAbs is H435. In IgG1, 2, and 4, the titratable histidine at this site is critical for pH-dependent FcRn binding and endosomal recycling. However, the presence of arginine slightly decreases FcRn affinity in the endosome, rendering IgG3 unable to compete with H135-containing mAbs for lysosomal salvage.[75] Interestingly, IgG3 half-life is similar to that of other IgG mAbs for individuals containing allotypes with H435.[7]

Of all IgG subclasses, IgG3 has the strongest effector functions as a result of tight FcγR interactions. Multivalent binding of IgG immune complexes to each of the FcγRs is strongest for IgG3.[76] Furthermore, IgG3 is the most potent of the IgG subclasses in fixing C1q for initiation of

the complement pathway.[7] While the potent immune activation of IgG3 may sound promising for treatment of cancer and infectious disease, the complexities of its long hinge region have not been adequately addressed to allow for the formation of stable and homogeneous biologics.

IgG3 contains the most polymorphisms of any Ig subclass in the form of 13 defined allotypes and several hinge variants with differing numbers of repeats. Each of the allotypes occur as one to three amino acid substitutions in the CH2 or CH3 domains.[67] These allotypes are combined into six common alleles, each of which contains four to seven allotypic variants.[67] It is not clear whether any of these alleles might have therapeutic advantages, especially since the IgG3 subclass has been studied relatively little in the biologics field. A more structurally dramatic polymorphism of IgG3 occurs due to heterogeneity in the hinge region. The sequence of the hinge contains one common exon, followed by one to four repeats of a second exon.[68] As a result, the hinge ranges from 27 to 83 residues, which suggests wide variation in conformation, proteolytic stability, and antigen cross-linking.

1.4.4 IgG4

The least naturally abundant of the IgG subtypes is IgG4, which makes up 4% of IgG mAbs or 3% of mAbs overall.[14] IgG4 mAbs are often associated with antigen exposure over an extended period, which may be related to its anti-inflammatory properties and gene locus as the last subtype of γ heavy chain.[7] Like IgG2, IgG4 is around 146 kDa and contains 12 amino acids in the hinge region. However, hinge disulfide bonds of IgG4 resemble those of IgG1, with two covalent linkages between heavy chains. The rigid CPPC motif in the hinge of IgG1 is replaced with CPSC in IgG4, conferring more flexibility. While IgG4 does not have any antigenically defined allotypes, there are several allelic variants containing isoallotypic substitutions.[67]

The increase in hinge flexibility of IgG4 allows for the formation of intrachain disulfide

bonds instead of the normal interchain linkages.[77] In addition, human IgG4 contains R409 instead of K409 that is present in IgG1, 2, and 3. The K409R substitution destabilizes interchain interactions in the CH3 domain and, combined with the labile hinge of IgG4, allows mAbs to dissociate into half-Abs and recombine into distinct pairings.[78] This process, termed Fab-arm exchange (FAE), has been observed *in vivo*, resulting in the formation of bispecific molecules that are monovalent for two different antigens.[79] Immunologically, this may be an anti-inflammatory mechanism to decrease antigen cross-linking due to loss of bivalency. Since the exchange of therapeutic half-Abs with endogenous Abs has the potential to create poorly defined bispecific mAbs upon human administration, the S228P mutation is now commonly used to prevent this process from occurring for therapeutic IgG4 mAbs.[77] The mutation prevents FAE by stabilizing the IgG4 hinge into a more rigid, IgG1-like state that forms proper interchain disulfide bonds.

IgG4 binds to most FcγRs, except perhaps FcγRIIIb, though generally more weakly than IgG1 or IgG3. Of all the IgG subtypes, IgG4 binds most strongly to the inhibitory FcγRIIb, which may explain its anti-inflammatory effects.[76] It is inefficient at complement fixation, with less C1q binding than even IgG2.[7] As with IgG2, IgG4 may be most applicable for therapeutics that require antigen binding without extensive immune activation.

1.4.5 IgA

Although IgG Abs dominate the current pool of biologics, IgA Abs elicit several effector mechanisms that may be useful therapeutically. Because IgA does not bind to FcRn, it is eliminated more quickly than IgG, with a serum half-life of around one week instead of three weeks. Nonetheless, its rate of production is the highest of any other Ig class.[80] IgA1and IgA2 collectively make up ~20% Abs in the serum, where they are mostly in the monomeric state; however, IgA is the dominant Ig isotype in secretions like saliva and breastmilk, and at mucosal surfaces such as

the gastrointestinal and respiratory tracts. At these sites, IgA is processed into polymeric forms (most commonly dimers, but up to tetramers) in which the 15-kDa joining (J) chain covalently links the monomers via disulfide bonds to their 18-residue C-terminal tailpiece domains.[81] In this polymeric form, IgA binds to pIgR and is processed to the lumen of mucosal sites, where it is released with SC as secretory IgA.

IgA1 can be distinguished from IgA2 in terms of structure and distribution. It contains a longer hinge due to sequence duplication, and is more prone to proteolysis. The hinge of IgA1 contains O-glycosylation sites that are absent in the IgA2 hinge.[82] In the serum, IgA is predominantly of the IgA1 subclass, whereas in mucosa IgA2 plays a larger role and even becomes the major subtype in the gut.[81] Both isoforms exist in monomeric and polymeric forms, and both can be processed into secretory IgA by pIgR. While IgA1 responds to protein and polysaccharide antigens, IgA2 seems to specialize in polysaccharide antigens.[83,84]

Despite its lack of FcγR interaction, IgA possesses significant effector functions that occur through binding to FcαRI on macrophages, neutrophils, and eosinophils. While binding to the former cell types elicits phagocytosis, the latter cells release cytotoxic granules in an ADCC mechanism similar to that of IgG-ligated NK cells. Studies with matched IgG and IgA Abs have demonstrated their complementary mechanisms of action. IgG recruits NK cells for ADCC activity and C1q for initiation of the classical complement pathway. IgA, on the other hand, can cause substantial ADCC in the absence of lymphocytes, and initiates CDC despite not binding to C1q.[81,85] Rather, IgA may recruit complement via the alternative and/or lectin pathways. It has been postulated that the complement-mediated lysis by IgA is an *in vitro* artifact, and that any observed CDC is independent of IgA.[81] Regardless of complement activity, the cross-linking of FcαRI by IgA clearly elicits potent ADCC and ADCP functions that have not yet been utilized by

clinical biologics.

There are three allotypes of IgA2 with notable differences in structure, if not function. While IgA2m2 and IgA2m3 contain the normal HC-LC disulfide bonds, IgA2m1 lacks any covalent linkage between paired heavy and light chains.[81] Rather, the two LCs of IgA2m1 form a LC-LC disulfide bond that is unique among all the human Igs. Presumably, this LC-LC linkage could constrict the movement of the Fabs in IgA2m1 while the lack of HC-LC linkage could destabilize the H_2L_2 complex. To address these concerns, the P221R mutation has been incorporated into IgA2m1 to instill it with more IgAm2-like disulfide pairing patterns.[86] In terms of glycosylation, IgA2m1 contains four N-glycosylation sites while IgA2m2 and IgA2m3 contain one additional site.[82] The effects of these structural changes on the function of each allotype have not yet been thoroughly investigated.

1.4.6 IgD

IgD is co-expressed with IgM in the membrane of mature naïve B cells, but little is known about its biological function. While IgD has a lengthy hinge region containing multiple O-glycosylation sites, IgM lacks a true hinge but instead contains an extra Ig domain.[87] The different structures of IgD and IgM allow for differences in the antigen specificities of B cell receptors. While IgM signaling can be triggered by antigens of low or high valency, IgD signaling appears to occur only for highly polyvalent antigens.[88] Thus, IgD may help to regulate B cell development by distinguishing soluble self-antigens from complexed or polyvalent pathogenic epitopes. Whether this same mechanism plays a role in the outcome of class switch recombination has not been investigated.

Nor is the function of soluble IgD entirely clear. The presence of IgD^+IgM^- plasmablasts in the upper respiratory mucosa, and the detectable levels of IgD in serum, support an

immunological role for Abs of this Ig subclass.[89] Circulating IgD has been shown to ligate receptors on basophils to elicit production of proinflammatory cytokines (TNFα, IL-1β) and antimicrobial factors (cathelicidin).[89] Thus, while IgD likely plays important immunological roles, these functions are not understood well enough to justify use of this framework in a clinical candidate.

1.4.7 IgE

IgE is best known for its ability to elicit highly inflammatory responses to allergens, but also to helminths and other pathogens. Its structure contains five Ig domains instead of the more typical four, causing monomeric IgE to be slightly larger than IgG despite lacking a hinge. Seven asparagine residues on the IgE heavy chain can be glycosylated, although one site has been shown to contain exclusively oligomannose sugars rather than complex glycans.[87] IgE in the serum is not only the least prevalent of any Ig class, but also the shortest-lived, having a half-life of just two days.[14] However, molecules of IgE can persist for weeks within tissues by binding to their high-affinity receptor on mast cells and basophils, since the half-life of the IgE-FcεRI complex is on the order of days.[24] This extremely slow dissociation rate also allows IgE to prime immune cells for immediate degranulation upon antigen binding and receptor crosslinking.[24]

A major effector mechanism of IgE is the FcεRI-mediated degranulation of mast cell and basophils, where important contents include histamine, serotonin, proteases, and inflammatory cytokines.[23] However, FcεRI is also expressed on eosinophils, which can similarly degranulate to achieve ADCC via release of cationic proteins, reactive oxygen species, and other inflammatory cytokines.[90] Furthermore, expression of CD32 on macrophages and monocytes allows for the phagocytosis of IgE-bound target cells. Thus, IgE Abs have a variety of clinically relevant effector functions in addition to potentially favorable properties such as long tissue residency, a lack of

inhibitory receptors, and interaction with tumor-resident macrophages.[90,91] Despite the lack of human trials, preclinical studies in mice have demonstrated that tumor-targeting IgE and IgG Abs have complementary modes of action, and that IgE Abs are in some cases superior.[90] The potential for anaphylactic reactions is a valid concern, but so far IgE has demonstrated no activation of effector cells in the absence of cross-linked antigen.[90] An ongoing clinical study using IgE Abs targeting folate receptor alpha will help inform whether IgE Abs are safe agents for the treatment of cancer.[92]

1.4.8 IgM

As mentioned previously, IgM is coexpressed with IgD on mature B lymphocytes as a result of differential splicing. Thus, IgM Abs play a pivotal role in the early immune response, where low antigen affinity, but high avidity and polyreactivity allow for the recognition of pathogens prior to the development of affinity matured Abs or other adaptive mechanisms.[14] Although IgM is found predominantly in the serum, where it makes up 8% of Abs and has a half-life of 10 days, it can also be transcytosed to mucosal surfaces via pIgR.[14] Like the ε heavy chain, the μ chain contains four constant Ig domains in addition to its variable region and has several conserved N-glycosylation sites.[93] However, IgM forms the largest quaternary structures composed of usually five, but sometimes six, IgM molecules.[14] While the pentameric species can form with or without the J chain, the more potent hexamer form lacks any J chain.[94,95] It appears that J chain is favorable for pIgR binding and transcytosis but inhibitory for complement-mediated lysis.[94,95] IgM heavy chains contain a single disulfide bond (in the Cμ2 domain) linking them to the other heavy chain of the IgM monomer, and two additional cysteine residues (in the Cμ3 and tailpiece domains) allow for formation of inter-monomer disulfide bonds.[93]

The polymeric structure of IgM is perfectly suited to ligation of C1q and potent activation

of the classical complement pathway. In addition, IgM has been shown to mediate phagocytosis. While this function was initially attributed to Fcα/μR, it was recently shown that any phagocytic may result as an extension of the complement cascade (via the opsonin C3 and complement receptor 3 on phagocytes).[20,96] Excluding the IgG class, IgM has the most extensive history of clinical use. One IgM Ab, nebacumab, was approved by several European countries in the early 1990s for treatment of Gram-negative sepsis; but it was subsequently withdrawn due to a variety of factors including high toxicity, high cost, and an inability to diagnose which cases of sepsis would be suitable for nebacumab use.[97] More recently, phase 1 clinical trials with IgM mAbs have demonstrated that these therapeutics are generally well-tolerated, with safety concerns including mild skin rash and nosebleed.[98-102] Furthermore, modest but favorable anti-tumor responses have been observed in some of these early trials.[98-101] Thus, the potent immune-activating function of IgM has shown promise for treatment of infection and cancer.

1.4.9 κ and λ light chain

Abs of all subclasses incorporate one of two types of light chains, κ or λ, whose genes are on chromosomes 2 or 22 respectively. Synthesis of a λ light chain only occurs if recombination at both κ alleles is unsuccessful. While the ratio of Abs containing κ and λ light chains is roughly 2:1 in humans, the ratio is over 9:1 for approved therapeutic mAbs.[2,3] This overwhelming preference for the κ isotype in biologics may be related to the use of hybridoma technology to generate mAb variable regions, since mouse B cells express Abs with a 20:1 κ:λ ratio.[103] Structurally, the third complementarity-determining region (CDR3) of λ light chains is on average longer, more hydrophobic, and more acidic than that of κ light chains.[104,105]

The κ and λ genes contain distinct types of genetic diversity. The κ constant region is encoded by a single gene locus, but this gene has three allotypes (Km1, Km2, Km3).[67] The allele

containing Km3 is most common in Caucasoid, Negroid, and Mongoloid populations. Accordingly, most therapeutic Abs utilize κ light chains of the Km3 allotype.[68] Meanwhile, individuals may have anywhere from 7 to 11 distinct lambda genes due to differences in haplotype.[67] Immunoglobulin constant lambda (IGLC) genes 1, 2, 3, 7, and sometimes 6 code for functional proteins, while the remaining loci are considered pseudogenes. None of the λ genes have serologically defined allotypes.

1.4.10 Cross-isotypes and cross-subtypes

Using protein engineering, it is possible to combine favorable features of different Ab isotypes into functionally optimized chimeric molecules.[106] For instance, the breadth of Ab effector mechanisms has been increased using an IgG1 framework containing IgA1 sequences in the lower Fc domain. The IgG1/A1 hybrid elicited strong ADCC, ADCP, and CDC by binding to FcαRI in addition to FcγRs and C1q.[107] Conversely, the clinically approved eculizumab combined the IgG2 C_H1 and hinge with the IgG4 C_H2 and C_H3 in order to abrogate both FcγR and C1q binding and serve as an immunologically silent cross-subtype.[108] The use of IgG2 sequences in otherwise IgG1 mAbs has also been used to reduce hinge proteolysis and induce a more agonistic antigen binding response while retaining the favorable properties of the IgG1 subclass.[109,110]

1.5 Identification of variable regions

1.5.1 Hybridoma

Multiple strategies can be used to generate and select the antigen-binding variable regions of therapeutic mAbs. The classical method, which is still the most common in successful clinical candidates, uses hybridoma technology.[111] This *in vivo* technique generates mAbs targeting antigens that are immunogenic in mice or other suitable mammalian hosts. Antigens are first injected into the mouse to elicit the expansion of antigen-specific B cells. After a humoral response

has been mounted, splenocytes are harvested and the mAb-producing B cells are fused with highly proliferative myeloma cells via strategies such as electroporation and polyethylene glycol treatment. Isolation of fused hybridoma cells is carried out by growing the mixture of cells in hypoxanthine-aminopterin-thymidine (HAT) media, which allows for selective proliferation of cells with properties of both B cells and the myeloma line. Unfused myeloma cells, which are modified to lack the HGPRT gene, cannot grow in HAT media as they are unable to make the nucleotides necessary for DNA replication. Conversely, unfused primary B cells quickly die in culture due to lack of immortalization. Thus, the hybridoma cells are selected and subsequently sorted into new cultures starting from individual cells. These immortalized, mAb-producing cells can then be tested for the desired specificity by conducting binding assays such as ELISA with cell supernatants. In addition to the hybridoma method, B cells can also be immortalized through transformation with Epstein-Barr virus or B cell lymphoma genes.[112,113]

Although the generation of mAbs using hybridoma technology was a huge step forward in the development of biologic therapeutics, it later became apparent that use of mouse proteins in humans led to a high incidence of immunogenicity.[114] Since this realization, the chimerization and humanization of mouse Abs has become commonplace. Chimeric Abs retain the entire variable region sequences of the hybridoma-generated mouse Ab, but the constant regions are of human origin. Thus, the amino acid sequence of chimeric Abs is still roughly 1/3 non-human. Humanized Abs contain a higher percentage of human sequences, as only the mouse CDRs are retained while the rest of the constant and variable framework is human. In some cases, grafting of mouse hypervariable loops onto the human framework leads to decreased antigen binding, in which case *in vitro* or *in silico* affinity maturation may be performed.[115,116] Fully human mAbs can be generated via mouse hybridoma by using transgenic animals that contain the human Ig genes in

place of their mouse counterparts.[117] In addition, isolation of B cells from immunized or infected individuals, or those with cancer, allows for formation of human hybridoma cells from which human Abs can be isolated.[118] While anti-drug antibody responses in patients correlate with the 'humanness' of the Ab sequence (mouse > chimeric > humanized), even fully human Abs can be immunogenic depending on the paratope that is formed.[114,119]

Since hybridoma technology functions in the context of an intact immune system, only certain antigens can be effectively targeted using this method.[120] A primary consideration is that antigens must be sufficiently immunogenic to elicit a humoral response in the host animal; thus, Abs targeting endogenous proteins may be difficult to generate *in vivo*. On the other hand, it is often not feasible or ethical to inject mice with pathogens or toxins that may prove fatal before the generation of a robust B cell response. In summary, while the hybridoma technique is still the standard for mAb production and allows for the formation of an immortalized mAb-producing cell line, its dependence on adaptive immunity necessitates Ab generation times of many months and limits the ability to control the precise epitope at which elicited Abs will bind.

1.5.2 Immunoglobulin sequencing

Another strategy for identifying mAbs of interest is to directly sequence all the V_H and V_L genes isolated from the B cells of immunized animals or humans. Immunoglobulin sequencing (Ig seq) uses next-generation sequencing to read the variable region sequences of up to several million Ig variants.[120] This method is useful not only for the mAb discovery, but also for detailed characterization of humoral immune responses.[121] While the peripheral blood compartment is the most accessible source of human B cells, the majority of B cells are found in extravascular milieu like the spleen, bone marrow, and lymph nodes, and can only be accessed in lab animals.[122] The localization and time since antigen exposure also affect the functional phenotype of B cells; for

example, plasmablasts are abundant in blood one week after antigen exposure, while memory B cells appear one to two weeks later.[120] The B cell subset, in turn, affects properties such as mRNA levels and extent of affinity maturation. Thus, the choice to use mRNA or genomic DNA as the template for Ig seq depends whether information on mRNA expression or B cell clonality is desired.[122]

One drawback of performing Ig seq analysis in bulk is the impossibility of knowing which combinations of V_H and V_L genes came from each B cell. Several strategies have been utilized to deduce the correct pairing of mAb HC and LC sequences, and thus to recreate Abs with intact paratopes. Pairing sequences based on ranking of clonal frequency is one option that has proven successful.[121] This method is especially powerful following immunization, when Ag-specific B cells make up a significant portion of total B cell pool.[120,122] For Abs that have undergone significant somatic hypermutation, pairing based on similar levels of mutation accumulation is another approach that has produced viable Abs.[122]

The most reliable way to ensure physiological pairings of variable sequences, however, is to clone individual B cells. Single B cells can be isolated by limiting dilution or flow cytometry, which has the added benefit of being able to sort different B cell subsets based on expression of surface markers.[123] Retention of pairing information can be achieved by fusion of V_H and V_L genes into a single amplicon, or by tagging each gene with a barcode unique to its B cell.[122] Selection of Ag-binding B cells can be performed using Ag-coated beads, flow cytometry with fluorescent antigen, and microarray and microengraving techniques.[123] Alternatively, soluble Abs secreted by B cells or expressed from cloned genes can be used for binding-based selection. While Ig seq in general is useful for discovery of high-affinity Abs that have undergone *in vivo* selection, single B cell methods facilitate identification of native gene pairs at the cost of reduced throughput.

1.5.3 Display

The essential aspects of *in vivo* immunological selection have been emulated *in vitro* to yield display technologies that allow for discovery of mAbs in the absence of an animal host.[115,121] Thus, mAbs to almost any antigen, even those that are toxic or weakly immunogenic, can be isolated in a fraction of the time. The first step for display technologies is to select a library of heavy and light chain genes that can be cloned into the system of interest. The library is either derived from immunized, infected, or otherwise immune-challenged individuals; or from universal donors that have not undergone specific immune activation. While the former libraries are more focused and potentially affinity-matured, naïve libraries have to potential to select mAbs against virtually any antigen. After cloning the library into the desired expression system, combinations of heavy and light chains, often in the scFv or Fab format, are displayed on the particle surface and selected by their ability to bind the antigen of interest. Non-binders are removed via wash steps to leave the best mAb candidates, which can be further refined through additional panning steps using the same or different binding conditions. Since the genes of interest are immediately available, the soluble protein can be expressed and used to quantify Ab-Ag affinity via methods such as ELISA. While hybridoma-derived mAbs still dominate the pool of therapeutics, six display-derived mAbs have been approved, and new *in vitro* methods for Ab selection continue to be discovered.[124]

The first display technology developed, and still the most widely used, uses bacteriophage for surface expression of Ab variable domains and selection of antigen binders.[125] Phage display, which uses viruses such as M13 phage, works by fusing the Ab scFv sequence with that of phage surface molecules like coat protein pIII.[126] The DNA sequence within the plasmid codes for the corresponding surface protein, allowing for phenotypic selection and subsequent genotypic

identification. Phage particles that bind antigen strongly are amplified via infection of bacterial hosts such as *E. coli*. This selective expansion of tightly binding phage particles allows for further rounds of panning or DNA sequencing of the associated scFvs. Several Abs in clinical use were derived from phage display technology, with the first being adalimumab in 2002.[124] Mammalian-derived Abs tend to have more favorable biophysical properties than phage-derived Abs, which might be related to *in vivo* selection of Abs with stable variable regions.[127]

In addition to phage display, various cell-based display platforms have also been developed. Bacterial, yeast, and mammalian display have all been used to select for Abs with the desired antigen binding properties.[128-130] The main advantage of cell display is the ability to quickly isolate the cells expressing the most active Ab domains using fluorescence-activated cell sorting. Cells containing extracellular scFv or Fab are bound to fluorescently labeled antigen and then sorted by brightness. The level of binding can be normalized for Ab expression on the surface using additional fluorescence channels. Cell-based display methods tend to have smaller library sizes due to low efficiency of transformation. However, the shift from a prokaryotic to eukaryotic, and ultimately mammalian system, has the advantage that the Abs selected will be expressed in cells with similar folding pathways and post-translational modifications.

Finally, ribosome and mRNA display are cell-free technologies that reduce the problem of Ab display to one of protein translation.[131] In ribosome display, mRNA sequences are *in vitro* translated, and the resulting polypeptide is left tethered to the ribosome due to lack of mRNA stop codon. After selection of antigen-binding proteins, the Ab-ribosome-mRNA complex is disassembled for sequencing of the selected mRNA. For mRNA display, puromycin serves as an adaptor molecule linking the translated polypeptide to its mRNA precursor. Since transformations into cells are not required in either case, these two methods have larger libraries and allow for

more diversity than other display techniques. The presence of a single antigen binding domain per complex prevents the avidity effects that sometimes complicate cell-based display. In addition to using high fidelity PCR for sequencing of the mRNA candidates, PCR using an error-prone polymerase can also be used for affinity maturation via random mutagenesis if necessary.

1.6 Expression system

1.6.1 Mammalian expression

The vast majority of approved therapeutic Abs are produced in mammalian cells due to their ability to express, fold, post-translationally modify, and secrete proteins in an analogous manner to endogenous human proteins, and thus to avoid unwanted immunogenicity.[132] Additionally, the ability of mammalian cells to properly glycosylate the conserved Asn-297 residue of IgG Abs is vital for solubility, stability, and effector function, while glycan composition also impacts Ab pharmacokinetics.[133-136]

Human cell lines such as human embryonic kidney 293 (HEK293) and its derivatives are commonly used for batch expressions in the discovery phase due to the favorable transfection efficiency of these cells.[137] Ab production with HEK cells is facilitated by their growth in chemically defined, serum-free media in suspension.[138] A significant advantage of HEK cells, and other human cells like PER.C6 embryonic retinoblasts and HT-1080 fibrosarcoma cells, is their production of proteins with fully human glycosylation patterns. Because human cell lines and human patients are of the same species, there is a risk of pathogen contamination and transmission; however, this ability to propagate virus also makes HEK cells useful in vaccine development.[137] Although no therapeutic Abs are currently expressed in human cells, other types of approved biologics have been produced in HEK293 and HT-1080 cells.[137]

Non-human mammalian cells exemplified by the Chinese hamster ovary (CHO) line are

used to produce most Ab therapeutics due to thorough characterization, high protein yield, and ability to be stably transfected.[139] While these cells can produce proteins with complex N-glycans, glycosylation patterns are not identical to those of human cells. CHO cells do not express all the human glycosylating enzymes and have been shown to sialylate proteins to a greater extent than HEK cells.[137,140] Some murine cell lines, such as NS0 and Sp2/0, express an α-galactosylating enzyme not present in humans, which introduces a potentially immunogenic epitope on glycoproteins produced in these systems.[137] Nonetheless, plasma-, CHO-K1-, and HEK293-derived IgG have core-fucosylated structures containing similar levels of galactose and sialic acid.[137] Cell engineering has created non-human cell lines with more human-like glycosylation patterns, as well as cell lines with targeted changes to Ab glycosylation and function.[137] For example, the Lec13 variant of CHO cells reduces synthesis of the fucosylation substrate to generate low-fucose Abs with increased ADCC via enhanced FcγRIIIa binding.[141] Thus, human and non-human mammalians cells form Abs with optimal folding and post-translational modifications, but genetic manipulation is relatively difficult and maintenance costly.

1.6.2 Other expression systems

Other cell-based expression systems can be used when cost and convenience are the primary considerations. While bacterial systems such as *Escherichia coli* may have difficulty producing complex full-length proteins, they have shown utility in generating Ab fragments such as Fab and Fv that do not require glycosylation to fulfill their intended functions.[138] In contrast to gram negative bacteria, which generally transport Ab products to the periplasm, gram positive bacteria have the advantage of secreting proteins directly into the media. Eukaryotic cells such as the yeast *Pichia Pastoris* and insect cells retain some of the advantages of prokaryotic systems while also being able to post-translationally modify expressed proteins.[138,139,142] Although

glycosylation in these cells is not identical to that of human cells, cell engineering of glycosylating enzymes allows for production of Abs with appropriate effector function.[138,139] Other genetic manipulation strategies include the co-expression of folding chaperones to facilitate assembly of complex Ab structures.[138] Besides cell-based expression, it is also possible to use prokaryotic and eukaryotic cell lysates in combination with template DNA and additional supplements to synthesize Ab fragments *in vitro*. These cell-free techniques eliminate the need for transformation of expression plasmids while enabling the facile incorporation of non-natural or isotopically labeled amino acids.[143]

For production of large batches of Ab-based proteins, whole-organism approaches have also been explored. Ab genes can be transformed into plants via the transfer DNA of *Agrobacterium tumefaciens*, which allows for purification of protein from tobacco leaves or rice seeds.[138,144] Alternatively, Abs can be harvested from mouse milk or chicken eggs using transgenic animals that have human Ig genes in place of the native Ig loci.[138] While these latter systems are expected to produce proteins with human-like glycosylation, plant systems have been engineered to prevent the attachment of potentially immunogenic sugars like xylose.[138] It seems unlikely that Ab expression in transgenic plants or animals will soon replace current mammalian cell production considering the time required to establish and maintain such protein-producing organisms.

1.7 Post-translational modifications

1.7.1 Glycosylation

Clearly, glycosylation of Abs is a vital determinant of their biological and therapeutic activity. Although Abs of various classes may have several N- and O-glycosylation sites, the best characterized glycans are those attached to Asn297 in the C_H2 region of IgG Abs (**Figure 1.3**). These complex N-glycans contain a core heptasaccharide motif with four N-acetyl glucosamine

(GlnNAc) residues and three mannose residues in a biantennary arrangement.[7,145] Fucose may be added to the protein-proximal GlnNAc residue, bisecting GlnNAc may be added to the central mannose residue, galactose may be added to each terminal mannose residue, and sialic acid (N-acetylneuraminic acid in mammals or N-glycolylneuraminic acid in some non-human mammals) may be additionally added to these galactose residues. All these possibilities for individual glycans, combined with the potential for differential glycosylation on each heavy chain, allow for significant heterogeneity in otherwise similar molecules of mAb. Studies from serum samples have demonstrated that >90% of endogenous IgG is core fucosylated, while only ~15% contains bisecting GlnNAc.[146] Glycoforms lacking galactose or containing a single galactose residue are more common than doubly galactosylated glycoforms.[147] Similarly, sialic acid is incorporated in <10% of structures, with disialylation even less common.[148] While hybrid and high-mannose type glycans are rare in endogenous human Abs (2% and <0.1%, respectively), they are important to study in the context of therapeutics since non-human recombinant systems like NS0 and CHO cells can produce ~29% and ~3.5% high-mannose glycans.[149,137] It should also be noted that ~20% of IgG Fabs contain saccharides as a result of N-glycosylation motifs in the variable regions.[150] Due to increased accessibility for glycosylating enzymes, Fab glycans tend to have higher levels of bisecting GlnNAc, galactose, and sialic aid compared to their Fc counterparts.[7] Interestingly, Fab glycans are less likely to contain fucose, which may be explained by the inhibitory effect of bisection on core fucosylation.[146]

There is substantial evidence that glycosylation of endogenous Abs is tailored to dampen or potentiate the elicited immune response. On the one hand, the frequency of different glycoforms is altered as a function of physiologic states like age, pregnancy, and inflammatory status.[7,151,152] Low inflammation is associated with increases in both galactosylation and sialylation, with

rheumatoid arthritis and lupus patients having higher levels of agalactosylated Abs.[151,153,154] On the other hand, glycan composition has direct effects on immune receptor binding and Ab function. Addition of sialic acid to terminal galactose residues causes decreased binding to inflammatory FcγRs and increased binding to anti-inflammatory lectins like DC-SIGN.[152] Fucose is a well-established immunoregulator, with afucosylated IgG Abs having more potent ADCC through tighter FcγRIIIa binding.[141] Likewise, the presence of bisecting GlnNAc inhibits core fucosylation, and therefore increases ADCC.[146,151] Complete lack of glycosylation all but eliminates binding to FcγRs and complement, and therefore ablates IgG effector functions.

Fc glycosylation affects the thermodynamic and serum stability of IgG Abs.[155,156] Structurally, the effect of IgG deglycosylation is increased flexibility of the C_H2 domain, which causes tighter packing in crystal structures but a larger radius of gyration in solution.[157,158] Deglycosylation decreases the thermal stability of the C_H2 domain and may cause increased aggregation relative to normally glycosylated IgG.[159] While complete loss of glycans does not significantly alter FcRn binding or pharmacokinetics, the presence of terminal mannose or galactose causes shorter half-life via lectin-mediated clearance. Abs with terminal mannose glycans can be cleared through the mannose receptor on endothelial and immune cells, while those lacking terminal sialic acid can be eliminated by the hepatic asialoglycoprotein receptor.[155,156] Thus, complex glycan-bearing Abs have longer half-lives than those containing hybrid or high-mannose glycans.[160] Similarly, IgG that has been degalactosylated, and therefore contains terminal GlnNAc, was shown to have extended pharmacokinetics compared to unmodified Abs.[161]

Given the substantial effect of Ab glycosylation on function and stability, numerous glycoengineering strategies have been developed to create next generation Ab therapeutics with more controlled glycan composition. One of the most explored methods to increase IgG effector

potency is to generate low fucose glycoforms that bind more tightly to FcγRIIIa. Common strategies to modify glycosylation in cell culture include the addition of glycan precursors to increase saccharide incorporation or glycosyltransferase inhibitors to decrease incorporation. [145,156] Additionally, the genes for glycosylating enzymes within host cells may be knocked out to reduce fucosylation and non-human glycosylation, or knocked in to provide a more human-like glycosylation profile. Clinical trials such as one with the FDA-approved obinutuzumab have demonstrated that low fucose glycovariants from engineered cell lines may lower the risk of disease progression, but increase adverse events, compared to non-glycoengineered mAbs.[162] Completely aglycosylated Abs have been extensively studied in contexts where strong immune recruitment is not necessary, since they can be expressed in prokaryotic hosts and lack the heterogeneity of glycosylated Abs.[163] Protein engineering strategies have identified Fc mutations that restore FcγR-mediated function to aglycosylated Abs, thus paving the way for Ab therapeutics that are both homogeneous and immune competent.

1.7.2 Amino acid modifications

Chemical alteration of amino acids is common both endogenously and in recombinant Ab preparations (**Figure 1.3**). Some types of modifications add or remove charges, which can interfere with antigen or receptor binding depending on the site of the altered residue.[156,164,165] Formation of pyroglutamate from N-terminal glutamine or glutamate removes the N-terminal positive charge, and also the negative charge of glutamate. Likewise, C-terminal amidation replaces a negatively charged carboxylate with an uncharged primary amide. Deamidation of interior asparagine or glutamine residues to aspartate or glutamate leads to introduction of negative charge, while isomerization of aspartate to isoaspartate can change protein conformation through alteration of the polypeptide backbone. Glycation of lysine residues removes a positive charge while

introducing new functionality.

Notably for IgG Abs, whose heavy chains terminate in a lysine residue, cleavage of this C-terminal lysine by carboxypeptidase B has important functional consequences.[166] While most endogenous Abs lack the terminal lysine and are thus better able to hexamerize for complement fixation, recombinant Abs can have higher levels of uncleaved heavy chain. Once recombinant Abs are localized to the serum, remaining lysine residues are efficiently cleaved with a half-life of approximately one hour. [167] However, it may be important to characterize C-terminal composition of purified Abs being compared in CDC assays, as those Abs with two C-terminal lysines elicit CDC with significantly weaker potency compared to unfractionated Abs from hybridoma cells.[166]

Oxidation of exposed amino acid side chains, especially those of methionine, tryptophan, and histidine, is commonly observed in Abs and other proteins, and has potential impacts on protein partner binding.[164,165] Methionine residues 252 and 428 located at the $C_\gamma2$-$C_\gamma3$ interface are particularly prone to oxidation, which can lead to weaker FcRn binding and in extreme cases, reduced half-life.[168,169] Oxidation of tryptophan residues within the hydrophobic antigen binding pocket can lead to significant decreases in antigen affinity.[170] Thus, it is important to optimize formulation conditions, or even replace liable residues, to reduce this source of heterogeneity.

On the other hand, reduced cysteines can also introduce unwanted complexity into Ab preparations.[164] In the native structure of an Ab, all framework cysteine residues are paired into either intra- or inter-chain disulfide bonds that serve to stabilize Ab tertiary and quaternary structure. The presence of free thiols represents a deviation from the proper Ab structure, and has been associated with decreased thermal stability and the ability to form covalent Ab aggregates.[171,172] Thus, it is common to ensure integrity of recombinant Abs by incorporating free sulfhydryl quantification into quality control assessments. Additional heterogeneity associated

with cysteine residues includes formation of trisulfides, thioethers, and racemized D-cysteine, although impacts of these modifications on function are less apparent.[164]

1.8 Fragmentation

1.8.1 Antigen-binding fragments

While whole Ab frameworks such as IgG are well-established as therapeutics, smaller frameworks of individual Ab domains may confer distinct biological advantages. The major difference between full Abs and Ab fragments is molecular size, with the 150-kDa IgG being reduced to 50 kDa in the case of Fabs, and even smaller sizes for other Ab fragments (**Figure 1.2**). One favorable result of small size is increased rate of diffusion, allowing for more efficient penetration into tissues and tumors that are being targeted.[173] Furthermore, small, non-glycosylated Ab fragments can be expressed efficiently in prokaryotic cells, reducing the time and cost of protein production. On the other hand, proteins <60 kDa are preferentially cleared via renal filtration, meaning 50-kDa Fabs and especially smaller Ab fragments are eliminated more quickly than 150-kDa IgG Abs.[173,174] Valency of binding is another consideration, since bivalent Abs have tighter avidity for antigen compared to monovalent Ab fragments.

Absence of Fc-mediated function is another major difference between full-length Abs and Ab fragments. Since the Fc domain is required for FcRn binding and endosomal recycling, Ab fragments lacking this domain are quickly cleared by lysosomal degradation in addition to renal filtration.[174] Thus, higher or more frequent dosing is usually required for small Ab-based therapeutics. Lack of the Fc domain also eliminates FcR- and complement-mediated effector functions. This loss of function may be advantageous for therapeutic mechanisms that require antigen binding without immune activation, but detrimental for indications like oncology, where ADCC, ADCP, and CDC are important tumor-killing functions. Finally, lack of an Fc domain may

eliminate binding to protein A- and G-based resins, necessitating the use of alternative purification strategies based on, for example, protein L. It should be noted that the fast clearance of Ab fragments, combined with their lack of FcR binding, makes them well-suited to diagnostic applications.[173]

In the laboratory, various Fab-containing fragments can be generated via enzymatic proteolysis. Traditionally, papain has been used to cleave above the hinge disulfide bonds to yield two monovalent Fabs and one Fc per molecule of IgG.[175] Pepsin cleaves below the hinge disulfides, producing one bivalent $F(ab')^2$ per IgG that can be further split into two F(ab') molecules in the presence of reducing agent. The apostrophe in these names denotes the presence of hinge/Fc sequences including oxidizable cysteines. Pepsin tends to cleave multiple sites in the Fc, preventing the purification of functional Fc using this enzyme. Following IgG cleavage, protein A or other affinity techniques can be used to purify the species of interest. Besides papain and pepsin, other enzymes like IdeS are used for site-specific IgG proteolysis.[176] While these enzymatic methods are useful for preparing small samples of Fab, recombinant expression of Ab fragments from custom genes may be more feasible for production of large, homogeneous preparations.

The Fab framework has the longest clinical history of all Ab fragments, with four molecules achieving approved status.[177] While ranibizumab and certolizumab pegol are expressed in *E. coli* as Fab or Fab' fragments, respectively, abciximab is produced as a full-length IgG in mammalian cells before papain digestion to Fab. Generally, Fabs have been successfully employed to treat acute indications where fast clearance is not a major concern. However, certolizumab pegol is used to treat chronic inflammatory conditions like rheumatoid arthritis and Crohn's disease. For this reason, the free cysteine near the heavy chain C-terminus is used for site-specific conjugation

to ~40-kDa polyethylene glycol (PEG), which increases its serum half-life.[178] Thus, Fab fragments are attractive options when the Fc region is unnecessary or detrimental, and modifications such as PEGylation or albumin-binding functionality can be used to mitigate drawbacks like fast clearance.

1.8.2 Single-chain variable fragments

The next most explored types of Ab fragment are the variable fragment (Fv), disulfide-stabilized variable fragment (dsFv), and most commonly, single-chain variable fragment (scFv).[179] These frameworks are composed of the V_H and V_L domains, which for the dsFv are stabilized by an engineered interchain disulfide bond, and for the scFv are covalently linked with a hydrophilic 10-25 amino acid linker. At roughly 28 kDa, the scFv is the smallest Ab-based protein that retains the native variable regions of a human Ab. Similar to Fabs, scFvs have the potential for low-cost prokaryotic expression and increased tissue penetration, at the cost of fast clearance and lack of effector function.

The modular nature of the scFv facilities its multimerization into homo-oligomers with increased antigen-binding valency or hetero-oligomers with multiple functionalities.[179] For example, use of progressively shorter linkers allows for formation of scFv dimer, trimer, and tetramer (diabody, triabody, tetrabody) since the V_H and V_L domains cannot properly pair when connected by a short peptide. It is possible to create bispecific scFvs by incorporating the V_H and V_L sequences for two separate Abs into a single 55-kDa polypeptide. This and other bsAb platforms are discussed in the section on multispecificity.

1.8.3 Single domain antibodies

Even smaller than scFvs are single domain Abs (sdAbs), which are 15-kDa V_L, V_H, or V_{HH} domains.[180] The most popular of these are V_{HH} sdAbs, or nanobodies, which are derived from heavy chain Abs that are produced by camelids. These 80-kDa heavy chain Abs (so named because

they lack light chains) contain a single antigen-binding domain, V_{HH}, directly N-terminal of the hinge. Since the V_{HH} domain is not complexed with other Ab domains, its surface tends to be much more hydrophilic than that of V_H and V_L domains, which are hydrophobic at their pairing interface. Therefore, camelid-derived V_{HH} nanobodies tend to have favorable biophysical characteristics like high solubility and low aggregation compared to human sdAbs.[181] In addition, the V_{HH} CDR3 is often longer than the V_H CDR3, potentially allowing it to form more favorable contacts with its binding epitope.[182] Besides camelids, cartilaginous fishes produce a distinct type of heavy chain Ab containing a single variable region, V_{NAR}, which could also serve as a therapeutic sdAb.[183]

Like scFvs, sdAbs are amenable to tandem multimerization. Fusion of the same nanobody allows for increased valency and decreased antigen dissociation, while fusion to distinct nanobodies allows for bispecific mechanisms to be explored. A common strategy is to pair antigen-binding and albumin-binding specificities into the same molecule, allowing it to fulfill its intended function while circulating longer in serum.[180] Additional engineering efforts have focused on reducing the immunogenicity of V_{HH} domains, which may not be crucial given their sequence similarity to human V_H3 domains and their size comparability to the non-human domains in full-length chimeric Abs.[180] While humanization of V_{HH} molecules may decrease their antigenicity, it can also confer unfavorable V_H properties like low solubility.[180] Thus, the complementary strengths of human and non-human sdAbs should be considered when designing therapeutics with these frameworks.

1.8.4 Crystallizable fragments

While most therapeutic Ab fragments retain Ag-binding domains, the free Fc domain can also be used to antagonize Fc receptors. This format is ideal when Fc receptors should be occupied without co-localizing a specific Ag. As one example, the IgG1 Fc has been engineered to bind

with high affinity and less pH dependence to FcRn.[184] Upon administration, the IgG mutant binds tightly to endosomal FcRn, preventing FcRn-mediated salvage of endogenous IgG Abs and accelerating their degradation. The utility of these Ab-degrading Fc molecules (Abdegs) has been explored for treatment of autoimmune diseases mediated by pathogenic IgG.[185] Since the Fab domains are unnecessary for the Abdeg mechanism, the Fc domain alone can be used therapeutically. A clinical example is ARGX-113, which has shown both depletion of endogenous IgG and efficacy treating myasthenia gravis.[185]

1.9 Multimerization

1.9.1 Antibody multimerization

Intuitively, Ab oligomers can have enhanced binding to antigen and FcRs, largely through multivalency and a decreased dissociation rate. The affinity of naturally low-abundant recombinant IgG1 dimers for low-affinity FcγRs is hundreds of times higher than that of the corresponding monomers.[186] Similarly, aggregates of thermally stressed IgG1 have enhanced affinity for FcRn, while immune complexed and hexamerized IgG1 have enhanced FcRn-mediated transepithelial transport.[187,188] For CD40 Abs, agonism is generally dependent on FcγIIb-mediated crosslinking. However, covalent multimers of mouse IgG2a were shown to activate CD40 in a FcγR-independent manner, allowing for increased survival in a mouse lymphoma model.[189] Thus, Ab multimerization can provide enhanced FcR- and Ag-mediated functions, but may introduce heterogeneity or potential for immunogenicity depending on the oligomerization strategy.

IgG hexamerization, which occurs on the surface of Ag-coated cells, can be augmented for improvement of complement-mediated effector function (**Figure 1.2**).[26] By mutating residues at the IgG complexation interface, hexamerization on the cell surface has been increased, allowing for improved C1q recruitment and CDC.[190] The requirement of antigen-expressing cells for

enhancement of effector function distinguishes this approach from other Fc engineering strategies, which tend to increase immune activation independent of target binding. Attachment of the IgM tailpiece to the IgG C-terminus is another hexamerization approach that allows for enhanced binding to Fc-binding proteins.[188,191189] Depending on structure and context, these multimerizing Abs may be useful for both potentiating and inhibiting the immune functions of complement and FcRs.

1.9.2 Domain multimerization

Duplication of Ag-binding domains is possible through tandem fusion of gene sequences, and may be used to maximize potency. As discussed previously, multimerization of scFvs and nanobodies allows for higher-avidity antigen binding, and introduces the opportunity for bispecific and multispecific mechanisms to be explored.[179,180] These Ag-binding domains may be used alone or as Fc fusions to improve pharmacokinetics and impart effector function.

The Fc domain can be analogously duplicated to generate Ab variants that are multivalent for both Ag and FcRs. Several studies have demonstrated the utility of IgG1 molecules that contain one or two extra Fc domains tandemly linked to the IgG C-terminus.[192-195] Whether the additional Fc domains are linked by the IgG2 hinge or a flexible linker, they elicit significantly stronger ADCC and ADCP than the wild-type IgG. Intriguingly, the Fc domains can also be of distinct classes. For example, fusion of the IgA2 Fc to the C-terminus of a normal IgG1 Ab led to enhanced ADCC through FcαRI binding.[196] Alternatively, Fc multimers that lack Ag binding display marked FcR antagonism, which could be useful for treatment of autoimmunity.[197] A potential drawback of these frameworks is faster clearance due to differences in FcRn binding avidity.[195] Regardless, Fc duplication is a creative engineering strategy for generating Abs with stronger effector functions. In contrast to the standard approach of introducing framework mutations that alter FcR

binding, this strategy uses the avidity effect to enhance binding. Use of the proper linker may allow for potent IgG derivatives that retain high stability and low immunogenicity through conservation of native Ab sequences.

1.10 Conjugation

1.10.1 Payload

A primary consideration for the design of ADCs is the type of cytotoxic agent that will be conjugated to the tumor-targeting Ab. Due to the limited number of Ab-targeting receptors on the cell surface, and the limited capacity of drugs per Ab, the delivery of traditional chemotherapeutic agents is often not sufficient to eliminate malignant cells.[198] Instead, ADCs have made use of increasingly potent drugs that are cytotoxic in the picomolar range, and therefore not therapeutically feasible without conjugation to Abs to increase their specificity.

While potent antitumor activity is essential for ADC payloads, other factors should also be considered. The physicochemical properties of the drug are important, as excessively hydrophobic agents can lead to low aqueous solubility, increased ADC aggregation, immunogenicity, or accelerated clearance.[198,199] For example, the hydrophobicity of some drugs limits the number of molecules that can be attached to the Ab before aggregation occurs. The warhead should also be amenable to linker attachment, and retain activity and stability after conjugation to the Ab. Finally, ideal conjugated drugs should not be substrates for efflux transporters like multidrug resistance protein 1 (MDR1), as this would increase their systemic toxicity and introduce the opportunity for resistance mechanisms.

Several classes of warheads have been conjugated to approved ADCs, and many more are conjugated to ADCs that have been in clinical trials. Auristatins and maytansinoids, potent tubulin inhibitors, are derivatives of compounds produced by *Dolabella auricularia* sea slugs and

Maytenus ovatus plants, respectively.[198] Monomethyl auristatins E and F (MMAE and MMAF), are two examples of auristatins that were selected for favorable potency and stability. MMAE is the cytotoxic component of the approved ADC brentuximab vedotin. Examples of stable and soluble maytansinoids include DM1 and DM4, with DM1 being the warhead for trastuzumab emtansine. The calicheamicins are a third class of payload found on approved ADCs, derived from a compound produced by the bacterium *Micromonospora echinospora*. Both gemtuzumab ozogamicin and inotuzumab ozogamicin utilize the DNA-cleaving N-acetyl-γ-calicheamicin to kill malignant cells. Notably, the distinct cytotoxic mechanism makes calicheamicins efficient at lysing all cells, in contrast to auristatins and maytansinoids, which preferentially target rapidly dividing cells.[200] While several other classes of cytotoxic compounds have been conjugated to Abs, they generally induce cell death via DNA, RNA, or tubulin interference and so far have not been used in approved ADCs.[198]

Antibody-radionuclide conjugates (ARCs) can be used diagnostically, but also therapeutically due to the damaging effects of radiation on DNA, membranes, and mitochondria.[201] Attachment of radionuclides to Abs is commonly achieved through Ab conjugation to metal chelators such as diethylenetriaminepentaacetic acid (DTPA) or 1,4,7,10-tetraazacyclododecane-1,4,7,10-tetraacetic acid (DOTA), or through iodination of tyrosine residues in the case of iodine isotopes.[202] Selection of the radionuclide is critical for delivery of optimal radiation energy at an appropriate pathlength. Most commonly used are β emitters, such as ^{90}Y and ^{131}I, which exert long-range (1-10 mm) effects but have low linear energy transfer.[202] Examples include the approved ^{90}Y-ibritumomab and the approved but withdrawn ^{131}I-tositumomab. Although both of these ARCs target CD20 for treatment of non-Hodgkin's lymphoma, it is thought that β emitters may be suitable for elimination of high-volume solid tumors, due to the large crossfire effect that damages

cells distant to the radionuclide.[201,202] Conversely, α emitters (e.g. ^{211}At, ^{213}Bi) and Auger emitters (e.g. ^{111}In, ^{125}I), which have a higher linear energy transfer but a lower range, may be more apt for treatment of small tumors or metastasized clusters of cells. For all types of emitters, another important consideration is the physical half-life of the radionuclide, which should ideally be similar to the biological half-life of the ARC.[203] An ongoing challenge for ARCs is the cost and expertise required for administration, which often involves complex dose calculations and the need for radioprotection and waste management.[202,203] Indeed, the declining sales and resulting withdrawal of ^{131}I-tositumomab was partly attributed to the complexity of administering the drug.[199] Overall, radionuclides serve as potent warheads when conjugated to Abs and provide beneficial crossfire effects for targeting heterogeneous tumors, but a deeper understanding of the underlying radiobiology would help clarify dose requirements and radioresistance mechanisms.

In addition to ADCs and ARCs, other types of Ab conjugates have been explored. Moxetumomab pasudotox, which was recently approved for treatment of hairy cell leukemia, is composed of an anti-CD22 dsFv linked to a truncated form of *Pseudomonas* endotoxin A.[204] Thus, protein toxins are viable alternatives to small molecule drugs and natural products, with sufficient activity at the low concentrations achieved by Ab conjugates. A concern for use of exogenous toxins is the possibility of immunogenicity and increased clearance, which is more problematic for larger toxins containing more potential epitopes. Abs can also be conjugated to more specific cytotoxic agents, like antibacterials, for treatment of intracellular infections.[205] The future will tell whether Ab-mediated delivery of other types of warheads can be used for additional non-cancer indications.

1.10.2 Conjugation strategy

Early ADCs used the intrinsic reactivity of native amino acids to couple drugs to Abs. The

primary amine of lysine sidechains readily reacts with activated esters on linker moieties, allowing for lysine-specific conjugation. Unfortunately, IgG molecules contain approximately 80 lysines which are largely surface exposed. This excess of reactive sites leads to significant heterogeneity both in drug-antibody ratio (DAR) and the site of conjugation, with possibility for reduced Ag binding or serum half-life.[206] Most approved ADCs (gemtuzumab ozogamicin, trastuzumab emtansine, and inotuzumab ozogamicin) have used this lysine conjugation strategy, which can result in some Abs being left unconjugated while others are overloaded with a DAR of up to 8.[198] Another straightforward conjugation strategy, employed by brentuximab vedotin, is reactivity of reduced interchain cysteines with the linker maleimide group. Although there are only 8 interchain cysteines per IgG, there is still significant heterogeneity associated with this method.[206] The loss of stabilizing interchain disulfide bonds can be rectified by using re-bridging groups that covalently link cysteines while also adding a handle for conjugation.[198,207] Overall, conjugation via native amino acids has produced several efficacious ADCs, but also left room for improvement of product homogeneity.

Molecular biology paved the way for site-specific ADCs via conjugation to mutated amino acids. At the forefront are THIOMABs, which contain engineered cysteine residues at ideal locations for drug attachment.[208] Since the introduced cysteines are unpaired, they react with Michael acceptors more readily than disulfide-bonded cysteine residues. Advantages of THIOMABs, and other engineered cysteine technologies, include homogeneity of structure and DAR, increased therapeutic index, and improved pharmacokinetics.[208] The site of the engineered cysteine has a large impact on the properties of the ADC. Introduced cysteines should not be too solvent accessible, for fear of thiol exchange with endogenous proteins; and they can be positioned at patches containing positive charge to improve linkage stability via succinimide hydrolysis. [209]

In addition to engineered cysteines, incorporation of peptide tags into the Ab sequence has allowed for enzymatic conversion to site-specific conjugation handles.[198,206] For example, presence of the CXPXR amino acid motif allows for introduction of an electrophilic formylglycine residue via formylglycine-generating enzyme, while the LLQGA motif allows for direct coupling of an amine-containing substrate to the internal glutamine residue via transglutaminase.

Incorporation of non-canonical or unnatural amino acids outside the standard 20 is another approach for generating site-specific ADCs.[210] Since selenocysteine has a lower pKa than cysteine and lysine, it is more reactive than other nucleophilic residues at low pH. This amino acid can be introduced at the Ab C-terminus using the UGA codon paired with the selenocysteine insertion sequence.[211] Unnatural amino acids like para-acetylphenylalanine and para-azidomethylphenylalanine can likewise be introduced using the amber codon (UAG) along with the proper charged tRNA.[212,213] These amino acids integrate orthogonal ketone and azide groups, respectively, into the Ab for conjugation to alkoxyamines and dibenzocyclooctynes. While use of unnatural residues requires a substantial initial investment and may affect protein yields, it ultimately allows for stable and well-defined conjugation.

Glycans attached to IgG Asn297 represent an additional target for site-specific conjugation.[198,206] Metabolic engineering with media supplementation has allowed for incorporation of 6-thiofucose in place of the normal fucose residue.[214] As with THIOMABs, the unpaired thiol group of 6-thiofucose is more prone to reduction and maleimide conjugation. Similarly, post-expression glycan engineering allows for introduction of galactose and sialic acid residues that contain azide or ketone functionality.[206,215] This is achieved using glycosylating enzymes that naturally have, or are mutated to have, expanded substrate specificity. Finally, chemical oxidation of vicinal diols within glycan residues such as sialic acid introduces

electrophilic aldehyde groups.[198,206] While periodate oxidation is a relatively straightforward method to incorporate a chemical handle for conjugation, it can cause off-target oxidation of prone methionine residues.[216]

Conjugation strategy directly determines the possible range of DAR values, as well as the chemical properties of the Ab-linker bond. While conjugation to native lysines or cysteines leads to heterogeneity in DAR and potential for excessive drug loading, introduction of engineered cysteines or unnatural amino acids allows for well-defined DAR values. Generally one or two sites are mutated (on each HC or LC), allowing for DAR values of 2 or 4.[198] This reduction in maximum DAR has benefits such as reduced aggregation propensity and improved pharmacokinetics.[206] Meanwhile, the conjugation chemistry also impacts ADC stability, with labile linkages allowing for drug loss and resulting off-target toxicity. Thiol-maleimide coupling is often used to load native and engineered cysteines due to its speed and selectivity; however, the resulting thioether is susceptible to thiol exchange with endogenous thiols.[206] By adding groups with positive charge adjacent to the maleimide, succinimide hydrolysis is favored for prevention of retro-Michael reactions.[217] Oxime, and to a greater extent hydrazone, linkages undergo acid-catalyzed hydrolysis, so the possible instability of these groups should also be considered.[206] As the number of site-specific conjugation strategies continues to increase, it will be interesting to see which sites and functionalities produce the safest and most efficacious ADCs.

1.10.3 Linker

The first step in linker design is choosing two functionalities that will allow for covalent bond formation between the Ab on one end and the payload on the other. Thus, the chemistry of the linker must be compatible with whichever conjugation site and drug are selected.

An important property of these two reactive ends is the extent to which their conjugated

products are cleavable by lysosomal proteases, acidic pH, and reducing conditions. Ideally, both of the Ab-linker-payload linkages would be completely stable in the blood, and only efficiently cleaved after delivery to the target cell. One strategy to release the warhead within the cell is to use dipeptide linkers such as valine-citrulline, which are C-terminally cleaved by cathepsin B in the lysosome.[218,219] Brentuximab vedotin is an ADC in clinical use with such a linker. A second strategy is to incorporate pH-sensitive linkages that allow for drug release specifically in the lysosome; for example, the hydrazone group which was mentioned previously for its acid lability.[218] Although ADCs like gemtuzumab ozogamicin and inotumomab ozogamicin have shown efficacy using such a linker, it is now appreciated that hydrazone groups may release the payload prematurely to increase off-target toxicity.[198,218] Thirdly, disulfide linkers are cleaved much more efficiently in the reducing environment within cells, and therefore also allow for targeted drug release. Sterically masking the disulfide bond may help to decrease reduction by low concentrations of reductant in the serum.[220] In contrast to cleavable linkers, linkers containing thioethers and other non-cleavable groups may be used to decrease the chances of unintended systemic drug exposure.[218] For trastuzumab emtansine, drug release from the Ab does not occur until the Ab has been proteolytically degraded. Because the metabolic product contains the payload linked to an Ab-derived amino acid, it is vital that the payload retain activity even with the added bulk and charge. In one comparison of linker types, it was found that ADCs containing a non-cleavable linker had similar potency, but a higher therapeutic window, than the corresponding ADCs containing a protease-cleavable linker.[221]

In addition to chemical reactivity, the physicochemical properties of the linker as a whole should also be considered. Since ADCs contain more hydrophobic surface area than naked Abs, they are generally more prone to aggregation.[218] Additionally, hydrophobic drugs are more likely

to be substrates for the transporter MDR1.[198] Therefore, polar linkers that contain solubilizing groups like sulfonate and PEG not only reduce ADC aggregation propensity, but also potentiate elimination of MDR1-expressing cells (assuming the polar functionality is retained in the final warhead).[222,223] As a result, properties like potency, pharmacokinetics, and therapeutic index can all be improved by using charged or polar linkers.[224] Presence of charge in the final drug moiety also largely determines its ability to elicit the bystander effect, as only uncharged molecules efficiently cross lipid membranes to reach neighboring cells. Whereas S-methyl metabolites originating from disulfide linkers are uncharged and therefore enable bystander killing, amino acid-conjugated payloads with non-cleavable linkers are charged and less likely to elicit these effects.[225,226] It should be noted that toxicity to neighboring cells can be favorable (in the case of targeting tumors with heterogenous antigen expression) or unfavorable (when the primary casualties are healthy cells).

1.10.4 Fusion proteins

Fusion proteins are another class of Ab conjugate that combine the favorable features of Abs with therapeutic properties of other biomolecules. Molecular biology approaches can be used to genetically fuse an Abs or Ab domain to the molecule of interest, allowing for recombinant expression of multifunctional proteins.

Some fusion proteins utilize the Ag-binding specificity of Abs for localization into targeted environments. For example, Ab-cytokine conjugates have been used to increase tumor accumulation of pro-inflammatory interleukins (e.g. IL-2, IL-12) for activation of cytotoxic T cells and NK cells.[227] For these immunomodulatory agents, the affinity and valency of the cytokine and Ab components should be optimized to maximize tumor localization and minimize off-target cytokine effects. Similarly, antibody-directed enzyme prodrug therapy (ADEPT) uses Ab

specificity to deliver enzymes to the site of malignancy, where they can activate low-toxicity prodrugs into the active cytotoxic agent.[228] Although immunogenicity is a concern, engineering of non-human enzymes, or use of human enzymes not present in blood (e.g. β-glucuronidase), can be used to mitigate this risk factor. A widely applicable strategy for half-life extension of biologics is incorporation of an albumin-binding domain. Nanobodies targeting albumin (AlbudAbs) take advantage of FcRn-mediated endosomal recycling to prolong the pharmacokinetics of other proteins while only adding a small ~12-kDa domain.[229]

Likewise, the Fc domain of an Ab can be conjugated to other proteins to impart physical and biological properties. Biomolecules like receptors, cytokines, enzymes, and peptides can be genetically fused to Ab Fc domains, and several such molecules are approved for clinical use.[230] An important advantage of IgG Fc fusion is the ability to bind FcRn and increase half-life, though Fc-fusion proteins generally have weaker FcRn binding and shorter half-lives (~2 weeks vs. ~3 weeks) than IgG molecules.[230,231] Depending on the groups attached, Fc-fusion may retain FcγR-mediated effector functions but generally lose the ability to fix complement.[231,232] Other potential benefits include increased stability and solubility, as well as facile purification using protein A- and G-based resins.[230] From a design standpoint, it is possible to fuse proteins to either end of the Fc. In practice, it is more common to attach functionality to the N-terminus of the Fc to more closely mimic the native IgG structure. Since the Fc domain is a dimer of heavy chains, the folded product will be a dimer of the fusion partner as well. While domain dimerization may be advantageous, in some cases it is preferable to generate molecules that are monomeric for the non-Ab component. For example, co-transfection of the protein-Fc fusion with a standard Fc domain allows for a mixture of products from which the desired species (monomeric protein, dimeric Fc) can be purified.[233] Such monomeric Fc-fusions may have improved pharmacokinetics, but

presumably a lower yield. Regardless of which design strategy is used, the Fc-fusion format has proven useful for instilling diverse biotherapeutics with beneficial properties of the Ab framework.

1.10.5 Conjugation to hydrophilic polymers

As mentioned previously, certolizumab pegol is a Fab' fragment that is site-specifically PEGylated to partially compensate for lack of FcRn-mediated recycling.[234] In fact, addition of PEG and other hydrophilic groups is a general strategy to increase solubility and apparent hydrodynamic radius of therapeutic proteins. The increase in apparent size prevents renal filtration of small proteins that would otherwise be quickly eliminated.[235] Conjugation can be achieved using the same amino acid-targeting chemistries discussed for ADCs, where modification of site-specific C-terminal Fab' thiols may be preferential to non-specific amine conjugation that can impede Ag binding. Favorable effects of PEG include increased stability, bioavailability, and half-life; and decreased immunogenicity and proteolysis.[234,235] On the other hand, anti-PEG Abs have been detected in patients before and after administration of PEGylated proteins and may lead to faster clearance of PEGylated proteins.[236] Several groups besides PEG, including sugars like polysialic acid and dextran, can be chemically conjugated to Ab fragments to similarly alter their biophysical characteristics.[235] Furthermore, proteins can be recombinantly modified to include hydrophilic peptide repeats or glycosylation motifs. These strategies reinforce the notion that covalent conjugation of Abs to drugs, polymers, and other proteins allows the properties of Abs to be tailored to their specific therapeutic purpose.

1.11 Multispecificity

1.11.1 Asymmetric IgG-like frameworks

As mentioned in the section on antigen selection, some mechanisms of action require multiple functionalities to be combined into one molecule. With deeper understanding of

molecular biology and protein engineering, it has become increasingly practical to design bispecific and multispecific Abs (bsAbs and msAbs) with a diverse array of architectures.[237,238] While it is outside the scope of this review to describe all the msAb technologies that have been developed, it is worthwhile to explain the main strategies used and to highlight demonstrative examples of their implementation. The first family of bsAb frameworks uses the whole IgG structure to generate bivalent, bispecific Abs that retain Fc-mediated properties like pharmacokinetic stability and immune activity.

Classically, IgG bsAbs could be generated by fusing two hybridomas into a quadroma that expresses two distinct Ig HCs (HC_A, HC_B) and two distinct LCs (LC_A-LC_B) targeting antigens A and B.[239] Similarly, expression hosts can be transfected with DNA sequences corresponding to the four polypeptide chains of interest. When the chain pairing possibilities are considered, it is easy to understand why these methods are inefficient at producing bsAb with the desired [LC_A-HC_A]-[HC_B-LC_B] composition. When left to chance, the HCs may homodimerize (HC_A-HC_A or HC_B-HC_B) instead of heterodimerizing (HC_A-HC_B), and each HC may associate with the wrong LC (e.g., HC_A-LC_B instead of HC_A-LC_A). These opportunities for chain mispairing have been termed the HC problem and LC problem, respectively. Assuming equal efficiency of transfection/expression of each chain and unbiased chain pairing, only 1/8 of the tetrameric protein product will have the desired composition. While it is possible to purify the bsAb fraction from the mixture, the low yield and additional steps are significant drawbacks. Use of Ab chains from different species (e.g. mouse and rat) simplifies the matter somewhat by minimizing the LC problem and allowing for pH step elution of the three possible HC dimers.[240] An example of such a Triomab is catumaxomab (α-CD3 x α-EPCAM), which was the first bsAb approved for clinical use in 2009 but later withdrawn for commercial reasons.[38]

To facilitate proper chain assembly without resorting to non-human frameworks, genetic engineering strategies have been employed with much success. The HC problem can be remedied by engineering a preference for HC heterodimerization over homodimerization, increasing yield of bsAb from 1/8 to 1/4 of tetrameric products in the absence of additional HC-LC pairing strategies. A pioneering technology in this field was the "Knobs-into-Holes" set of mutations that creates a "knob" in the C_H3 domain of one HC (T366Y) that fits into a "hole" of the other HC (Y407T).[241] A second generation framework used the same concept with the addition of an engineered disulfide bond to stabilize the HC heterodimer.[242] In addition to steric complementarity, electrostatic steering is another way to create a preference for the HC heterodimer. By making one C_H3 domain more negatively charged (K392D/K409D) and the other more positively charged (E356K/D399K), the HCs of the same types are repelled while opposite HCs attract.[243] Charge-based HC heterodimerization methods, combined with a common LC, were used to create the recently approved bsAb emicizumab (α-factor IXa x α-factor X).[244] A third strategy is to use IgA/IgG chimeric strand-exchange engineered domain (SEED) C_H3 domains where the heterodimer contains more class-matched area at the C_H3 interface.[245] An advantage of each of these methods is the ability to drive heterodimerization in cells that would otherwise assemble HCs randomly.

Combination of HC-HC pairing and HC-LC pairing strategies generates IgG bsAbs with high purity. One way to circumvent the LC problem is to combine the HC and LC into a single chain, as for scFv-Fc or scFab-Fc fusions.[237] Alternatively, the correct HC-LC pairings can be favored by incorporating mutations into each chain that generate orthogonal Fab interfaces.[246] Moving the site of the HC-LC disulfide bond on only one of the Fab domains (as with DuetMab) is another way to drive correct HC-LC assembly.[247] A particularly elegant solution to the LC

problem is to swap the C_H1 and C_L domains on only one Fab arm.[248] This CrossMab approach reliably generates the desired HC-LC pairings without the use of potentially destabilizing mutations and has inspired a whole family of multispecific Ig frameworks.[249] In cases where it is possible to generate functional Fvs against two distinct antigens using a common LC or common HC, the LC and HC problems can be avoided and these chain pairing strategies become unnecessary.

The bsAb technologies covered so far rely on co-transfection of Ig chains directed toward distinct antigens into the same batch of Ab-expressing cells. It is also possible to separately express and purify parental Abs before recombining them *in vitro* to the corresponding bsAb. For example, parental Abs containing "knob" or "hole" mutations can be separately purified and then incubated together in the presence of reducing agent to allow for hinge reduction and half-Ab exchange driven by the energetic preference for HC heterodimer.[250] Mutation of the hinge to lack disulfide bonds facilitates this process by obviating the need for reducing agent, but also eliminates stabilizing disulfide bonds in the product.[251] A similar method takes advantage of the Fab-arm exchange process that takes place naturally for IgG4 due to the weaker C_H3 interactions and hinge lability of this subtype. For controlled Fab-arm exchange, parental Abs containing the F405L or K409R mutations are combined under reducing conditions to allow formation of >90% pure bsAb.[252] Since the correct HC-LC pairing is not disrupted, even in the presence of reductant, these methods sidestep the LC problem and only require mutations for HC heterodimerization. Another benefit of the post-expression recombination approach is the ability to generate panels of parental Abs containing complementary mutations, which can be recombined to evaluate the synergy of each combination.

Rather than driving proper HC-HC and HC-LC pairings, strategies have also been devised

to facilitate purification of bsAb from mixtures of other chain combinations. For instances where two Fv fragments are discovered or engineered to use the same V_H sequence (i.e. common HC) and each V_L is from a different class (κ and λ), κ/λ bodies can be easily purified.[253] After transfecting cells with the single HC, Ag A-specific κ LC, and Ag B-specific λ LC, the desired product will contain two HCs and one of each LC. Thus, successive KappaSelect and LambdaSelect chromatography steps allow for purification of bsAbs of the desired composition. For any two mAbs containing a common LC, bsAb purification can be expedited by incorporating mutations that ablate protein A binding into one of the parental HCs.[254] After co-expression of the two HCs and common LC, bsAb can be purified from the mixture using protein A resin combined with incremental decreases in buffer pH. The species containing two mutated HCs flows through the column, while the heterodimer elutes at intermediate pH and the wild-type HC homodimer elutes only at low pH due to strong protein A avidity. If recombination of half-Abs is performed using purified parental mAbs or culture supernatants (rather than co-expression), the process can be used to purify bsAb without the requirement for a common LC.[255]

In summary, several strategies exist for the preferential formation and purification of IgG-like bsAbs. Although bsAbs with the whole IgG framework necessitate methods for proper HC-HC and HC-LC pairing, they inherit many of the favorable structural and functional features of the well-characterized IgG framework. Selection of which bsAb technology to employ may be guided by considerations including ease of implementation and minimization of mutational load, while patent rights are a valid concern for commercial projects.

1.11.2 Fusion of Ag-binding domains

To avoid the HC and LC pairing problems, or to alter properties like size, valency, and geometry, msAbs lacking the Fc domain can be formed via fusion of Ag-binding domains. Small

size in particular may be beneficial for tissue penetration, while the resulting decrease in half-life can be overcome through incorporation of albumin-binding capacity, for example.[173,175] Lack of the Fc domain eliminates FcR- and C1q-mediated functions, but specific immune activity can be achieved by domains that bind receptors of interest (e.g. CD3). Without the constraints of the IgG framework, factors like flexibility and inter-Ag distance can be optimized using different binding domains and linkers. Although chemical conjugation to generate, for example, bispecific $F(ab')_2$ is possible, most work has focused on genetic engineering approaches to create bsAbs from Ag-binding fragments.[256,257]

The scFv format is well-suited for bsAb applications, as scFv domains with different specificities can be easily combined using single or multiple polypeptide chains. For cancer indications, tandem linkage of scFv domains targeting a target-associated antigen and a T cell or NK cell antigen (CD3 or FcγRIIIa) are used to create bispecific T cell engagers (BiTEs) or bispecific killer cell engagers (BiKEs).[258,259] For example, the BiTE blinatumomab (α-CD3 x α-CD19) was approved in 2014 for treatment of specific leukemias, and is thought to function by stimulating cytotoxic T cells to act on co-localized tumor cells. In addition to $scFv_2$ formats, $scFv_3$ proteins can be engineered to bind three separate antigens, or to bind one antigen bivalently and a second antigen monovalently.[237] The scFv-based Diabody framework is also amenable to multispecificity. Since Diabody chains may undergo unwanted homodimerization, derivatives like dual-affinity retargeting (DART) proteins and single-chain Diabodies have been engineered to drive heterodimerization through incorporation of a stabilizing disulfide bond and consolidation into a single polypeptide chain, respectively.[260,261] Shortening the linker of the single-chain Diabody allows for generation of TandAbs, which bind bivalently to each of two Ags.[262]

Like scFvs, distinct Fab fragments can be combined into bifunctional agents. For example,

HCs can be fused in tandem and co-expressed with both LCs.[263] The correct HC-LC pairing is driven by strategies such as the orthogonal Fab interface mutations that resolve the LC problem. sdAbs are particularly amenable to genetic fusion, since their binding capacity resides in a single domain that does not require chain pairing. Tandem fusion of sdAbs allows for generation of multispecific and multivalent proteins that retain low molecular weights.[237]

In summary, sdAbs, scFvs, and Fabs of distinct specificities can be combined into compact and multifunctional agents. These Fc-less bsAbs are not limited to sdAb-sdAb, scFv-scFv, or Fab-Fab fusions; indeed, combination of different frameworks may be beneficial. For instance, Fab-scFv and Fab-sdAb fusions do not have the chain-pairing problem of Fab-Fab fusions, and the increased spacing creates geometry distinct from that of scFv-scFv and sdAb-sdAb fusions. Differences in bsAb properties like Ag affinity, expression yield, and aggregation propensity can vary between bsAb formats.[264] Thus, careful consideration and experimentation are likely required to determine the optimal domain configurations for a given application.

1.11.3 Fusion of Ag-binding domains to IgG

Finally, Ag-binding fragments can be fused to the IgG or Fc framework to create msAbs that are often multivalent for each antigen. A straightforward strategy is to append Ag-binding domains to the native IgG framework. Domains such as scFv, and dAb can be fused either N- or C-terminally to the HC or LC, allowing many symmetrical constructs to be explored that may differ in their geometry and ability to co-engage with two antigens.[237] Because bispecificity results from the native IgG and appended domain targeting different antigens, it is not necessary to address the HC and LC problems. An example of this approach is the dual-variable-domain Ab (DVD-Ig), in which a distinct V_H and V_L are fused N-terminally to the standard IgG HC and LC, respectively.[265] If the size of IgG fusions is deemed too large, the same strategies can be applied

to make bispecific molecules based on Fc or C_H3 homodimerizing domains. Combinations of different domain types, linkers, and appendage sites allow for almost limitless possibilities to be explored.

At the same time, domains can also be appended to heterodimerizing Fc domains to generate asymmetric architectures with opportunities for multispecificity. For example, the trispecific scFab-Fc-scFv contains heterodimerizing HCs attached to different scFabs at the N-terminus and a distinct scFv at one or both of the C-termini.[266] Applying the DVD-Ig format together with Knobs-into-Holes mutations to drive HC heterodimerization and CrossMab domain swapping to drive correct HC-LC pairing allow for creation of tetraspecific Abs that are monovalent for each antigen.[267] It has become increasingly clear that combinations of protein engineering strategies can be used to generate multifunctional frameworks that are custom-tailored to the application at hand.

1.12 Protein engineering

1.12.1 Mutations that alter effector function

Early work in the IgG engineering field revealed residues important for FcγR binding via alanine scanning, and also showed that mutation of selected residues could enhance FcγR affinity and FcγR-mediated effector functions.[268] Since then, numerous studies have reported sets of 1-5 amino acid mutations that significantly improve both FcγR binding and ADCC/ADCP.[269-271] While all of the FcγRs share a binding site comprising the lower hinge and upper C_H2, slight differences in binding modes means that a given set of mutations may differentially impact affinity to each of the FcγRs. Improved binding to FcγRIIIa for more potent ADCC is a common goal that can be achieved through amino acid mutation in addition to the glycan engineering methods mentioned previously. Similarly, variants with tighter FcγRIIa binding have enhanced

macrophage-mediated ADCP. Although it may be important in some contexts to maximize the relative affinity for activating and inhibitory FcγRs, one study showed that FcγRIIa affinity was more important than the FcγRIIa/FcγRIIb affinity ratio for ADCP function.[272,273] Because the IgG HCs bind FcγRs asymmetrically, each HC can be made to contain a distinct set of mutations that synergistically enhance FcγR binding.[274] As all of these mutation strategies incorporate framework changes and potentially novel epitopes, they may have altered properties, such as stability and immunogenicity, compared to a native IgG.

Mutations in the C_H2 domain can also alter affinity for C1q binding, and thus modulate CDC activity. Since FcγRs and C1q bind at proximal sites in the IgG Fc domain, improvement of CDC may come at the cost of decreased ADCC.[270,271] For example, one study found that a set of three mutations caused a 7-fold increase in CDC, but a 20-fold decrease in ADCC.[275] Addition of two additional mutations not only increased CDC further, but also caused a modest increase in ADCC relative to the wild-type IgG. Another approach designed an IgG1/3 chimera by fusing the IgG1 C_H1 and hinge with the IgG3 C_H2 and C_H3 domains.[276] By combining the properties of each subclass, CDC was increased relative to IgG1 while ADCC was increased relative to IgG3. As mentioned previously, mutations in the lower Fc domain can also be used to enhance CDC by increasing IgG hexamerization.[26]

Conversely, Fc engineering can be used to generate silent antagonists that have minimal effector function. Previously mentioned strategies to reduce FcγR and C1q binding include deglycosylation and hybridization of weakly activating subclasses like IgG2 and IgG4.[108,150] In addition, the C_H2 domain can be mutated to decrease engagement with activating receptors and the resulting release of inflammatory cytokines.[271,277] Different sets of 2-6 amino acid mutations in the IgG1, IgG2, and IgG4 framework in some cases caused complete elimination of ADCC,

ADCP, and CDC functions.[278] Meanwhile, properties like stability, immunogenicity, and biological half-life appeared to be minimally affected by the mutations. Rather than reducing binding to all FcγRs, it may be desirable to increase affinity for the inhibitory FcγRIIb in some immunosuppressive applications.[277] Overall, the introduction of even a few amino acid mutations can have powerful and specific effects on the biological and biophysical properties of Abs which enables effector functions to be fine-tuned based on indication.

1.12.2 Mutations that alter pharmacokinetics

Structural and mutational studies have identified residues at the Cγ2-Cγ3 elbow that are responsible for FcRn binding.[271] This knowledge, in combination with display technologies, has allowed for the discovery of IgG Fc point mutations that strengthen the interaction with FcRn at endosomal pH.[269,271,277,279] Since FcRn is vital for endosomal salvage of IgG, it was thought that tight-binding IgG mutants might have an extended PK profile. Indeed, one set of mutations (M252Y/S254T/T256E, YTE) not only increased affinity for FcRn at pH 6.0 by ~10-fold, but also prolonged serum half-life in humans by 2- to 4-fold.[280,281] Functionally, the long-lived LS mutants (M428L/N434S) have been shown to elicit stronger anti-tumor activity due to maintenance of higher serum concentrations.[282] Other studies have stressed the importance of retaining pH sensitivity, showing that an increased affinity for FcRn at physiological pH may actually accelerate clearance.[269,279] It seems that strong FcRn affinity at pH 6.0 generally extends half-life, but that some threshold for pH 7.4 affinity exists which, if surpassed, counteracts this effect.[283] Although FcRn and FcγRs bind at distal sites, potential allosteric effects have been suggested based on the decreases in effector function observed for mutants with enhanced FcRn binding.[284] FcRn and protein A, on the other hand, bind to the same Cγ2/Cγ3 region; thus, care should be taken not to interfere with protein A binding if it is required for purification. Due to advantages such as lower

dose requirements, less frequent dosing, and lower cost, PK-enhancing mutations will likely be incorporated into more novel Abs and biosuperiors in the future.

By contrast, mutations that weaken FcRn binding may be useful for IgG diagnostics or other agents that should be quickly cleared.[285] IgG mutants that bind FcRn with high affinity at acidic and neutral pH can be used to accelerate degradation of endogenous Abs or Ags. The systemic load of potentially autoreactive, pathogenic Abs can be depleted by antagonizing FcRn and preventing its salvage of endogenous IgG.[279] Because this FcRn-blocking strategy is not dependent on Fab activity, the Abdeg format uses Fc fragments containing mutations that enhance FcRn binding at a broad pH range.[184] For Abs that antagonize soluble antigens, the long IgG half-life may be conferred to the antigen unwantedly.[279] To accelerate clearance of pathogenic antigens, sweeping Abs can be used that have enhanced FcRn affinity at neutral pH.[286] This improved FcRn binding allows for receptor-mediated cellular uptake and lysosomal degradation. Concomitant engineering of the variable regions can be used to release antigen in the endosome and prevent it from recycling with IgG.[279,286] It is important to note that Abdegs and sweeping Abs have shorter half-lives than native IgGs, which may necessitate more frequent dosing. Nevertheless, it is apparent that alteration of pH-dependent FcRn binding is a powerful tool for half-life modulation of IgGs as well as their targeted antigens.

1.13 Biophysical properties

1.13.1 Stability and aggregation

The conformational stability of an Ab is defined by the relative free energies of the native and unfolded states. These energies are based on fundamental forces like hydrogen bonds, hydrophobic and van der Waals interactions, and electrostatic attraction and repulsion, both between protein atoms and between protein and solvent. Aggregation is closely coupled to

stability.[287,288] While all proteins undergo continuous conformational sampling, less stable proteins are more likely to partially unfold and reveal hydrophobic residues that are buried in the native state. Transient exposure of hydrophobic, uncharged patches allows for intermolecular association of these regions. Because aggregation of this sort locks proteins in non-native conformations, it is often considered to be irreversible.[288] Some regions of Abs are more likely than others to initiate aggregation. The intra- and interdomain contacts, such as those between V_H and V_L domains, are especially prone to aggregation due to their hydrophobic character. For this reason, sdAbs (V_H, V_L) are often engineered to reduce hydrophobicity at the normal domain interface, and scFvs may be modified to minimize transient opening that can lead to aggregation.[288,289] IgG binding sites (CDRs for antigen binding, lower hinge and upper Cγ2 for FcγR and C1q binding, and the Cγ2/Cγ3 elbow for FcRn binding) also tend to have hydrophobic residues that contribute to the energy of binding.[288] For ADCs and other conjugates, hydrophobic linkers or payloads have the potential to increase aggregation.[288] Although IgG molecules are considered especially stable proteins, efforts to improve developability have focused on protein engineering and formulation strategies to further reduce the incidence of aggregation.

Clinical IgGs are routinely concentrated to >100 mg/mL in order to deliver sufficient quantities of drug via small-volume injection.[290] Because aggregation is more likely at higher concentrations, there is a clear need to quantify aggregation and understand its effects. Indeed, Abs and other therapeutic proteins must be thoroughly characterized to ensure that no more than a few percent of the drug consists of non-monomeric species. This homogeneity is essential because pre-clinical data is usually available only for the species of interest. Oligomers and large aggregates do not necessarily share the same biological properties as the monomer, and in many cases aggregates have less desirable characteristics.[287,288] For example, the repeated epitopes or

misfolded regions on protein multimers may make them more immunogenic.[291] The generation of an immune response to aggregates not only compromises patient safety, but may also lead to immune recognition of the active, monomeric species. Thus, aggregation-induced immunogenicity can increase clearance of a drug (often via anti-drug antibodies), reducing exposure and efficacy.[292]

The negative effects of aggregation can be minimized by protein engineering, either through rational alteration of problematic sequences or through evolutionary screening approaches.[288] In both cases, a common strategy is to decrease the free energy of the folded protein in order to disfavor the unfolded states that are more likely to initiate aggregation. An example of rational design is the inclusion of a novel intradomain disulfide bond into sdAbs, which increases thermal stability and decreases aggregation.[293] Certain HCs and LCs may be selected to generate Abs with more favorable biophysical properties. For example, the sub-family V_H3 has superior thermodynamic stability compared to other V_H domains, and V_κ is generally more stable than V_λ.[294] The pairings of these domains are also important to consider, as certain V_H and V_L combinations are more stable and more common *in vivo*.[294,295] Engineering to decrease intermolecular encounters is another option for decreasing aggregation. For instance, addition of charge (especially acidification) may be used to induce molecular repulsion, while addition of hydrophilic residues into otherwise hydrophobic stretches decreases hydrophobic nucleation.[288] When engineering for increased stability, it is important to consider functional sites that could be impacted by proximal or even distant mutations. In contrast to rational mutagenesis, evolutionary approaches generate libraries of variants and isolate those with enhanced biophysical properties by screening under destabilizing conditions.[288]

Several methods exist for assessing the conformational stability and aggregation propensity of drug candidates, as well as related properties like colloidal stability and self-association.[127,296,297]

In general, stress tests attempt to quickly predict the long-term stability of proteins by exposing them to conditions that allow for exploration of non-native conformations. In principle, aggregation can be accelerated by increasing the free energy of the native state, decreasing the free energy of the unfolded state, or adding energy to the system to overcome kinetic barriers between states. Temperature ramping methods like differential scanning calorimetry are frequently used to compare protein stability based on the thermal unfolding of each domain. Alternatively, the percent of monomer can be tracked using size-based analyses such as size-exclusion chromatography.[298] These methods allow for assessment of aggregation under short- and long-term conditions of normal or high stress. Stability at low pH is frequently tested since elution from affinity resin and viral inactivation are performed in low pH buffers. The presence of aggregation-prone regions may also be predicted using sequence-based computational modeling approaches.[299] While *in silico* methods may be helpful in guiding lead selection, they are unlikely to replace *in vitro* stability tests that experimentally evaluate the presence of problematic aggregation pathways.

1.13.2 Immunogenicity

It is logical that exogenous proteins have the potential to elicit an immune response when administered to animals or patients. On the one hand, some anti-drug antibody (ADA) responses lead to non-neutralizing antibodies that minimally impact the therapeutic mechanism but may accelerate clearance.[292] On the other hand, ADAs developed against important drug epitopes can reduce potency and decrease half-life. Severe immune reactions may inactivate the therapeutic agent while also causing potentially fatal infusion reactions and anaphylaxis.[291] Immunogenicity depends not only on extrinsic factors like dose, frequency, route of administration, formulation, and patient background; but also on intrinsic biophysical properties of the therapeutic agent.[292] Thus, it is important to understand which molecular features are likely to be immunogenic in order

to develop safer and more effective biologics.

As previously mentioned, aggregated antibodies and other proteins are often more immunogenic than their monomers.[291,292] This may be due in part to the presence of regularly repeated epitopes that mimic pathogenic patterns of surface expression. Repeated structures present on other antibody-based drugs can also be cause for concern. For example, conjugation of hydrophobic drugs to antibodies can not only increase immunogenicity through aggregation, but also through the repeated linker and payload motifs present on a monomeric ADC.[300] Formation of ADC immune complexes and subsequent uptake into phagocytes can also lead to off-target toxicities and loss of efficacy.

The main source of immunogenicity is novel structures not present in endogenous antibodies. Thus, mouse antibodies elicit a stronger ADA response than chimeric antibodies, which in turn elicit a stronger response than humanized antibodies.[114] Antibody fusions may be immunogenic due to the presence of non-human proteins or unnatural peptide linkers.[300] Small molecules and other cytotoxic payloads can also serve as antigenic haptens when present on ADCs, as can the linkers connecting them to the protein. Even minimally disruptive amino acid mutations and oxidative or chemical modifications have been suggested as sources of immunogenicity.[165,301] Strategies to avoid the development of ADAs include the introduction of masking groups like PEG and glycans, which can limit exposure to neoepitopes.[301]

Although it is difficult to replicate the complexity of the human immune systems, a number of preclinical models exist for the prediction of immunogenicity in humans.[302] Since immunity is species-specific, it is preferable to do *in vivo* studies in non-human primates which have high homology with humans. While rodents may develop an immune response to human proteins and could thus overestimate immunogenicity, they may be decent predictors of relative

immunogenicity.[292,302] A more efficient approach is to use transgenic mice that express the human antibody genes and/or human HLA. Although this should generate immune tolerance for the administered antibody and allow for identification of neoepitopes, ongoing challenges include lack of genetic diversity in these models and incomplete understanding of mechanisms that induce human immunogenicity.[302] In addition to whole organisms, immunogenicity can be predicted *in vitro* by incubating cells with the antibody and monitoring surface expression of receptors on antigen-presenting cells, T cell proliferation, or cytokine release.[292] Identification of T cell epitopes in silico may also be useful for predicting antigenicity of novel sequences.[292] In summary, immunogenicity can be avoided by rationally minimizing novel and repeated epitopes, and by masking and formulation strategies. While several methods exist for preclinical prediction of immunogenicity, it remains challenging to fully replicate the complexity of the immune response in humans.

1.13.3 Charge and isoelectric point

An important biophysical property of antibodies is their surface charge, both in terms of net charge and distribution. Patches of uncharged, hydrophobic amino acids can serve as hot spots for antibody aggregation.[288] Thus, incorporation of acidic or basic residues into these regions can help to prevent intermolecular association. However, positively charged patches can also increase non-specific tissue uptake and reduce exposure of antibodies. Studies have demonstrated that engineering variable regions to reduce patches of positive charge can enhance the pharmacokinetic stability of antibodies.[303,304] In these instances, the decreased clearance might also be related to small decreases in the isoelectric point (pI) of the proteins.

The overall charge of a protein at physiological pH is determined by its pI, which in turn is related to the number of titratable side chains it contains. It is well-established that antibodies

with more basic pI values tend to have increased tissue uptake and faster clearance.[285,305] This phenomenon is likely related to the propensity of positively charged residues to interact with negatively charged cell membranes. Reducing the pI of an antibody, e.g. by engineering the variable domains, allows for improvement of several PK parameters. Acidification is thought to decrease interactions at cell surfaces, decrease non-specific tissue uptake, decrease clearance, and increase bioavailability.[305] On the other hand, increasing pI tends to increases clearance and volume of distribution, but could possibly be used to favor penetration of the blood-brain barrier. Significant changes in PK properties have been proposed to occur only once the pI has been changed by >1 pH unit.[285] Engineering to modulate charge and pI is therefore a valid option to control aggregation and PK properties of antibodies.

1.13.4 Formulation

The conformational stability of a protein is a function of intramolecular interactions, but also of interactions between the protein and its surrounding solvent. Thus, formulation is a powerful tool to stabilize antibodies and prevent them from aggregating or degrading over the normal shelf life of several years.[290] One variable to optimize is pH, where intermediate pH formulations tend to have maximum viscosity, but extreme pH formulations may accelerate degradation pathways like isomerization and deamidation. In cases where protein self-association is controlled by electrostatic interactions, ionic strength may be modulated to prevent self-association and high viscosity.

Addition of excipients to formulation buffers is broadly used to improve long-term stability.[290,306] Surfactants like polysorbates 20 and 80 may be added to mitigate aggregation that occurs at air-liquid interfaces. Similarly, amino acids like arginine and histidine and non-reducing sugars like sucrose and trehalose are commonly used to prevent aggregation at high protein

concentrations. These same components may also have stabilizing effects in the context of protein lyophilization and freeze-thaws.[290] Since each antibody is structurally distinct and may contain unique instabilities, panels of buffers conditions are often tested to determine the ideal formulation on a case-by-case basis. Type of storage vessel is another important consideration, as different materials are known to leach potentially destabilizing components into the antibody formulation.[290] While intravenous and subcutaneous administration routes remain the most widely used, several novel delivery strategies have been proposed to expand the options available to patients and physicians.[307]

1.13.5 Behavior in serum

Although formulations are optimized to maximize long-term antibody stability, these therapeutics are ultimately delivered to complex biological compartments where their behavior may differ from that in simple buffers. The primary environment for most therapeutic antibodies is the blood, where they are delivered directly via infusion or indirectly via injection and the lymphatic system.[285] Plasma is a crowded matrix that contains high concentrations of endogenous proteins and other components.[308] The excluded volume effect can increase the apparent concentration of antibodies while the abundance of other proteins introduces opportunities for non-specific interactions.[309] Thus, it is important to determine whether administered antibodies interact with serum components in a way that alters their functional properties.

The presence of high concentrations of endogenous proteins complicates the analysis of antibody behavior in serum. Due to the high background and heterogeneity of serum samples, it is difficult to monitor individual proteins using traditional (e.g., absorbance-detected) methods. However, strategies such as fluorescent labeling have allowed for comparison of antibody behavior in buffers and in serum. Intriguingly, differences in antibody-antigen affinity, stoichiometry, and

complex size have been noted based on serum matrix effects.[310,311] Thus, measures of binding affinity in dilute buffers may not accurately represent the binding that occurs *in vivo*. Furthermore, mixing of formulated antibodies with serum can result in aggregation of antibodies with serum proteins in an antibody- and excipient-dependent manner.[312,313] Administration of certain antibody/formulation combinations could therefore result in aggregation-induced infusion reactions or loss of effective drug. Differences in the number and size of aggregates has also been reported based on environment.[314] Whereas heat-stressed antibodies aggregated similarly in buffer and serum, pH-stressed antibodies formed smaller but more numerous aggregates in serum. Because serum allows for both self-association or aggregation with serum components, nanoparticle-based techniques have been developed to distinguish between these mechanisms.[315] Clearly, antibody functionality can vary significantly between formulated buffers and complex biological matrices. In the future, it will be important to characterize antibody functions in biologically relevant environments in order to increase understanding of therapeutic mechanisms as they occur *in vivo*.

1.14 Summary

The first generation of antibody therapeutics focused primarily on specific binding of molecular targets to elicit simple inhibitory mechanisms. While these early molecules established large molecules as a valid class of drugs, they did not fully capitalize on all aspects of the antibody platform. More recently, therapeutic mechanisms have been customized not only based on type of antigen, but by antigen affinity, valency, and epitope. Use of different antibody subclasses allows for fine-tuning of pharmacokinetics and effector function due to differential binding to endogenous FcRs and complement proteins. Meanwhile, antigen-binding domains can be used to eliminate effector function, multimerizing antibodies increase complement fixation, and antibody fusions

instill other proteins with favorable properties of the antibody framework. Conjugation of cytotoxic agents to antibodies allows for specific delivery of payloads to tumors, while multispecific antibodies grant novel mechanisms that increase specificity and facilitate delivery to historically intractable compartments. In parallel with these framework innovations, antibody engineering allows for incorporation of amino acid and glycan changes that selectively alter biological and physical properties.

In conclusion, the humoral immune response creates astoundingly complex antibody molecules with the ability to bind both antigens and elements of the adaptive immune system. This antibody format has proven to be extremely amenable to protein engineering, which allows for modular design of structural domains that best integrate the desired therapeutic functions. With increased understanding of immunobiology and the continued development of molecular biological methods, the possibilities for antibody-based therapeutics are bounded only by the scope of human ingenuity.

FIGURES

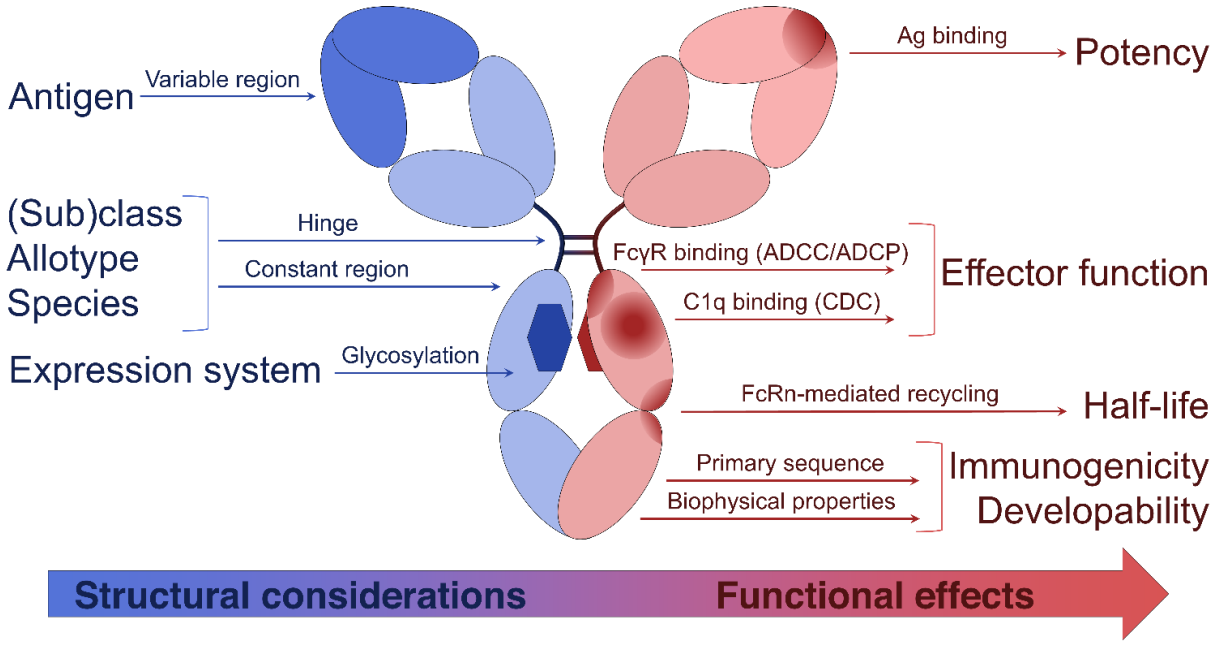

Figure 1.1: Structural considerations for the design of IgG-based therapeutics and their effects on biological and clinical function.

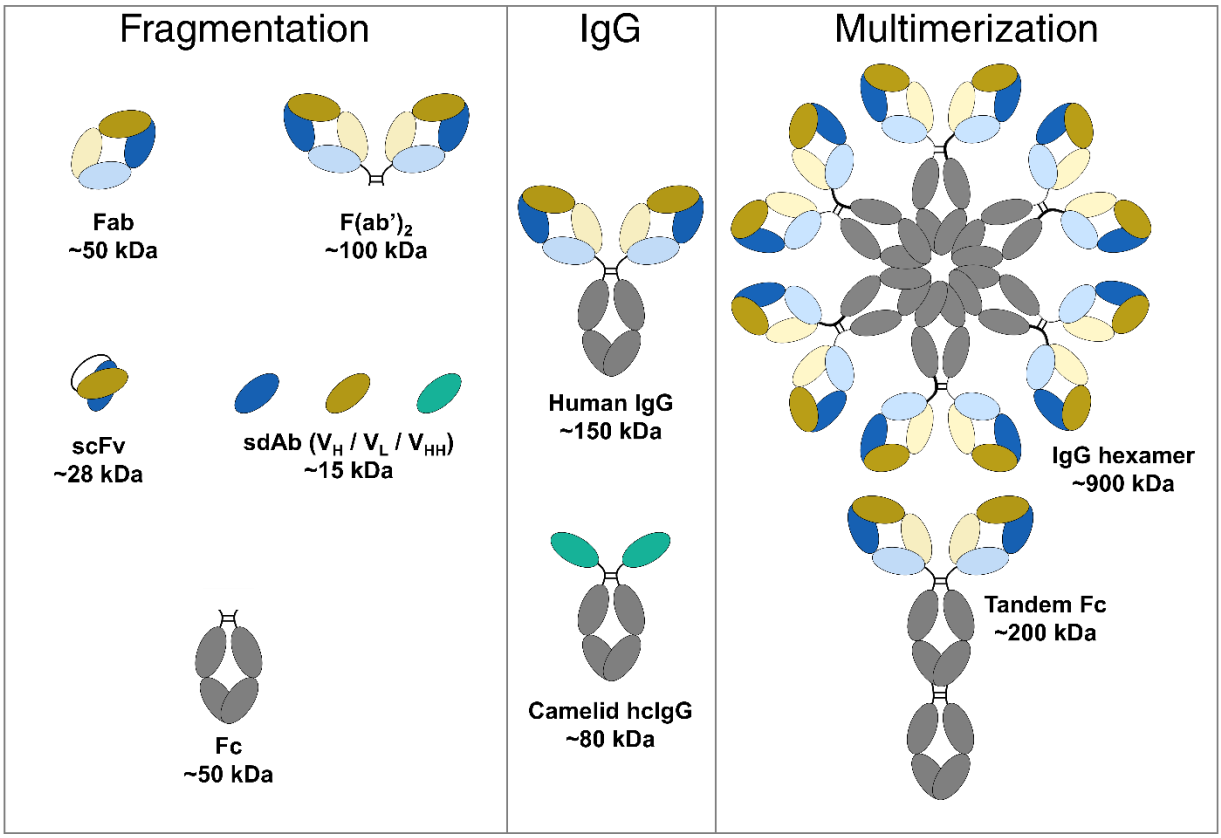

Figure 1.2: Antibody frameworks based on fragmentation (left) or multimerization (right) of human or non-human IgG domains.

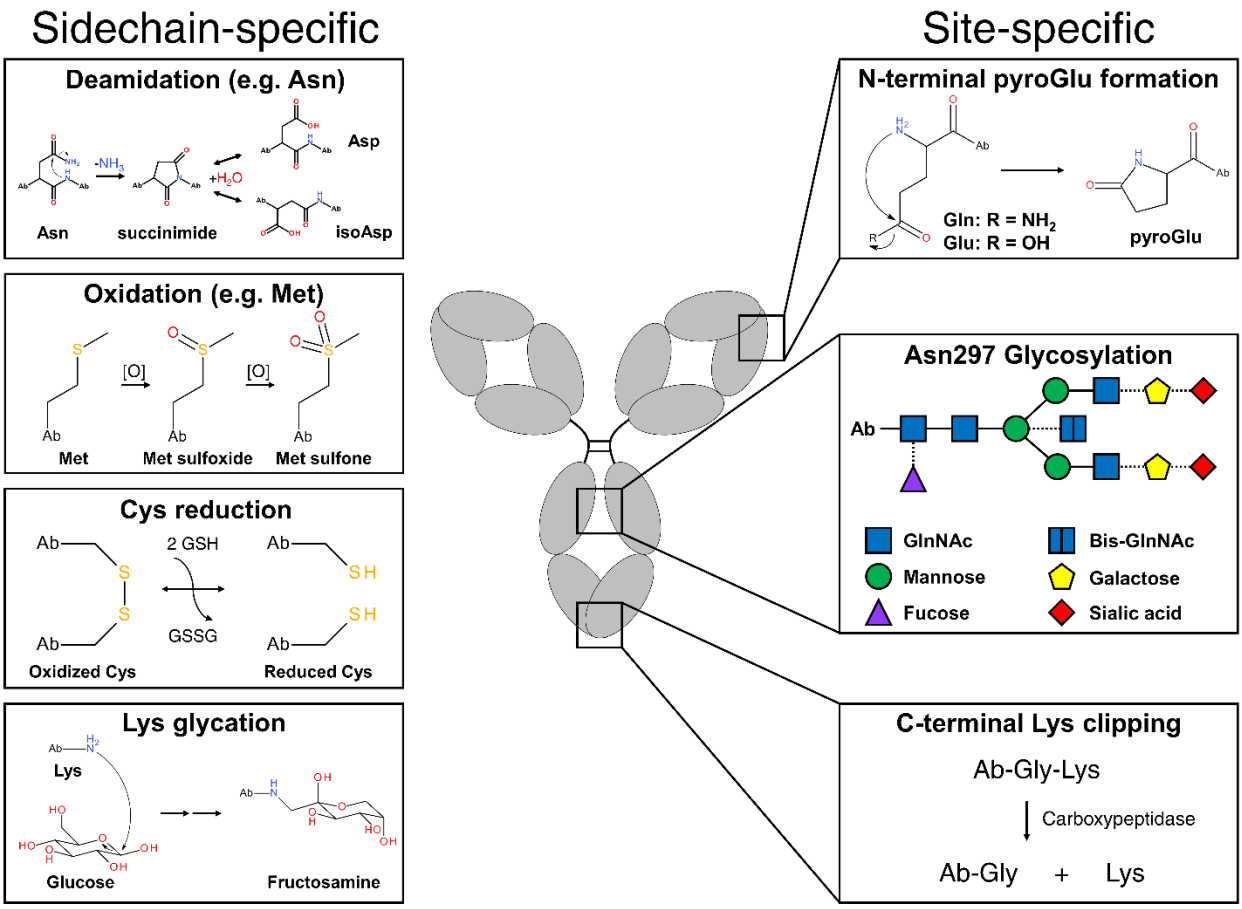

Figure 1.3: Common post-translational modifications of IgG antibodies. Shown on the left are amino acid modifications that occur in a side-chain dependent but site-independent manner. These chemical alterations may negatively affect properties like antigen or receptor binding. Shown on the right are amino acid modifications that occur at specific locations. While N-terminal formation of pyroglutamate occurs only for chains that begin with glutamine or glutamate, C-terminal lysine clipping occurs for all IgG antibodies, whose heavy chains terminate with a glycine-lysine motif. Glycosylation at asparagine 297 leads to a core glycan (solid lines) to which additional sugars may be added (dotted lines). These differences in glycan composition have significant effects on binding to Fc receptors.

TABLES

Table 1.1: Types of antigens and the indications for which they are appropriate

Indication	Antigen type	Example antigen	Approved antibodies
Cancer	Lineage-defining	CD19	Blinatumomab (CD19xCD3)
		CD20	Rituximab I-131 Tositumomab* Ibritumomab tiuxetan Obinutuzumab Ofatumumab
		CD22	Inotuzumab ozogamicin
		CD30	Brentuximab vedotin
		CD33	Gemtuzumab ozogamicin
		CD38	Daratumumab
		SLAMF7	Elotuzumab
	Overexpressed	EpCAM	Catumaxomab* (EpCAMxCD3) Edrecolomab*
		EGFR	Cetuximab Necitumumab Panitumumab
		HER2	Pertuzumab Trastuzumab (emtansine)
		PDGRFα	Olaratumab
	Immunomodulatory	CTLA4	Ipilimumab
		PD1	Nivolumab Pembrolizumab
		PDL1	Atezolizumab Avelumab Durvalumab
Inflammatory disease	Soluble cytokine	BAFF	Belimumab
		IL-1β	Canakinumab
		IL-5	Mepolizumab Reslizumab
		IL-12	Ustekinumab (IL-12/23)
		IL-17A	Ixekizumab Secukinumab
		IL-23	Guselkumab Tildrakizumab
		TNFα	Adalimumab Certolizumab pegol Golimumab Infliximab
Infection	Pathogen	*B. anthracis*	Obiltoxaximab Raxibacumab
		C. difficile enterotoxin B	Bezlotoxumab
		RSV protein F	Palivizumab

*Withdrawn

Table 1.2: Properties of antibody subclasses

	IgA1	IgA2	IgD	IgE	IgG1	IgG2	IgG3	IgG4	IgM
Structure									
Heavy chain	α_1	α_2	δ	ε	γ_1	γ_2	γ_3	γ_4	μ
Ig domains per HC	4	4	4	5	4	4	4	4	5
Monomer size (kDa)	160	160	184	188	146	146	165	146	194
Oligomeric forms	1-4	1-4	1	1	1	1-2	1	0.5-1	5-6
Hinge amino acids	23	10	64	0	15	12	62[a]	12	0
HC-HC disulfide bonds	3	3	1	2	2	4	11	2	3[b]
N-glycans per HC	2	5[c]	3	7	1	1	1	1	5
O-glycans per HC	5	0	5	0	0	0	3[d]	0	0
Biology									
Serum level (mg/mL)	3	0.5	0.03	0.00005	9	3	1	0.5	1.5
% of serum Ig	16	3	0.2	0.0003	49	16	5	3	8
Serum half-life (d)	6	6	3	2	21	20	7	21	10
Predominant antigen (protein, carb, allergen)	p	c	-	a	p	c	p	a	c
Allotypes	0	3	0	1	4	1	13	0	0
Distribution									
Mucosal transcytosis[e]	+++	+++	-	-	-	-	-	-	+
Placental transfer	-	-	-	-	+++	+	++	+	+
Extravascular diffusion[f]	++	++	-	+	+++	+++	+++	+++	-
Effector function									
Cytotoxicity (ADCC)[g]	++	++	-	++	+++	+	+++	+	-
Phagocytosis (ADCP)	++	++	-	-	+++	-	+++	+	+
Complement (CDC)[h]	+	+	-	-	++	+	+++	-	+++

[a]IgG3 hinge length varies from 27-83 residues based on allotype
[b]Polymeric IgM contains 1 HC-HC disulfide bond within each monomer, and an additional 2 disulfide bonds linking each HC to HCs of other monomers
[c]IgA2m(1) contains 4 N-glycosylation sites while IgA2m(2) and IgA2m(3) contain 5
[d]IgG3 contains 1-3 O-glycosylation sites due to allotypic differences in the number of hinge repeats
[e]Only polymeric IgA (predominantly dimer) is transported to secretions
[f]Only monomeric IgA has significant diffusion to extravascular sites
[g]ADCC is mediated primarily by NK cells (IgG) and myeloid cells (IgA, IgE)
[h]Complement activation of IgA occurs through the alternative or lectin, rather than classical, pathway

1.15 References

[1] Kuhn C, Weiner HL. Therapeutic anti-CD3 monoclonal antibodies: from bench to bedside. *Immunotherapy*. 2016;8(8):889-906.

[2] Reichert JM. Antibodies to watch in 2018. *mAbs*. 2018;10(2):183-203.

[3] Molé CM, Béné MC, Montagne PM, Seilles E, Faure GC. Light chains of immunoglobulins in human secretions. *Clin Chim Acta*. 1994;224:191-197.

[4] Bruhns P. Properties of mouse and human IgG receptors and their contribution to disease models. *Blood*. 2015;119(24):5640-5650.

[5] Stewart R, Hammond SA, Oberst M, Wilkinson RW. The role of Fc gamma receptors in the activity of immunomodulatory antibodies for cancer. *J Immunother Cancer*. 2014;2(1):1-10.

[6] Hanson QM, Barb AW. A perspective on the structure and receptor binding properties of immunoglobulin G Fc. *Biochemistry*. 2015;54:2931-2942.

[7] Vidarsson G, Dekkers G, Rispens T. IgG subclasses and allotypes: From structure to effector functions. *Front Immunol*. 2014;5(520):1-17.

[8] Mellor JD, Brown MP, Irving HR, Zalcberg JR, Dobrovic A. A critical review of the role of Fc gamma receptor polymorphisms in the response to monoclonal antibodies in cancer. *J Hematol Oncol*. 2013;6(1):1.

[9] Weng WK, Levy R. Two immunoglobulin G fragment C receptor polymorphisms independently predict response to rituximab in patients with follicular lymphoma. *J Clin Oncol*. 2003;21(21):3940-3947.

[10] Roopenian DC, Akilesh S. FcRn: the neonatal Fc receptor comes of age. *Nat Rev Immunol*. 2007;7(9):715-725.

[11] Martin WL, West AP, Gan L, Bjorkman PJ. Crystal structure at 2.8 Å of an FcRn/heterodimeric Fc complex: Mechanism of pH-dependent binding. *Mol Cell*. 2001;7(4):867-877.

[12] Baker K, Rath T, Pyzik M, Blumberg RS. The Role of FcRn in Antigen Presentation. *Front Immunol*. 2014;5(August):1-12.

[13] Bakema JE, Van Egmond M. The human immunoglobulin A Fc receptor FcαRI: A multifaceted regulator of mucosal immunity. *Mucosal Immunol*. 2011;4(6):612-624.

[14] Schroeder HW, Cavacini L, Schroeder Jr. HW, Cavacini L, Schroeder HW, Cavacini L. Structure and function of immunoglobulins. *J Allergy Clin Immunol*. 2010;125(2):S41-52.

[15] Aleyd E, Heineke MH, van Egmond M. The era of the immunoglobulin A Fc receptor FcαRI; its function and potential as target in disease. *Immunol Rev*. 2015;268(1):123-138.

[16] Ouchida R, Mori H, Hase K, et al. Critical role of the IgM Fc receptor in IgM homeostasis, B-cell survival, and humoral immune responses. *Proc Natl Acad Sci*. 2012;109(40):E2699-E2706.

[17] Wang H, Coligan JE, Morse HC. Emerging functions of natural IgM and its Fc receptor FCMR in immune homeostasis. *Front Immunol*. 2016;7(99):1-7.

[18] Shibuya A, Honda S. Immune regulation by Fcα/μ receptor (CD351) on marginal zone B cells and follicular dendritic cells. *Immunol Rev*. 2015;268(1):288-295.

[19] Shibuya A, Honda SI, Shibuya K. A pro-inflammatory role of Fcα/μR on marginal zone B cells in sepsis. *Int Immunol*. 2017;29(11):519-524.

[20] Shibuya A, Sakamoto N, Shimizu Y, et al. Fcα/μ receptor mediates endocytosis of IgM-coated microbes. *Nat Immunol*. 2000;1(5):441-446.

[21] Kaetzel CS. The polymeric immunoglobulin receptor: bridging innate and adaptive immune responses at mucosal surfaces. *Immunol Rev*. 2005;206:83-99.

[22] Turula H, Wobus C. The Role of the Polymeric Immunoglobulin Receptor and Secretory Immunoglobulins during Mucosal Infection and Immunity. *Viruses*. 2018;10(5):237.

[23] Kinet J-P. The high-affinity IgE receptor (FcεRI): From Physiology to Pathology. *Annu Rev Immunol*. 1999;17(1):931-972.

[24] Sutton BJ, Davies AM. Structure and dynamics of IgE-receptor interactions: FcεRI and CD23/FcεRII. *Immunol Rev*. 2015;268(1):222-235.
[25] Yokota A, Yukawa K, Yamamoto A, et al. Two forms of the low-affinity Fc receptor for IgE differentially mediate endocytosis and phagocytosis: identification of the critical cytoplasmic domains. *Proc Natl Acad Sci U S A*. 1992;89(11):5030-5034.
[26] Diebolder CA, Beurskens FJ, de Jong RN, et al. Complement is activated by IgG hexamers assembled at the cell surface. *Science*. 2014;343(6176):1260-1263.
[27] Czajkowsky DM, Shao Z. The human IgM pentamer is a mushroom-shaped molecule with a flexural bias. *Proc Natl Acad Sci U S A*. 2009;106(35):14960-14965.
[28] Choe W, Durgannavar TA, Chung SJ. Fc-binding ligands of immunoglobulin G: An overview of high affinity proteins and peptides. *Materials (Basel)*. 2016;9(994):1-17.
[29] Bouvet J-P. Immunoglobulin Fab Fragment-binding Proteins. *Int J Immunopharmacol*. 1994;16:419-424.
[30] Grover RK, Zhu X, Nieusma T, et al. A Structurally Distinct Human Mycoplasma Protein that Generically Blocks Antigen-Antibody Union. *Science*. 2014;343(6171):656-662.
[31] Capone M, Bryant JM, Sutkowski N, Haque A. Fc Receptor-Like Proteins in Pathophysiology of B-cell Disorder. *J Clin Cell Immunol*. 2016;7(3).
[32] Rhodes DA, Isenberg DA. TRIM21 and the Function of Antibodies inside Cells. *Trends Immunol*. 2017;38(12):916-926.
[33] Jennewein MF, Alter G. The Immunoregulatory Roles of Antibody Glycosylation. *Trends Immunol*. 2017.
[34] Weiner LM, Murray JC, Shuptrine CW. Antibody-based immunotherapy of cancer. *Cell*. 2012;148(6):1081-1084.
[35] Redman JM, Hill EM, AlDeghaither D, Weiner LM. Mechanisms of action of therapeutic antibodies for cancer. *Mol Immunol*. 2015;67(2):28-45.
[36] Hoos A. Development of immuno-oncology drugs - from CTLA4 to PD1 to the next generations. *Nat Rev Drug Discov*. 2016;15(4):235-247.
[37] Vonderheide RH, Glennie MJ. Agonistic CD40 antibodies and cancer therapy. *Clin Cancer Res*. 2013;19(5):1035-1043.
[38] Carter PJ, Lazar GA. Next generation antibody drugs: pursuit of the "high-hanging fruit." *Nat Rev Drug Discov*. 2017;17(3):197-223.
[39] Lu LL, Suscovich TJ, Fortune SM, Alter G. Beyond binding: Antibody effector functions in infectious diseases. *Nat Rev Immunol*. 2018;18(1):46-61.
[40] Zhou Y, Goenaga A-L, Harms BD, et al. Impact of Intrinsic Affinity on Functional Binding and Biological Activity of EGFR Antibodies. *Mol Cancer Ther*. 2012;11(7):1467-1476.
[41] Kostolanský F, Varečková E, Betáková T, Mucha V, Russ G, Wharton SA. The strong positive correlation between effective affinity and infectivity neutralization of highly cross-reactive monoclonal antibody IIB4, which recognizes antigenic site B on influenza A virus haemagglutinin. *J Gen Virol*. 2000;81(7):1727-1735.
[42] Igawa T, Tsunoda H, Kuramochi T, Sampei Z, Ishii S, Hattori K. Engineering the variable region of therapeutic IgG antibodies. *MAbs*. 2011;3:37-41.
[43] Beckman RA, Weiner LM, Davis HM. Antibody constructs in cancer therapy: Protein engineering strategies to improve exposure in solid tumors. *Cancer*. 2007;109:170-179.
[44] Rudnick SI, Adams GP. Affinity and Avidity in Antibody-Based Tumor Targeting. *Cancer Biother Radiopharm*. 2009;24(2):155-161.
[45] Klein C, Lammens A, Schäfer W, et al. Epitope interactions of monoclonal antibodies targeting CD20 and their relationship to functional properties. *MAbs*. 2013;5(1):22-33.

[46] Beers SA, Chan CHT, French RR, Cragg MS, Glennie MJ. CD20 as a target for therapeutic type i and ii monoclonal antibodies. *Semin Hematol*. 2010;47(2):107-114.
[47] Shim H. One target, different effects: A comparison of distinct therapeutic antibodies against the same targets. *Exp Mol Med*. 2011;43(10):539-549.
[48] Baselga J, Cortés J, Kim S-B, et al. Pertuzumab plus Trastuzumab plus Docetaxel for Metastatic Breast Cancer. *N Engl J Med*. 2012;366(2):109-119.
[49] Lühder F, Huang Y, Dennehy KM, et al. Topological Requirements and Signaling Properties of T Cell–activating, Anti-CD28 Antibody Superagonists. *J Exp Med*. 2003;197(8):955-966.
[50] Yu X, Chan HTC, Orr CM, et al. Complex Interplay between Epitope Specificity and Isotype Dictates the Biological Activity of Anti-human CD40 Antibodies. *Cancer Cell*. 2018;33(4):664-675.
[51] Fan G, Wang Z, Hao M, Li J. Bispecific antibodies and their applications. *J Hematol Oncol*. 2015;8(130):1-14.
[52] Kontermann RE, Brinkmann U. Bispecific antibodies. *Drug Discov Today*. 2015;20:838-847.
[53] Moores SL, Chiu ML, Bushey BS, et al. A novel bispecific antibody targeting EGFR and cMet is effective against EGFR inhibitor-resistant lung tumors. *Cancer Res*. 2016;76:3942-3953.
[54] Mazor Y, Sachsenmeier KF, Yang C, et al. Enhanced tumor-targeting selectivity by modulating bispecific antibody binding affinity and format valence. *Sci Rep*. 2017;7(40098):1-11.
[55] Zhukovsky EA, Morse RJ, Maus M V. Bispecific antibodies and CARs: Generalized immunotherapeutics harnessing T cell redirection. *Curr Opin Immunol*. 2016;40:24-35.
[56] Pardridge WM. Re-engineering therapeutic antibodies for Alzheimer's disease as blood-brain barrier penetrating bi-specific antibodies. *Expert Opin Biol Ther*. 2016;16(12):1455-1468.
[57] Watts RJ, Dennis MS. Bispecific antibodies for delivery into the brain. *Curr Opin Chem Biol*. 2013;17(3):393-399.
[58] Strohl WR. Current progress in innovative engineered antibodies. *Protein Cell*. 2018;9(1):86-120.
[59] Beck A, Goetsch L, Dumontet C, Corvaïa N. Strategies and challenges for the next generation of antibody–drug conjugates. *Nat Rev Drug Discov*. 2017;16(5):315-337.
[60] Liu R, Wang RE, Wang F. Antibody-drug conjugates for non-oncological indications. *Expert Opin Biol Ther*. 2016;16(5):591-593.
[61] Kalim M, Chen J, Wang S, et al. Intracellular trafficking of new anticancer therapeutics: Antibody–drug conjugates. *Drug Des Devel Ther*. 2017;11:2265-2276.
[62] Opaliński Ł, Szymczyk J, Szczepara M, et al. High affinity promotes internalization of engineered antibodies targeting FGFR1. *Int J Mol Sci*. 2018;19(5):1-14.
[63] Carter PJ, Senter PD. Antibody-drug conjugates for cancer therapy. *Cancer J*. 2008;14(3):154-169.
[64] Ito T, Tsumoto K. Effects of subclass change on the structural stability of chimeric, humanized, and human antibodies under thermal stress. *Protein Sci*. 2013;22:1542-1551.
[65] Magdelaine-Beuzelin C, Vermeire S, Goodall M, et al. IgG1 heavy chain-coding gene polymorphism (G1m allotypes) and development of antibodies-to-infliximab. *Pharmacogenet Genomics*. 2009;19(5):383-387.
[66] Bartelds GM, de Groot E, Nurmohamed MT, et al. Surprising negative association between IgG1 allotype disparity and anti-adalimumab formation: A cohort study. *Arthritis Res Ther*. 2010;12(6):1-7.
[67] Lefranc M-P, Lefranc G. Human Gm, Km, and Am allotypes and their molecular characterization: a remarkable demonstration of polymorphism. *Methods Mol Biol*. 2012;882:635-680.
[68] Jefferis R, Lefranc M-P. Human IgG Isotypes, Allotypes and Idiotypes. *MAbs*. 2009;1(4):1-7.
[69] Ternant D, Arnoult C, Pugnière M, et al. IgG1 Allotypes Influence the Pharmacokinetics of Therapeutic Monoclonal Antibodies through FcRn Binding. *J Immunol*. 2016;196(2):607-613.
[70] Liu H, May K. Disulfide bond structures of IgG molecules. *MAbs*. 2012;4(1):17-23.
[71] Beers SA, Glennie MJ, White AL. Influence of immunoglobulin isotype on therapeutic antibody function. *Blood*. 2016;127(9):1097-1101.

[72] Salfeld JG. Isotype selection in antibody engineering. *Nat Biotechnol*. 2007;25(12):1369-1372.
[73] Jonsson G, Oxelius V-A, Truedsson L, Braconier JH, Sturfelt G, Sjoholm AG. Homozygosity for the IgG2 Subclass Allotype G2M(n) Protects against Severe Infection in Hereditary C2 Deficiency. *J Immunol*. 2006;177(1):722-728.
[74] Plomp R, Dekkers G, Rombouts Y, et al. Hinge-Region O-Glycosylation of Human Immunoglobulin G3 (IgG3). *Mol Cell Proteomics*. 2015;14(5):1373-1384.
[75] Stapleton NM, Andersen JT, Stemerding AM, et al. Competition for FcRn-mediated transport gives rise to short half-life of human IgG3 and offers therapeutic potential. *Nat Commun*. 2011;2(599):1-9.
[76] Bruhns P, Iannascoli B, England P, Mancardi D a, Fernandez N, Jorieux S. Specificity and affinity of human Fcγ receptors and their polymorphic variants for human IgG subclasses. *Receptor*. 2009;113(16):3716-3725.
[77] Schuurman J, Perdok GJ, Gorter AD, Aalberse RC. The inter-heavy chain disulfide bonds of IgG4 are in equilibrium with intra-chain disulfide bonds. *Mol Immunol*. 2001;38(1):1-8.
[78] van der Neut Kolfschoten M, Schuurman J, Losen M, et al. Anti-Inflammatory Activity of Human IgG4 Antibodies by Dynamic Fab Arm Exchange. *Science*. 2007;317(September):1554-1557.
[79] Labrijn AF, Buijsse AO, van den Bremer ETJ, et al. Therapeutic IgG4 antibodies engage in Fab-arm exchange with endogenous human IgG4 in vivo. *Nat Biotechnol*. 2009;27(8):767-771.
[80] Leusen JHW. IgA as therapeutic antibody. *Mol Immunol*. 2015;68(1):35-39.
[81] Woof JM, Russell MW. Structure and function relationships in IgA. *Mucosal Immunol*. 2011;4(6):590-597.
[82] Arnold JN, Royle L, Dwek RA, Rudd PM, Sim RB. Human immunoglobulin glycosylation and the lectin pathway of complement activation. *Adv Exp Med Biol*. 2005;564(Cl):27-43.
[83] Simell B, Kilpi T, Käyhty H. Subclass distribution of natural salivary IgA antibodies against pneumococcal capsular polysaccharide of type 14 and pneumococcal surface adhesin A (PsaA) in children. *Clin Exp Immunol*. 2006;143(3):543-549.
[84] Ladjeva I, Peterman JH, Mestecky J. IgA subclasses of human colostral antibodies specific for microbial and food antigens. *Clin Exp Immunol*. 1989;78(1):85-90.
[85] Kretschmer A, Lohse S, Rösner T, et al. CD20 Antibodies of Human IgA Isotype Mediate CDC, and ADCC By Myeloid Effector Cells. *Blood*. 2016;128:1835.
[86] Lohse S, Brunke C, Derer S, et al. Characterization of a mutated IgA2 antibody of the m(1) allotype against the epidermal growth factor receptor for the recruitment of monocytes and macrophages. *J Biol Chem*. 2012;287(30):25139-25150.
[87] Arnold JN, Radcliffe CM, Wormald MR, et al. The Glycosylation of Human Serum IgD and IgE and the Accessibility of Identified Oligomannose Structures for Interaction with Mannan-Binding Lectin. *J Immunol*. 2004;173(11):6831-6840.
[88] Übelhart R, Hug E, Bach MP, et al. Responsiveness of B cells is regulated by the hinge region of IgD. *Nat Immunol*. 2015;16(5):534-543.
[89] Chen K, Xu W, Wilson M, et al. Immunoglobulin D enhances immune surveillance by activating antimicrobial, proinflammatory and B cell-stimulating programs in basophils. *Nat Immunol*. 2009;10(8):889-898.
[90] Josephs DH, Spicer F, Karagiannis P, Gould HJ, Karagiannis SN. IgE immunotherapy A novel concept with promise for the treatment of cancer. *MAbs*. 2014;6(1):54-72.
[91] Karagiannis SN, Josephs DH, Bax HJ, Spicer JF. Therapeutic IgE antibodies: Harnessing a macrophage-mediated immune surveillance mechanism against cancer. *Cancer Res*. 2017;77(11):2779-2783.
[92] ClinicalTrials.gov [Internet]. Bethesda (MD): National Library of Medicine (US). Identifier NCT02546921, Phase I Study of Mov18, a First in Class Chimeric IgE Antibody in Patients With Advanced Solid Tumors; 2015 Sept 11 [cited 2018 Dec 10]; Available from: https://clinicaltrials.gov/ct2/show/NCT02546921

[93] Muller R, Grawert MA, Kern T, et al. High-resolution structures of the IgM Fc domains reveal principles of its hexamer formation. *Proc Natl Acad Sci*. 2013;110(25):10183-10188.
[94] Johansen F-E, Braathen R, Brandtzaeg P. Role of J chain in secretory immunoglobulin formation. *Scand J Immunol*. 2000;52(3):240-248.
[95] Wiersma EJ, Collins C, Fazel S, Shulman MJ. Structural and functional analysis of J chain-deficient IgM. *J Immunol*. 1998;160(12):5979-5989.
[96] Weinstein JR, Quan Y, Hanson JF, et al. IgM-Dependent Phagocytosis in Microglia Is Mediated by Complement Receptor 3, Not Fc / Receptor. *J Immunol*. 2015;195(11):5309-5317.
[97] Marks L. The birth pangs of monoclonal antibody therapeutics: The failure and legacy of centoxin. *MAbs*. 2012;4(3):403-412.
[98] Irie RF, Ollila DW, O'Day S, Morton DL. Phase I pilot clinical trial of human IgM monoclonal antibody to ganglioside GM3 in patients with metastatic melanoma. *Cancer Immunol Immunother*. 2004;53(2):110-117.
[99] Liedtke M, Twist CJ, Medeiros BC, et al. Phase I trial of a novel human monoclonal antibody mab216 in patients with relapsed or refractory B-cell acute lymphoblastic leukemia. *Haematologica*. 2012;97(1):30-37.
[100] Hensel F, Timmermann W, Von Rahden BHA, Rosenwald A, Brändlein S, Illert B. Ten-year follow-up of a prospective trial for the targeted therapy of gastric cancer with the human monoclonal antibody PAT-SC1. *Oncol Rep*. 2014;31(3):1059-1066.
[101] Rasche L, Duell J, Castro IC, et al. GRP78-directed immunotherapy in relapsed or refractory multiple myeloma - results from a phase 1 trial with the monoclonal immunoglobulin M antibody PAT-SM6. *Haematologica*. 2015;100(3):377-384.
[102] Eisen A, Greenberg BM, Bowen JD, Arnold DL, Caggiano AO. A double-blind, placebo-controlled, single ascending-dose study of remyelinating antibody rHIgM22 in people with multiple sclerosis. *Mult Scler J – Exp Transl Clin*. 2017;3(4):205521731774309.
[103] Hood L, Gray WR, Sanders BG, Dreyer WJ. Light chain evolution. *Cold Spring Harb Symp Quant Biol*. 1967;32:133-146.
[104] Townsend CL, Laffy JMJ, Wu YCB, et al. Significant differences in physicochemical properties of human immunoglobulin kappa and lambda CDR3 regions. *Front Immunol*. 2016;7:1-12.
[105] DeKosky BJ, Lungu OI, Park D, et al. Large-scale sequence and structural comparisons of human naive and antigen-experienced antibody repertoires. *Proc Natl Acad Sci*. 2016;113(19):E2636-E2645.
[106] Brezski RJ, Georgiou G. Immunoglobulin isotype knowledge and application to Fc engineering. *Curr Opin Immunol*. 2016;40(May 2015):62-69.
[107] Kelton W, Mehta N, Charab W, et al. IgGA: A "cross-isotype" engineered human Fc antibody domain that displays both IgG-like and IgA-like effector functions. *Chem Biol*. 2014;21(12):1603-1609.
[108] Rother RP, Rollins SA, Mojcik CF, Brodsky RA, Bell L. Discovery and development of the complement inhibitor eculizumab for the treatment of paroxysmal nocturnal hemoglobinuria. *Nat Biotechnol*. 2007;25(11):1256-1264.
[109] White AL, Chan HTC, French RR, et al. Conformation of the human immunoglobulin G2 hinge imparts superagonistic properties to immunostimulatory anticancer antibodies. *Cancer Cell*. 2015;27(1):138-148.
[110] Kinder M, Greenplate AR, Grugan KD, et al. Engineered protease-resistant antibodies with selectable cell-killing functions. *J Biol Chem*. 2013;288(43):30843-30854.
[111] Köhler G, Milstein C. Continuous cultures of fused cells secreting antibody of predefined specificity. *Nature*. 1975;256(5517):495-497.
[112] Tosatao G, Cohen JI. Generation of Epstein-Barr Virus (EBV)-immortalized B cell lines. Curr Protoc Immunol. 2007;7.22.1-7.22.4.

[113] Kwakkenbos MJ, Diehl SA, Yasuda E, et al. Generation of stable monoclonal antibody-producing B cell receptor-positive human memory B cells by genetic programming. *Nat Med*. 2010;16(1):123-128.
[114] Hwang WYK, Foote J. Immunogenicity of engineered antibodies. *Methods*. 2005;36(1):3-10.
[115] Kennedy PJ, Oliveira C, Granja PL, Sarmento B. Monoclonal antibodies: technologies for early discovery and engineering. *Crit Rev Biotechnol*. 2018;38(3):394-408.
[116] Barderas R, Desmet J, Timmerman P, Meloen R, Casal JI. Affinity maturation of antibodies assisted by in silico modeling. *Proc Natl Acad Sci*. 2008;105(26):9029-9034.
[117] Lonberg N. Human antibodies from transgenic animals. *Nat Biotechnol*. 2005;23(9):1117-1125.
[118] Sheehan J, Marasco WA. Phage and Yeast Display. *Microbiol Spectr*. 2015;3(1):1-12.
[119] Harding FA, Stickler MM, Razo J, DuBridge RB. The immunogenicity of humanized and fully human antibodies: Residual immunogenicity resides in the CDR regions. *MAbs*. 2010;2(3):256-265.
[120] Lushova AA, Biazrova MG, Prilipov AG, Sadykova GK, Kopylov TA, Filatov A V. Next-Generation Techniques for Discovering Human Monoclonal Antibodies. *Mol Biol*. 2017;51(6):782-787.
[121] Parola C, Neumeier D, Reddy ST. Integrating high-throughput screening and sequencing for monoclonal antibody discovery and engineering. *Immunology*. 2018;153(1):31-41.
[122] Georgiou G, Ippolito GC, Beausang J, Busse CE, Wardemann H, Quake SR. The promise and challenge of high-throughput sequencing of the antibody repertoire. *Nat Biotechnol*. 2014;32(2):158-168.
[123] Tiller T. Single B cell antibody technologies. *N Biotechnol*. 2011;28(5):453-457.
[124] Frenzel A, Schirrmann T, Hust M. Phage display-derived human antibodies in clinical development and therapy. *MAbs*. 2016;8(7):1177-1194.
[125] Smith GP. Filamentous Fusion Phage : Novel Expression Vectors that Display Cloned Antigens on the Virion Surface. *Science*. 1985;228(4705):1315-1317.
[126] Kuhn P, Fï¿½hner V, Unkauf T, et al. Recombinant antibodies for diagnostics and therapy against pathogens and toxins generated by phage display. *Proteomics - Clin Appl*. 2016;10(9-10):922-948.
[127] Jain T, Sun T, Durand S, et al. Biophysical properties of the clinical-stage antibody landscape. *Proc Natl Acad Sci U S A*. 2017;114(5):944-949.
[128] Daugherty PS, Chen G, Olsen MJ, Iverson BL, Georgiou G. Antibody affinity maturation using bacterial surface display. *Protein Eng*. 1998;11(9):825-832.
[129] Cherf GM, Cochran JR. Yeast Surface Display. *Methods Mol Biol*. 2015;1319:155-175.
[130] Bowers PM, Horlick RA, Kehry MR, et al. Mammalian cell display for the discovery and optimization of antibody therapeutics. *Methods*. 2014;65(1):44-56.
[131] Lipovsek D, Plückthun A. In-vitro protein evolution by ribosome display and mRNA display. *J Immunol Methods*. 2004;290(1-2):51-67.
[132] Frenzel A, Schirrmann T, Hust M. Phage display-derived human antibodies in clinical development and therapy. *MAbs*. 2016;8(7):1177-1194.
[133] Solá RJ, Griebenow KAI. Effects of Glycosylation on the Stability of Protein Pharmaceuticals. *Biochemistry*. 2010;98(4):1223-1245.
[134] Zheng K, Bantog C, Bayer R. The impact of glycosylation on monoclonal antibody conformation and stability. *MAbs*. 2011;3(6):568-576.
[135] Abès R, Teillaud JL. Impact of glycosylation on effector functions of therapeutic IgG. *Pharmaceuticals*. 2010;3(1):146-157.
[136] Liu L. Antibody glycosylation and its impact on the pharmacokinetics and pharmacodynamics of monoclonal antibodies and Fc-fusion proteins. *J Pharm Sci*. 2015;104(6):1866-1884.
[137] Goh JB, Ng SK. Impact of host cell line choice on glycan profile. *Crit Rev Biotechnol*. 2018;38(6):851-867.
[138] Frenzel A, Hust M, Schirrmann T. Expression of recombinant antibodies. *Front Immunol*. 2013;4(JUL):1-20.

[139] Kunert R, Reinhart D. Advances in recombinant antibody manufacturing. *Appl Microbiol Biotechnol*. 2016;100(8):3451-3461.
[140] Croset A, Delafosse L, Gaudry JP, et al. Differences in the glycosylation of recombinant proteins expressed in HEK and CHO cells. *J Biotechnol*. 2012;161(3):336-348.
[141] Shields RL, Lai J, Keck R, et al. Lack of fucose on human IgG1 N-linked oligosaccharide improves binding to human FcγRIII and antibody-dependent cellular toxicity. *J Biol Chem*. 2002;277(30):26733-26740.
[142] Ayyar BV, Arora S, Ravi SS. Optimizing antibody expression: The nuts and bolts. *Methods*. 2017;116:51-62.
[143] Stech M, Kubick S. Cell-Free Synthesis Meets Antibody Production: A Review. *Antibodies*. 2015;4(1):12-33.
[144] de Marco A. Recombinant antibody production evolves into multiple options aimed at yielding reagents suitable for application-specific needs. *Microb Cell Fact*. 2015;14(1):1-17.
[145] Li W, Zhu Z, Chen W, Feng Y, Dimitrov DS. Crystallizable fragment glycoengineering for therapeutic antibodies development. *Front Immunol*. 2017;8(NOV).
[146] Baković MP, Selman MHJ, Hoffmann M, et al. High-throughput IgG Fc N-glycosylation profiling by mass spectrometry of glycopeptides. *J Proteome Res*. 2013;12(2):821-831.
[147] Zauner G, Selman MHJ, Bondt A, et al. Glycoproteomic Analysis of Antibodies. *Mol Cell Proteomics*. 2013;12(4):856-865.
[148] Wuhrer M, Stam JC, Van De Geijn FE, et al. Glycosylation profiling of immunoglobulin G (IgG) subclasses from human serum. *Proteomics*. 2007;7(22):4070-4081.
[149] Flynn GC, Chen X, Liu YD, Shah B, Zhang Z. Naturally occurring glycan forms of human immunoglobulins G1 and G2. *Mol Immunol*. 2010;47(11-12):2074-2082.
[150] Jefferis R. Glycosylation as a strategy to improve antibody-based therapeutics. *Nat Rev Drug Discov*. 2009;8(3):226-234.
[151] Alter G, Ottenhoff THM, Joosten SA. Antibody glycosylation in inflammation, disease and vaccination. *Semin Immunol*. 2018;(May).
[152] Jennewein MF, Alter G. The Immunoregulatory Roles of Antibody Glycosylation. *Trends Immunol*. 2017;38(5):358-372.
[153] Parekh RB, Dwek RA, Sutton BJ, et al. Association of rheumatoid arthritis and primary osteoarthritis with changes in the glycosylation pattern of total serum IgG. *Nature*. 1985;316(1):452-457.
[154] Vučkovïc F, Krištïc J, Gudelj I, et al. Association of systemic lupus erythematosus with decreased immunosuppressive potential of the IgG glycome. *Arthritis Rheumatol*. 2015;67(11):2978-2989.
[155] Liu L. Antibody glycosylation and its impact on the pharmacokinetics and pharmacodynamics of monoclonal antibodies and Fc-fusion proteins. *J Pharm Sci*. 2015;104(6):1866-1884.
[156] Higel F, Seidl A, Sörgel F, Friess W. N-glycosylation heterogeneity and the influence on structure, function and pharmacokinetics of monoclonal antibodies and Fc fusion proteins. *Eur J Pharm Biopharm*. 2016;100:94-100.
[157] Krapp S, Mimura Y, Jefferis R, Huber R, Sondermann P. Structural analysis of human IgG-Fc glycoforms reveals a correlation between glycosylation and structural integrity. *J Mol Biol*. 2003;325(5):979-989.
[158] Borrok MJ, Jung ST, Kang TH, Monzingo AF, Georgiou G. Revisiting the role of glycosylation in the structure of human IgG Fc. *ACS Chem Biol*. 2012;7(9):1596-1602.
[159] Zheng K, Bantog C, Bayer R. The impact of glycosylation on monoclonal antibody conformation and stability. *MAbs*. 2011;3(6):568-576.
[160] Kanda Y, Yamada T, Mori K, et al. Comparison of biological activity among nonfucosylated therapeutic IgG1 antibodies with three different N-linked Fc oligosaccharides: The high-mannose, hybrid, and complex types. *Glycobiology*. 2007;17(1):104-118.

[161] Newkirk MM, Novick J, Stevenson MM, Fournier MJ, Apostolakos P. Differential clearance of glycoforms of IgG in normal and autoimmune-prone mice. *Clin Exp Immunol*. 1996;106(2):259-264.
[162] Marcus R, Davies A, Ando K, et al. Obinutuzumab for the First-Line Treatment of Follicular Lymphoma. *N Engl J Med*. 2017;377(14):1331-1344.
[163] Ju M-S, Taek Jung S. Aglycosylated full-length IgG antibodies: steps toward next-generation immunotherapeutics. *Curr Opin Biotechnol*. 2014;30:128-139.
[164] Liu H, Ponniah G, Zhang H-M, et al. In vitro and in vivo modifications of recombinant and human IgG antibodies. *MAbs*. 2014;6(5):1145-1154.
[165] Jefferis R. Posttranslational modifications and the immunogenicity of biotherapeutics. *J Immunol Res*. 2016;2016:1-15.
[166] van den Bremer ETJ, Beurskens FJ, Voorhorst M, et al. Human IgG is produced in a pro-form that requires clipping of C-terminal lysines for maximal complement activation. *MAbs*. 2015;7(4):672-680.
[167] Cai B, Pan H, Flynn GC. C-terminal lysine processing of human immunoglobulin G2 heavy chain in vivo. *Biotechnol Bioeng*. 2011;108(2):404-412.
[168] Bertolotti-Ciarlet A, Wang W, Lownes R, et al. Impact of methionine oxidation on the binding of human IgG1 to FcRn and Fcγ receptors. *Mol Immunol*. 2009;46(8-9):1878-1882.
[169] Wang W, Vlasak J, Li Y, et al. Impact of methionine oxidation in human IgG1 Fc on serum half-life of monoclonal antibodies. *Mol Immunol*. 2011;48(6-7):860-866.
[170] Wei Z, Feng J, Lin HY, et al. Identification of a single tryptophan residue as critical for binding activity in a humanized monoclonal antibody against respiratory syncytial virus. *Anal Chem*. 2007;79(7):2797-2805.
[171] Lacy ER, Baker M, Brigham-Burke M. Free sulfhydryl measurement as an indicator of antibody stability. *Anal Biochem*. 2008;382(1):66-68.
[172] Huh JH, White AJ, Brych SR, Franey H, Matsumura M. The Identification of Free Cysteine Residues Within Antibodies and a Potential Role for Free Cysteine Residues in Covalent Aggregation Because of Agitation Stress. *J Pharm Sci*. 2013;102(6):1701-1711.
[173] Xenaki KT, Oliveira S, van Bergen en Henegouwen PMP. Antibody or Antibody Fragments: Implications for Molecular Imaging and Targeted Therapy of Solid Tumors. *Front Immunol*. 2017;8(October).
[174] Herrington-Symes AP, Farys M, Khalili H, Brocchini S. Antibody fragments: Prolonging circulation half-life special issue-antibody research. *Adv Biosci Biotechnol*. 2013;04(05):689-698.
[175] Andrew SM, Titus JA. Fragmentation of Immunoglobulin G. *Curr Protoc Cell Biol*. 2003;Chapter 16:16.4.1-16.4.10.
[176] von Pawel-Rammingen U, Johansson BP, Björck L. IdeS, a novel streptococcal cysteine proteinase with unique speci®city for immunoglobulin G. *EMBO J*. 2002;21(7):1607-1615.
[177] Sheridan C. Ablynx's nanobody fragments go places antibodies cannot. *Nat Biotechnol*. 2017;35(12):1115-1117.
[178] Dozier JK, Distefano MD. Site-specific pegylation of therapeutic proteins. *Int J Mol Sci*. 2015;16(10):25831-25864.
[179] Weisser NE, Hall JC. Applications of single-chain variable fragment antibodies in therapeutics and diagnostics. *Biotechnol Adv*. 2009;27(4):502-520.
[180] Bannas P, Hambach J, Koch-Nolte F. Nanobodies and nanobody-based human heavy chain antibodies as antitumor therapeutics. *Front Immunol*. 2017;8(NOV):1-13.
[181] Ewert S, Cambillau C, Conrath K, Plückthun A. Biophysical properties of camelid VHH domains compared to those of human VH3 domains. *Biochemistry*. 2002;41(11):3628-3636.

[182] Muyldermans S. Nanobodies: Natural Single-Domain Antibodies. *Annu Rev Biochem*. 2013;82(1):775-797.
[183] Matz H, Dooley H. Shark IgNAR-derived binding domains as potential diagnostic and therapeutic agents. *Dev Comp Immunol*. 2019;90(September 2018):100-107.
[184] Vaccaro C, Zhou J, Ober RJ, Ward ES. Engineering the Fc region of immunoglobulin G to modulate in vivo antibody levels. *Nat Biotechnol*. 2005;23(10):1283-1288.
[185] Fernandes JC. Therapeutic application of antibody fragments in autoimmune diseases: current state and prospects. *Drug Discov Today*. 2018;00(00):1-7.
[186] Luo Y, Lu Z, Raso SW, Entrican C, Tangarone B. Dimers and multimers of monoclonal IgG1 exhibit higher in vitro binding affinities to Fcγ receptors. *MAbs*. 2009;1(5):491-504.
[187] Bajardi-Taccioli A, Blum A, Xu C, Sosic Z, Bergelson S, Feschenko M. Effect of protein aggregates on characterization of FcRn binding of Fc-fusion therapeutics. *Mol Immunol*. 2015;67(2):616-624.
[188] Foss S, Grevys A, Sand KMK, et al. Enhanced FcRn-dependent transepithelial delivery of IgG by Fc-engineering and polymerization. *J Control Release*. 2016;223:43-52.
[189] White AL, Dou L, Chan HTC, et al. Fcγ Receptor Dependency of Agonistic CD40 Antibody in Lymphoma Therapy Can Be Overcome through Antibody Multimerization. *J Immunol*. 2014;193(4):1828-1835.
[190] de Jong RN, Beurskens FJ, Verploegen S, et al. A Novel Platform for the Potentiation of Therapeutic Antibodies Based on Antigen-Dependent Formation of IgG Hexamers at the Cell Surface. *PLoS Biol*. 2016;14(1):1-24.
[191] Tradtrantip L, Felix CM, Spirig R, Morelli AB, Verkman AS. Recombinant IgG1 Fc hexamers block cytotoxicity and pathological changes in experimental in vitro and rat models of neuromyelitis optica. *Neuropharmacology*. 2018;133:345-353.
[192] Nagashima H, Tezuka T, Tsuchida W, Maeda H, Kohroki J, Masuho Y. Tandemly repeated Fc domain augments binding avidities of antibodies for Fcγ receptors, resulting in enhanced antibody-dependent cellular cytotoxicity. *Mol Immunol*. 2008;45(10):2752-2763.
[193] Nagashima H, Ootsubo M, Fukazawa M, Motoi S, Konakahara S, Masuho Y. Enhanced antibody-dependent cellular phagocytosis by chimeric monoclonal antibodies with tandemly repeated Fc domains. *J Biosci Bioeng*. 2011;111(4):391-396.
[194] Jain A, Poonia B, So EC, et al. Tumour antigen targeted monoclonal antibodies incorporating a novel multimerisation domain significantly enhance antibody dependent cellular cytotoxicity against colon cancer. *Eur J Cancer*. 2013;49(15):3344-3352.
[195] Wang Q, Chen Y, Pelletier M, et al. Enhancement of antibody functions through Fc multiplications. *MAbs*. 2017;9(3):393-403.
[196] Borrok MJ, Luheshi NM, Beyaz N, et al. Enhancement of antibody-dependent cell-mediated cytotoxicity by endowing IgG with FcαRI (CD89) binding. *MAbs*. 2015;7(4):743-751.
[197] Ortiz DF, Lansing JC, Rutitzky L, et al. Elucidating the interplay between IgG-Fc valency and Fc R activation for the design of immune complex inhibitors. *Sci Transl Med*. 2016;8(365):365ra158-365ra158.
[198] Beck A, Goetsch L, Dumontet C, Corvaïa N. Strategies and challenges for the next generation of antibody–drug conjugates. *Nat Rev Drug Discov*. 2017;16(5):315-337.
[199] Bakhtiar R. Antibody drug conjugates. *Biotechnol Lett*. 2016;38(10):1655-1664.
[200] Shor B, Gerber HP, Sapra P. Preclinical and clinical development of inotuzumab-ozogamicin in hematological malignancies. *Mol Immunol*. 2015;67(2):107-116.
[201] Kumar C, Shetake N, Desai S, Kumar A, Samuel G, Pandey BN. Relevance of radiobiological concepts in radionuclide therapy of cancer. *Int J Radiat Biol*. 2016;92(4):173-186.
[202] Steiner M, Neri D. Antibody-radionuclide conjugates for cancer therapy: Historical considerations and new trends. *Clin Cancer Res*. 2011;17(20):6406-6416.

[203] Navarro-Teulon I, Lozza C, Pèlegrin A, Vivès E, Pouget JP. General overview of radioimmunotherapy of solid tumors. *Immunotherapy*. 2013;5(5):467-487.
[204] Teicher BA, Chari RVJ. Antibody conjugate therapeutics: Challenges and potential. *Clin Cancer Res*. 2011;17(20):6389-6397.
[205] Mariathasan S, Tan MW. Antibody–Antibiotic Conjugates: A Novel Therapeutic Platform against Bacterial Infections. *Trends Mol Med*. 2017;23(2):135-149.
[206] Agarwal P, Bertozzi CR. Site-Specific Antibody–Drug Conjugates: The Nexus of Bioorthogonal Chemistry, Protein Engineering, and Drug Development. *Bioconjug Chem*. 2015;26(2):176-192.
[207] Hu Q-Y, Berti F, Adamo R. Towards the next generation of biomedicines by site-selective conjugation. *Chem Soc Rev*. 2016;45(6):1691-1719.
[208] Junutula JR, Raab H, Clark S, et al. Site-specific conjugation of a cytotoxic drug to an antibody improves the therapeutic index. *Nat Biotechnol*. 2008;26(8):925-932.
[209] Shen B-Q, Xu K, Liu L, et al. Conjugation site modulates the in vivo stability and therapeutic activity of antibody-drug conjugates. *Nat Biotechnol*. 2012;30(2):184-189.
[210] Hallam TJ, Wold E, Wahl A, Smider V V. Antibody conjugates with unnatural amino acids. *Mol Pharm*. 2015;12(6):1848-1862.
[211] Li X, Yang J, Rader C. Antibody conjugation via one and two C-terminal selenocysteines. *Methods*. 2014;65(1):133-138.
[212] Tian F, Lu Y, Manibusan A, et al. A general approach to site-specific antibody drug conjugates. *Proc Natl Acad Sci*. 2014;111(5):1766-1771.
[213] Zimmerman ES, Heibeck TH, Gill A, et al. Production of site-specific antibody-drug conjugates using optimized non-natural amino acids in a cell-free expression system. *Bioconjug Chem*. 2014;25(2):351-361.
[214] Okeley NM, Toki BE, Zhang X, et al. Metabolic engineering of monoclonal antibody carbohydrates for antibody-drug conjugation. *Bioconjug Chem*. 2013;24(10):1650-1655.
[215] Qasba PK. Glycans of Antibodies as a Specific Site for Drug Conjugation Using Glycosyltransferases. *Bioconjug Chem*. 2015;26(11):2170-2175.
[216] Zhou Q, Stefano JE, Manning C, et al. Site-specific antibody-drug conjugation through glycoengineering. *Bioconjug Chem*. 2014;25(3):510-520.
[217] Akkapeddi P, Azizi SA, Freedy AM, Cal PMSD, Gois PMP, Bernardes GJL. Construction of homogeneous antibody-drug conjugates using site-selective protein chemistry. *Chem Sci*. 2016;7(5):2954-2963.
[218] Jain N, Smith SW, Ghone S, Tomczuk B. Current ADC Linker Chemistry. *Pharm Res*. 2015;32(11):3526-3540.
[219] Dubowchik GM, Firestone RA, Padilla L, et al. Cathepsin B-labile dipeptide linkers for lysosomal release of doxorubicin from internalizing immunoconjugates: Model studies of enzymatic drug release and antigen-specific in vitro anticancer activity. *Bioconjug Chem*. 2002;13(4):855-869.
[220] Lewis Phillips GD, Li G, Dugger DL, et al. Targeting HER2-positive breast cancer with trastuzumab-DM1, an antibody-cytotoxic drug conjugate. *Cancer Res*. 2008;68(22):9280-9290.
[221] Doronina SO, Mendelsohn BA, Bovee TD, et al. Enhanced activity of monomethylauristatin F through monoclonal antibody delivery: Effects of linker technology on efficacy and toxicity. *Bioconjug Chem*. 2006;17(1):114-124.
[222] Zhao RY, Wilhelm SD, Audette C, et al. Synthesis and evaluation of hydrophilic linkers for antibody-maytansinoid conjugates. *J Med Chem*. 2011;54(10):3606-3623.
[223] Kovtun Y V., Audette CA, Mayo MF, et al. Antibody-maytansinoid conjugates designed to bypass multidrug resistance. *Cancer Res*. 2010;70(6):2528-2537.
[224] Lyon RP, Bovee TD, Doronina SO, et al. Reducing hydrophobicity of homogeneous antibody-drug conjugates improves pharmacokinetics and therapeutic index. *Nat Biotechnol*. 2015;33(7):733-735.

[225] Hong EE, Erickson H, Lutz RJ, et al. Design of coltuximab ravtansine, a CD19-targeting antibody-drug conjugate (ADC) for the treatment of B-cell malignancies: Structure-activity relationships and preclinical evaluation. *Mol Pharm*. 2015;12(6):1703-1716.

[226] van der Lee MMC, Groothuis PG, Ubink R, et al. The Preclinical Profile of the Duocarmycin-Based HER2-Targeting ADC SYD985 Predicts for Clinical Benefit in Low HER2-Expressing Breast Cancers. *Mol Cancer Ther*. 2015;14(3):692-703.

[227] Müller D. Antibody fusions with immunomodulatory proteins for cancer therapy. *Pharmacol Ther*. 2015;154:57-66.

[228] Sharma SK, Bagshawe KD. Antibody Directed Enzyme Prodrug Therapy (ADEPT): Trials and tribulations. *Adv Drug Deliv Rev*. 2017;118:2-7.

[229] Holt LJ, Basran A, Jones K, et al. Anti-serum albumin domain antibodies for extending the half-lives of short lived drugs. *Protein Eng Des Sel*. 2008;21(5):283-288.

[230] Jafari R, Zolbanin NM, Rafatpanah H, Majidi J, Kazemi T. Fc-fusion Proteins in Therapy: An Updated View. *Curr Med Chem*. 2017;24(12):1228-1237.

[231] Levin D, Golding B, Strome SE, Sauna ZE. Fc fusion as a platform technology: Potential for modulating immunogenicity. *Trends Biotechnol*. 2015;33(1):27-34.

[232] Czajkowsky DM, Hu J, Shao Z, Pleass RJ. Fc-fusion proteins: New developments and future perspectives. *EMBO Mol Med*. 2012;4(10):1015-1028.

[233] Dumont JA, Low SC, Peters RT, Bitonti AJ. Monomeric Fc fusions: Impact on pharmacokinetic and biological activity of protein therapeutics. *BioDrugs*. 2006;20(3):151-160.

[234] Pasut G. Pegylation of biological molecules and potential benefits: Pharmacological properties of certolizumab pegol. *BioDrugs*. 2014;28(SUPPL. 1):15-23.

[235] Chen C, Constantinou A, Deonarain M. Modulating antibody pharmacokinetics using hydrophilic polymers. *Expert Opin Drug Deliv*. 2011;8(9):1221-1236.

[236] Zhang P, Sun F, Liu S, Jiang S. Anti-PEG antibodies in the clinic: Current issues and beyond PEGylation. *J Control Release*. 2016;244:184-193.

[237] Brinkmann U, Kontermann RE. The making of bispecific antibodies. *MAbs*. 2017;9(2):182-212.

[238] Spiess C, Zhai Q, Carter PJ. Alternative molecular formats and therapeutic applications for bispecific antibodies. *Mol Immunol*. 2015;67(2):95-106.

[239] Suresh MR, Cuello AC, Milstein C. Bispecific monoclonal antibodies from hybrid hybridomas. *Methods Enzymol*. 1986;121:210-228.

[240] Lindhofer H, Mocikat R, Steipe B, Thierfelder S. Preferential species-restricted heavy/light chain pairing in rat/mouse quadromas. Implications for a single-step purification of bispecific antibodies. *J Immunol*. 1995;155(1):219-225.

[241] Ridgway JB, Presta LG, Carter P. "Knobs-into-holes" engineering of antibody CH3 domains for heavy chain heterodimerization. *Protein Eng*. 1996;9:617-621.

[242] Merchant AM, Zhu Z, Yuan JQ, et al. An efficient route to human bispecific IgG. *Nat Biotechnol*. 1998;16(7):677-681.

[243] Gunasekaran K, Pentony M, Shen M, et al. Enhancing antibody Fc heterodimer formation through electrostatic steering effects: Applications to bispecific molecules and monovalent IgG. *J Biol Chem*. 2010;285(25):19637-19646.

[244] Sampei Z, Igawa T, Soeda T, et al. Identification and Multidimensional Optimization of an Asymmetric Bispecific IgG Antibody Mimicking the Function of Factor VIII Cofactor Activity. *PLoS One*. 2013;8(2).

[245] Davis JH, Aperlo C, Li Y, et al. SEEDbodies: Fusion proteins based on strand-exchange engineered domain (SEED) CH3 heterodimers in an Fc analogue platform for asymmetric binders or immunofusions and bispecific antibodies. *Protein Eng Des Sel*. 2010;23(4):195-202.

[246] Lewis SM, Wu X, Pustilnik A, et al. Generation of bispecific IgG antibodies by structure-based design of an orthogonal Fab interface. *Nat Biotechnol*. 2014;32(2):191-198.
[247] Mazor Y, Oganesyan V, Yang C, et al. Improving target cell specificity using a novel monovalent bispecific IgG design. *MAbs*. 2015;7(2):377-389.
[248] Schaefer W, Regula JT, Bähner M, et al. Immunoglobulin domain crossover as a generic approach for the production of bispecific IgG antibodies. *Proc Natl Acad Sci U S A*. 2011;108(27):11187-11192.
[249] Klein C, Schaefer W, Regula JT. The use of CrossMAb technology for the generation of bi- and multispecific antibodies. *MAbs*. 2016;8(6):1010-1020.
[250] Shatz W, Chung S, Li B, et al. Knobs-into-holes antibody production in mammalian cell lines reveals that asymmetric afucosylation is sufficient for full antibody-dependent cellular cytotoxicity. *MAbs*. 2013;5(6):872-881.
[251] Jackman J, Chen Y, Huang A, et al. Development of a two-part strategy to identify a therapeutic human bispecific antibody that inhibits IgE receptor signaling. *J Biol Chem*. 2010;285(27):20850-20859.
[252] Labrijn AF, Meesters JI, de Goeij BECG, et al. Efficient generation of stable bispecific IgG1 by controlled Fab-arm exchange. *Proc Natl Acad Sci U S A*. 2013;110(13):5145-5150.
[253] Fischer N, Elson G, Magistrelli G, et al. Exploiting light chains for the scalable generation and platform purification of native human bispecific IgG. *Nat Commun*. 2015;6(6113):1-12.
[254] Tustian AD, Endicott C, Adams B, Mattila J, Bak H. Development of purification processes for fully human bispecific antibodies based upon modification of protein A binding avidity. *MAbs*. 2016;8(4):828-838.
[255] Zwolak A, Leettola CN, Tam SH, et al. Rapid Purification of Human Bispecific Antibodies via Selective Modulation of Protein A Binding. *Sci Rep*. 2017;7(1):1-11.
[256] Graziano RF, Guptill P. Chemical production of bispecific antibodies. *Methods Mol Biol*. 2004;283(10):71-85.
[257] Williams AJ, Ovadia RD, Giese GS. Improving Stepwise Assembly of a Bispecific F(ab′) 2 from Two Different Fab′ Molecules. *Ind Eng Chem Res*. 2017;56(7):1713-1722.
[258] Baeuerle PA, Reinhardt C. Bispecific T-cell engaging antibodies for cancer therapy. *Cancer Res*. 2009;69:4941-4944.
[259] Wolf E, Hofmeister R, Kufer P, Schlereth B, Baeuerle PA. BiTEs: Bispecific antibody constructs with unique anti-tumor activity. *Drug Discov Today*. 2005;10(18):1237-1244.
[260] Johnson S, Burke S, Huang L, et al. Effector cell recruitment with novel Fv-based dual-affinity re-targeting protein leads to potent tumor cytolysis and in vivo B-cell depletion. *J Mol Biol*. 2010;399:436-449.
[261] Brusselbach S, Korn T, Volkel T, Muller R, Kontermann RE. Enzyme recruitment and tumor cell killing in vitro by a secreted bispecific single-chain diabody. *Tumor Target*. 1999;4:115-123.
[262] Völkel T, Korn T, Bach M, Müller R, Kontermann RE. Optimized linker sequences for the expression of monomeric and dimeric bispecific single-chain diabodies. *Protein Eng*. 2001;14(10):815-823.
[263] Wu X, Sereno AJ, Huang F, et al. Fab-based bispecific antibody formats with robust biophysical properties and biological activity. *MAbs*. 2015;7(3):470-482.
[264] Durben M, Schmiedel D, Hofmann M, et al. Characterization of a bispecific FLT3 X CD3 antibody in an improved, recombinant format for the treatment of leukemia. *Mol Ther*. 2015;23:648-655.
[265] Wu C, Ying H, Grinnell C, et al. Simultaneous targeting of multiple disease mediators by a dual-variable-domain immunoglobulin. *Nat Biotechnol*. 2007;25(11):1290-1297.
[266] Castoldi R, Jucknischke U, Pradel LP, et al. Molecular characterization of novel trispecific ErbB-cMet-IGF1R antibodies and their antigen-binding properties. *Protein Eng Des Sel*. 2012;25(10):551-559.

[267] Hu S, Fu W, Xu W, et al. Four-in-one antibodies have superior cancer inhibitory activity against EGFR, HER2, HER3, and VEGF through disruption of HER/MET crosstalk. *Cancer Res*. 2015;75(1):159-170.
[268] Shields RL, Namenuk AK, Hong K, et al. High resolution mapping of the binding site on human IgG1 for FcγRI, FcγRII, FcγRIII, and FcRn and design of IgG1 variants with improved binding to the FcγR. *J Biol Chem*. 2001;276(9):6591-6604.
[269] Saxena A, Wu D. Advances in Therapeutic Fc engineering – Modulation of igG-Associated effector Functions and Serum Half-life. *Front Immunol*. 2016;7(580):1-11.
[270] Kellner C, Otte A, Cappuzzello E, Klausz K, Peipp M. Modulating cytotoxic effector functions by Fc engineering to improve cancer therapy. *Transfus Med Hemotherapy*. 2017;44(5):327-336.
[271] Wang X, Mathieu M, Brezski RJ. IgG Fc engineering to modulate antibody effector functions. *Protein Cell*. 2017;9(1):1-11.
[272] Nimmerjahn F, Ravetch J V. Divergent Immunoglobulin G Subclass Activity through Selective Fc Receptor Binding. *Science (80)*. 2005;310(5753):1510-1512.
[273] Richards JO, Karki S, Lazar GA, Chen H, Dang W, Desjarlais JR. Optimization of antibody binding to Fc RIIa enhances macrophage phagocytosis of tumor cells. *Mol Cancer Ther*. 2008;7(8):2517-2527.
[274] Mimoto F, Igawa T, Kuramochi T, et al. Novel asymmetrically engineered antibody Fc variant with superior FcγR binding affinity and specificity compared with afucosylated Fc variant. *MAbs*. 2013;5(2):229-236.
[275] Moore GL, Chen H, Karki S, Lazar GA. Engineered Fc variant antibodies with enhanced ability to recruit complement and mediate effector functions. *MAbs*. 2010;2(2):181-189.
[276] Natsume A, In M, Takamura H, et al. Engineered Antibodies of IgG1/IgG3 Mixed Isotype with Enhanced Cytotoxic Activities. *Cancer Res*. 2008;68(10):3863-3872.
[277] Sondermann P, Szymkowski DE. Harnessing Fc receptor biology in the design of therapeutic antibodies. *Curr Opin Immunol*. 2016;40:78-87.
[278] Tam SH, Mccarthy SG, Armstrong AA, et al. Functional, biophysical, and structural characterization of human IgG1 and IgG4 Fc variants with ablated immune functionality. *Antibodies*. 2017;6(3):12.
[279] Ward ES, Devanaboyina SC, Ober RJ. Targeting FcRn for the modulation of antibody dynamics. *Mol Immunol*. 2015;67:131-141.
[280] Dall'Acqua WF, Kiener PA, Wu H. Properties of Human IgG1s engineered for enhanced binding to the neonatal Fc Receptor (FcRn). *J Biol Chem*. 2006;281(33):23514-23524.
[281] Robbie GJ, Criste R, Dall'Acqua WF, et al. A novel investigational Fc-modified humanized monoclonal antibody, motavizumab-YTE, has an extended half-life in healthy adults. *Antimicrob Agents Chemother*. 2013;57(12):6147-6153.
[282] Zalevsky J, Chamberlain AK, Horton HM, et al. Enhanced antibody half-life improves in vivo activity. *Nat Biotechnol*. 2010;28(2):157-159.
[283] Borrok MJ, Wu Y, Beyaz N, et al. pH-dependent binding engineering reveals an FcRn affinity threshold that governs IgG recycling. *J Biol Chem*. 2015;290(7):4282-4290.
[284] Grevys A, Bern M, Foss S, et al. Fc Engineering of Human IgG1 for Altered Binding to the Neonatal Fc Receptor Affects Fc Effector Functions. *J Immunol*. 2015;194:5497-5508.
[285] Liu L. Pharmacokinetics of monoclonal antibodies and Fc-fusion proteins. *Protein Cell*. April 2017:1-18.
[286] Igawa T, Tsunoda H, Kuramochi T, Sampei Z, Ishii S, Hattori K. Engineering the variable region of therapeutic IgG antibodies. *MAbs*. 2011;3:37-41.
[287] Roberts CJ. Therapeutic protein aggregation: mechanisms, design, and control. *Trends Biotechnol*. 2014;32(7):372-380.

[288] Li W, Prabakaran P, Chen W, Zhu Z, Feng Y, Dimitrov D. Antibody Aggregation: Insights from Sequence and Structure. *Antibodies*. 2016;5(3):1-23.
[289] Barthelemy PA, Raab H, Appleton BA, et al. Comprehensive analysis of the factors contributing to the stability and solubility of autonomous human VH domains. *J Biol Chem*. 2008;283(6):3639-3654.
[290] Shire SJ. Formulation and manufacturability of biologics. *Curr Opin Biotechnol*. 2009;20(6):708-714.
[291] Moussa EM, Panchal JP, Moorthy BS, et al. Immunogenicity of Therapeutic Protein Aggregates. *J Pharm Sci*. 2016;105(2):417-430.
[292] Ratanji KD, Derrick JP, Dearman RJ, Kimber I. Immunogenicity of therapeutic proteins: Influence of aggregation. *J Immunotoxicol*. 2014;11(2):99-109.
[293] Kim DY, Kandalaft H, Ding W, et al. Disulfide linkage engineering for improving biophysical properties of human VHdomains. *Protein Eng Des Sel*. 2012;25(10):581-589.
[294] Ewert S, Huber T, Honegger A, Plückthun A. Biophysical properties of human antibody variable domains. *J Mol Biol*. 2003;325(3):531-553.
[295] Jayaram N, Bhowmick P, Martin ACR. Germline VH/VL pairing in antibodies. *Protein Eng Des Sel*. 2012;25(10):523-530.
[296] Jarasch A, Koll H, Regula JT, Bader M, Papadimitriou A, Kettenberger H. Developability assessment during the selection of novel therapeutic antibodies. *J Pharm Sci*. 2015;104(6):1885-1898.
[297] Thiagarajan G, Semple A, James JK, Cheung JK, Shameem M. A comparison of biophysical characterization techniques in predicting monoclonal antibody stability. *MAbs*. 2016;8(6):1088-1097.
[298] den Engelsman J, Garidel P, Smulders R, et al. Strategies for the assessment of protein aggregates in pharmaceutical biotech product development. *Pharm Res*. 2011;28(4):920-933.
[299] Hamrang Z, Rattray NJW, Pluen A. Proteins behaving badly: Emerging technologies in profiling biopharmaceutical aggregation. *Trends Biotechnol*. 2013;31(8):448-458.
[300] Gorovits B, Wakshull E, Pillutla R, Xu Y, Manning MS, Goyal J. Recommendations for the characterization of immunogenicity response to multiple domain biotherapeutics. *J Immunol Methods*. 2014;408:1-12.
[301] Hermeling S, Crommelin DJA, Schellekens H, Jiskoot W. Structure-immunogenicity relationships of therapeutic proteins. *Pharm Res*. 2004;21(6):897-903.
[302] Brinks V, Jiskoot W, Schellekens H. Immunogenicity of therapeutic proteins: The use of animal models. *Pharm Res*. 2011;28(10):2379-2385.
[303] Datta-Mannan A, Thangaraju A, Leung D, et al. Balancing charge in the complementarity-determining regions of humanized mAbs without affecting pl reduces non-specific binding and improves the pharmacokinetics. *MAbs*. 2015;7(3):483-493.
[304] Yadav DB, Sharma VK, Boswell CA, et al. Evaluating the use of antibody variable region (Fv) charge as a risk assessment tool for predicting typical cynomolgus monkey pharmacokinetics. *J Biol Chem*. 2015;290(50):29732-29741.
[305] Leipold D, Prabhu S. Pharmacokinetic and pharmacodynamic considerations in the design of therapeutic antibodies. *Clin Transl Sci*. 2018.
[306] Awwad S, Angkawinitwong U. Overview of antibody drug delivery. *Pharmaceutics*. 2018;10(3):1-24.
[307] Mitragotri S, Burke PA, Langer R. Overcoming the challenges in administering biopharmaceuticals: formulation and delivery strategies. *Nat Rev Drug Discov*. 2014;13(9):655-672.
[308] Correia IR. Stability of IgG isotypes in serum. *MAbs*. 2010;2(3):221-232.
[309] Zhou H-X, Rivas G, Minton AP. Macromolecular crowding and confinement: biochemical, biophysical, and potential physiological consequences. *Annu Rev Biophys*. 2008;37:375-397.
[310] Demeule B, Shire SJ, Liu J. A therapeutic antibody and its antigen form different complexes in serum than in phosphate-buffered saline: A study by analytical ultracentrifugation. *Anal Biochem*. 2009;388(2):279-287.

[311] Krayukhina E, Noda M, Ishii K, et al. Analytical ultracentrifugation with fluorescence detection system reveals differences in complex formation between recombinant human TNF and different biological TNF antagonists in various environments. *MAbs*. 2017;9(4):664-679.
[312] Arvinte T, Palais C, Green-Trexler E, et al. Aggregation of biopharmaceuticals in human plasma and human serum: Implications for drug research and development. *MAbs*. 2013;5(3):491-500.
[313] Luo S, Zhang B. Dextrose-mediated aggregation of therapeutic monoclonal antibodies in human plasma: Implication of isoelectric precipitation of complement proteins. *MAbs*. 2015;7(6):1094-1103.
[314] Filipe V, Poole R, Oladunjoye O, Braeckmans K, Jiskoot W. Detection and characterization of subvisible aggregates of monoclonal IgG in serum. *Pharm Res*. 2012;29(8):2202-2212.
[315] Li X, Geng SB, Chiu ML, Saro D, Tessier PM. High-Throughput Assay for Measuring Monoclonal Antibody Self-Association and Aggregation in Serum. *Bioconjug Chem*. 2015;26(3):520-528.

CHAPTER 2

Diffusion of Soluble Aggregates of Antibodies in Serum

Note: This chapter was adapted with permission from:
Goulet DR, Zwolak A, Chiu ML, Nath A, Atkins WM. Diffusion of Soluble Aggregates of THIOMABs and Bispecific Antibodies in Serum. *Biochemistry*. **2017**, *56*, 2251-2260.

2.1 Introduction

Therapeutic proteins including monoclonal antibodies (mAbs), Fc-fusion proteins, bispecific antibodies (bsAbs) and other proteins that are based on the immunoglobulin (Ig) framework dominate the pool of biologics currently in commercial development.[1-3] Collectively, these drugs have the potential to treat many diseases that have been intractable to treatment with small molecule drugs.[1] Antibody-based therapeutics can be challenging and expensive to characterize and manufacture, and regulatory criteria concerning their production are still being revised. Aggregation status is a critical property often determined in standard dilute solutions, but difficult to measure in biological tissue or serum.

Part of the concern over protein aggregates is their potential for increasing immunogenicity, which can negatively impact the safety and efficacy of a drug.[4-6] The mechanism by which aggregates activate the immune system likely involves the introduction of novel epitopes from partial unfolding and the presence of regularly repeated epitopes.[7] Binding of C1q as the first step of the complement pathway is highly dependent on oligomeric state, with surface-bound IgG hexamers causing maximal complement activation.[8,9] Similarly, Ab multimers have been shown to have higher affinities for Fc receptors than the monomeric molecules, and this trend may contribute to immune response.[10] The generation of anti-drug Abs may result in anaphylaxis, cytokine release syndrome, and other potentially fatal infusion reactions in addition to increased clearance and resulting loss of efficacy.[11,12]

Many methods are available to monitor the aggregation of biologics in formulation buffers. Size-exclusion chromatography (SEC) and dynamic light scattering (DLS) are commonly used to determine size distributions, and DLS has the advantage of detecting aggregation that occurs at high concentration. However, it is not possible to assess aggregation state in biological media at therapeutic concentrations using these and other optical techniques. Since the aggregation status can change with environment, the behavior of a protein in buffer is not necessarily predictive of its properties in serum.[13,14] In addition, distinct aggregation states of antibody-based drugs could interact with serum or tissue proteins differently and thereby impact their functional and therapeutic properties. Methods that directly monitor the aggregation in serum could facilitate our ability to better predict aggregation behavior or to better understand clinical properties of biologics. While there has been success using surface plasmon resonance and Ab-coated nanoparticles to achieve these ends, the majority of strategies involve the use of covalent labeling to monitor protein interactions within complex mixtures.[15,16]

Fluorescence correlation spectroscopy (FCS) exploits confocal microscopy to monitor the diffusion of highly dilute solutions of a fluorescently labeled molecule. The autocorrelation function of the fluorescence signal provides the translational diffusion time (τ_D) of the molecules, which is linearly proportional to the hydrodynamic (or Stokes) radius and therefore can be used to report on the aggregation state.[17,18] Crucially, FCS enables the measurement of diffusive properties in optically dense and non-ideal samples such as tissue or serum that cannot be analyzed by standard optical or light scattering methods. Although FCS has been applied in biological media, its utility for monitoring the aggregation status of therapeutic proteins in the serum has not been documented. Here we utilize fluorescently labeled THIOMABs and a bispecific IgG with defined, irreversible aggregation states as models to study their tendency to further aggregate in serum, or

to interact with serum proteins. The results indicate a modest, viscosity-independent, increase in τ_Ds for dimers or trimers compared to monomers in serum versus buffer, and a significant increase in τ_D for aggregates of bsAbs with molecular weight corresponding to pentamers when they are placed into serum. This highlights the important effects that even relatively small changes in the nanometer-scale aggregation profile of a biologic may have on its aggregation state in serum, and therefore potentially on its efficacy and disposition.

2.2 Experimental procedures

2.2.1 Proteins and other materials

Ab residues are identified using Eu numbering. THIOMAB (trastuzumab, anti-Her2 S400C in human IgG1) was provided by Genentech, Inc. OneShot FBS was purchased from Thermo Fisher (A3160401) and chemicals were purchased from Sigma.

The parental Abs used to create bsAb, anti-respiratory syncytial virus F405L and anti-gp120 K409R (both in human IgG1), were expressed in Expi293 cells (Thermo Fisher, A14635) according to the manufacturer's protocol by co-transfecting heavy and light chain plasmids at a 1:3 molar ratio. Purification was performed by equilibrating a protein A column in 1x phosphate-buffered saline (PBS), loading the filtered supernatant, washing with PBS, and eluting Abs with 100 mM sodium citrate, pH 3.5, followed by immediate dialysis into fresh PBS.

2.2.2 Generation of disulfide cross-linked THIOMAB

3 mg of THIOMAB capped with cysteine and/or glutathione was first uncapped as described previously by incubating with a 20x molar equivalent of dithiothreitol for 16 hours at room temperature.[19] Following reduction, the Ab was purified using a 1-mL cation exchange column. The column was equilibrated in 20 mM succinate, pH 5.0 and the sample was diluted in the same buffer prior to loading to allow binding to the column. Following a 10-mL wash at pH

5.0, the Ab was eluted using Tris buffer (50 mM Tris, 150 mM NaCl, pH 7.5).

After preparation of reduced thiols in THIOMAB, a 6x equivalent (40 µM) of $CuSO_4$ was added to catalyze re-oxidation of cysteines including the creation of inter-Ab disulfides. This reaction was incubated for two hours at room temperature and resulted in a small amount of visible precipitate. Immediately following oxidation, a 6x equivalent of Alexa 488 maleimide (Thermo Fisher, A10254) was added to the sample from a 5 mg/mL stock in dimethyl sulfoxide (DMSO) and incubated for three hours at room temperature. An additional buffer exchange was required after SEC to remove free dye using a 0.5-mL desalting column with 7K MWCO. Afterwards, the ratio of dye to Ab was 0.2 for monomer and 0.1 for dimer as determined by absorbance at 280 nm and 493 nm.

2.2.3 Generation of glutaraldehyde cross-linked Abs

3 mg of THIOMAB was uncapped as above, but using PBS (20 mM NaPi, 150 mM NaCl, pH 7.2) to elute from the cation exchange column rather than Tris buffer. A 6x equivalent of Alexa 488 maleimide was added immediately after uncapping from a 5 mg/ml stock in DMSO and incubated for two hours at room temperature. The sample was concentrated to 400 µL and then 2 µL of 12% glutaraldehyde (w/v) in water was added. After ten minutes at room temperature, 30 µL of 1 M Tris, pH 8.0 was added to quench the reaction. Insoluble aggregate was removed by spinning the sample for ten minutes at 16,000×g. Following SEC, the labeling efficiency was ~2 fluorophores per Ab for each THIOMAB oligomer.

bsAb was generated using cFAE as described previously.[20,24] Briefly, 2.5 mg of anti-RSV F405L and 2.5 mg of anti-gp120 K409R in human IgG1 were co-incubated with 75 mM mercaptoethylamine for five hours at 31 ºC, followed by dialysis into PBS. After formation of bsAb, 1 M $NaHCO_3$ was added to equal 1/10 the reaction volume and a 6x molar equivalent of

Alexa 488 NHS ester (Thermo Fisher, A20000) was also added from a 5 mg/ml stock in DMSO. Labeling was carried out for two hours at room temperature. The sample was then glutaraldehyde cross-linked as with THIOMAB above. Ratios of dye to Ab ranged from 0.5 to 2, with lower dye incorporation for the larger oligomers.

2.2.4 Purification and characterization of antibody oligomers

Purification of cross-linked oligomers was achieved with a Superdex 200 10/300 GL (GE, 17517501) column with PBS as the running buffer at 0.5 mL/min and collection of 0.3-mL fractions. To estimate the size of larger oligomers, a standard curve of molecular weight versus retention time was generated using a gel filtration standard (Bio-Rad, 151-1901). Although Vitamin B_{12} is included in the mix of standards, it was excluded from the calibration curve as it deviated from the trend of the other standards (likely due to its small mass of 1,350 Da and extended shape relative to proteins).

Purified oligomers were run on non-reducing SDS-PAGE to visualize their composition. Gels containing 4-15% (w/v) acrylamide were used with a Tris-glycine running buffer containing 0.1% (w/v) SDS and a Laemmli sample buffer lacking reductant. Lanes contained either the starting monomer sample, the cross-linked sample, or 5-25 µL of an SEC-purified fraction. For determination of aggregation reversibility, the loading buffer contained 50 mM DTT for reduced samples. The percentage of each species in a sample was calculated by dividing the density of its band by the total density of bands in its lane.

2.2.5 Preparation of viscosity-matched buffers

The dynamic viscosities of Tris buffer, Tris buffer with 9.90% glycerol (v/v), and FBS were determined at 20 ºC using a Lovis 2000 M/ME rolling ball viscometer at 70º relative to horizontal. Values in the text are the average and standard deviation of 10 replicates.

2.2.6 Fluorescence correlation spectroscopy

Experiments were performed on an Axio Observer D1 microscope (Zeiss) equipped with an LDH-D-C-485 picosecond pulsed diode 485 nm laser, Tau-SPAD single photon counting module, and HydraHarp 400 for autocorrelation (PicoQuant). Time traces and autocorrelations were collected using SymPhoTime 64 software (PicoQuant).

Free dye and tagged Ab samples were analyzed at 1.5 µg/mL regardless of oligomer size or 10 nM fluorophore in the case of free dye. In some cases, Ab samples had to be concentrated after SEC so that they could be diluted 1:100 in the appropriate medium. All buffers were filtered through a 0.22 µm filter prior to sample dilution. Sample aliquots of 50 µL were placed onto 22x22-1 cover glass. With the laser power at 140 µW, ten 60-second traces (or five 120-second traces) were obtained for each sample and contained 200 sampling points and a maximum lag time of 10 seconds. Traces were fit individually using Igor Pro over the range of 0.01 ms to 1,000 ms, initially using the following one-component three-dimensional diffusion model[17,18]:

$$G_{1comp}(\tau) = \frac{1}{N}\left(\frac{1}{1+\frac{\tau}{\tau_D}}\right)\left(\frac{1}{1+\frac{\tau}{s^2\tau_D}}\right)^{0.5}$$

where G(τ) is the autocorrelation at a given lag time τ, N is the average number of particles in the focal volume, τ_D is the translational diffusion time, and s is the ratio of long to short axes of the focal volume. The value of s was fixed at 10 for all samples based on its value for free dye in Tris buffer. For larger oligomer samples in particular, autocorrelations did not fit well to a one-component model and were instead fit to include two components. When both τ_D values were allowed to float, one τ_D was similar to that of free dye. Therefore, final fits for all samples include two components with one τ_D fixed at the τ_D obtained for chemically passivated free dye in the corresponding medium. Additional parameters ρ_{dye} and ρ_{Ab} represent the fraction of each species

where the sum of ρ_{dye} and ρ_{Ab} was fixed at 1.

$$G_{2comp}(\tau) = \frac{1}{N}\left[\rho_{dye}\left(\frac{1}{1+\frac{\tau}{\tau_{D,dye}}}\right)\left(\frac{1}{1+\frac{\tau}{s^2\tau_{D,dye}}}\right)^{0.5} + \rho_{Ab}\left(\frac{1}{1+\frac{\tau}{\tau_{D,Ab}}}\right)\left(\frac{1}{1+\frac{\tau}{s^2\tau_{D,Ab}}}\right)^{0.5}\right]$$

The Ab τ_D, which was allowed to float, is the τ_D plotted in **Figure 2.8**. For the majority of samples, the τ_D of the Ab contributed more than 85% of the total signal with the remainder from the free dye component. The dye component did not exceed 50% of the overall signal for any sample.

Since diffusion times were not normally distributed for all datasets, the Mann-Whitney test was used for comparison of τ_Ds in glycerol buffer and FBS. Significant differences ($P < 0.05$) are indicated in **Table 2.2**.

2.3 Results

2.3.1 Generation of oligomeric standards

To determine whether Ab oligomers have different propensities for self-association in serum or association with serum components, we prepared three distinct types of Ab oligomers using covalent cross-linking strategies. Firstly, THIOMABs containing engineered cysteine residues at a solvent-exposed region of the C_H3 region (S400C), were labeled and site-specifically cross-linked.[21] The engineered thiol groups (initially capped with cysteine or glutathione) were reduced prior to addition of a small amount of $CuSO_4$ to yield dimers with inter-Ab disulfide bonds (**Figure 2.1A**). As a result of disulfide bond formation at the site of the engineered Cys, this method creates Ab dimers that are uniform in size as well as shape. After oxidation to dimer, the sample was labeled at the remaining reduced cysteines using Alexa 488 maleimide. Importantly, there are two free thiols per Ab molecule regardless of oligomeric state, since each disulfide bond involves only one cysteine of each Ab. Therefore, labeling was performed after oxidation to allow for maximum dimerization. Monomeric THIOMAB that was reduced and labeled retained function as

assessed by binding to protein A (**Figure 2.2**).

Secondly, as an alternative to well-defined disulfide linkages, glutaraldehyde was used to randomly tether nucleophilic residues of different Ab molecules via two reactive aldehydes separated by five carbon atoms (**Figure 2.1B**). The abundance of lysine residues in IgG, coupled with several possible mechanisms of glutaraldehyde cross-linking, leads to a heterogeneous mixture of Ab oligomers.[22,23] Therefore, even dimers of the same mass may have significant differences in shape or exposed surfaces owing to distinct sites of cross-linking. Prior to amine-targeted cross-linking, the solvent-exposed cysteine residues of the THIOMAB were fluorescently labeled using a maleimide derivative of Alexa 488.

As a third model system, a bsAb was created using controlled Fab-arm exchange (cFAE), which involves the co-incubation under reducing conditions of parental Abs harboring complementary mutations that drive bsAb formation.[24] Full formation of bsAb from parental Abs was verified by hydrophobic interaction chromatography, where a single peak corresponding to bsAb was observed between the peaks for parental Abs (**Figure 2.3**). Because the Abs used for creation of bsAb did not contain engineered cysteine residues, they were instead labeled at primary amines groups using Alexa 488 N-hydroxysuccinimide (NHS) ester. After labeling, glutaraldehyde was added to cross-link molecules of bsAb at unreacted amines (**Figure 2.1C**). As with glutaraldehyde cross-linked THIOMAB, this sample is expected to have significant heterogeneity in the site of cross-linking as well as oligomer shape.

The type of linkage for cross-linked samples was verified by non-reducing and reducing SDS-PAGE (**Figure 2.4**). Any covalent oligomer that can be reduced to heavy and light chain with DTT was likely oligomerized via inter-Ab disulfide bonds. Thus, the copper-oxidized sample was expected to be fully dissociated in the presence of 50 mM dithiothreitol (DTT) due to reduction of

intra- and inter-Ab disulfide bonds. Conversely, the glutaraldehyde cross-linked samples contain non-reducible linkages between Ab heavy and light chains. Indeed, addition of DTT converted $CuSO_4$-oxidized THIOMAB to free heavy chain (50 kDa) and light chain (25 kDa) while the oligomers formed with glutaraldehyde still contained larger species corresponding to irreversibly linked Ab domains.

After cross-linking and labeling, different oligomeric states of Ab were purified using size-exclusion chromatography (SEC). The purified fractions were run on non-reducing SDS-PAGE to visualize the purity of oligomeric standards (**Figure 2.5**). For each preparation of cross-linked Ab, a distribution of oligomeric states was obtained with small oligomers being the most abundant. While the disulfide-linked sample contained mostly monomeric and dimeric Ab, the glutaraldehyde cross-linked samples also contained larger oligomeric species. Thus, monomer and dimer molecules were isolated from the $CuSO_4$-treated mixture, while monomer, dimer, trimer, and a mixture of larger oligomers were purified from glutaraldehyde-treated Abs. Densitometry of electrophoretic gels revealed the proportion of each oligomer in the purified fractions (**Table 2.1**). Monomer and dimer fractions were >75% pure while larger oligomers were significantly more heterogeneous. It is important to note that monomers purified from the cross-linking reactions were used for FCS experiments, rather than using the unreacted monomer. In the case of the chemically cross-linked samples, both the monomer and the oligomers may be coupled to molecules of glutaraldehyde that did not react with other molecules of Ab but that may have reacted with the Tris used to quench the reaction. In addition to separating the different oligomers, SEC was also useful for removing unreacted molecules of free dye and cross-linking reagents.

Gel filtration was used to estimate the size of species in the larger oligomer fractions (**Figure 2.6**). Based on their known masses and measured retention times, fractions of monomer,

dimer, and trimer from glutaraldehyde cross-linked THIOMAB and monomer and dimer from cross-linked bsAb fell close to a calibration curve generated using gel filtration standards. The retention time of larger oligomer fractions was then used to estimate the size of these species. For glutaraldehyde cross-linked THIOMAB, the larger oligomers were roughly consistent with a hexameric species, having a calculated mass of 840 kDa and estimated aggregation state of 5.60. Large oligomers of bsAb were found to correspond roughly to pentamers based on a calculated mass of 728 kDa which is 4.85 times that of monomer.

2.3.2 Benchmarks of viscosity

The diffusion of a labeled particle is dependent not only on the size of the particle, but also on the viscosity of the medium in which it is diffusing.[25,26] Therefore, transferring Ab from buffer to serum results in an increased τ_D simply due to the higher viscosity of the serum. To control for the viscosity of the medium, a buffer was prepared to have the same viscosity as fetal bovine serum (FBS). By comparing the τ_D of an Ab in FBS with that in the viscosity-matched buffer, it is possible to determine whether any changes in hydrodynamic properties have occurred; in particular, whether Abs have formed interactions with serum components or other molecules of Ab.

The dynamic viscosity, which is independent of density, was determined for Tris buffer and FBS at 20 ºC. As expected, the Tris buffer had a significantly lower viscosity than that of FBS (1.0294 ± 0.0006 cP and 1.3657 ± 0.0010 cP, respectively). To account for the effect of viscosity on diffusion properties, a solution containing 9.90% glycerol (v/v) in Tris buffer was prepared that matched the viscosity of FBS but lacked protein. The glycerol-containing buffer had a viscosity of 1.3658 ± 0.0014 cP, which is well within experimental error of the measured viscosity of serum.

2.3.3 Diffusion of Ab oligomers in buffer and serum

FCS is a sensitive single-molecule/small-ensemble technique that reports on the

hydrodynamic properties of fluorescent particles based on how rapidly they diffuse through the ~1 fL observation volume of a confocal microscope. An increase in a particle's diffusion time (τ_D) may result from an increase in complex size (as occurs during binding or aggregation) or a decrease in compactness (as occurs during unfolding). Independent of the diffusion time, FCS also reports on the brightness per particle, an orthogonal measure of aggregation state. Thus, FCS is well-suited for determining whether Ab oligomers have altered hydrodynamic properties in serum compared to viscosity-matched buffer. Any increase in τ_D above that seen in the matched buffer would suggest that labeled Abs are associating with proteins present in the serum sample, or undergoing self-association that is facilitated by the crowded environment of the serum.

The τ_D of labeled Ab oligomers was determined after dilution into simple Tris buffer, high-viscosity glycerol buffer, and FBS. Oligomers were diluted for FCS analysis so that the final solution contained >99% of the appropriate medium. FCS autocorrelation curves of glutaraldehyde cross-linked THIOMAB (**Figure 2.7**) demonstrate that Abs diffuse more slowly in high-viscosity glycerol buffer than in simple Tris buffer based on a shift of the curve to longer lag times. Interestingly, the autocorrelation curves of monomeric, dimeric, and trimeric THIOMAB (**Figure 2.7B-D**) appeared very similar between glycerol buffer and FBS, suggesting that small oligomers do not associate significantly with the serum. However, larger THIOMAB oligomers (**Figure 2.7F**) showed an increase in τ_D in FBS compared to buffers based on the shift in autocorrelation to longer lag times. The clearest example of serum associations was seen with the reactive Alexa 488 maleimide (**Figure 2.7A**), which exhibited a modest increase in τ_D from Tris buffer to glycerol buffer and a large increase in τ_D upon dilution into FBS. The significant right-shift of the curve in FBS indicates that molecules of free dye interact covalently with serum proteins through reaction to cysteine residues. When the reactive maleimide was first inactivated with 2-

mercaptoethylamine, the autocorrelation curve in FBS was similar to that in glycerol buffer.

In order to calculate τ_D values from autocorrelation curves, a three-dimensional diffusion equation was fit to the data. Fits were significantly improved by using a two-component model, suggesting that some samples contained residual molecules of free dye (**Figure 2.7E, F**). Thus, one τ_D was fixed at the value of passivated free dye in the appropriate medium and the other τ_D was a fitted parameter. Diffusion times for Ab oligomers in Tris buffer, glycerol buffer, and FBS are plotted in **Figure 2.8** with a data point shown for each individual replicate. All dye and Ab samples experienced slightly slower diffusion in glycerol buffer than in Tris buffer due to the viscosity effect. As previously noted, both maleimide and NHS esters of free Alexa 488 had significantly longer τ_D values in FBS than in either buffer as a result of covalent reaction with serum proteins. Dyes passivated with 2-mercaptoethylamine or Tris did not show this increase in τ_D, demonstrating that significant non-covalent interactions did not occur.

For disulfide-linked THIOMAB, there was a small increase in τ_D from monomer to dimer in each of the media examined. These THIOMAB monomers and dimers showed similar τ_D values in glycerol buffer and FBS, indicating that long-lived serum interactions did not occur. Diffusion times of glutaraldehyde cross-linked THIOMAB oligomers were similar to those of copper-oxidized THIOMAB oligomers, and did not vary greatly with environment. Although larger oligomers appeared to have longer τ_Ds, the differences were within experimental error.

A similar pattern was observed with glutaraldehyde cross-linked bsAb for which the τ_D again increased with the size of the oligomer and with the viscosity of the medium. There was a large variability in the τ_D when large oligomers were placed into FBS, which likely results from the tendency of large oligomers to interact with serum components. The crude mixture of cross-linked bsAb oligomers was analyzed and was similar to the sample of monomer. Since the mixture

contained mostly monomer and small amounts of larger oligomers, this result is not unexpected.

The FCS results are summarized quantitatively in **Table 2.2**. In accordance with the autocorrelation data, the τ_Ds were longer in FBS and glycerol buffer than they were in Tris buffer. To determine whether different oligomers interacted with the serum, the τ_D values of each oligomer in glycerol buffer and FBS were compared. Since the viscosities of these two media were the same, any differences in τ_D indicate serum-induced interactions. Interestingly, glutaraldehyde cross-linked THIOMAB dimer and hexamer and glutaraldehyde cross-linked bsAb dimer and trimer appeared significantly larger ($P < 0.05$) in FBS than in glycerol buffer. This result suggests that glutaraldehyde-generated oligomers in general are more likely to interact with serum than the more homogeneous disulfide-linked oligomers. Furthermore, the pentamer fraction of glutaraldehyde cross-linked bsAb was quite different ($P < 0.001$) in these two media. Such a difference in τ_D indicates that these large oligomers behave distinctly in the serum environment than in simple buffers. The implication is that oligomers larger than trimers may experience serum interactions, but that aggregation is dependent upon Ab framework.

(2.3.4 Antibody-antigen binding in buffer and serum

2.4 Discussion

Small amounts of subvisible or submicron aggregates are present in many preparations of therapeutic antibodies and related platforms.[27] However, the behavior of small oligomers in serum or tissue is not well characterized and their interactions with serum components, or with each other, could impact their clearance, their immunogenicity, and their efficacy. To assess the tendency of small aggregates to further oligomerize in serum, or to interact with serum components, we prepared fluorescently labeled standards of defined oligomer composition and applied FCS to monitor changes in apparent size in serum versus viscosity-matched buffers

The use of a two-component model was required since a single component could not adequately describe the data in all cases. Particularly for the larger oligomers, there was a significant contribution to the autocorrelation from a free dye component. Although all samples were purified by SEC prior to analysis, it is likely that the hydrophobic dye molecules were selectively trapped in larger oligomer fractions. After dilution of Abs for FCS analysis, the non-covalently bound dye could dissociate from the protein component. A measurable contribution from free dye is not uncommon in FCS experiments, and is routinely dealt with using two-component fitting as employed here.[28,29] Although some samples likely contained free dye, monomeric Ab, and large aggregate, it was not possible to use a three-component model without overfitting.

Based on measured τ_D, the following equations can be used to calculate the hydrodynamic radius (R_H) of a particle:

$$R_H = \frac{k_B T}{6\pi\eta D} \qquad\qquad D = \frac{r^2}{4\tau_D}$$

where k_B is the Boltzmann constant, T is the absolute temperature, η is the viscosity, D is the translational diffusion coefficient, and r is the short axis of the focal volume. Using the measured τ_D of 0.24 ms for Alexa 488 NHS ester along with its diffusion coefficient from the literature allows for calculation of the r parameter for this experimental setup.[30] Then, the average τ_D of 2.52 ms for all Ab monomer samples yields a R_H of 54 Å, which is in good agreement with other reported values of 55-56 Å obtained by FCS.[31,32] The increase in τ_D from Ab monomers to dimers was subtle but within the precision of the method, averaging just a 1.14-fold increase in apparent size. This similarity in diffusion properties for distinct oligomeric states is expected, since a given change in mass will cause a much smaller change in diffusion. For globular proteins the τ_D is proportional to the cube root of the particle's mass, meaning that a doubling of mass from

monomer to dimer would cause only a 1.26-fold increase in τ_D.[17] Because antibodies are not perfectly spherical, it is reasonable to expect an even smaller change in diffusion if dimerization results in a more compact shape. Studies on unstressed Abs by analytical ultracentrifugation have yielded R_H values of 54 Å and 62 Å for monomer and compact dimer, respectively, which match the values of 54 Å and 61 Å obtained here by FCS.[33] Thus, the modest differences in diffusion properties between oligomeric fractions are fully consistent with changes in their apparent sizes.

Abs experienced slower diffusion in serum or glycerol-containing buffer than in Tris buffer, consistent with the more viscous environment. In fact, τ_D values increased overall 1.31-fold from Tris buffer to glycerol buffer, consistent with the 1.33-fold difference in viscosity. Across the oligomers tested, diffusion was slightly slower in FBS than in glycerol buffer. This trend may represent weak or transient interactions between labeled Abs and proteins in the serum. Significant differences ($P < 0.05$) between these two media were only seen, however, for certain samples of glutaraldehyde cross-linked Ab. Because glutaraldehyde modifies the Ab surface in addition to cross-linking, it was not entirely unexpected that Abs incubated with the agent would interact more with the serum. For instance, single molecules or polymers of glutaraldehyde could react with nucleophilic Ab side chains to introduce strands of glutaraldehyde or Tris-capped glutaraldehyde, in addition to the inter- and intra-Ab cross-links. These surface modifications add more area to the Abs that may interact with molecules in the serum. Consistent with this hypothesis, the τ_D of THIOMAB monomer reacted with $CuSO_4$ (an unmodified Ab monomer) was lower than that of THIOMAB monomer or bsAb monomer that was reacted with glutaraldehyde. Thus, while all Ab oligomers showed serum-induced differences in diffusion, these differences were only significant when the Ab contained surface modifications from the glutaraldehyde cross-linking step. Alternatively, the higher incorporation of dye for the glutaraldehyde cross-linked

samples could have increased serum interactions by the additive effects of several weak dye-serum interactions. In either case, the result has implications for antibody-drug conjugates prepared via lysine coupling, which frequently contain more than two drug-linker moieties that presumably provide a source of nonspecific interactions with serum proteins analogous to those proposed here for glutaraldehyde.[34]

However, the difference between Ab diffusion in glycerol and FBS was far more significant ($P < 0.001$) for the large oligomer fraction of bsAb despite a large increase in variability for this sample. This substantial increase in τ_D suggests interactions with serum beyond those caused by surface decoration with glutaraldehyde adducts. Larger Ab oligomers may form stronger or longer-term interactions with serum components simply due to their increased surface area. Partial unfolding may be increased in certain large oligomers to accommodate inter-Ab linkages, and this could introduce the opportunity for hydrophobic oligomer-serum interactions. Likewise, bridging flocculation from the domains present in the larger oligomers could result in serum component interactions.[35] Besides interacting directly with components of FBS, it is also possible that serum facilitates the self-association of large Ab oligomers via the excluded volume effect.[36] The possibility that multiple weakly interacting dye molecules could cause serum association through an avidity effect was considered, and would be possible for the THIOMAB hexamers that contained ~12 dye molecules per molecule of hexamer. However, for bsAb samples the pentamer fraction contained fewer dye molecules than the dimer fraction (~4 and ~3, respectively), while the pentamer had slower diffusion than the dimer in serum. Thus, the serum interactions observed for this sample were protein- rather than dye-mediated.

It is notable that large oligomers of the bsAb showed slower diffusion in FBS than in buffer, while this shift did not occur for similarly sized oligomers of THIOMABs generated by the same

cross-linking method. A likely explanation is that serum interactions are dependent upon the variable region of the Ab. It is known that differences in Fab sequence can cause substantial changes in melting temperature which are related to stability.[37] Thus, if either Fab from the bsAb is inherently more prone to unfolding or aggregation than the Fab from the THIOMAB, the bsAb may have slower diffusion. This effect would be accentuated at large oligomer states in which the molecules become multivalent for each Fab. An alternative explanation is that the framework plays a role, and that bsAbs in general experience more serum interactions than mAbs. But because bsAbs generated by cFAE contain only two point mutations that minimally affect biophysical properties and stability, the variable region is perhaps the more feasible cause for the difference in diffusion.[38]

These studies highlight the utility of FCS as a means of assessing protein aggregation and other association events in biological media such as the serum. Although FCS is useful for monitoring a specific protein within complex mixtures, there is concern that the hydrophobic dye molecule could accelerate aggregation or otherwise alter Ab properties. In fact, the Ab-dye conjugates used here are in many ways similar to antibody-drug conjugates, which are known to have altered properties relative to naked Abs.[34] To minimize dye-induced changes, the average incorporation of dye was kept below two molecules for each molecule of Ab. Previous studies have shown no significant differences between naked and Alexa 488-labeled Abs with a dye:Ab ratio of 2 by SEC, nanoparticle tracking analysis, and light obscuration.[15] This is consistent with the FCS result showing that free dye interacts with serum only when it contains a reactive moiety for covalent modification. If dye molecules did significantly alter the properties of the Abs, then higher dye:Ab ratios would be expected to yield larger τ_D values by FCS. However, dye incorporation was slightly lower for higher order oligomers (possibly due to competition of cross-

linking and labeling chemistries) and it was these oligomers that showed the slowest diffusion.

Taken together, these experiments demonstrate that a range of soluble Ab oligomers generated with distinct cross-linking strategies experience slower diffusion in the serum than would be expected based on viscosity. This finding suggests that Abs in general interact transiently with components of the serum. Based on increases in average τ_D and variability, nanometer-scale soluble oligomers estimated as bsAb pentamer aggregate in serum to a greater extent than bsAb monomers, dimers, and trimers. Although this aggregation phenomenon was shown to be Ab-dependent, it implies that oligomerization results in significant hydrodynamic changes only after a certain size threshold is exceeded. Thus, the time- and cost-intensive practice of removing all traces of dimer may be unnecessary in terms of preventing adverse reactions. On the other hand, there are important pharmacokinetic and immunological responses that depend on the size and conformation of administered proteins which have not been investigated here. For example, submicron Ab aggregates (0.1-1 μm) may have altered distribution compared to monomers and micron oligomers, and small native-like oligomers (10-40 nm) have been shown to be more immunogenic than monomer or micron-sized aggregates.[39,40] As the large bsAb oligomers generated here exhibited altered diffusion in FBS (forming aggregates of 6-50 nm), these findings may suggest a correlation between serum interactions and immunogenicity. But while techniques like FCS are useful for detecting serum-induced changes in protein behavior, more work is needed to elucidate the precise causes and mechanisms of aggregate-induced immunogenicity.

FIGURES

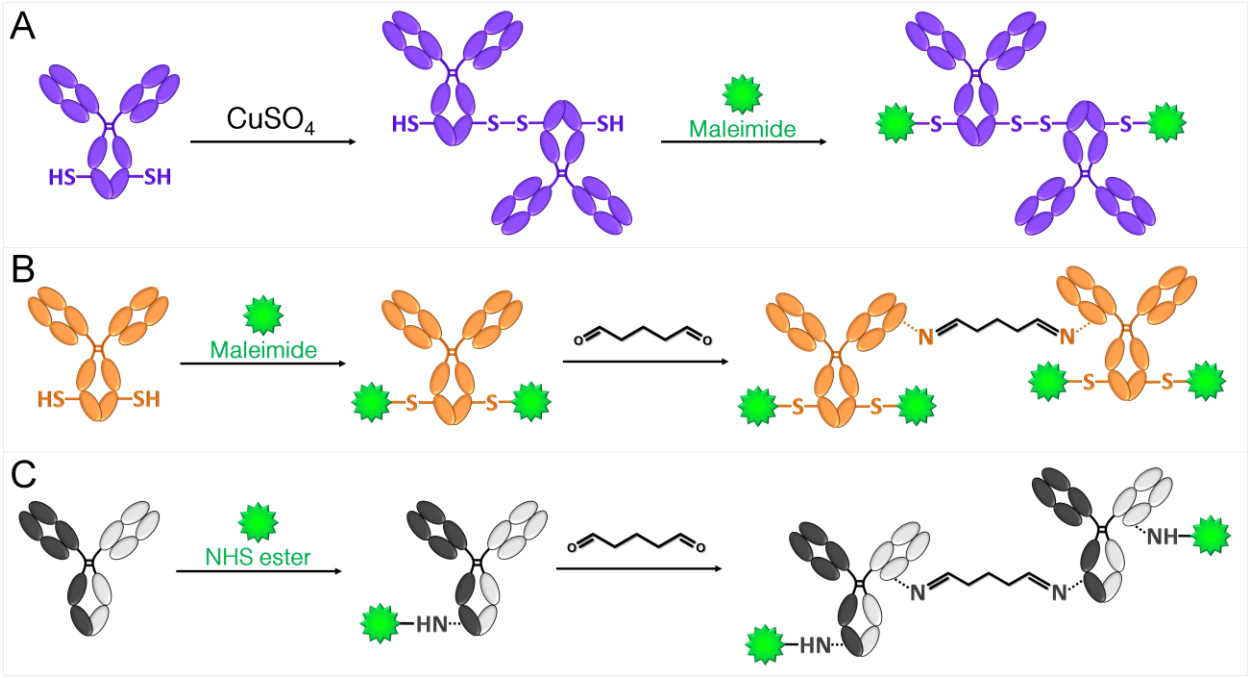

Figure 2.1: Preparation of covalent Ab oligomers. (A) THIOMAB was oxidized with $CuSO_4$ to induce inter-Ab disulfide bonds and then labeled at remaining reduced cysteines using Alexa 488 maleimide. (B) THIOMAB was labeled with Alexa 488 maleimide and subsequently cross-linked with glutaraldehyde to create larger oligomers. (C) A sample of bsAb was labeled with Alexa 488 NHS ester and then cross-linked with glutaraldehyde. Green stars represent molecules of Alexa 488 and dashed lines denote cross-linking through undefined sites on the Abs.

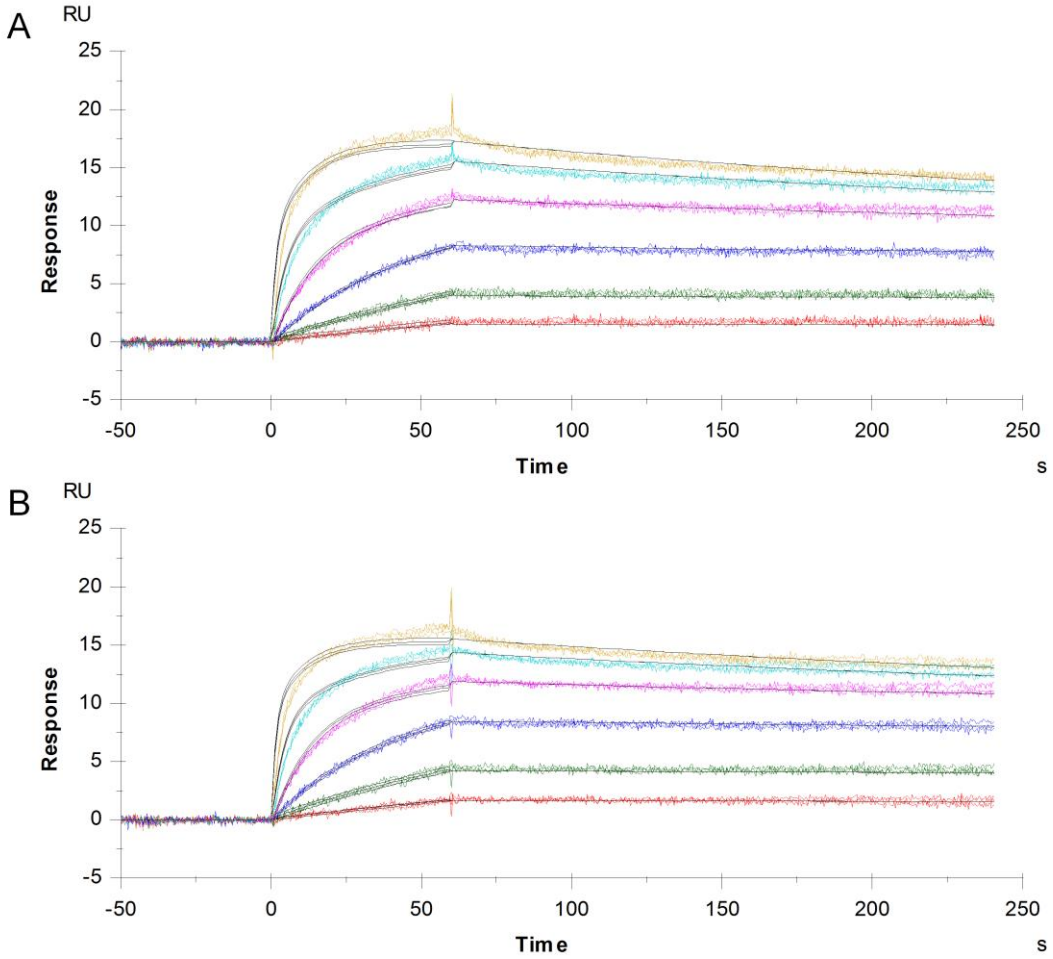

Figure 2.2: Surface plasmon resonance using a Biacore T100 shows surface-bound capped (A) or uncapped and Alexa 488-labeled (B) THIOMAB binding to protein A (ThermoFisher, 21181) in solution at 10 nm (red), 30 nM (green), 90 nM (blue), 270 nM (magenta), 810 nM (cyan), and 2.43 μM (yellow). THIOMAB was immobilized to ~85 RU onto a CM5 chip in 10 mM acetate buffer, pH 5.5 and protein A was flowed over at 50 μL/min for 60 seconds followed by a 180-second wash using 1x DPBS pH 7.2 with 0.1% casein and 0.05% Tween 20 as the running buffer. Regeneration was achieved with a 20-second pulse of 10 mM glycine pH 3.0 at 20 μL/min followed by a 5-minute stabilization in running buffer. After double subtraction (reference flow cell and zero protein A), triplicate traces were globally fit to the heterogeneous ligand model in Biacore Evaluation software where the major K_D was 84.1 ± 11.5 nM for capped THIOMAB and 75.4 ± 19.2 nM for uncapped and A488-labeled THIOMAB. The other component K_Ds were in the femtomolar range and had less contribution, so were deemed less important for the sake of this comparison.

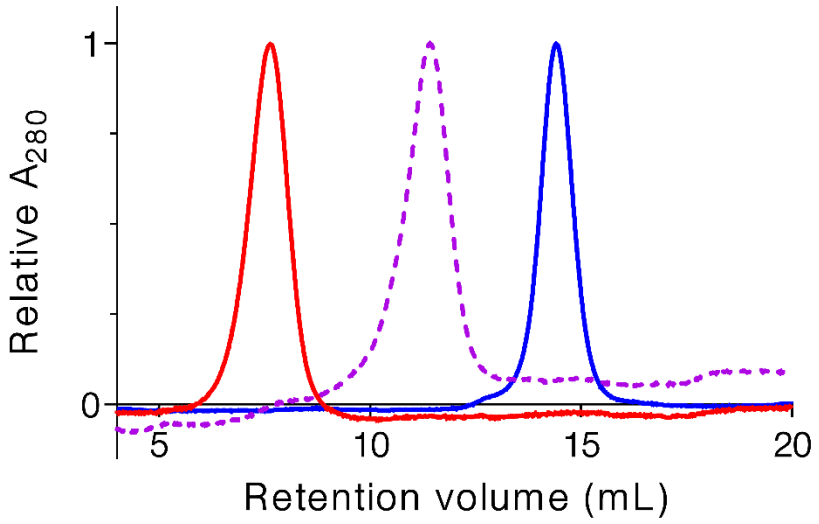

Figure 2.3: Hydrophobic interaction chromatography shows formation of bsAb (purple dashed trace) after five-hour incubation of anti-RSV F405L (blue solid trace) and anti-gp120 K409R (red solid trace) with 75 mM MEA. HPLC was performed with a TSKgel Ether-5PW column (Tosoh, 08641) at 0.5 mL/min using a gradient from 1.5 M (buffer A) to 0 M (buffer B) ammonium sulfate in 0.1 M sodium phosphate, pH 6.5. Abs were separated using a 40-minute gradient from 25 to 50% buffer B.

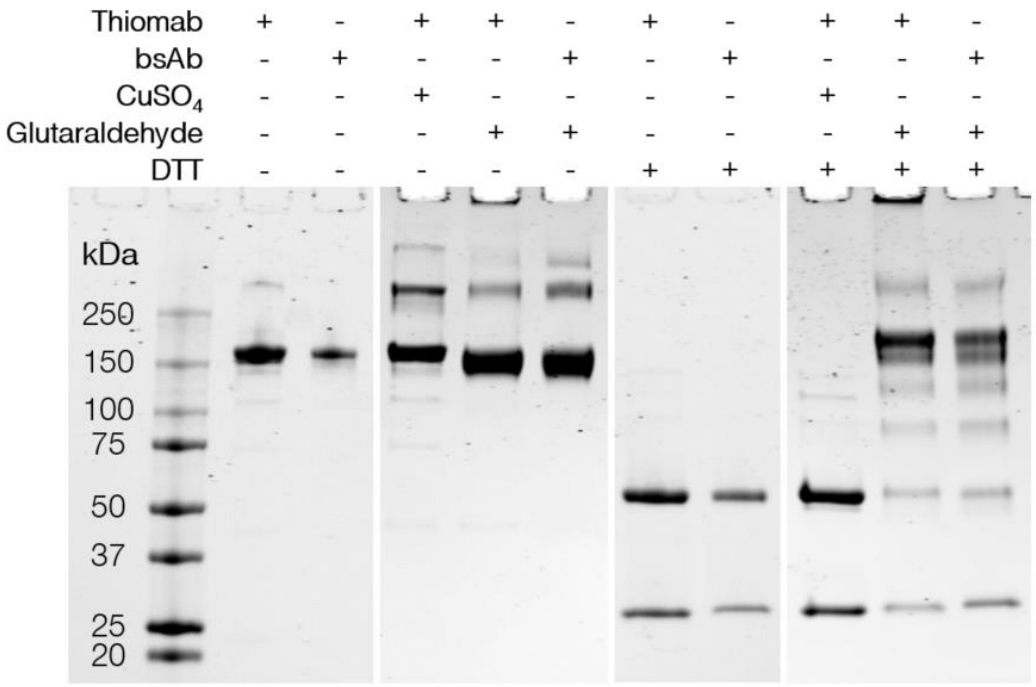

Figure 2.4: SDS-PAGE of Ab oligomers reveals the chemical nature of cross-links. THIOMAB oligomers induced by oxidation with $CuSO_4$ were dissociated to heavy and light chains with addition of 50 mM DTT to the sample loading buffer. Glutaraldehyde cross-linked samples retain heavier species in the presence of DTT, indicative of non-reducible linkages.

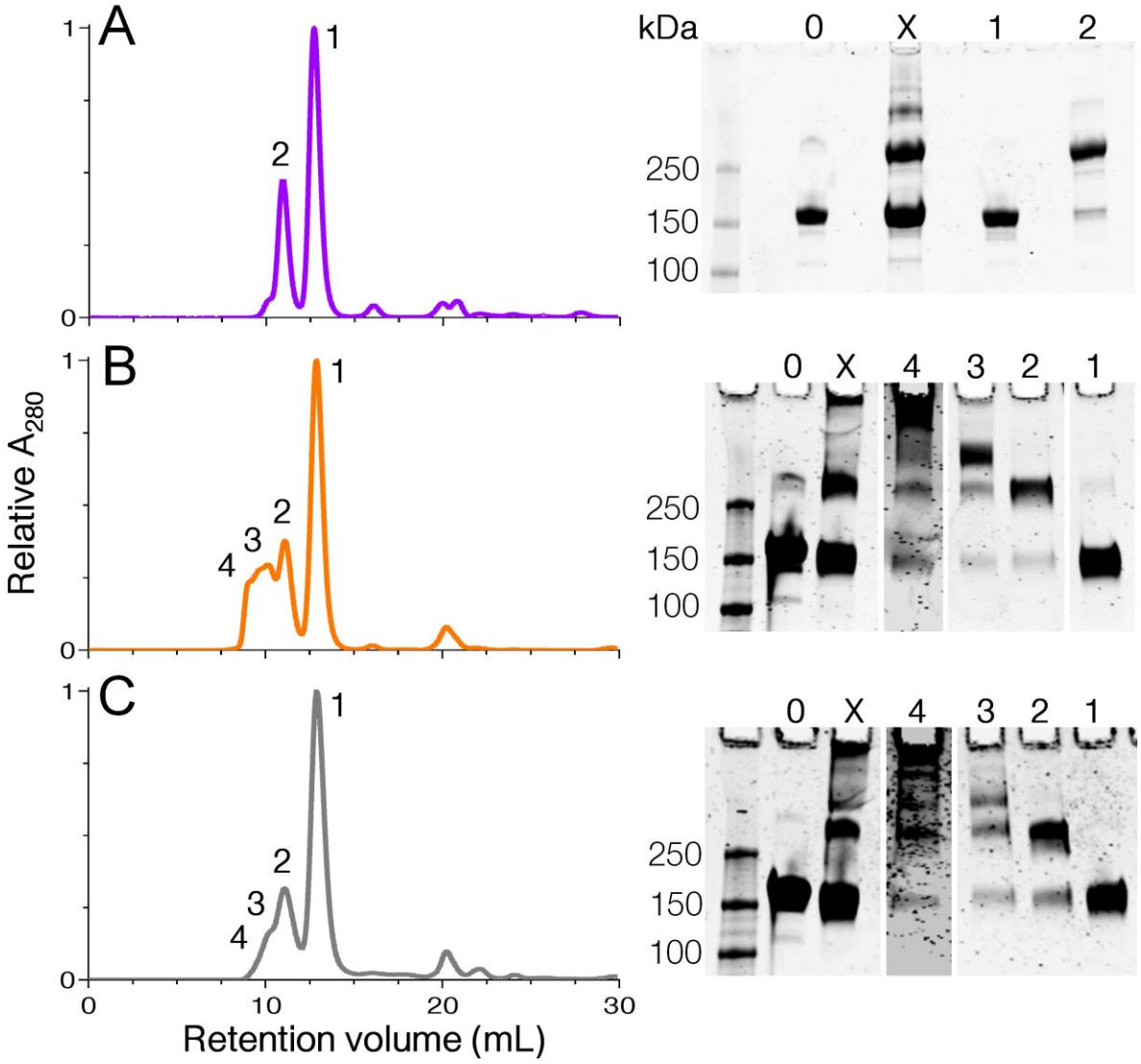

Figure 2.5: Size-exclusion chromatograms plotted as normalized absorbance at 280 nm (left) and non-reducing SDS-PAGE gels (right) showing the purification of disulfide-linked THIOMAB (A), glutaraldehyde cross-linked THIOMAB (B), and glutaraldehyde cross-linked bsAb (C) oligomers. Monomer (1) and dimer (2) fractions were purified for all samples, while trimer (3) and larger oligomer (4) fractions were also obtained for glutaraldehyde cross-linked Abs. Gels include lanes for unreacted Ab (0) and the cross-linked reaction mixture (X). For the large oligomer fractions, contrast was increased compared to other lanes to resolve faint bands.

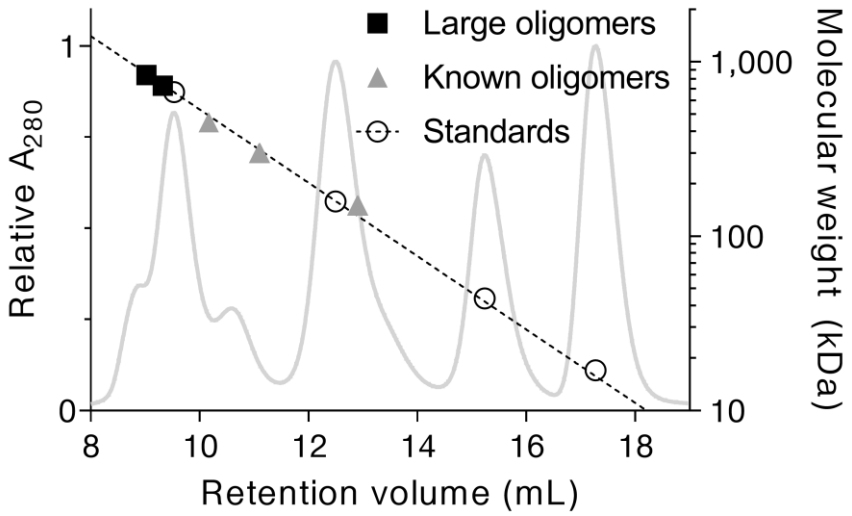

Figure 2.6: SEC calibration curve generated from gel filtration standards (open circles) was used to estimate the size of larger oligomers (black closed squares) as roughly hexamer (THIOMAB) and pentamer (bsAb). Known Ab oligomers are shown for comparison (gray closed triangles) and include glutaraldehyde cross-linked THIOMAB monomer, dimer, and trimer, and glutaraldehyde cross-linked bsAb monomer and dimer. The monomer and dimer points overlap for the different Ab samples. Standards include bovine thyroglobulin (670 kDa), bovine γ-globulin (158 kDa), chicken ovalbumin (44 kDa), and horse myoglobin (17 kDa).

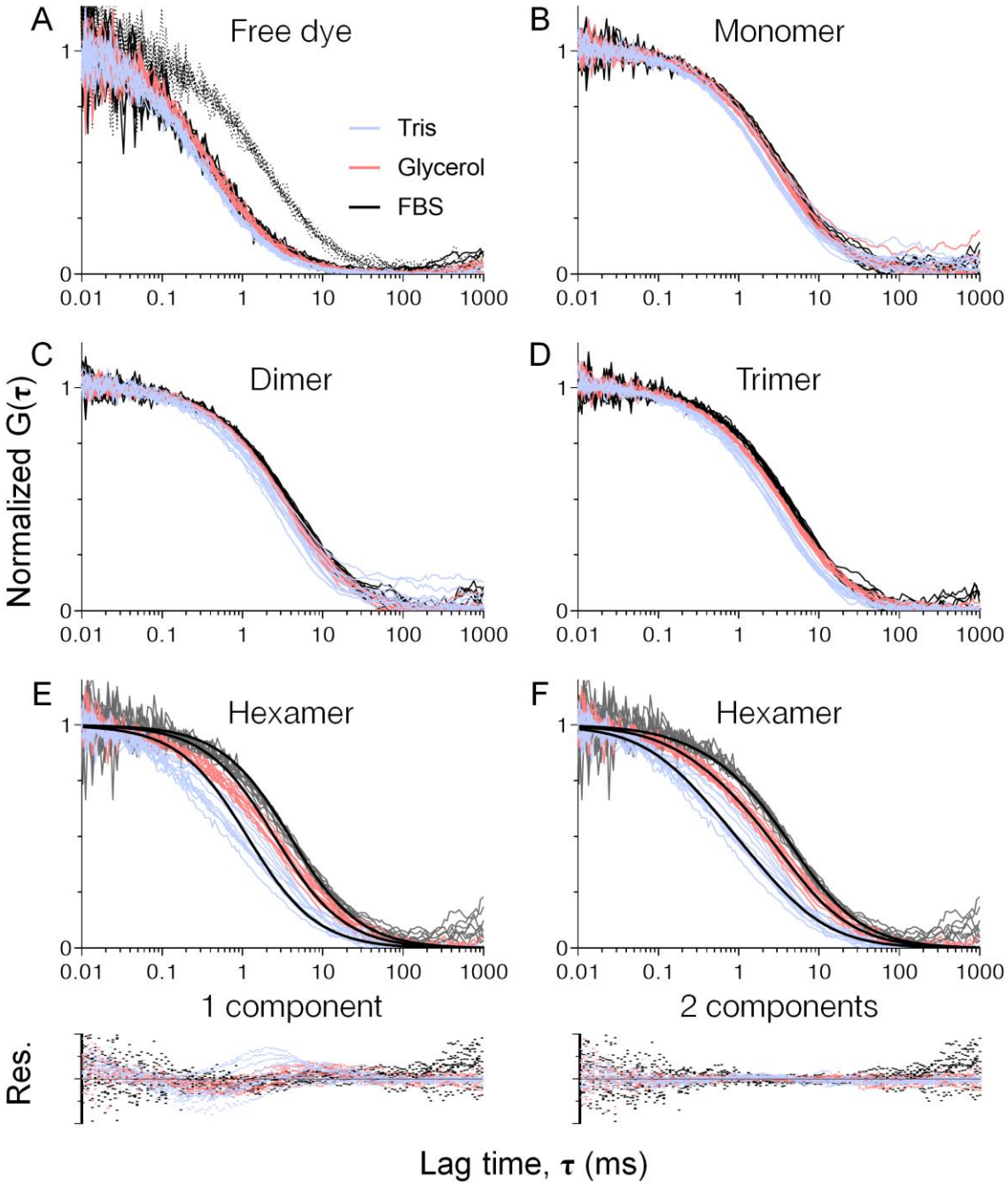

Figure 2.7: Normalized FCS autocorrelations of free Alexa 488 maleimide (A) and glutaraldehyde-reacted THIOMAB monomer (B), dimer (C), and trimer (D) in Tris buffer (blue), glycerol buffer (red), and FBS (black). Free dye in FBS is shown as Alexa 488 maleimide that was inactivated with 2-mercaptoethylamine (black solid lines) and as the reactive maleimide (black dotted lines). The autocorrelations of the larger oligomer fraction are plotted along with one- (E) and two-component (F) fits; lower panels show fit residuals. Ten replicates are overlaid for each oligomer/media combination.

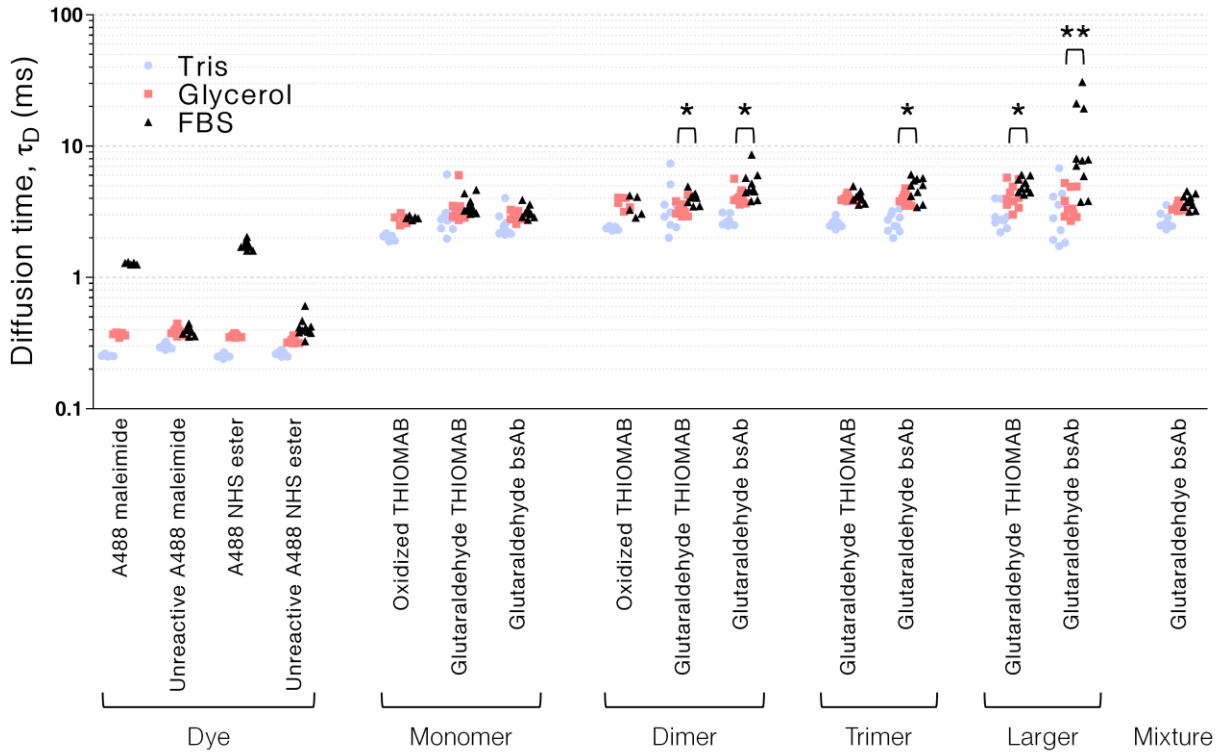

Figure 2.8: Diffusion times resulting from fits of FCS autocorrelation to a two-component model (with one τ_D fixed to that of chemically passivated free dye in the appropriate medium). Purified oligomers of disulfide-linked THIOMAB, glutaraldehyde cross-linked THIOMAB, and glutaraldehyde cross-linked bsAb were analyzed in a simple Tris buffer (blue circles), glycerol-containing buffer (red squares), and FBS (black triangles). Free Alexa 488 was tested as the reactive maleimide and NHS ester derivatives and after inactivating with 2-mercaptoethylamine or Tris. Significant differences in diffusion time between a given Ab oligomer in glycerol buffer and FBS are indicated (* $P < 0.05$, ** $P < 0.001$).

TABLES

Table 2.1: Purity of oligomer fractions assessed by SDS-PAGE densitometry

Sample	Fraction	% Monomer	% Dimer	% Trimer	% ≥Tetramer
Disulfide THIOMAB	Monomer	**99**	1	--	--
	Dimer	13	**83**	4	--
Glutaraldehyde THIOMAB	Monomer	**97**	3	--	--
	Dimer	16	**83**	1	--
	Trimer	11	20	**67**	3
	Hexamer	6	5	3	**86**
Glutaraldehyde bsAb	Monomer	**99**	1	--	--
	Dimer	22	**77**	1	--
	Trimer	24	40	**33**	3
	Pentamer	16	17	13	**55**

Table 2.2: Average diffusion times (ms) ± standard deviation of Ab oligomers reported by FCS

Sample	Fraction	Tris	Glycerol	FBS
Disulfide THIOMAB	Monomer	2.02 ± 0.12	2.78 ± 0.24	2.85 ± 0.08
	Dimer	2.37 ± 0.08	3.68 ± 0.38	3.50 ± 0.62
Glutaraldehyde THIOMAB	Monomer	3.02 ± 1.14	3.41 ± 0.95	3.57 ± 0.55
	Dimer	3.56 ± 1.58	3.39 ± 0.42	4.07 ± 0.43 *
	Trimer	2.62 ± 0.18	4.03 ± 0.19	4.14 ± 0.41
	Hexamer	3.04 ± 0.69	4.26 ± 0.92	5.08 ± 0.64 *
Glutaraldehyde bsAb	Monomer	2.52 ± 0.59	2.93 ± 0.22	3.17 ± 0.35
	Dimer	2.69 ± 0.23	4.17 ± 0.60	5.15 ± 1.41 *
	Trimer	2.66 ± 0.44	4.03 ± 0.39	4.87 ± 0.92 *
	Pentamer	3.31 ± 1.56	3.71 ± 0.96	11.6 ± 9.1 **

* $P < 0.05$ between glycerol buffer and FBS

** $P < 0.001$ between glycerol buffer and FBS

2.5 References

[1] Smith, A. J. (2014) New horizons in therapeutic antibody discovery: opportunities and challenges versus small-molecule therapeutics. *J. Biomol. Screen. 20*, 437–453.

[2] Thakur, A., and Lum, L. G. (2016) "NextGen" biologics: bispecific antibodies and emerging clinical results. *Expert Opin. Biol. Ther. 16*, 675–688.

[3] Sievers, E. L., and Senter, P. D. (2013) Antibody-drug conjugates in cancer therapy. *Annu. Rev. Med. 64*, 15–29.

[4] Rosenberg, A. S. (2006) Effects of protein aggregates: an immunologic perspective. *AAPS J. 8*, E501–E507.

[5] Ratanji, K. D., Derrick, J. P., Dearman, R. J., and Kimber, I. (2013) Immunogenicity of therapeutic proteins: influence of aggregation. *J. Immunotoxicol. 11*, 99–109.

[6] Ahmadi, M., Bryson, C. J., Cloake, E. A., Welch, K., Filipe, V., Romeijn, S., Hawe, A., Jiskoot, W., Baker, M. P., and Fogg, M. H. (2015) Small amounts of sub-visible aggregates enhance the immunogenic potential of monoclonal antibody therapeutics. *Pharm. Res. 32*, 1383–1394.

[7] Hermeling, S., Crommelin, D. J. A., Schellekens, H., and Jiskoot, W. (2004) Structure-immunogenicity relationships of therapeutic proteins. *Pharm. Res. 21*, 897–903.

[8] Beurskens, F. J., van Schaarenburg, R. A., and Trouw, L. A. (2015) C1q, antibodies and anti-C1q autoantibodies. *Mol. Immunol. 68*, 6–13.

[9] Diebolder, C. A, Beurskens, F. J., de Jong, R. N., Koning, R. I., Strumane, K., Lindorfer, M. A., Voorhorst, M., Ugurlar, D., Rosati, S., Heck, A. J. R., van de Winkel, J. G. J., Wilson, I. A., Koster, A. J., Taylor, R. P., Saphire, E. O., Burton, D. R., Schuurman, J., Gros, P., and Parren, P. W. H. I. (2014) Complement is activated by IgG hexamers assembled at the cell surface. *Science 343*, 1260–1263.

[10] Luo, Y., Lu, Z., Raso, S. W., Entrican, C., and Tangarone, B. (2009) Dimers and multimers of monoclonal IgG1 exhibit higher in vitro binding affinities to Fcγ receptors. *MAbs 1*, 491–504.

[11] Food and Drug Administration Center for Biologics Evaluation and Research (2014) Guidance for industry: immunogenicity assessment for therapeutic protein products. Silver Spring, MD.

[12] Keizer, R. J., Huitema, A. D. R., Schellens, J. H. M., and Beijnen, J. H. (2010) Clinical pharmacokinetics of therapeutic monoclonal antibodies. *Clin. Pharmacokinet. 49*, 493–507.

[13] Arvinte, T., Palais, C., Green-Trexler, E., Gregory, S., Mach, H., Narasimhan, C., and Shameem, M. (2013) Aggregation of biopharmaceuticals in human plasma and human serum: Implications for drug research and development. *MAbs 5*, 491–500.

[14] Demeule, B., Shire, S. J., and Liu, J. (2009) A therapeutic antibody and its antigen form different complexes in serum than in phosphate-buffered saline: a study by analytical ultracentrifugation. *Anal. Biochem. 388*, 279–287.

[15] Filipe, V., Poole, R., Oladunjoye, O., Braeckmans, K., and Jiskoot, W. (2012) Detection and characterization of subvisible aggregates of monoclonal IgG in serum. *Pharm. Res. 29*, 2202–2212.

[16] Li, X., Geng, S. B., Chiu, M. L., Saro, D., and Tessier, P. M. (2015) High-throughput assay for measuring monoclonal antibody self-association and aggregation in serum. *Bioconjug. Chem. 26*, 520–528.

[17] Sahoo, B., Drombosky, K. W., and Wetzel, R. (2016) Fluorescence correlation spectroscopy: a tool to study protein oligomerization and aggregation in vitro and in vivo. *Methods Mol. Biol. 1345*, 67–87.

[18] Bulseco, D. A., and Wolf, D. E. (2013) Fluorescence correlation spectroscopy: molecular complexing in solution and in living cells. *Methods Cell Biol. 114*, 489–524.

[19] Bhakta, S., Raab, H., and Junutula, J. R. (2013) Engineering THIOMABs for site-specific conjugation of thiol-reactive linkers. *Methods Mol. Biol. 1045*, 189–203.

[20] Labrijn, A. F., Meesters, J. I., Priem, P., de Jong, R. N., van den Bremer, E. T. J., van Kampen, M. D., Gerritsen, A. F., Schuurman, J., and Parren, P. W. H. I. (2014) Controlled Fab-arm exchange for the generation of stable bispecific IgG1. *Nat. Protoc. 9*, 2450–2463.
[21] Shen, B. Q., Xu, K., Liu, L., Raab, H., Bhakta, S., Kenrick, M., Parsons-Reponte, K. L., Tien, J., Yu, S. F., Mai, E., Li, D., Tibbitts, J., Baudys, J., Saad, O. M., Scales, S. J., McDonald, P. J., Hass, P. E., Eigenbrot, C., Nguyen, T., Solis, W. A., Fuji, R. N., Flagella, K. M., Patel, D., Spencer, S. D., Khawli, L. A., Ebens, A., Wong, W. L., Vandlen, R., Kaur, S., Sliwkowski, M. X., Scheller, R. H., Polakis, P., and Junutula, J. R. (2012) Conjugation site modulates the in vivo stability and therapeutic activity of antibody-drug conjugates. *Nat. Biotechnol. 30*, 184–189.
[22] Cheung, D. T., and Nimni, M. E. (1982) Mechanism of crosslinking of proteins by glutaraldehyde I: reaction with model compounds. *Connect. Tissue Res. 10*, 187–199.
[23] Wine, Y., Cohen-Hadar, N., Freeman, A., and Frolow, F. (2007) Elucidation of the mechanism and end products of glutaraldehyde crosslinking reaction by X-ray structure analysis. *Biotechnol. Bioeng. 98*, 711–718.
[24] Labrijn, A. F., Meesters, J. I., de Goeij, B. E. C. G., van den Bremer, E. T. J., Neijssen, J., van Kampen, M. D., Strumane, K., Verploegen, S., Kundu, A., Gramer, M. J., van Berkel, P. H. C., van de Winkel, J. G. J., Schuurman, J., and Parren, P. W. H. I. (2013) Efficient generation of stable bispecific IgG1 by controlled Fab-arm exchange. *Proc. Natl. Acad. Sci. U. S. A. 110*, 5145–5150.
[25] Zimmerman, S. B., and Minton, A. P. (1993) Macromolecular crowding: biochemical, biophysical, and physiological consequences. *Annu. Rev. Biophys. Biomol. Struct. 22*, 27–65.
[26] Banks, D. S., and Fradin, C. (2005) Anomalous diffusion of proteins due to molecular crowding. *Biophys. J. 89*, 2960–2971.
[27] Philo, J. (2009) A critical review of methods for size characterization of non-particulate protein aggregates. *Curr. Pharm. Biotechnol. 10*, 359–372.
[28] Bahns, J. T., Liu, C. M., and Chen, L. (2004) Characterizing specific phage-protein interactions by fluorescence correlation spectroscopy. *Protein Sci. 13*, 2578–2587.
[29] Krouglova, T., Vercammen, J., and Engelborghs, Y. (2004) Correct diffusion coefficients of proteins in fluorescence correlation spectroscopy. Application to tubulin oligomers induced by Mg^{2+} and Paclitaxel. *Biophys. J. 87*, 2635–2646.
[30] Petrov, E. P., and Schwille, P. (2008) State of the art and novel trends in fluorescence correlation spectroscopy. *Springer Ser. Fluoresc. 6*, 145–197.
[31] Nag, M., Bera, K., and Basak, S. (2015) Intermolecular disulfide bond formation promotes immunoglobulin aggregation: investigation by fluorescence correlation spectroscopy. *Proteins 83*, 169–177.
[32] Jøssang, T., Feder, J., and Rosenqvist, E. (1988) Photon correlation spectroscopy of human IgG. *J. Protein Chem. 7*, 165–171.
[33] Plath, F., Ringler, P., Graff-Meyer, A., Stahlberg, H., Lauer, M. E., Rufer, A. C., Graewert, M. A., Svergun, D., Gellermann, G., Finkler, C., Stracke, J. O., Koulov, A., and Schnaible, V. (2016) Characterization of mAb dimers reveals predominant dimer forms common in therapeutic mAbs. *MAbs 8*, 928–940.
[34] Singh, S. K., Luisi, D. L., and Pak, R. H. (2015) Antibody-crug conjugates: design, formulation and physicochemical stability. *Pharm. Res. 32*, 3541–3571.
[35] Israelachvili, J. N. (1991) Intermolecular and Surface Forces 2nd ed. Academic Press, London.
[36] Zhou, H. X., Rivas, G., and Minton, A. P. (2008) Macromolecular crowding and confinement: biochemical, biophysical, and potential physiological consequences. *Annu. Rev. Biophys. 37*, 375–397.
[37] Ionescu, R. M., Vlasak, J., Price, C., and Kirchmeier, M. (2008) Contribution of variable domains to the stability of humanized IgG1 monoclonal antibodies. *J. Pharm. Sci. 97*, 1414–1426.

[38] Gramer, M. J., van den Bremer, E. T. J., van Kampen, M. D., Kundu, A., Kopfmann, P., Etter, E., Stinehelfer, D., Long, J., Lannom, T., Noordergraaf, E. H., Gerritsen, J., Labrijn, A. F., Schuurman, J., van Berkel, P. H. C., and Parren, P. W. H. I. (2013) Production of stable bispecific IgG1 by controlled Fab-arm exchange: scalability from bench to large-scale manufacturing by application of standard approaches. *MAbs 5*, 962–973.

[39] Kijanka, G., Bee, J. S., Bishop, S. M., Que, I., Löwik, C., and Jiskoot, W. (2016) Fate of multimeric oligomers, submicron, and micron size aggregates of monoclonal antibodies upon subcutaneous injection in mice. *J. Pharm. Sci. 105*, 1693–1704.

[40] Fathallah, A. M., Chiang, M., Mishra, A., Kumar, S., Xue, L., Middaugh, R., and Balu-Iyer, S. V. (2015) The effect of small oligomeric protein aggregates on the immunogenicity of intravenous and subcutaneous administered antibodies. *J. Pharm. Sci. 104*, 3691–3702.

CHAPTER 3

A Combinatorial Approach to the Prediction of Antibody Pharmacokinetics

Note: This chapter was adapted with permission from:
Goulet DR, Watson MJ, Tam SH, Zwolak A, Chiu ML, Atkins WM, Nath A. Toward a Combinatorial Approach for the Prediction of IgG Half-Life and Clearance. *Drug Metab. Dispos*. **2018**, *46*, 1900-1907.

3.1 Introduction

Monoclonal antibodies (mAbs) are an important class of drugs that have proven invaluable for the treatment of cancer, autoimmune disease, and other indications. In 2017, 10 mAb-based drugs were approved by the U.S. Food and Drug Administration, and over 50 mAbs were in late-stage clinical trials.[1] The ability to design a wide range of agonistic or antagonistic drugs that target any soluble or cell-surface antigen, while conserving a well-defined protein scaffold, makes mAbs extremely attractive as therapeutic agents. Engineered mAb-based molecules such as bispecific antibodies and antibody-drug conjugates have introduced novel mechanisms for the treatment of disease.[2,3]

One reason for the success of mAb therapeutics, particularly of the immunoglobulin G (IgG) class, is their slow elimination kinetics. The serum stability of IgG mAbs makes intravenous or subcutaneous administration a feasible approach, as drug can be delivered with a dosing interval of several weeks. The biological mechanism for the slow clearance of IgGs relies on escape from lysosomal degradation by binding to the neonatal Fc receptor (FcRn) via the crystallizable fragment (Fc) of the mAb constant region.[4,5] When serum proteins are pinocytosed by endothelial cells for lysosomal proteolysis, the acidic pH of the endosome (pH <6.5) allows IgG mAbs to bind FcRn located in the endosomal membrane. The complex is then trafficked back to the cell surface, where mAbs are released at the neutral pH (pH 7.4) of the blood. Thus, the importance of pH-

dependent FcRn binding has long been recognized as an important determinant of IgG half-life.[6]

Although mAbs have an average elimination half-life of several weeks in humans, there is a large variability associated with this parameter. It is not uncommon for IgG mAbs to have half-lives as short as one week or as long as four weeks.[7,8] Mutation of the FcRn binding interface can further broaden the range of IgG clearance parameters.[9] Part of the variation in IgG half-life can be attributed to target-dependent effects, such as receptor-mediated internalization and degradation.[10] However, even mAbs that target soluble antigens and lack receptor-mediated clearance have a wide range of elimination kinetics. A consequence of this variation is the investment in mAb candidates that have sub-optimal pharmacokinetic parameters, which necessitates higher doses or more frequent dosing.

To increase the convenience and cost-effectiveness of mAb therapies, there is a need for predictive models that can accurately determine pharmacokinetic properties before candidates are investigated in animals or humans. Ideally, these models would be based on biophysical parameters that can be readily measured early in the drug pipeline.[11,12] Historically, FcRn binding at endosomal and neutral pH have both been shown to affect mAb elimination, and accounting for the interaction at both pH values may provide more predictive success.[13,14] Thermal stability, and related properties like aggregation propensity, may also affect half-life, though less is known about this possible relationship.[15] While these and other biophysical parameters, such as non-specific binding or electrostatic interactions, may be predictively important, their relative contributions and the underlying mechanistic relationships remain unclear.[16-18]

In this work, we characterized the FcRn binding properties and thermal stability of a panel of IgG1 mAbs and, using the LASSO (least absolute shrinkage and selection operator) machine learning technique, identified the combination of parameters that best correlated with their half-

life and clearance values from the literature.[19] The most important parameters were then used to predict the half-life and clearance of each mAb, revealing that just two biophysical determinants could be used to accurately predict human pharmacokinetics (PK) for this set of mAbs. Crucially, this empirical approach to the problem allows us to identify predictive parameters in an unbiased fashion, and highlights correlations that could guide future mechanistic studies. Predictions could be further improved by refining this approach, perhaps by incorporating and testing some of the many other parameters that have been proposed to affect mAb PK.

3.2 Experimental procedures

3.2.1 Proteins and other materials

Clinical mAbs were obtained through clinical vendors by S.T., Janssen R & D. Size-exclusion chromatography and SDS-PAGE were performed to ensure the integrity of mAbs. Human FcRn with β_2-microglobulin was purchased from Sino Biological (CT009-H08H-50). Presence of both the FcRn α chain and β_2-microglobulin was verified by SDS-PAGE.

3.2.2 Biolayer interferometry

Kinetic experiments were performed at 25 ºC on an Octet RED384 using 96-well half-area plates at 1000 rpm and a total 100 µL per well. First, 2.5 µg/mL His-tagged human FcRn in 1x PBS pH 7.2 (8.10 mM Na_2HPO_4, 1.47 mM KH_2PO_4, 137 mM NaCl, 2.67 mM KCl) was loaded onto Ni-NTA sensor tips for 300 seconds to obtain a response of 2 nm. Two baseline steps were performed for 120 seconds and then 60 seconds by blocking with 1x PBS containing 1% casein (w/v) and 0.05% Tween 20 (v/v) brought to pH 6.0 or pH 7.0 using HCl. A 180-second association phase was performed with 66.7, 16.7, 4.17, and 1.04 nM IgG at pH 6.0 or 6670, 1670, 417, and 104 nM IgG at pH 7.0 (same buffer as in baseline steps). Dissociation was performed for 180 seconds in fresh buffer matching the baseline/association buffer.

Analysis was performed in Octet Data Analysis software version 7. Reference data (mAb binding to tips lacking FcRn) were subtracted from sample data. Association and dissociation data for a given mAb at pH 6.0 were globally fit using the 1:1 model with a linked R_{max} for the four concentrations. For pH 7.0 data, none of the models produced adequate global fits, so the response at the highest IgG concentration (6.67 μM) was used as a model-independent measure of pH 7.0 binding.

3.2.3 Differential scanning calorimetry

Thermal unfolding experiments were performed on a MicroCal VP-Capillary DSC using 0.15 or 0.5 mg/mL IgG in 1x PBS pH 7.2. IgG samples and reference buffer were scanned from 40 to 100 ºC at 60 ºC/hr. Three buffer/buffer scans were run between each sample/buffer scan. After subtracting the buffer/buffer scan immediately preceding the sample/buffer scan and normalizing concentration, "Progress Baseline" subtraction was performed to obtain a thermogram with a flat baseline using Origin 7 software. Thermodynamic parameters T_m and ΔH were obtained by fitting to a non-2-state model containing 3 peaks. The total ΔH was calculated as the sum of individual ΔH values. The weight-averaged T_m was obtained using the T_m and ΔH from each peak according to the following equation:

$$T_{m,avg} = \frac{\sum_{i=1}^{3} T_{m,i} \cdot \Delta H_i}{\sum_{i=1}^{3} \Delta H_i}$$

The change in heat capacity upon unfolding (ΔC_P) was determined by using the "Step at Half Area" baseline option and calculating the difference between baselines before and after the step. Using the "Step at Peak" option yielded essentially identical ΔC_P values (R^2 = 0.99). DSC parameters presented are the average of two independent experiments (one at 0.15 mg/mL and one at 0.5 mg/mL).

3.2.4 Literature reports of antibody pharmacokinetics

Literature reports of half-life and clearance were found by searching for a given antibody and "half-life" in PubMed (https://www.ncbi.nlm.nih.gov/pubmed) and selected based on description of human clinical studies. FDA package inserts were used as additional references. Volumes of distribution at steady state for the various mAbs ranged within 2-fold (0.060–0.106 L/kg). All the studies either explicitly reported linear PK or did not specifically mention non-linearity. When multiple doses or routes of administration were investigated, the average pharmacokinetic value of all conditions was used.

3.2.5 Regression analysis

Analysis was performed in MATLAB R2017b using the 'regress' and 'lasso' functions. Prior to regression analysis, the six parameters (FcRn k_a at pH 6.0, FcRn k_d at pH 6.0, FcRn response at pH 7.0, ΔH, T_m, and ΔC_P) were tabulated with each column as a predictor and each row as a mAb. Parameters were normalized by subtracting the mean of the column and dividing by the standard deviation of the column. Thus, the normalized columns all had a mean of 0 and standard deviation of 1, but retained their distribution of values for the different mAbs, ensuring that each parameter contributed equally to regression calculations. In linear regression, coefficients for each parameter are optimized so as to minimize the root-mean-square difference between observed and predicted values of a dependent variable (here, either half-life or clearance). LASSO involves a similar optimization, with the additional constraint that the sum of all the coefficients must be lower than a regularization parameter λ.[19] Higher values of λ favor simpler models with fewer non-zero coefficients, allowing us to rigorously explore the trade-off between model accuracy and model complexity.

Following LASSO regression, models based on the optimal parameter pairs were

calculated using the following equation:

$$y = m_1 \cdot x_1 + m_2 \cdot x_2 + b$$

where y is the 2-parameter score, x_1 and x_2 are the parameter values (e.g., FcRn-IgG response at pH 7.0 and ΔC_P), m_1 and m_2 are the best-fit regression coefficients, and b is the regression intercept. For leave-one-out analysis, the half-life of each mAb in turn was predicted by performing a regression with the other seven mAbs, and then using the resulting intercept and coefficients along with the parameter values of the mAb to calculate its 2-parameter score.

3.3 Results

3.3.1 Review of literature on antibody pharmacokinetics

To determine the relation between biophysical parameters of therapeutic mAbs and their pharmacokinetic characteristics, a small selection of mAbs with existing human half-life data was required. Eight clinical IgG1κ mAbs targeting soluble antigens were selected based on FDA package inserts and clinical trials describing half-lives ranging from 7.2 to 24.5 days (**Table 3.1**). These half-life values, and separately the mAb clearance values, were used as the dependent variables to which the independent variables (biophysical parameters) would be correlated.

3.3.2 Antibody binding to the neonatal Fc receptor at endosomal pH

Since FcRn is known to salvage IgG from lysosomal degradation and thus affect serum stability, the affinity of these eight mAbs for FcRn was examined as one potential determinant of half-life and clearance. In particular, both the association rate (k_a) and dissociation rate (k_d) of the interaction at endosomal pH (pH 6.0) were determined by BLI because both kinetic parameters could be important predictors. The kinetic data fit well to the simplest 1:1 binding model, from which k_a and k_d parameters were extracted for each mAb (**Table 3.1**, **Figures 3.1A**, **3.2**). When the IgG-FcRn k_a and k_d were compared to half-life and clearance, they unexpectedly revealed very

weak correlations (**Figure 3.3A**, **B**). This suggests that FcRn affinity at endosomal pH is not the most important determinant of half-life and clearance for IgG1 mAbs containing different variable regions.

3.3.3 Antibody binding to the neonatal Fc receptor at physiological pH

IgG-FcRn binding is highly pH dependent, with tight binding occurring only below pH ~6.5. For the FcRn salvage mechanism to be effective, an IgG must associate tightly with FcRn in the endosome; however, it also must be efficiently released from FcRn upon exposure to the neutral pH (pH 7.4) of the blood. Thus, the binding kinetics of the mAbs to FcRn at neutral pH were considered as another possible determinant of serum half-life, as previously considered by others.[13,32] Well-defined binding was not observed at pH 7.4, even with >1 mg/mL of IgG binding to immobilized FcRn. Instead, binding and dissociation were examined at pH 7.0, which was the highest pH with quantifiable binding. The pH 7.0 data did not fit well to any simple models such as 1:1 or bivalent analyte, preventing determination of accurate k_a and k_d values. This complexity may result from avidity in IgG-FcRn interactions.[20] As an alternative, the maximum response achieved was tabulated as an objective, model-independent measure of binding at pH 7.0 (**Table 3.1**, **Figures 3.1B**, **3.4**). Comparison of these response values with mAb half-lives revealed an inverse correlation, indicating that long mAb half-life is associated with weak FcRn binding at neutral pH (**Figure 3.3C**). Conversely, FcRn response at pH 7.0 was positively correlated to clearance. Independent experiments confirmed the observed trends in FcRn binding at pH 6.0 and 7.0 (**Figures 3.5-3.7**).

3.3.4 Antibody thermal stability

Thermal stability, which varies based on the amino acid sequence, is another biophysical property of mAbs that may affect half-life. DSC was used to monitor unfolding as a function of

temperature. Since IgG unfolding thermograms have been shown to be similar at endosomal and neutral pH, the experiments were performed only at pH 7.2.[21] After subtracting buffer scans and normalizing by concentration, the DSC data were fit to a non-2-state model with three components, which was the smallest number of components that accurately described each of the mAbs (**Figures 3.8A**, **3.9**, **3.10**). From these fits, the total change in enthalpy (ΔH) of unfolding (sum of the ΔH values for each component) was tabulated and revealed a weak negative correlation with half-life and a weak positive correlation with clearance (**Table 3.1**, **Figure 3.3D**). The weight-averaged melting temperature (T_m) was also calculated as the T_m of each fit component multiplied by that component's contribution to the total ΔH. This T_m parameter showed a weak positive correlation with half-life and a weak negative correlation with clearance (**Table 3.1**, **Figure 3.3E**). As a final predictor of half-life from DSC data, the difference in heat capacity between folded and unfolded states (ΔC_P) was calculated for each mAb. ΔC_P was inversely correlated with half-life and positively correlated with clearance (**Table 3.1**, **Figures 3.3F**, **3.8B**, **3.11**).

3.3.5 Multiple regression to identify combinations of pharmacokinetic predictors

Comparing individual BLI or DSC parameters yielded generally weak correlations to half-life and clearance with $R^2 < 0.8$. Multiple regression was performed with all six parameters and yielded very strong correlations with $R^2 = 0.99$, but as expected the data were severely undersampled and overfit, resulting in large standard errors in parameter coefficients. To determine which subset of coefficients would yield the best correlation with half-life and clearance, LASSO regression was applied to reduce the number of predictors by introducing the regularization parameter λ.[19,22] Applying LASSO to the tabulated mAb parameters revealed different solutions to the regression problem depending on the value of λ. As the value of λ was increased, the number of non-zero coefficients decreased while the mean-squared error increased

(**Figure 3.12**). Based on this analysis, the best single parameter for half-life prediction was FcRn response at pH 7.0 (consistent with the high R^2 value for this individual correlation). Examining solutions for lower values of λ revealed that the combination of two parameters most strongly associated with half-life was FcRn response at pH 7.0 and ΔC_P. These same two parameters were also the best combination of clearance determinants, though in the opposite order of importance. To ensure that this analysis was not discounting the pH 6.0 binding data because it was represented by two distinct parameters, LASSO regression was also performed using the maximum response at pH 6.0 instead of both k_a and k_d. This 5-parameter regression yielded results similar to the original 6-parameter solution: response at pH 7.0 and ΔC_P remained the top pair of predictors for both half-life and clearance (**Figure 3.13**).

Next, normal multiple regression was performed using FcRn response at pH 7.0 and ΔC_P as the only two predictors for half-life. This was done to determine best-fit coefficients for the parameters without applying any penalty function for the number of parameters. The resulting correlation between the linear combination of these two parameters and half-life or clearance was much stronger than the correlation for each individual parameter (R^2 = 0.91 and R^2 = 0.96, respectively, **Figure 3.14A**, **B**). Because the parameter matrix was normalized to have a mean of 0 and a standard deviation of 1 prior to analysis, any differences in the magnitude or range of parameters were eliminated. In other words, regression results will depend on relative differences rather than absolute values of biophysical parameters. Thus, the regression coefficients reflect the relative importance of each parameter for half-life or clearance prediction. In this case, the half-life coefficient for pH 7.0 response was -4.63 ± 0.83 and for ΔC_P was -2.88 ± 0.83 with an intercept of 16.8 ± 0.8. In other words, both pH 7.0 response and ΔC_P were negatively correlated with half-life, but pH 7.0 response was somewhat more important for the 2-parameter correlation. For

clearance, ΔC_P was the more important of the two determinants. The pH 7.0 response coefficient was 1.86 ± 0.35, the ΔC_P coefficient was 3.15 ± 0.35, and the intercept was 5.67 ± 0.32.

3.3.6 Testing the predictive power of the model

To test the robustness of the 2-parameter correlation and assess its predictive power, we performed leave-one-out (a.k.a. jackknife) subsampling: the half-life and clearance of each mAb were predicted based on its measured biophysical parameters and a regression model trained on the other seven mAbs. When LASSO analysis was performed for each subset of mAbs, all but one subset yielded pH 7.0 response and ΔC_P as the primary two determinants for both half-life and clearance. When omalizumab was excluded, these two parameters were most important for clearance; but for half-life, pH 7.0 response, ΔH, and ΔC_P were the first three determinants. Despite this single exception, for consistency, the pH 7.0 response and ΔC_P of each mAb were used to predict its half-life and clearance. The values of the regression intercept and coefficients were similar when any one of the mAbs was omitted from the correlations (**Table 3.2**). Indeed, the standard deviations for the intercept, pH 7.0 response coefficient, and ΔC_P coefficient from subsampling analysis were all under 16% for both half-life and clearance.

Prediction of mAb half-life based on its pH 7.0 response and ΔC_P was fairly accurate, with differences between measured and predicted half-life ranging from 0 to 4.7 days (0-38%) and a root-mean-squared deviation (RMSD) of 2.7 days (16%). Comparing the leave-one-out 2-parameter predicted half-life of a mAb to the reported value resulted in a correlation with R^2 = 0.79 (**Figure 3.14C**). Analogous prediction of mAb clearance based on the same two parameters resulted in an RMSD of 1.4 mL/d/kg (24%). In this case, the correlation between predicted and reported clearance indicated strong predictive power (R^2 = 0.88, **Figure 3.14D**).

3.4 Discussion

The half-life of a therapeutic mAb is a vital biological characteristic that determines how frequently the drug must be administered. In many cases it is desirable to invest in mAbs that have slow elimination kinetics, so they can be administered at a lower dose or reduced frequency, ultimately saving time and money for both patients and companies. Despite the incentive for characterizing mAb half-life early in the drug pipeline, it has been difficult to predict the PK properties of mAbs before they enter human trials. Many individual parameters, including biological properties like FcRn affinity or glycosylation state, biophysical properties like non-specific binding or aggregation propensity, and sequence-based properties like allotype, have been correlated to half-life with varying degrees of interdependence.[13,15,17,23] It appears that no single property of a mAb can be used to accurately predict PK properties. At the same time, it would be advantageous to know the smallest, most tractable set of parameters that would be predictively useful. Thus, we took a combinatorial approach to determine whether half-life prediction could be improved using multiple parameters incorporated into a cohesive model. The LASSO machine learning approach provides a statistically rigorous method to identify parameter combinations that best predict outcomes.

In forming a panel of mAbs to analyze, various factors were considered. The primary goal was to obtain a small sample of mAbs with a large spread of human half-life values based on published clinical data. Thus, mAbs were selected with half-lives ranging from one week to over three weeks. Because the subtype of IgG heavy chain is known to affect mAb PK, with IgG3 having a shorter serum half-life than other subtypes, only IgG1 mAbs were considered for analysis.[24] Likewise, all the selected mAbs contained kappa light chains. Only mAbs that target soluble antigens were selected, to minimize differences in half-life that occur as a result of

receptor-mediated disposition or other target-dependent processes, and emphasize intrinsic biophysical parameters. Of course, it was not possible to eliminate every source of variation with the relatively small number of mAbs available to us. The panel contains mAbs that are chimeric, humanized, or fully human, and allotypes m3,1; m17,1; and m17,-1 are all represented. However, neither framework nor allotype were associated with significant differences in half-life or clearance (**Figure 3.15**).

The FcRn binding data at pH 6.0 yielded tight K_D values relative to some literature reports, due to the level of FcRn immobilized and the bivalent mechanism of FcRn-IgG binding.[7,13] Nevertheless, the data within this experiment are directly comparable and revealed modest differences in association and dissociation rates that were not correlated with half-life. As the FcRn binding interface of these mAbs is identical, it is possible that the observed differences in FcRn binding are caused by charge-mediated Fab-FcRn interactions.[25] Previous studies have noted that stronger FcRn binding at endosomal pH leads to enhanced IgG half-life.[26-28] It should be noted that these studies compare the clearance of a given mAb with and without mutations that affect FcRn binding. The variable regions of the mAb are conserved and the biophysical properties of the mutants are expected to be similar. Localization of mutations to the FcRn binding site creates large (10- to 30-fold) increases in FcRn affinity that are much larger than the 3-fold span in affinity observed here. In these cases, it makes sense that FcRn binding would be a primary determinant of half-life. Other studies have shown that FcRn binding at pH 6 is not strongly associated with half-life when distinct clinical mAbs are examined, or even when the variable regions are maintained.[13,29-31]

The ability of mAbs to bind FcRn at pH 7.0, however, was strikingly related to their half-lives in humans. Although it was not possible to reliably extract k_a and k_d values at pH 7, the

maximum response achieved at the highest mAb concentration provided an objective measure of binding that was negatively correlated with half-life. As the mass and concentration of mAbs were effectively equal and the association times were identical, the response parameter provides an unbiased measure of FcRn binding. The inverse correlation between neutral pH binding and half-life has been observed previously by groups showing that weak FcRn binding at neutral pH is just as important as tight binding in the endosome.[13,32] The observation that excessive binding at neutral pH accelerates clearance may be due to FcRn-dependent endocytosis and degradation, or FcRn-independent processes related to non-specific binding. The inability to globally fit the pH 7 data, while inconvenient, may suggest the presence of multiple conformations or protonation states of the Fc or FcRn at this pH, or of polyvalent interactions, which complicates simple 1:1 fits.

It is reasonable that the serum stability of a mAb would be related to its inherent thermal stability. Molecules containing unstable variable regions may be more prone to unfold or aggregate. Both processes would be expected to accelerate clearance, either due to the generation of an immune response or the loss of FcRn binding capacity.[33,34] This hypothesis is supported by DSC data showing a weak but positive correlation between weight-averaged T_m and half-life. Interestingly, the correlation for ΔC_P and half-life was negative, suggesting that mAbs containing more buried hydrophobic residues are more likely to have shorter half-lives. Indeed, ΔC_P was moderately positively correlated with the grand average of hydropathy (GRAVY) score ($R^2 = 0.33$, **Figure 3.16**) based on the amino acid sequence of the mAb variable regions.[35] An abundance of buried hydrophobic residues can stabilize the folded state in buffer, but may introduce opportunities for aggregation and other non-specific interactions in the presence of other proteins or tissue constituents. Thus, the biological matrix could actually destabilize the monomeric folded state if nonspecific, hydrophobically driven interactions pull the equilibrium toward unfolding or

aggregation with serum components. While previous efforts have examined less direct measures of stability such as non-specific binding or self-association, our use of DSC enables the delineation of the precise thermodynamic parameters that provide the most predictive value.[12]

A challenge associated with half-life prediction is how to account for the effects of multiple determinants without overparameterizing the model. Here, LASSO was used to identify the most powerful combination of two biophysical parameters for half-life and clearance prediction. The advantage of using LASSO was the ability to explore all possible combinations of parameters and to vary the value of λ so that the number of non-zero coefficients ranged from 0 to 6. In this way, the response at pH 7.0 and the ΔC_P were identified as the two parameters that, in combination, yielded the best correlation to both half-life and clearance. Thus, accounting for both FcRn binding at neutral pH and thermodynamic stability allows for the most accurate prediction of mAb PK.

The approach taken here was fundamentally empirical in nature, and designed more to generate hypotheses than to test them. Experiments were devised to allow for extraction of biophysical parameters that may be associated with mAb serum stability. While the limited set of predictors selected for analysis were guided by current knowledge of mAb PK, the analysis was not biased by our current mechanistic understanding of mAb recycling and clearance. This approach is therefore useful for generating new hypotheses about the phenomenon of interest. In this case, analysis identified pH 7 response and ΔC_P as predictors that are inversely correlated with half-life and positively correlated with clearance. While the importance of FcRn release at neutral pH has been demonstrated, we did not encounter any previous reports that low ΔC_P values contribute to long mAb half-life. Perhaps the relationship between ΔC_P and clearance can be further explored to clarify the mechanism behind this observation.

Importantly, the parameters we considered by no means encompass all the factors that

could affect the disposition of a particular mAb. A number of additional biophysical properties, reflective of protein stability, non-specific binding and aggregation propensity, have been advanced as important predictive metrics of PK and pharmacodynamics.[17,18] Expanding the use of LASSO and similar regression analyses to larger datasets, covering more samples and including more biophysical parameters, could prove informative, particularly in clarifying which *in vitro* parameters should be emphasized. Empirical, combinatorial approaches such as the one developed here could be generally useful for many different mAb-based therapeutics, or for non-mAb therapeutics whose PK can be predicted by other combinations of biophysical determinants.

FIGURES

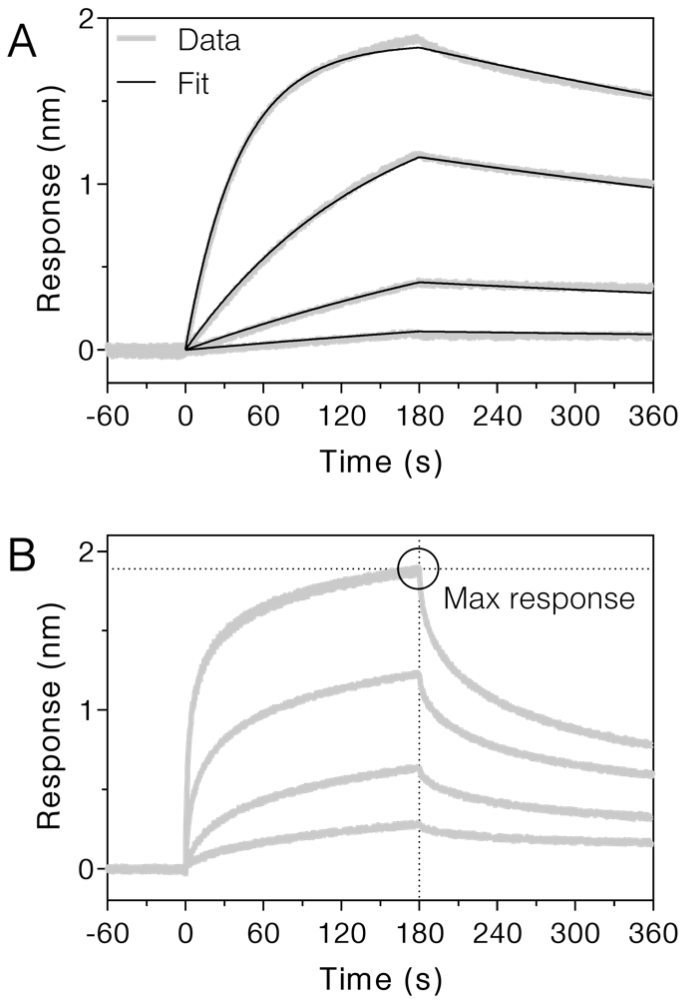

Figure 3.1: Biolayer interferometry sensorgrams of bevacizumab binding to immobilized human FcRn at pH 6.0 (A) and 7.0 (B). At pH 6.0, Ni-NTA tips loaded with FcRn were dipped in buffer containing 66.7, 16.7, 4.17, or 1.04 nM of bevacizumab to observe the association phase for 3 minutes, followed by dipping in buffer lacking bevacizumab to observe the dissociation phase for 3 minutes. Thick gray lines show the data and narrow black lines show a global fit of all four concentrations to a 1:1 binding model, which yielded kinetic parameters k_a and k_d. At pH 7.0, Ni-NTA tips loaded with FcRn were dipped in buffer containing 6670, 1670, 417, or 104 nM of bevacizumab to observe the association phase for 3 minutes, followed by dipping in buffer lacking bevacizumab to observe the dissociation phase for 3 minutes. Thick gray lines show the data and the black circle highlights the maximum binding response achieved for the 6.67 μM concentration.

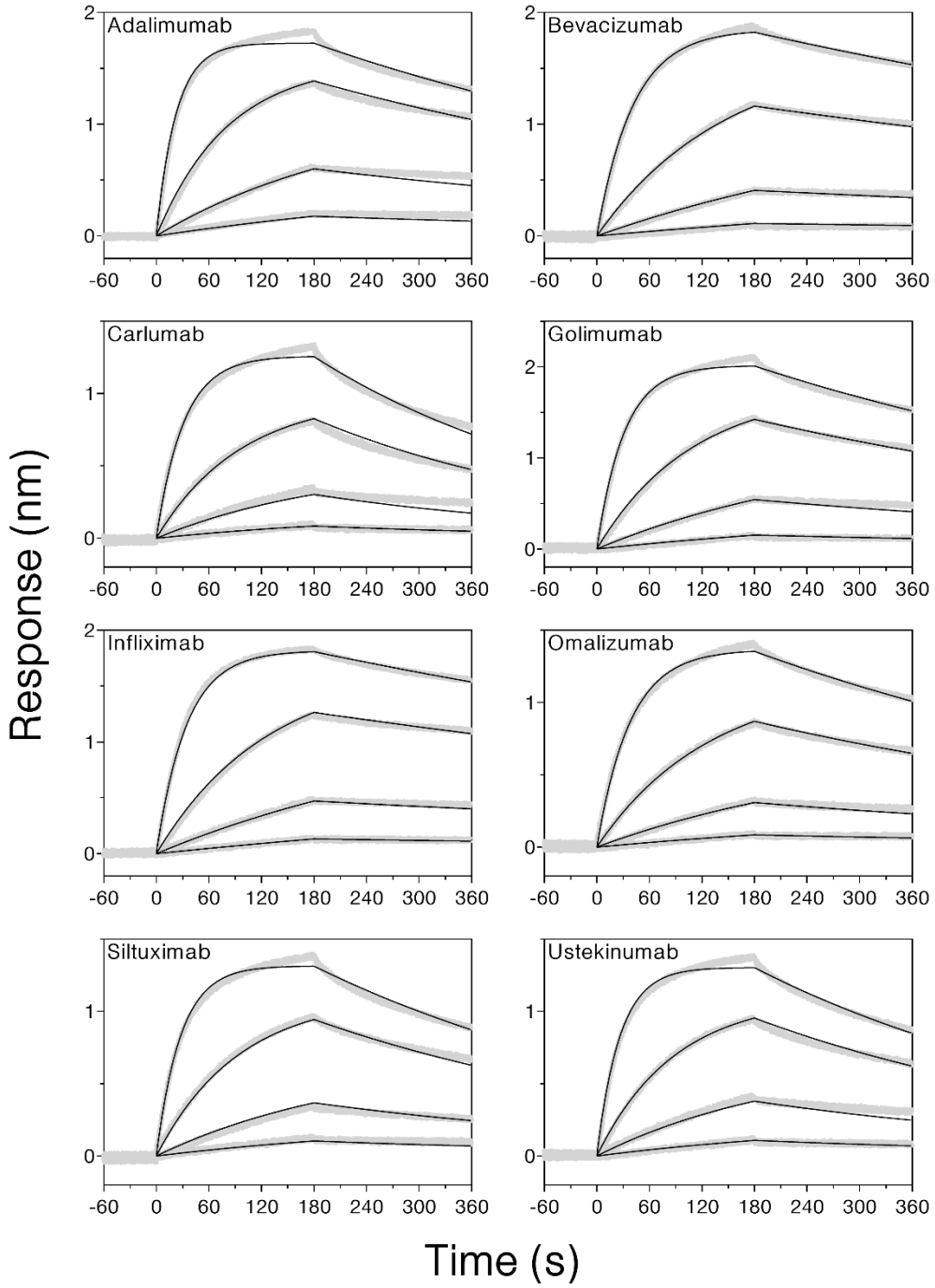

Figure 3.2: Biolayer interferometry sensorgrams showing binding of immobilized human FcRn to therapeutic mAbs at pH 6.0. Data for all four concentrations of IgG (66.7, 16.7, 4.17, and 1.04 nm) were globally fit to a 1:1 binding model to extract k_a and k_d values (Table 3.1). Data are shown in gray and fits are in black.

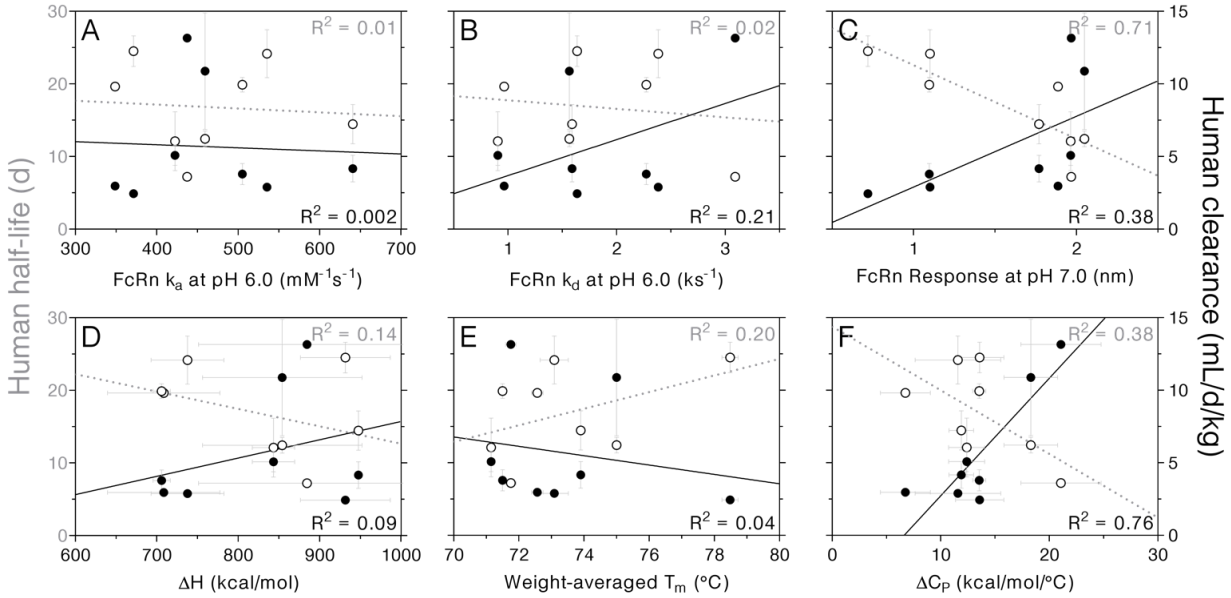

Figure 3.3: Correlations between mAb half-life or clearance and individual biophysical parameters. The FcRn k_a values at pH 6.0 (A), FcRn k_d values at pH 6.0 (B), and FcRn maximum binding response after 3 min at pH 7.0 (C) were obtained from BLI experiments. The total ΔH (D), weight-averaged T_m (E), and ΔC_P of unfolding (F) were obtained from DSC experiments. Half-life values are plotted on the left axis as open circles, with linear fits plotted as gray dotted lines containing the gray R^2 values listed at the top-right. Clearance values are plotted on the right axis as closed circles, with linear fits plotted as black solid lines containing the black R^2 values listed at the bottom-right.

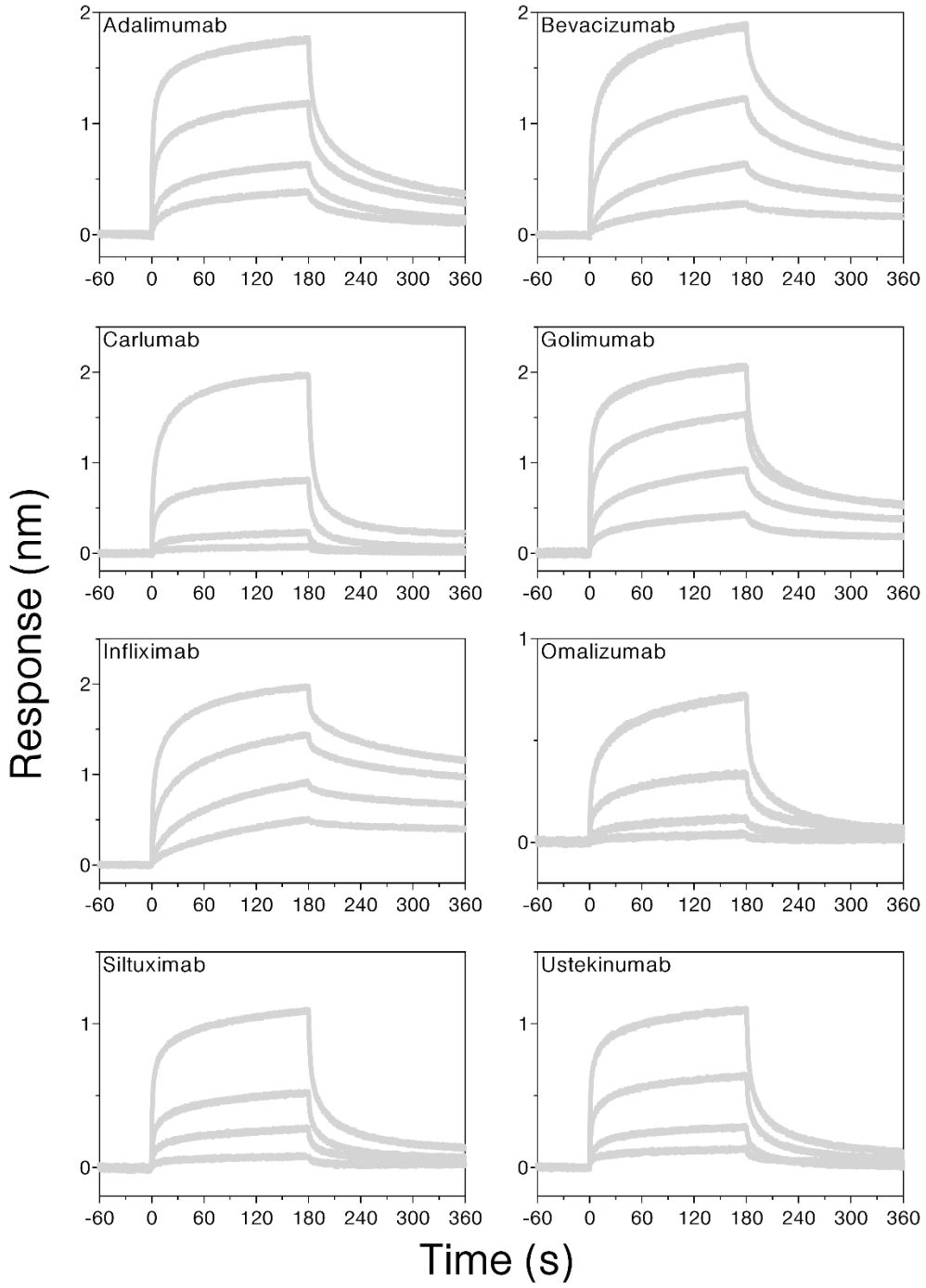

Figure 3.4: Biolayer interferometry sensorgrams showing binding of immobilized human FcRn to 6670, 1670, 417, or 104 nM therapeutic mAbs at pH 7.0. As the data did not fit well to simple binding models, the maximum response of the highest concentration (6.67 μM IgG) was tabulated as a model-independent readout of binding (Table 3.1).

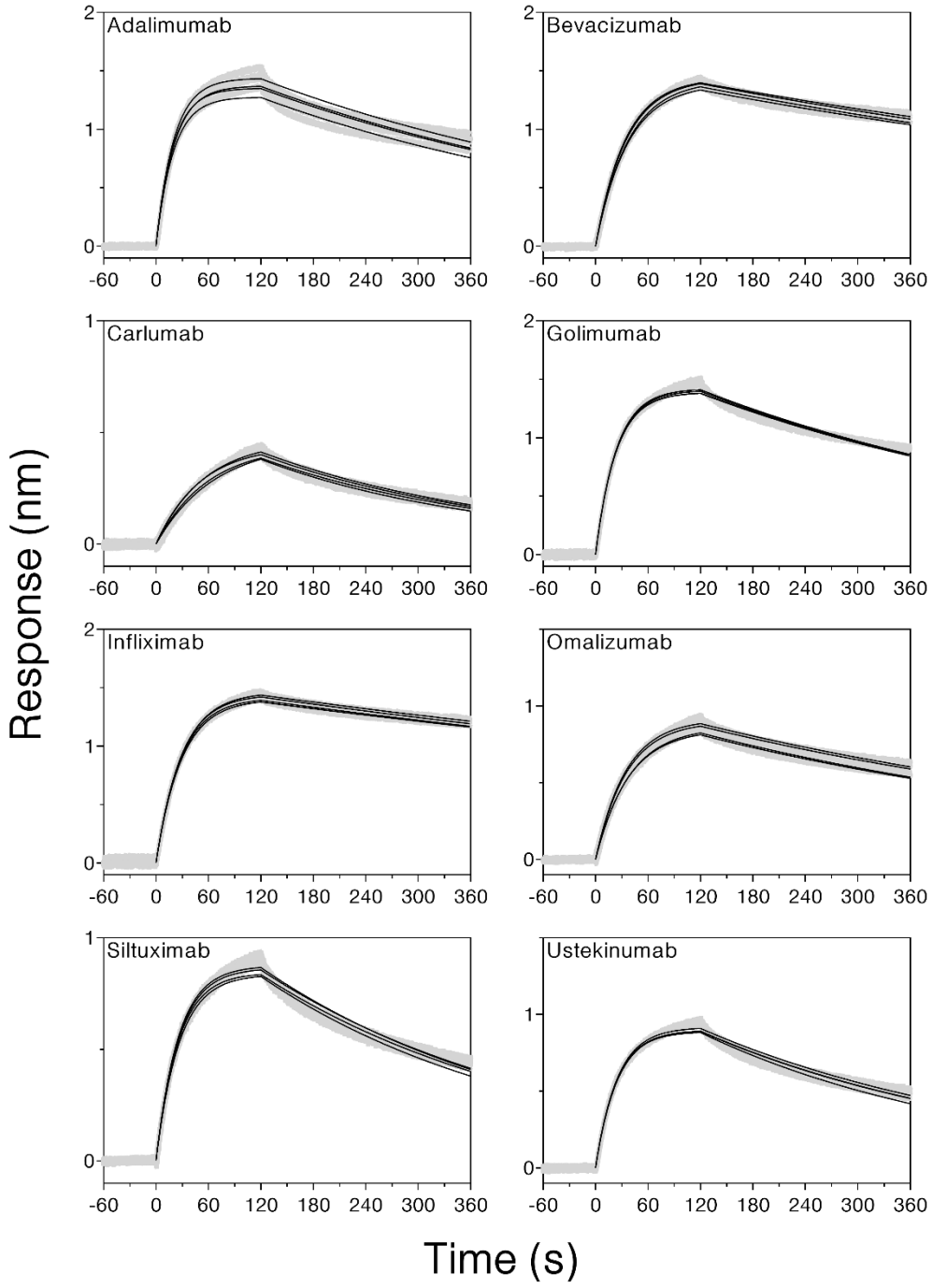

Figure 3.5: Biolayer interferometry sensorgrams showing binding of immobilized human FcRn to therapeutic mAbs at pH 6.0. Four replicates of 66.7 nM of IgG were individually fit to a 1:1 binding model to extract k_a and k_d values. Data are shown in gray and fits are in black.

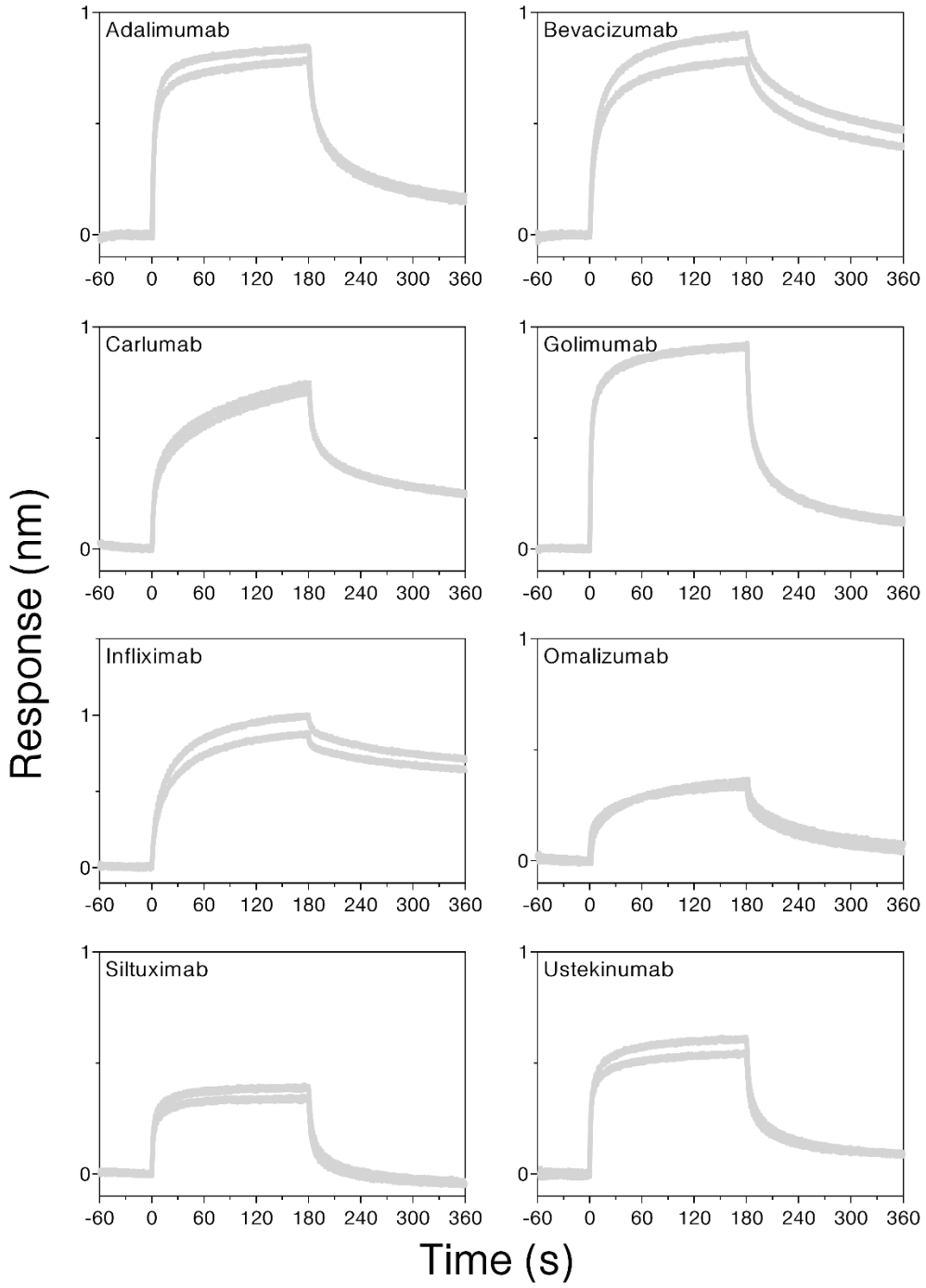

Figure 3.6: Biolayer interferometry sensorgrams showing binding of immobilized human FcRn to therapeutic mAbs at pH 7.0. Data were collected as in the methods section of the main paper, except that FcRn was loaded for 180 seconds rather than 300 seconds. The maximum response for two replicates of 6667 nM of IgG was determined for comparison to original experiments.

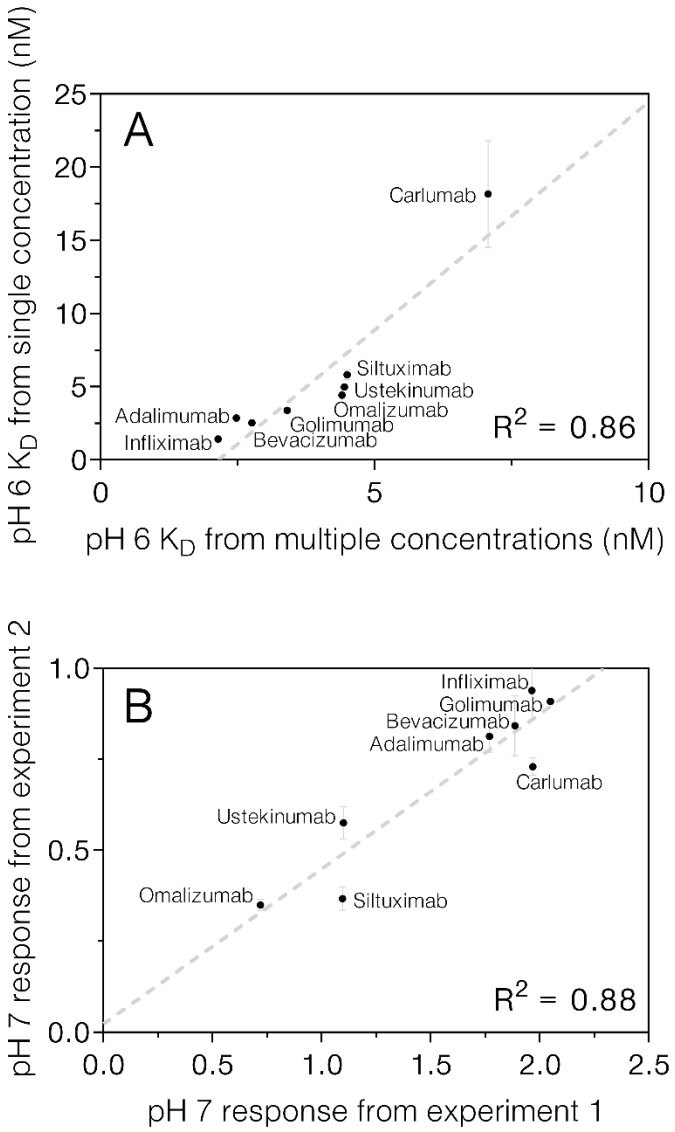

Figure 3.7: Comparison of FcRn-IgG binding trends from independent experiments. For pH 6 binding (A), K_D values from original experiments with multiple IgG concentrations (x-axis, data in Figure 3.2) were compared to K_D values from follow-up experiments with a single IgG concentration (y-axis, data in Figure 3.5). For pH 7 binding (B), the maximum response from original experiments (x-axis) was compared to the response from follow-up experiments (y-axis).

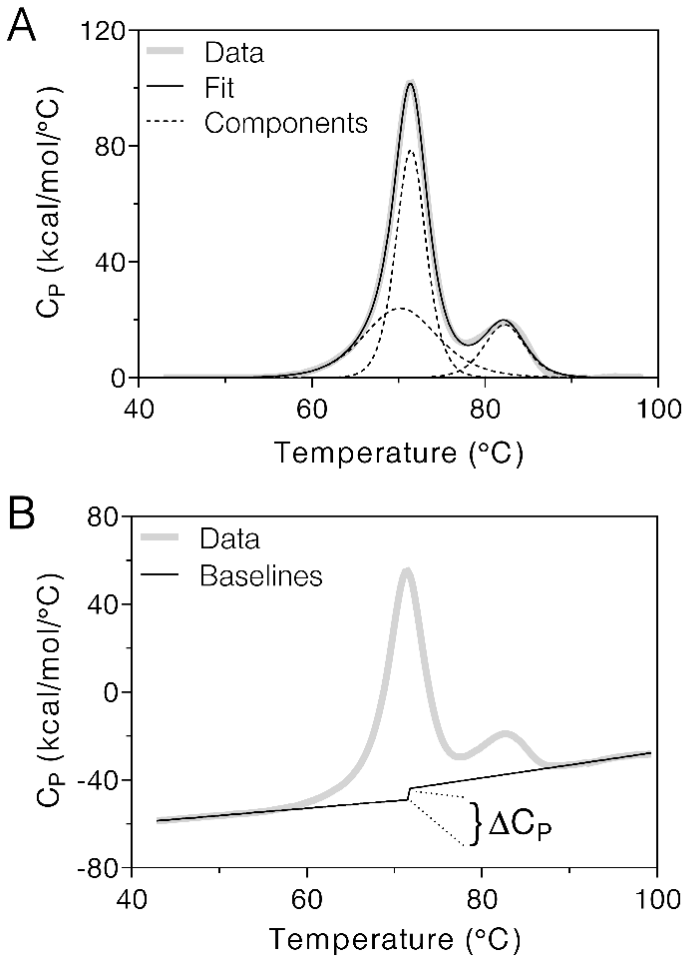

Figure 3.8: Differential scanning calorimetry thermograms showing the unfolding of bevacizumab at pH 7.2. (A) After performing "Progress Baseline" subtraction, the data were fit to a 3-component, non-2-state model to extract the ΔH and T_m associated with three unfolding events. Data is shown as a thick gray line, the fit as a narrow black line, and the fitted components as black dotted lines. (B) Baselines of the folded and unfolded states were fit using the "Step at Half Area" baseline option. The difference in C_P at half area was calculated as the ΔC_P.

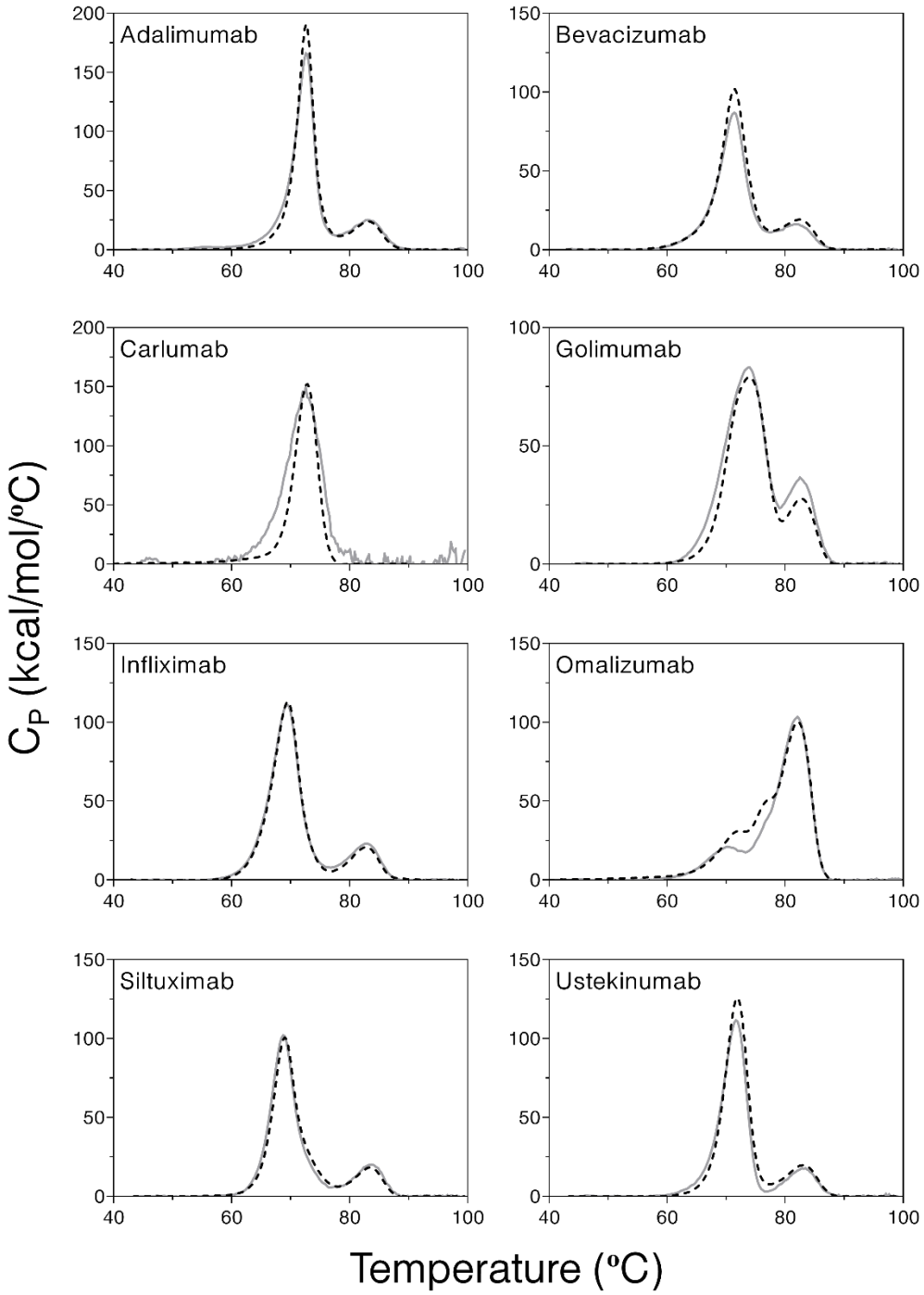

Figure 3.9: Differential scanning calorimetry thermograms for the eight clinical mAbs. Two independent replicates are shown in solid gray lines (0.15 mg/mL) and dotted black lines (0.5 mg/mL). Thermograms were reference subtracted (using the buffer/buffer scan immediately preceding the sample/buffer scan), normalized by concentration, and "Progress Baseline" subtracted.

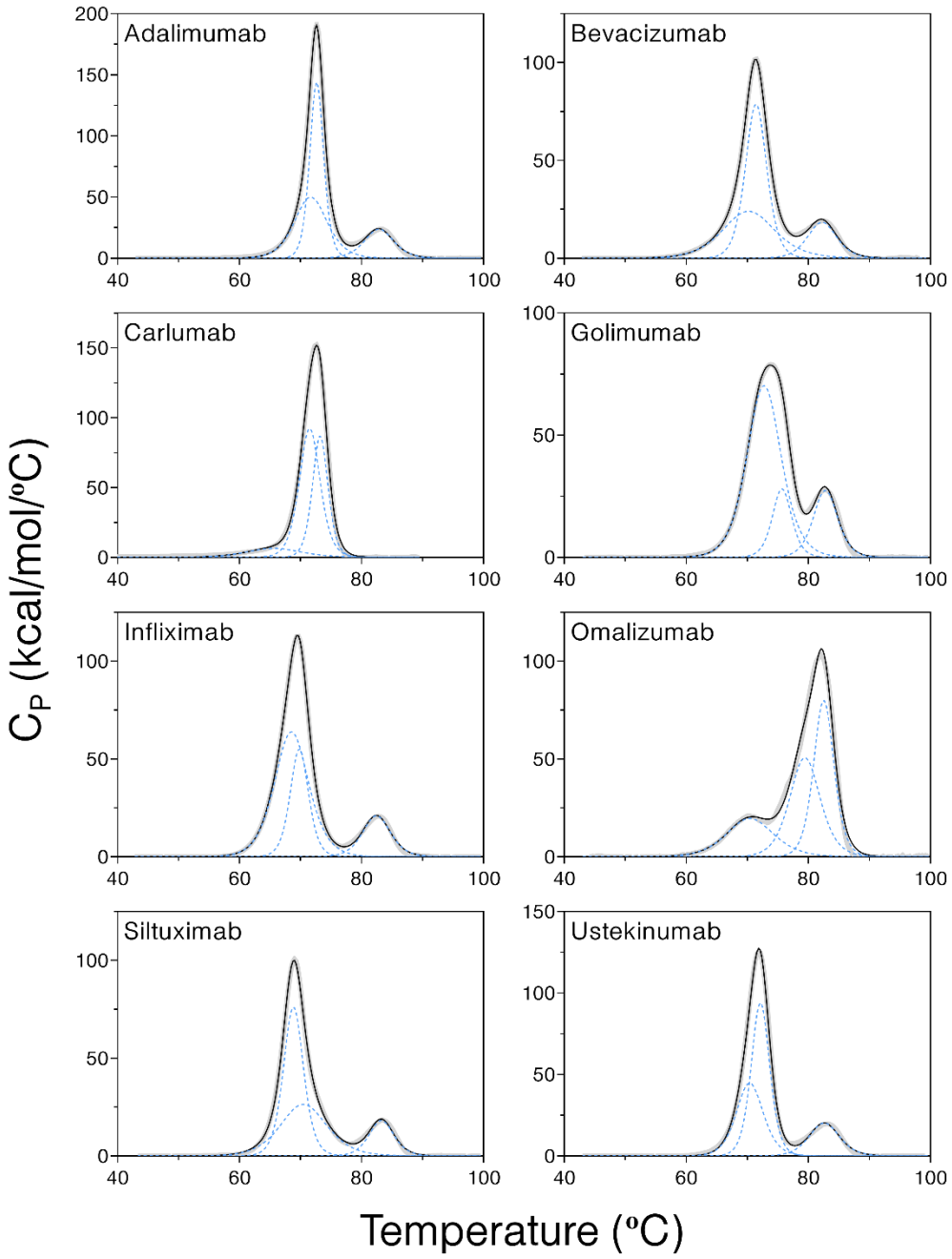

Figure 3.10: Differential scanning calorimetry thermograms fit to a 3-component, non-2-state model. Thermograms were reference subtracted (using the buffer/buffer scan immediately preceding the sample/buffer scan), normalized by concentration, and "Progress Baseline" subtracted before fitting to the model. The data are represented by thick gray lines, the fits are shown by narrow black lines, and the fitted components are shown as blue dotted lines.

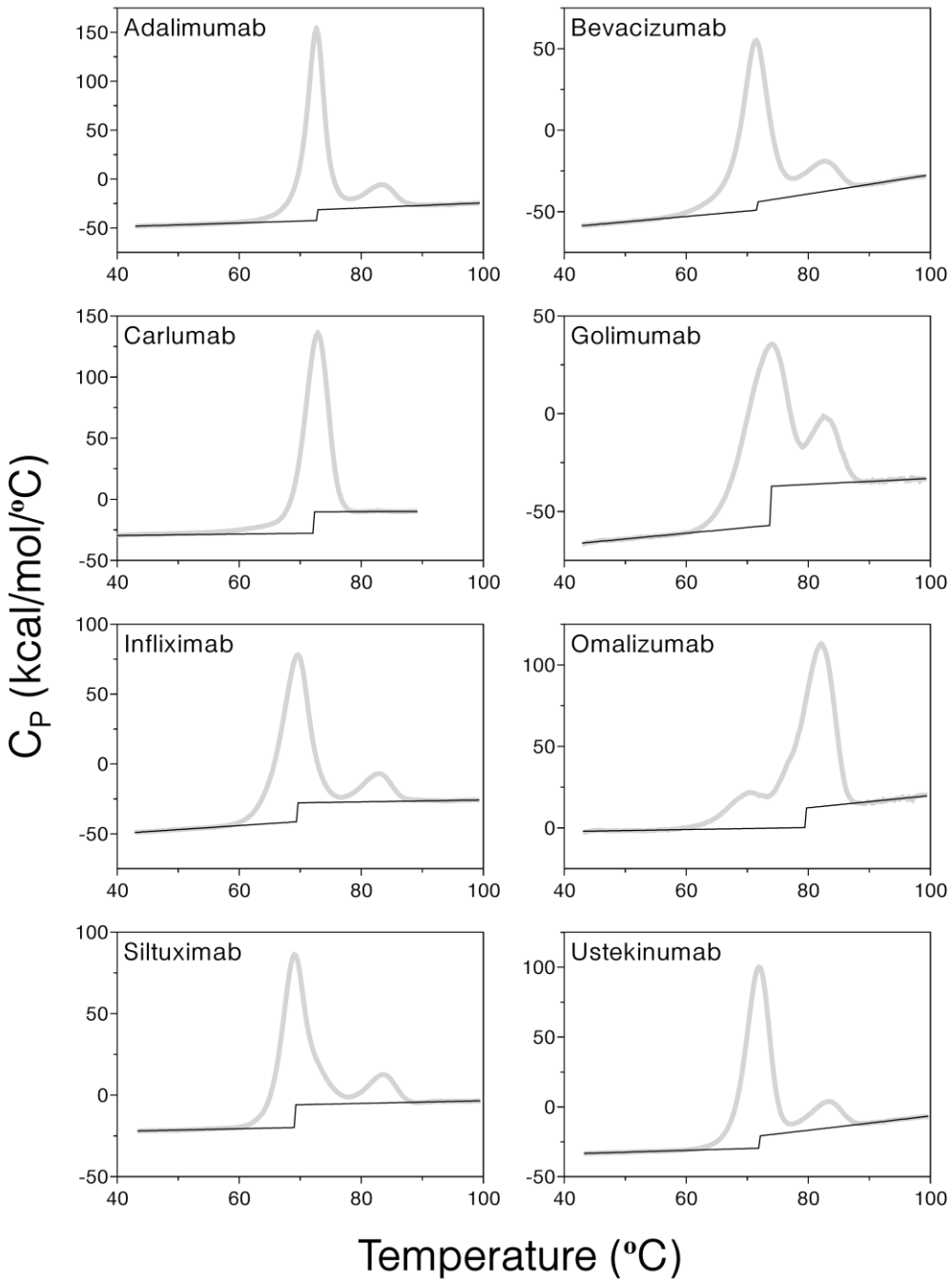

Figure 3.11: Differential scanning calorimetry was used to determine the ΔC_P of unfolding for each mAb. Thermograms were reference subtracted (using the buffer/buffer scan immediately preceding the sample/buffer scan) and normalized by concentration. The value of ΔC_P was obtained by fitting the baseline for the folded and unfolded state and determining their difference using the "Step at Half Area" baseline option. Data are shown in gray and baseline fits are shown in black.

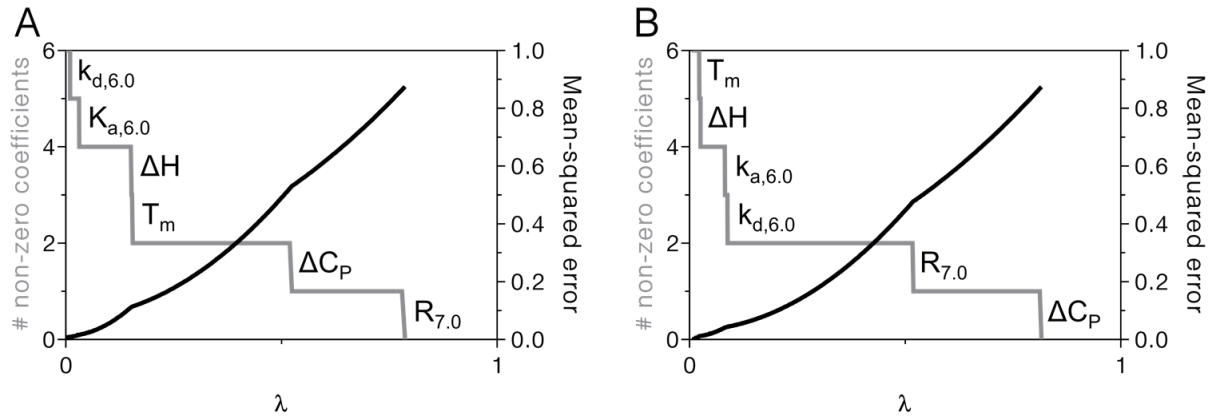

Figure 3.12: LASSO analysis to determine the most important predictors of mAb half-life (A) and clearance (B). As the value of the regularization parameter λ increased, the number of non-zero coefficients (gray line, left axis) decreased while the mean-squared error (black line, right axis) increased. The most important parameters for multiple regression of half-life (introduced at the highest values of λ) were pH 7.0 response ($R_{7.0}$), ΔC_P of unfolding, weight-averaged T_m, total ΔH of unfolding, pH 6.0 k_a ($k_{a,6.0}$), and pH 6.0 k_d ($k_{d,6.0}$), in that order. For clearance, the order of importance was ΔC_P, $R_{7.0}$, $k_{d,6.0}$, $k_{a,6.0}$, ΔH, and T_m.

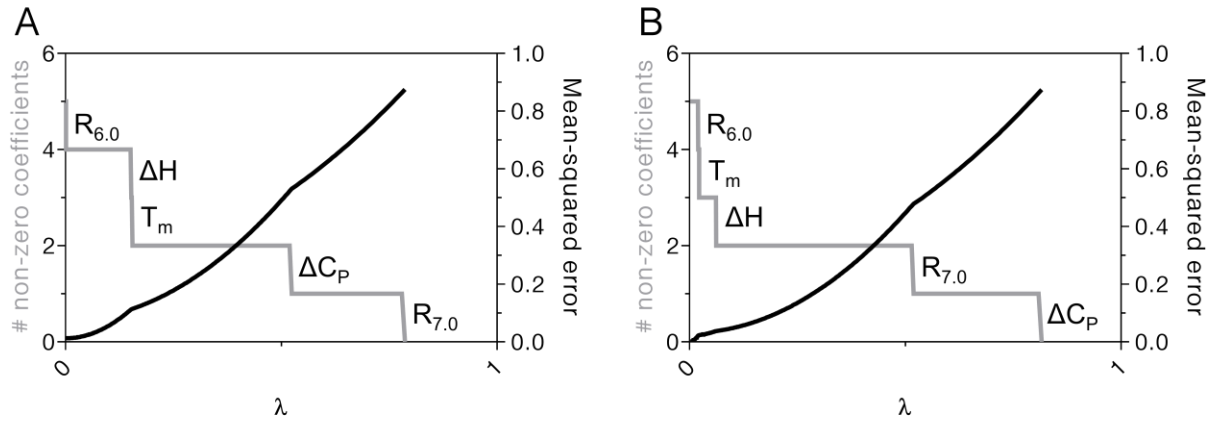

Figure 3.13: LASSO analysis for prediction of half-life (A) and clearance (B) using FcRn-IgG binding response at pH 6.0 instead of pH 6.0 k_a and k_d. The most important parameters for multiple regression of half-life (introduced at the highest values of λ) were pH 7.0 response, ΔC_P of unfolding, weight-averaged T_m, total ΔH of unfolding, and pH 6.0 response, in that order. For clearance, the order of importance was ΔC_P, pH 7.0 response, ΔH, T_m, and pH 6.0 response.

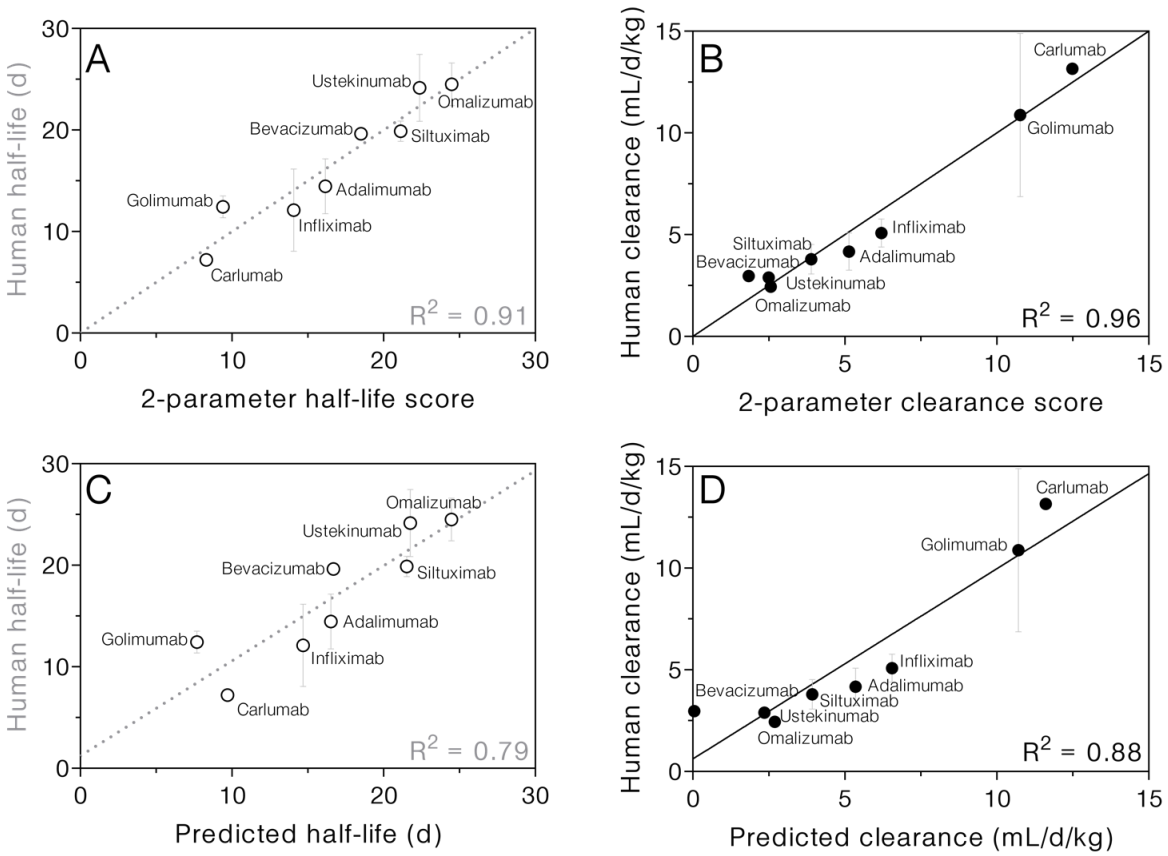

Figure 3.14: mAb half-life (A) and clearance (B) correlated strongly with the respective 2-parameter scores, which are based on the FcRn response at pH 7.0 and ΔC_P. Half-life (C) and clearance (D) predictions were validated using leave-one-out analysis. Multiple regression was performed using response at pH 7.0 and ΔC_P as predictors. Each mAb in turn was omitted from the regression, and then its values of pH 7 response and ΔC_P were used to predict its half-life or clearance using the regression results of the remaining seven mAbs.

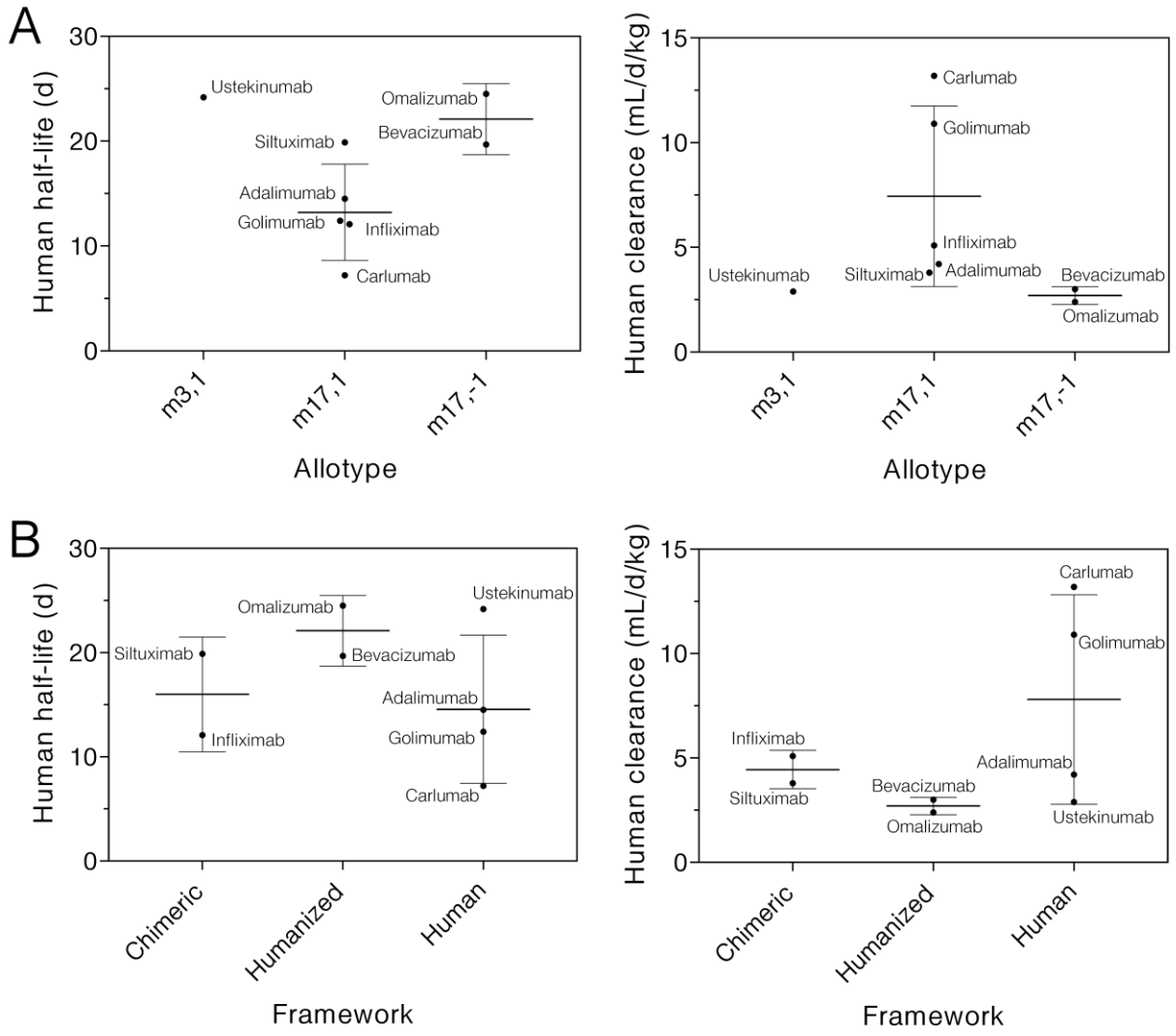

Figure 3.15: Effect of IgG1 allotype (A) and framework (B) on mAb pharmacokinetics. There is no significant difference between the half-lives or clearance values of m17,1 and m17,-1 mAbs ($p = 0.19$ and $p = 0.10$, respectively). There is also no significant difference between the half-lives or clearance of chimeric and humanized ($p = 0.67$, $p = 0.33$), chimeric and human ($p > 0.99$, $p = 0.80$), or humanized and human ($p = 0.27$, $p = 0.27$) mAbs. It was not possible to test for significance of m3 versus m17 allotypes as there is only one m3 mAb.

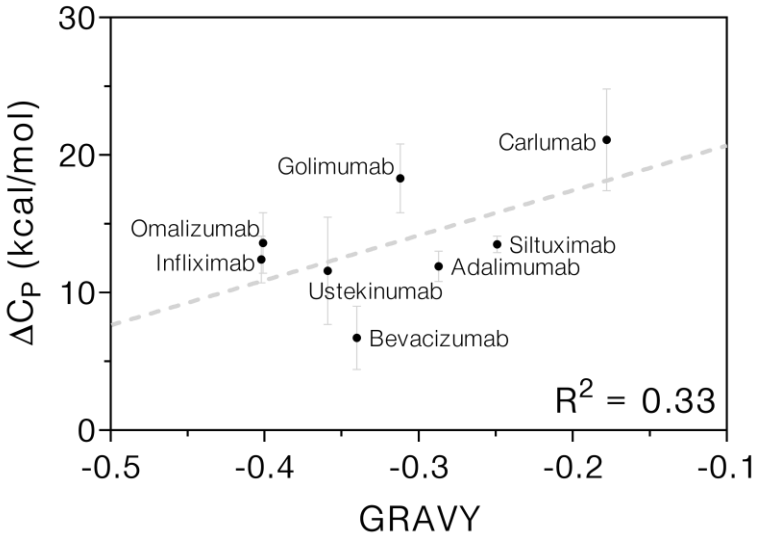

Figure 3.16: Comparison of ΔC_P measured by DSC and grand average of hydropathy (GRAVY) score based on the amino acid sequence of the mAb variable regions. GRAVY scores were calculated by inputting the sequence for a mAb heavy and light chain variable regions into the ExPASy ProtParam calculator (https://web.expasy.org/protparam/protparam-doc.html).

Table 1: Literature pharmacokinetics and biophysical parameters for clinical mAbs

Antibody	Human half-life (d)	Human clearance (mL/d/kg)	FcRn k_a, pH 6.0 ($mM^{-1}s^{-1}$)	FcRn k_d, pH 6.0 (ks^{-1})	FcRn response, pH 7.0 (nm)	ΔH (kcal/mol)	Wt avg T_m (ºC)	ΔC_P (kcal/mol/ºC)
Adalimumab[36-38]	14.5 ± 2.7	4.2 ± 0.9	641 ± 1	1.59 ± 0.01	1.77	948 ± 1	73.9 ± 0.1	11.9 ± 1.1
Bevacizumab[39-42]	19.7 ± 0.4	3.0 ± 0.3	349 ± 0	0.96 ± 0.00	1.89	709 ± 69	72.6 ± 0.2	6.7 ± 2.3
Carlumab[43,44]	7.2 ± 0.4	13.2	437 ± 1	3.09 ± 0.01	1.97	884 ± 133	71.8 ± 0.2	21.1 ± 3.7
Golimumab[45-50]	12.4 ± 1.1	10.9 ± 4.0	459 ± 1	1.56 ± 0.00	2.05	854 ± 98	75.0 ± 0.1	18.3 ± 2.5
Infliximab[51-55]	12.1 ± 4.0	5.1 ± 0.7	423 ± 0	0.91 ± 0.00	1.96	843 ± 26	71.2 ± 0.1	12.4 ± 1.7
Omalizumab[56,57]	24.5 ± 2.1	2.4 ± 0.1	371 ± 0	1.64 ± 0.00	0.72	932 ± 55	78.5 ± 0.2	13.6 ± 2.2
Siltuximab[58,59]	19.9 ± 1.0	3.8 ± 0.7	505 ± 1	2.27 ± 0.01	1.10	706 ± 11	71.5 ± 0.1	13.5 ± 0.6
Ustekinumab[60,61]	24.2 ± 3.3	2.9	535 ± 1	2.38 ± 0.01	1.10	738 ± 45	73.1 ± 0.4	11.6 ± 3.9

Table 3.2: Prediction of mAb half-life and clearance using leave-one-out regression

	Half-life prediction			Clearance prediction		
Antibody omitted and predicted	**Intercept**	**FcRn response, pH 7.0 coefficient**	**ΔC_P coefficient**	**Intercept**	**FcRn response, pH 7.0 coefficient**	**ΔC_P coefficient**
Adalimumab	17.1 ± 0.8	-4.48 ± 0.87	-3.03 ± 0.87	5.82 ± 0.33	1.94 ± 0.34	3.07 ± 0.34
Bevacizumab	16.4 ± 0.9	-5.04 ± 0.99	-2.13 ± 1.25	5.31 ± 0.19	1.45 ± 0.20	3.90 ± 0.26
Carlumab	17.1 ± 0.9	-4.47 ± 0.90	-2.31 ± 1.17	5.48 ± 0.35	1.76 ± 0.35	2.80 ± 0.46
Golimumab	16.2 ± 0.6	-5.13 ± 0.60	-3.50 ± 0.62	5.65 ± 0.39	1.84 ± 0.41	3.13 ± 0.43
Infliximab	17.1 ± 0.8	-4.31 ± 0.87	-3.05 ± 0.83	5.86 ± 0.30	2.04 ± 0.32	3.06 ± 0.31
Omalizumab	16.8 ± 1.0	-4.62 ± 1.26	-2.89 ± 0.94	5.71 ± 0.40	1.80 ± 0.53	3.17 ± 0.40
Siltuximab	17.0 ± 0.9	-4.85 ± 0.96	-2.84 ± 0.89	5.69 ± 0.39	1.84 ± 0.42	3.16 ± 0.39
Ustekinumab	16.5 ± 0.8	-4.34 ± 0.89	-2.78 ± 0.84	5.61 ± 0.38	1.93 ± 0.41	3.18 ± 0.38
Average	16.8 ± 0.4	-4.66 ± 0.32	-2.82 ± 0.43	5.64 ± 0.18	1.83 ± 0.18	3.18 ± 0.31
(None omitted)	16.8 ± 0.8	-4.63 ± 0.83	-2.88 ± 0.83	5.67 ± 0.32	1.86 ± 0.35	3.15 ± 0.35

3.5 References

[1] Kaplon H, Reichert JM (2017) Antibodies to watch in 2018. *mAbs* **10**:183-203

[2] Spiess C, Zhai Q, and Carter PJ (2015) Alternative molecular formats and therapeutic applications for bispecific antibodies. *Mol Immunol* **67**:95–106.

[3] Beck A, Goetsch L, Dumontet C, and Corvaïa N (2017) Strategies and challenges for the next generation of antibody–drug conjugates. *Nat Rev Drug Discov* **16**:315–337.

[4] Roopenian DC and Akilesh S (2007) FcRn: the neonatal Fc receptor comes of age. *Nat Rev Immunol* **7**:715–25.

[5] Roopenian DC, Christianson GJ, Sproule TJ, Brown AC, Akilesh S, Jung N, Petkova S, Avanessian L, Choi EY, Shaffer DJ, Eden PA, and Anderson CL (2003) The MHC class I-like IgG receptor controls perinatal IgG transport, IgG homeostasis, and fate of IgG-Fc-coupled drugs. *J Immunol* **170**:3528–3533.

[6] Raghavan M, Bonagura VR, Morrison SL, and Bjorkman PJ (1995) Analysis of the pH dependence of the neonatal Fc receptor/immunoglobulin G interaction using antibody and receptor variants. *Biochemistry* **34**:14649–14657.

[7] Suzuki T, Ishii-Watabe A, Tada M, Kobayashi T, Kanayasu-Toyoda T, Kawanishi T, and Yamaguchi T (2010) Importance of neonatal FcR in regulating the serum half-life of therapeutic proteins containing the Fc domain of human IgG1: A comparative study of the affinity of monoclonal antibodies and Fc-fusion proteins to human neonatal FcR. *J Immunol* **184**:1968–1976.

[8] Tam SH, McCarthy SG, Brosnan K, Goldberg KM, and Scallon BJ (2013) Correlations between pharmacokinetics of IgG antibodies in primates vs. FcRn-transgenic mice reveal a rodent model with predictive capabilities. *mAbs* **5**:397–405.

[9] Robbie GJ, Criste R, Dall'Acqua WF, Jensen K, Patel NK, Losonsky GA, and Griffin MP (2013) A novel investigational Fc-modified humanized monoclonal antibody, motavizumab-YTE, has an extended half-life in healthy adults. *Antimicrob Agents Chemother* **57**:6147–6153.

[10] Wang W, Wang EQ, and Balthasar JP (2008) Monoclonal antibody pharmacokinetics and pharmacodynamics. *Clin Pharmacol Ther* **84**:548–558.

[11] Dostalek M, Prueksaritanont T, and Kelley RF (2017) Pharmacokinetic de-risking tools for selection of monoclonal antibody lead candidates. *mAbs* **9**:756-766.

[12] Avery LB, Wade J, Wang M, Tam A, King A, Piche-Nicholas N, Kavosi MS, Penn S, Cirelli D, Kurz JC, Zhang M, Cunningham O, Jones R, Fennell BJ, McDonnell B, Sakorafas P, Apgar J, Finlay WJ, Lin L, Bloom L, and O'Hara DM (2018) Establishing *in vitro in vivo* correlations to screen monoclonal antibodies for physicochemical properties related to favorable human pharmacokinetics. *mAbs* **10**:244–255.

[13] Wang W, Lu P, Fang Y, Hamuro L, Pittman T, Carr B, Hochman J, and Prueksaritanont T (2011) Monoclonal antibodies with identical Fc sequences can bind to FcRn differentially with pharmacokinetic consequences. *Drug Metab Dispos* **39**:1469–1477.

[14] Souders CA, Nelson SC, Wang Y, Crowleya AR, Klempner MS, and Thomas W Jr. (2015) A novel in vitro assay to predict neonatal Fc receptor-mediated human IgG half-life. *mAbs* **7**:912– 921.

[15] Datta-Mannan A, Lu J, Witcher DR, Leung D, Tang Y, and Wroblewski VJ (2015) The interplay of non-specific binding, target-mediated clearance and FcRn interactions on the pharmacokinetics of humanized antibodies. *mAbs* **7**:1084–1093.

[16] Datta-Mannan A, Thangaraju A, Leung D, Tang Y, Witcher DR, Lu J, Wroblewski VJ (2015) Balancing charge in the complementarity-determining regions of humanized mAbs without affecting pI reduces non-specific binding and improves the pharmacokinetics. mAbs **7**:483–493.

[17] Tibbitts J, Canter D, Graff R, Smith A, Khawli LA (2016) Key factors influencing ADME properties of therapeutic proteins: A need for ADME characterization in drug discovery and development. *mAbs* **8**:229-245.

[18] Jain T, Sun T, Durand S, Hall A, Houston NR, Nett JH, Sharkey B, Bobrowicz B, Caffry I, Yu Y, Cao Y, Lynaugh H, Brown M, Baruah H, Gray LT, Krauland EM, Xu Y, Vásquez M, Wittrup KD. (2017) Biophysical properties of the clinical-stage antibody landscape. *Proc Natl Acad Sci U S A* **114**:944-949.
[19] Tibshirani R (1996) Regression selection and shrinkage via the lasso. *J R Stat Soc B* **58**:267–288.
[20] Abdiche YN, Yeung YA, Chaparro-Riggers J, Barman I, Strop P, Chin SM, Pham A, Bolton G, McDonough D, Lindquist K, Pons J, Rajpal A. (2015) The neonatal Fc receptor (FcRn) binds independently to both sites of the IgG homodimer with identical affinity. *mAbs* **7**:331-343.
[21] Majumdar R, Esfandiary R, Bishop SM, Samra HS, Middaugh CR, Volkin DB, and Weis DD (2015) Correlations between changes in conformational dynamics and physical stability in a mutant IgG1 mAb engineered for extended serum half-life. *mAbs* **7**:84–95.
[22] Tibshirani R (2011) Regression shrinkage and selection via the lasso: A retrospective. *J R Stat Soc B* **73**:273–282.
[23] Ternant D, Arnoult C, Pugnière M, Dhommée C, Drocourt D, Perouzel E, Passot C, Baroukh N, Mulleman D, Tiraby G, Watier H, Paintaud G, and Gouilleux-Gruart V (2016) IgG1 allotypes influence the pharmacokinetics of therapeutic monoclonal antibodies through FcRn binding. *J Immunol* **196**:607–613.
[24] Stapleton NM, Andersen JT, Stemerding AM, Bjarnarson SP, Verheul RC, Gerritsen J, Zhao Y, Kleijer M, Sandlie I, de Haas M, Jonsdottir I, van der Schoot E, Vidarsson G (2011) Competition for FcRn-mediated transport gives rise to short half-life of human IgG3 and offers therapeutic potential. *Nat Comm* 2:1-9.
[25] Schoch A, Kettenberger H, Mundigl O, Winter G, Engert J, Heinrich J, and Emrich T (2015) Charge-mediated influence of the antibody variable domain on FcRn-dependent pharmacokinetics. *Proc Natl Acad Sci U S A* **112**:5997–6002.
[26] Dall'Acqua WF, Kiener PA, and Wu H (2006) Properties of human IgG1s engineered for enhanced binding to the neonatal Fc Receptor (FcRn). *J Biol Chem* **281**:23514–23524.
[27] Hinton PR, Xiong JM, Johlfs MG, Tang MT, Keller S, and Tsurushita N (2006) An engineered human IgG1 antibody with longer serum half-life. *J Immunol* **176**:346–356.
[28] Zalevsky J, Chamberlain AK, Horton HM, Karki S, Leung IWL, Sproule TJ, Lazar GA, Roopenian DC, and Desjarlais JR (2010) Enhanced antibody half-life improves in vivo activity. *Nat Biotechnol* **28**:157–159.
[29] Datta-Mannan A, Chow CK, Dickinson C, Driver D, Lu J, Witcher DR, and Wroblewski VJ (2012) FcRn affinity-pharmacokinetic relationship of five human IgG4 antibodies engineered for improved in vitro FcRn binding properties in cynomolgus monkeys. *Drug Metab Dispos* **40**:1545–1555.
[30] Dall'Acqua WF, Woods RM, Ward ES, Palaszynski SR, Patel NK, Brewah YA, Wu H, Kiener PA, and Langermann S (2002) Increasing the Affinity of a Human IgG1 for the Neonatal Fc Receptor: Biological Consequences. *J Immunol* **169**:5171–5180.
[31] Gurbaxani B, Dela Cruz L., Chintalacharuvu K, and Morrison SL (2006) Analysis of a family of antibodies with different half-lives in mice fails to find a correlation between affinity for FcRn and serum half-life. *Mol Immunol* **43**:1462–1473.
[32] Borrok MJ, Wu Y, Beyaz N, Yu X-Q, Oganesyan V, Dall'Acqua WF, and Tsui P (2015) pH-dependent binding engineering reveals an FcRn affinity threshold that governs IgG recycling. *J Biol Chem* **290**:4282–4290.
[33] Ratanji KD, Derrick JP, Dearman RJ, and Kimber I (2014) Immunogenicity of therapeutic proteins: Influence of aggregation. *J Immunotoxicol* **11**:99–109.
[34] Roberts CJ (2014) Therapeutic protein aggregation: mechanisms, design, and control. *Trends Biotechnol* **32**:372–380.
[35] Kyte J and Doolittle RF (1982) A simple method for displaying the hydropathic character of a protein. *J Mol Biol* **157**:105–132.

[36] Humira (adalimumab) label, US Food and Drug Administration, revised 03/2017: https://www.accessdata.fda.gov/drugsatfda_docs/label/2017/125057s399lbl.pdf

[37] Weisman MH, Moreland LW, Furst DE, Weinblatt ME, Keystone EC, Paulus HE, Teoh LS, Velagapudi RB, Noertersheuser PA, Granneman GR, Fischkoff SA, and Chartash EK (2003) Efficacy, pharmacokinetic, and safety assessment of adalimumab, a fully human anti-tumor necrosis factor-alpha monoclonal antibody, in adults with rheumatoid arthritis receiving concomitant methotrexate: A pilot study. *Clin Ther* **25**:1700–1721.

[38] den Broeder A, van de Putte LBA, Rau R, Schattenkirchner M, Van Riel PLCM, Sander O, Binder C, Fenner H, Bankmann Y, Velagapudi R, Kempeni J, and Kupper H (2002) A single dose, placebo controlled study of the fully human anti-tumour necrosis factor-alpha antibody adalimumab (D2E7) in patients with rheumatoid arthritis. *J Rheumatol* **29**:2288–2298.

[39] Avastin (bevacizumab) label, US Food and Drug Administration, revised 12/2016: https://www.accessdata.fda.gov/drugsatfda_docs/label/2016/125085s317lbl.pdf.

[40] Han K, Peyret T, Marchand M, Quartino A, Gosselin NH, Girish S, Allison DE, and Jin J (2016) Population pharmacokinetics of bevacizumab in cancer patients with external validation. *Cancer Chemother Pharmacol* **78**:341–351.

[41] Li J, Gupta M, Jin D, Xin Y, Visich J, and Allison DE (2013) Characterization of the long-term pharmacokinetics of bevacizumab following last dose in patients with resected stage II and III carcinoma of the colon. *Cancer Chemother Pharmacol* **71**:575–580.

[42] Lu J-F, Bruno R, Eppler S, Novotny W, Lum B, and Gaudreault J (2008) Clinical pharmacokinetics of bevacizumab in patients with solid tumors. *Cancer Chemother Pharmacol* **62**:779–786.

[43] Janssen 2014 Compound Information CTNO888, National Institutes of Health, 2014: https://ncats.nih.gov/files/CNTO-888.pdf.

[44] Sandhu SK, Papadopoulos K, Fong PC, Patnaik A, Messiou C, Olmos D, Wang G, Tromp BJ, Puchalski TA, Balkwill F, Berns B, Seetharam S, de Bono JS, and Tolcher AW (2013) A first-in-human, first-in-class, phase I study of carlumab (CNTO 888), a human monoclonal antibody against CC-chemokine ligand 2 in patients with solid tumors. *Cancer Chemother Pharmacol* **71**:1041–1050.

[45] Simponi (golimumab) label, US Food and Drug Administration, revised 08/2015: https://www.accessdata.fda.gov/drugsatfda_docs/label/2015/125433s014lbl.pdf.

[46] Zhuang Y, Xu Z, Frederick B, de Vries DE, Ford JA, Keen M, Doyle MK, Petty KJ, Davis HM, and Zhou H (2012) Golimumab pharmacokinetics after repeated subcutaneous and intravenous administrations in patients with rheumatoid arthritis and the effect of concomitant methotrexate: An open-label, randomized dtudy. *Clin Ther* **34**:77–90.

[47] Zhuang Y, Lyn S, Lv Y, Xu Z, Bouman-Thio E, Masterson T, Ford JA, Keen M, Petty KJ, Davis HM, and Zhou H (2013) Pharmacokinetics and safety of golimumab in healthy Chinese subjects following a single subcutaneous administration in a randomized phase I trial. *Clin Drug Investig* **33**:795–800.

[48] Ling J, Lyn S, Xu Z, Achira M, Bouman-Thio E, Shishido A, Ford J, Shankar G, Wagner C, Kim KT, Davis HM, and Zhou H (2010) Lack of racial differences in the pharmacokinetics of subcutaneous golimumab in healthy Japanese and caucasian male subjects. *J Clin Pharmacol* **50**:792–802.

[49] Xu Z, Wang Q, Zhuang Y, Frederick B, Yan H, Bouman-Thio E, Marini JC, Keen M, Snead D, Davis HM, and Zhou H (2010) Subcutaneous bioavailability of golimumab at 3 different injection sites in healthy subjects. *J Clin Pharmacol* **50**:276–284.

[50] Zhou H, Jang H, Fleischmann RM, Bouman-Thio E, Xu Z, Marini JC, Pendley C, Jiao Q, Shankar G, Marciniak SJ, Cohen SB, Rahman MU, Baker D, Mascelli MA, Davis HM, and Everitt DE (2007) Pharmacokinetics and safety of golimumab, a fully human anti-TNF-α monoclonal antibody, in subjects with rheumatoid arthritis. *J Clin Pharmacol* **47**:383–396.

[51] Remicade (infliximab) label, US Food and Drug Administration, revised 11/2013: https://www.accessdata.fda.gov/drugsatfda_docs/label/2013/103772s5359lbl.pdf.

[52] Dotan I, Ron Y, Yanai H, Becker S, Fishman S, Yahav L, Ben Yehoyada M, and Mould DR (2014) Patient factors that increase infliximab clearance and shorten half-life in inflammatory bowel disease. *Inflamm Bowel Dis* **20**:2247–2259.

[53] Fasanmade AA, Adedokun OJ, Blank M, Zhou H, and Davis HM (2011) Pharmacokinetic properties of infliximab in children and adults with Crohn's disease: A retrospective analysis of data from 2 Phase III clinical trials. *Clin Ther* **33**:946–964.

[54] Cornillie F, Shealy D, D'Haens G, Geboes K, Van Assche G, Ceuppens J, Wagner C, Schaible T, Plevy SE, Targan SR, and Rutgeerts P (2001) Infliximab induces potent anti-inflammatory and local immunomodulatory activity but no systemic immune suppression in patients with Crohn's disease. *Aliment Pharmacol Ther* **15**:463–473.

[55] Ternant D, Aubourg A, Magdelaine-Beuzelin C, Degenne D, Watier H, Picon L, and Paintaud G (2008) Infliximab pharmacokinetics in inflammatory bowel disease patients. *Ther Drug Monit* **30**:523–529.

[56] Xolair (omalizumab) label, US Food and Drug Administration, Revised 07/2016: https://www.accessdata.fda.gov/drugsatfda_docs/label/2016/103976s5225lbl.pdf.

[57] Hayashi N, Tsukamoto Y, Sallas WM, and Lowe PJ (2007) A mechanism-based binding model for the population pharmacokinetics and pharmacodynamics of omalizumab. *Br J Clin Pharmacol* **63**:548–561.

[58] Sylvant (siltuximab) label, US Food and Drug Administration, 2014: https://www.accessdata.fda.gov/drugsatfda_docs/label/2014/125496s000lbl.pdf.

[59] Kurzrock R, Voorhees PM, Casper C, Furman RR, Fayad L, Lonial S, Borghaei H, Jagannath S, Sokol L, Usmani SZ, van de Velde H, Qin X, Puchalski TA, Hall B, Reddy M, Qi M, and van Rhee F (2013) A phase I, open-label study of siltuximab, an anti-IL-6 monoclonal antibody, in patients with B-cell non-Hodgkin lymphoma, multiple myeloma, or Castleman disease. *Clin Cancer Res* **19**:3659–3670.

[60] Stelara (ustekinumab) label, US Food and Drug Administration, revised 09/2016: https://www.accessdata.fda.gov/drugsatfda_docs/label/2016/761044lbl.pdf

[61] Zhu Y, Wang Q, Frederick B, Bouman-Thio E, Marini JC, Keen M, Petty KJ, Davis HM, and Zhou H (2013) Comparison of the pharmacokinetics of subcutaneous ustekinumab between Chinese and non-Chinese healthy male subjects across two phase 1 studies. *Clin Drug Investig* **33**:291–301.

CHAPTER 4

Mechanism of Controlled Fab-Arm Exchange to Form Bispecific Antibodies

Note: This chapter was adapted with permission from:
Goulet DR, Orcutt SJ, Zwolak A, Rispens T, Labrijn AF, de Jong RN, Atkins WM, Chiu ML. Kinetic Mechanism of Controlled Fab-Arm Exchange for the Formation of Bispecific Immunoglobulin G1 Antibodies. *J. Biol. Chem*. **2018**, *293*, 651-661.

4.1 Introduction

Bispecific antibodies (bsAbs) combine the antigen specificities of two parental Abs to create multifunctional molecules capable of simultaneously binding two distinct targets. In the pharmaceutical industry, bsAbs offer several biological mechanisms for treating disease that are not possible using traditional small molecule or monoclonal Ab therapies.[1-4] For example, targeting two tumor antigens allows for inhibition of orthogonal signaling pathways and can increase specificity for cancer cells versus healthy tissue while also mitigating the incidence of resistance mechanisms.[5-7] BsAbs can also facilitate co-localization of different cell types for applications such as T-cell redirection, where the immune system is activated against tumor cells.[8] With two clinical approvals in 2009 and 2014 and many molecules in ongoing clinical trials, bsAbs are a relatively novel class of biotherapeutics whose development has been aided by protein engineering. [1,9,10]

Currently, there are several platforms of bsAbs which can be categorized based on their inclusion of the Fc region.[1,11,12] BsAb formats omitting the Fc domain, such as bispecific T-cell engagers (BiTEs) and dual-affinity retargeting proteins (DARTs), generally contain Ab variable fragments connected via polypeptide linkers.[13,14] Although the small size of these Abs relative to intact immunoglobulin G (IgG) may allow for increased penetration to solid tumors, the absence of the Fc region abrogates binding to Fc receptors responsible for mediating immune effector

functions and long serum half-life.[15,16] Bispecific molecules based on the structure of full-length IgG retain Fc receptor binding but must be engineered to drive formation of the heavy chain heterodimer while retaining the correct pairing of heavy and light chains. The heavy chain pairing problem has been addressed by incorporating complementary mutations into the C_H3 region using technologies such as knobs-into-holes, electrostatic steering, and controlled Fab-arm exchange (cFAE).[17-19] cFAE uses a minimal set of mutations and avoids the light chain pairing issue, as exchange of half-Abs can be performed without perturbing the correct heavy-light chain interaction.

The cFAE reaction for formation of bispecific IgG1 was modeled after Fab-arm exchange (FAE) that occurs naturally in human IgG4, but not in other IgG subclasses.[20-22] In general, the dimerization of heavy chains in the Fc relies on a combination of covalent interchain disulfide bonds mediated by hinge cysteine residues and non-covalent interactions primarily mediated by the C_H3 domain. Like other isotypes, IgG4 Abs contain heavy chains that are normally linked by disulfide bonds in the hinge region. However, in IgG4 these hinge cysteines are contained within the motif "CPSC", whereas other isotypes contain "CPPC". The presence of serine at position 228 confers the hinge with extra flexibility that allows for the formation of intrachain disulfide bonds instead of the stabilizing interchain disulfide bonds.[23] Additionally, IgG4 Abs contain arginine at position 409 (versus lysine in IgG1) which destabilizes the non-covalent interaction between heavy chains in the C_H3 domain.[24] This combination of a labile hinge region and a destabilized C_H3 domain allows IgG4 to undergo half-Ab exchange.[22] The F405L substitution similarly serves to decrease heavy chain dimerization affinity, but importantly, the interaction of complementary mutants is energetically preferred over the interaction of either homodimer.[19] For the sake of clarity, exchange of any pair of half-Abs is here referred to as "Fab-arm exchange," while the term

"controlled Fab-arm exchange" is reserved for the process of generating bsAbs from parental Abs containing F405L / K409R mutations.

To create bispecific IgG1 using cFAE, two parental Abs are separately expressed with the F405L or K409R mutations. Following purification, the parental Abs are combined under mildly reducing conditions to selectively reduce the hinge disulfide bonds between parental heavy chains. Upon re-oxidation, intact bsAb is generated with yields over 90%.[19,25] The formation of therapeutic bsAbs is mechanistically more complex than the naturally occurring exchange that takes place with IgG4 molecules, because two heavy chains with chemically distinct C_H3 domains allow for three possible half-Ab interactions. As a result, each parental Fc dissociation rate must be considered and could contribute to the overall rate of the reaction.

Although cFAE is used for the formation of several bispecific therapeutic IgGs in clinical trials, a full description of its mechanism has not been reported, and rates of its individual steps have not been accurately determined.[26-28] Identification of rate-limiting steps of the reaction and conditions that affect the reaction rates will help to optimize large-scale production of bsAbs using cFAE and control the conjugation of drugs to the hinge cysteines of antibodies.[29] A mechanistic analysis of cFAE is presented here, with description of each elementary step from oxidized parental Abs to oxidized bsAb product. The use of Förster resonance energy transfer (FRET) allowed for real-time monitoring of cFAE as half-Abs with donor or acceptor labels assembled into a single Ab molecule. Affinities for half-Ab homo- and heterodimerization were compared and confirmed a thermodynamic preference for bsAb over parental Abs. The rate constants of reduction and re-oxidation of inter-heavy chain disulfide bonds were determined based on non-reducing SDS-PAGE of the reaction contents over time. Together, the results elucidate a series of disulfide redox and protein-protein interaction events that can be experimentally regulated based

on subtle changes to conditions such as pH and ionic strength.

4.2 Experimental procedures

4.2.1 Proteins and other materials

Abs against respiratory syncytial virus (RSV, clone B21M, containing F405L) and HIV envelope glycoprotein gp120 (clone B12, containing K409R) in human IgG1 and human IgG1 lacking hinge disulfides (C226S/C229S) were expressed transiently in EXPI293F cells (Thermo Fisher, A14527) according to the manufacturer's protocol.[30,31] Purification was performed using a mAbSelect SuRe column (GE Life Sciences, 11-0034-94) according to the manufacturer's protocol, followed by immediate buffer exchange over a desalting column (GE Life Sciences, 17-5087-01) into fresh phosphate-buffered saline (PBS: 2.67 mM KCl, 1.47 mM KH_2PO_4, 138 mM NaCl, 8.06 mM Na_2HPO_4, pH 7.2). SDS-PAGE and analytical size-exclusion chromatography (SEC) were used to analyze proteins. Hydrophobic interaction chromatography was used to ensure that cFAE went to completion (>90% bsAb) for both $IgG1_{WT}$ and $IgG1_{C\rightarrow S}$.

4.2.2 Hydrophobic interaction chromatography

HIC was used as an orthogonal technique to FRET to ensure formation of >90% bsAb for $IgG1_{WT}$ and $IgG1_{C\rightarrow S}$ Abs containing F405L/K409R mutations. After performing cFAE reactions including dialysis to remove reducing agent, 20 µg of protein was injected onto a butyl-NPR column (Tosoh Bioscience, 42168) and parental Abs were separated from bsAb using a gradient from 1.5 M to 0 M $(NH_4)_2SO_4$ in 0.1 M sodium phosphate, pH 6.5 at 0.5 mL/min. HIC of purified parental Abs was also performed to identify which protein each peak represents.

4.2.3 Fluorescent labeling

Abs were diluted to 5 mg/mL in PBS containing 100 mM sodium bicarbonate, pH 8.3 and labeling was performed by adding a 6-fold molar equivalent of Alexa 488 or Alexa 594 NHS esters

(ThermoFisher A-20000, A-20004) from a 10 mg/mL stock in DMSO. The reaction was incubated in the dark for one hour at room temperature, followed by two rounds of buffer exchange (GE Life Sciences, 28-9180-04). Concentration of labeled Ab and dye were calculated using absorbance as follows:

$$[Ab] = \frac{A_{Ab} - (A_{dye} \times CF)}{\varepsilon_{Ab}} \qquad [Dye] = \frac{A_{dye}}{\varepsilon_{dye}}$$

where α-RSV F405L had ε_{280} = 220,000 $M^{-1}cm^{-1}$, α-gp120 K409R had ε_{280} = 231,000 $M^{-1}cm^{-1}$, the donor (Alexa 488) had ε_{494} = 73,000 $M^{-1}cm^{-1}$ and correction factor (CF) = 0.143 in PBS, and the acceptor (Alexa 594) had ε_{590} = 92,000 $M^{-1}cm^{-1}$ and CF = 0.564 in PBS. The final dye:Ab ratio was 1-2.

4.2.4 IgG cleavage to generate Fc fragments

After labeling 1 mg each of α-RSV F405L and α-gp120 K409R in $IgG1_{WT}$ with 10x Alexa 488 as described above, Fc and $F(ab')_2$ were generated using IdeS enzyme (FabRICATOR, Genovis) according to the manufacturer's instructions. The Fc fraction was purified using protein A chromatography as described above. SEC was also performed using a Superdex 200 10/300 GL column (GE, 17517501) in PBS at 0.5 mL/min to remove undigested or singly digested IgG and residual free dye. Purity of Fc domains was analyzed by SDS-PAGE (**Figure 4.1**). The final dye:Ab ratio was ~2.

4.2.5 Förster resonance energy transfer

Experiments were performed in black half-area 96-well plates (Corning, 3993) using 100 nM of each parental Ab-dye conjugate in 50 μL of PBS at 25 ºC. The FAE reaction was initiated either by adding 50 mM MEA or 10 mM DTT to the mixture of $IgG1_{WT}$, or by combining pairs of Abs in the case of $IgG1_{C \rightarrow S}$ and was monitored every 30 seconds (or every 10 seconds in the case of the different Ab pairs) by exciting at 494 nm and measuring emission at 617 nm (corresponding

to fluorescence of the acceptor fluorophore) on a SpectraMax M5 plate reader. FRET signal was normalized by subtracting the minimum fluorescence and dividing by the maximum FRET in a dataset. cFAE reactions were performed once with the α-RSV F405L Alexa 488 / α-gp120 K409R Alexa 594 pairing and once with the α-RSV F405L Alexa 494 / α-gp120 K409R Alexa 488 pairing, with reported rates as the average ± standard deviation. The effect on kinetics of labeling with different amounts of dye was determined over a dye:Ab range of ~0.5 to ~15 (**Figure 4.2**). Rates were determined using monoexponential fits in GraphPad Prism 7.

To clarify the effect of different Ab concentrations, the reaction was performed using 1:3 dilutions of Ab starting with 4 μM total Ab. To clarify the role of the reductant, MEA or DTT was added from 1:2 dilutions starting with a final concentration of 200 mM. To determine pH dependence, the reaction buffer was 100 mM potassium phosphate, 100 mM sodium chloride with a pH ranging from 5 to 9 in 0.5-pH increments. To determine salt dependence, the reaction buffer was 20 mM potassium phosphate containing 1:2 serial dilutions of sodium chloride, starting at 2.5 M. When comparing rates of FAE for different pairs of Abs, the concentration was increased to 200 nM of each parental Ab to increase signal, since only half of products were FRET-active.

4.2.6 Fluorescence correlation spectroscopy

Experiments were performed on an Axio Observer D1 microscope (Zeiss) equipped with an LDH-D-C-485 picosecond pulsed diode 485 nm laser, Tau-SPAD single photon counting module, and HydraHarp 400 for autocorrelation (PicoQuant). Time traces and autocorrelations were collected using SymPhoTime 64 software (PicoQuant).

All buffers were filtered through a 0.22 μm filter prior to sample preparation. Samples contained a constant 50 pM of Alexa 488-labeled half-Fc and 1:3 or 1:4 dilutions of unlabeled half-Ab ($IgG1_{C\rightarrow S}$) and were equilibrated at room temperature overnight before analysis. Sample

aliquots of 50 µL were placed onto 22x22-1 cover glass. With the laser power at 250 µW, several replicate traces were obtained for each sample and contained 200 sampling points and a maximum lag time of 10 seconds. Data collection intervals varied from 60 to 180 seconds in different datasets, but did not significantly affect measured diffusion times. Inclusion of two components significantly improved fits, where one component was fixed at the diffusion time of free Alexa 488 to account for residual free dye in samples. Traces were fit individually using Igor Pro over the range of 0.01 to 1,000 ms using the following two-component three-dimensional diffusion model[32]:

$$G(\tau) = \frac{1}{N}\left[\rho_{dye}\left(\frac{1}{1+\frac{\tau}{\tau_{D,dye}}}\right)\left(\frac{1}{1+\frac{\tau}{s^2\tau_{D,dye}}}\right)^{0.5} + \rho_{prot}\left(\frac{1}{1+\frac{\tau}{\tau_{D,prot}}}\right)\left(\frac{1}{1+\frac{\tau}{s^2\tau_{D,prot}}}\right)^{0.5}\right]$$

where $G(\tau)$ is the autocorrelation at a given lag time τ, N is the average number of particles in the focal volume, $\tau_{D,dye}$ and $\tau_{D,prot}$ are the translational diffusion times of the free dye and protein components, ρ_{dye} and ρ_{prot} represent the fraction of each component, and s is the ratio of long to short axes of the focal volume. The values of s and $\tau_{D,dye}$ were fixed at 10 and 0.25 ms for all samples based on their values for free Alexa 488. The τ_D of the protein component was the value used for binding curves. For all samples, the labeled half-Fc contributed >80% of the total signal with the remainder from the free dye component.

Binding curves plot the diffusion times from FCS versus the concentration of unlabeled half-Ab. Each point represents the average of 3-10 replicates, and each interaction contained datasets from three different days. Curves were globally fit to a custom fitting equation (**Scheme 4.1**) that accounts for half-Fc and half-Ab homodimerization in addition to the heterodimerization interaction.

4.2.7 Disulfide redox kinetics

To determine rates of hinge reduction and re-oxidation, 1 mg/mL each of α-RSV F405L and α-gp120 K409R were reduced with 50 mM MEA or 10 mM DTT and incubated for four hours at 25 ºC with shaking at 300 rpm. At each time point, a 5 µL aliquot was removed from the reaction and quenched with 5 µL of 375 mM iodoacetamide (ThermoFisher, 90034) in 200 mM sodium bicarbonate, pH 8.0. Later, all the quenched samples were analyzed by non-reducing SDS-PAGE on a NuPAGE 4-12% gel (ThermoFisher, NP0323BOX), loading 3 µL per lane. Band densities were quantified using ImageLab software, and the percentage of oxidized hinge was calculated by dividing the sum of densities of the 150, 125, and 100 kDa bands by the sum of densities of the 150, 125, 100, 75, and 50 kDa bands. The datasets were fit to a sum of an exponential decay and an exponential association equation to extract reduction and re-oxidation rates. Each reaction was performed in duplicate with rates reported as average ± standard deviation.

4.2.8 Simulation

The SimBiology toolbox of Mathematica R2017a was used to model cFAE kinetics. Equilibria included F405L half-Ab homodimerization, K409R half-Ab homodimerization, and half-Ab heterodimerization. The FAE rates measured by kinetic FRET experiments of $IgG1_{C\rightarrow S}$ antibodies was used for the k_d of each binding reaction. The k_a values were determined using k_d values from FRET and K_D values from FCS ($k_a = k_d/K_D$). In addition to half-Ab binding, the equilibria between oxidized and reduced hinges were also included. The k_{red} and k_{ox} values were based on SDS-PAGE experiments with 50 mM MEA. The simulated reaction initially contained 222 nM of each oxidized parental Ab and was monitored for 180 minutes using the ode23t solver. The total amount of bsAb was defined as the sum of oxidized and reduced bsAb.

4.3 Results

4.3.1 Characterization of IgG hinge mutants

The formation of bsAb from two parental Abs requires the reduction of hinge disulfides, which allows for the exchange of half-Abs from parental homodimers to heterodimers. Parental IgG1 Abs with a native hinge contain a pair of inter-heavy chain disulfide bonds mediated by C226 and C229 from each half-Ab and therefore undergo exchange only under reducing conditions ($IgG1_{WT}$, **Figure 4.3A**). IgG1 hinge variants containing the C226S/C229S mutations provide a powerful mechanistic probe of cFAE ($IgG1_{C\rightarrow S}$, **Figure 4.3B**). These mutations eliminate the covalent bonds between heavy chains and allow FAE to occur even in the absence of reductant. The $IgG1_{C\rightarrow S}$ constructs had typical human IgG1 expression levels and purification properties as well as normal bsAb yield via cFAE (**Figures 4.4-4.6**). Comparison of the kinetic profiles for cFAE with these constructs helped to elucidate which steps of the reaction involve redox chemistry at the hinge, and which are related to inter-heavy chain interactions occurring in the C_H3 domain. Note that both $IgG1_{WT}$ and $IgG1_{C\rightarrow S}$ Abs contain the appropriate cFAE mutations (F405L or K409R); the term "wild-type" for $IgG1_{WT}$ refers to the Ab hinge region.

4.3.2 Kinetics of controlled Fab-arm exchange

Progress of cFAE was monitored using Förster resonance energy transfer (FRET), with each parental Ab labeled with a different fluorophore (**Figure 4.3C**). For example, an α-RSV Ab containing F405L was labeled with Alexa 488 as the FRET donor and an α-gp120 Ab containing K409R was labeled with Alexa 594 as the acceptor. The labeled Abs were then combined in equimolar amounts, and upon reduction of hinge disulfides, the Abs undergo FAE to form the bsAb which contains both fluorophores. In this bsAb, donor and acceptor dyes are within the Förster radius of ~60 Å, and FRET increases the fluorescence of the acceptor fluorophore.[33] The

increase in FRET signal provides a real-time readout of bsAb formation and can be used to characterize the kinetics of cFAE.[22,34] When cFAE was performed with two distinct sets of IgG1 Abs containing cFAE mutations, there was no significant difference in the observed rates (**Figure 4.7**). However, cFAE proceeded slightly faster for IgG1 Abs than the corresponding IgG4 S228P L234A L235A subtype Abs (**Figure 4.8**).

4.3.3 Effect of antibody concentration

To determine whether association of Abs or half-Abs is involved in the rate-determining step of cFAE, the reaction was performed with varying concentrations of parental Ab. If the slow step of cFAE were association of half-Abs to full Ab or association of intact Abs to Ab dimer, the reaction would proceed faster with increasing Ab concentrations. In contrast, if the rate-limiting step were a dissociation event, the overall rate of cFAE would be concentration independent. FRET was used to monitor the cFAE reaction using various concentrations of $IgG1_{WT}$ or $IgG1_{C\rightarrow S}$ Abs. The rate was not affected by the concentration of antibody over the range of 16 nM to 4 μM, whether exchange was initiated by adding 2-mercaptoethylamine (MEA) to a mixture of parental $IgG1_{WT}$ Abs or by combining parental $IgG1_{C\rightarrow S}$ Abs (**Figure 4.9**). This result eliminates the possibility that association controls the overall rate, but instead indicates that dissociation to half-Ab is rate-limiting. For $IgG1_{WT}$, (**Figure 4.9A**) there was a lag phase in the kinetic trace for the first 15 minutes of the reaction. Because this lag is not seen for the $IgG1_{C\rightarrow S}$ constructs (**Figure 4.9B**), it could be caused by the hinge reduction step. Thus, the requirement for an initial reduction of hinge disulfides reduces the rate of cFAE for $IgG1_{WT}$ compared to $IgG1_{C\rightarrow S}$ and causes a lag phase at early extent of reaction.

4.3.4 Effect of reducing agent

The role of the reducing agent was further explored by performing cFAE in the presence

of different concentrations of MEA or dithiothreitol (DTT). For $IgG1_{WT}$, there was a strong rate dependence on the concentration of MEA or DTT used to initiate the reaction (**Figure 4.10A**, **B**), with higher reductant concentrations leading to faster rates. In general, the rates with MEA were slower than those with an equivalent concentration of DTT, which is consistent with the stronger reduction potential of DTT.[35,36] The type and concentration of reducing agent played a less significant role when the reaction was performed with $IgG1_{C\rightarrow S}$. The concentration of MEA did not significantly affect the rate of cFAE for these hinge mutants (**Figure 4.10C**), nor did the concentration of DTT alter the rate at concentrations below 25 mM (**Figure 4.10D**). However, the reaction was accelerated in the presence of very high concentrations of DTT.

A summary of these experimental results (**Figure 4.11**) illustrates that cFAE does not proceed in the absence of reducing agent for $IgG1_{WT}$, but proceeds at an appreciable rate for $IgG1_{C\rightarrow S}$ even without reducing agent. As the concentration of MEA or DTT is increased, the rate of exchange remains constant for $IgG1_{C\rightarrow S}$, since hinge reduction is not necessary. The rate of cFAE for $IgG1_{WT}$ increases from zero until reaching a plateau that is similar to the rate for $IgG1_{C\rightarrow S}$. In both cases, high concentrations of DTT accelerate the reaction beyond this plateau. Since cFAE occurs at similar rates under these conditions in the absence or presence of hinge disulfides, it is likely that the effects of DTT are mediated at other sites within the proteins.

4.3.5 Effects of pH and ionic strength

Because IgG1 hinge reduction clearly contributes to the rate of cFAE, and because disulfide chemistry involves thiolates as the active species[37], the reaction was expected to proceed faster at higher pH for $IgG1_{WT}$. In fact, cFAE with $IgG1_{WT}$ came to completion faster at higher pH in the presence of 50 mM MEA (**Figure 4.12A**) or 10 mM DTT (**Figure 4.12B**). Although the minimum rates were larger, there was also a pH dependence for $IgG1_{C\rightarrow S}$, which suggests that the

pH effect is not entirely the result of thiol redox chemistry at the hinge (**Figure 4.12C**). The effect of pH is more apparent when plotting the fitted rate of the reaction at each pH value (**Figure 4.14A**) and emphasizes that the reaction is greatly hindered by lowering the pH to <6 for $IgG1_{WT}$. For $IgG1_{C\rightarrow S}$ the effect is similar but less dramatic. The pKa values recovered from sigmoidal fits of the rate vs. pH curves are similar for all conditions: 6.77 ± 0.04 for $IgG1_{WT}$ with 50 mM MEA, 6.76 ± 0.08 for $IgG1_{WT}$ with 10 mM DTT, and 6.96 ± 0.44 for $IgG1_{C\rightarrow S}$. When cFAE is performed with Abs containing a native hinge, the reaction appears to proceed fastest at pH 8, regardless of whether MEA or DTT is used.

Similarly, changes in ionic strength were expected to alter the reaction kinetics due to the dominance of charge effects at low ionic strength and of hydrophobic interactions at high ionic strength. Thus, cFAE was performed in buffers containing 0 to 2.5 M NaCl, which resulted in a similar trend in the rate profiles of $IgG1_{WT}$ with 50 mM MEA (**Figure 4.13A**), $IgG1_{WT}$ with 10 mM DTT (**Figure 4.13B**), and $IgG1_{C\rightarrow S}$ (**Figure 4.13C**). Rate vs. ionic strength curves could be described by a Debye-Huckel-like approximation that has been used previously.[38,39] Although the reaction with MEA reached a slower maximum rate, the reaction clearly proceeded more quickly in buffers with lower ionic strength (**Figure 4.14B**). The maximum rate occurs when the ionic strength is <100 mM regardless of hinge mutations or type of reductant. This result presents two possibilities for the rate-limiting dissociation step. First, the half-Ab interface in the C_H3 could contain repulsive electrostatic interactions that are accentuated in the low salt condition, leading to increased dissociation rate. Second, the half-Ab dimerization interface may contain stabilizing hydrophobic interactions which are dampened at low salt, again resulting in faster dissociation as salt is decreased. In either case, the similarity of trends for $IgG1_{WT}$ and $IgG1_{C\rightarrow S}$ indicates that salt effects occur due to protein-protein interactions in the C_H3 rather than redox chemistry at the hinge.

4.3.6 Kinetics with different pairs of parental Abs

Although the data demonstrate that the rate of cFAE is controlled by dissociation into half-Abs, the dissociation rate varies for each type of parental Ab due to the presence of the F405L or K409R mutations in the C_H3 domain. Thus, the slower of these two dissociation events dictates the overall rate of the reaction. To determine the dissociation rates of each parental Ab into half-Ab, the FRET assay was used with different combinations of labeled parental $IgG1_{C\rightarrow S}$ (**Figure 4.15B**). For example, the reaction with α-RSV F405L Alexa 488 and α-RSV F405L Alexa 594 reports on the rate of dissociation of the F405L parental Ab into half-Ab. In comparing the rate of each exchange reaction, the F405L parental Ab dissociates significantly faster than the K409R parental Ab ($2.25\times10^{-2} \pm 0.62\times10^{-2}$ versus $6.73\times10^{-4} \pm 0.22\times10^{-4}$ s^{-1}). Thus, the slower dissociation of the K409R parental Ab into half-Ab ultimately limits the rate of cFAE. Consistent with these observations, the rate of FAE for the K409R/K409R pair is similar to that of cFAE for the F405L/K409R pair ($6.73\times10^{-4} \pm 0.22\times10^{-4}$ and $7.72\times10^{-4} \pm 1.86\times10^{-4}$ s^{-1}, **Figure 4.15B**, blue and gray curves). When pre-formed bsAb was labeled with donor and acceptor fluorophores and allowed to exchange, the rate was the slowest ($1.98\times10^{-4} \pm 0.05\times10^{-4}$ s^{-1}), indicating that dissociation of the half-Ab heterodimer is slower than dissociation of either homodimer.

4.3.7 Equilibrium dissociation constants

Because binding affinity is proportional to dissociation rate ($K_D = k_d/k_a$), the half-Ab dissociation rates measured by the kinetic assay were expected to correlate with the equilibrium dimerization affinities. To measure K_D values for different pairs of Fc mutants, binding titrations were performed and the fraction bound at each concentration was determined by fluorescence correlation spectroscopy (FCS). This technique monitors the apparent size of a fluorescently labeled particle based on its rate of diffusion through the ~1 fL focal volume. To maximize the

difference in size between bound and unbound states (and therefore maximize signal), titrations were performed with a fixed concentration of labeled half-Fc (~25 kDa) in the presence of varying concentrations of unlabeled half-Ab ($IgG_{C\rightarrow S,}$ ~75 kDa). Upon binding of the labeled half-Fc to half-Ab, the ~4-fold increase in mass leads to a change in translational diffusion time (τ_D) that is observable by FCS. The sensitivity of FCS allowed very dilute concentrations to be explored (50 pM of labeled half-Fc), which was crucial given the tight affinity of these interactions and ensured that most half-Fc was in the monomeric state in the absence of added half-Ab.

After obtaining FCS autocorrelations, curves were fit to a two-component three-dimensional diffusion model with one component fixed to the diffusion time of free dye. Since only ~10% of fluorescence was from free dye, the two-component fits allowed for accurate determination of the τ_D of the protein component. **Figure 4.15C** shows a representative dataset of FCS autocorrelations generated by titrating 50 pM of A488-labeled K409R half-Fc with 0 to 500 pM of K409R half-Ab. Resulting τ_D values were plotted against concentration of half-Ab to generate binding curves, which were fit to equations derived specifically for these FCS experiments (**Figure 4.15D**, **Scheme 4.1**). The equations account for the competitive, non-two state nature of the experiment (since half-Fc and half-Ab may homodimerize or heterodimerize) by having K_D values for each interaction. The K_D values for F405L homodimerization, K409R homodimerization, and bsAb heterodimerization were determined by globally fitting datasets from all four half-Fc/half-Ab combinations. The resulting K_D values were 12.2 ± 3.7, 0.337 ± 0.076, and 0.0656 ± 0.0343 nM for the F405L, K409R, and bsAb interactions, respectively, consistent with the trend for dissociation rates measured kinetically.

4.3.8 Kinetics of hinge redox reactions

Since hinge reduction occurs more quickly than half-Ab exchange, FRET cannot be used

to characterize the rates of Ab reduction and re-oxidation. Instead, non-reducing SDS-PAGE with iodoacetamide quenching was used for this purpose. At the start of the experiment, cFAE of $IgG1_{WT}$ was initiated using 50 mM MEA or 10 mM DTT. Then at each time point, a reaction aliquot was removed and free thiols in the reaction were quenched with an excess of the alkylating agent to prevent further disulfide exchange from occurring. Samples were analyzed by non-reducing SDS-PAGE to monitor the change in Ab redox states with time (**Figure 4.16A**, **B**). Densitometry was used to calculate the percentage of Ab hinge that was oxidized at each time point, and the resulting kinetic trace was fit to a sum of two exponential equations to yield rates of reduction and re-oxidation (**Figure 4.16C**). The rate of reduction of inter-heavy chain disulfide bonds was $9.34\times10^{-4} \pm 1.80\times10^{-4}$ s^{-1} for 50 mM MEA and $2.23\times10^{-3} \pm 0.12\times10^{-3}$ s^{-1} for 10 mM DTT. From the second exponential component, re-oxidation to form inter-heavy chain disulfides occurred at a rate of $1.80\times10^{-4} \pm 0.08\times10^{-4}$ s^{-1} with 50 mM MEA; re-oxidation did not occur to a significant extent in four hours in the presence of 10 mM DTT. To account for the possibility that rates of hinge redox reactions could be framework dependent, the procedure was performed for each parental Ab as well as the combination of Abs. However, the reduction profiles for α-RSV F405L, α-gp120 K409R, and the mixture were similar with rates of $1.48\times10^{-3} \pm 0.04\times10^{-3}$, $1.49\times10^{-3} \pm 0.07\times10^{-3}$, and $1.54\times10^{-3} \pm 0.06\times10^{-3}$ s^{-1}, respectively at 31 ºC (**Figure 4.17**). The re-oxidation kinetics were also similar, with rates of $4.60\times10^{-4} \pm 0.15\times10^{-4}$, $4.00\times10^{-4} \pm 0.26\times10^{-4}$, and $4.19\times10^{-4} \pm 0.24\times10^{-4}$ s^{-1} for F405L parental, K409R parental, and the mixture to form bsAb.

4.3.9 Mechanistic model of controlled Fab-arm exchange

These experiments yield a mechanistic model for the elementary steps of cFAE that occur on the path from oxidized parental Abs to oxidized bsAb for $IgG1_{WT}$ (**Table 4.1**, **Figure 4.18A**). First, the inter-heavy chain disulfide bonds of parental Abs must be reduced, which occurs at a

similar rate for the different Abs used here. The indicated rate was observed using 50 mM MEA as a reducing agent, but reduction kinetics will vary with the concentration and type of reductant as shown in **Figure 4.11**. Next, the parental Abs with reduced hinge disulfides undergo dissociation into half-Abs, which occurs at different rates for the two cFAE mutants. Importantly, the much slower rate of dissociation of the K409R parental Ab is what ultimately determines the rate of cFAE. After dissociation occurs, half-Abs re-associate to form the intact bsAb containing reduced hinge disulfides. This half-Ab heterodimerization competes with homodimerization to parental Ab, but is driven toward the thermodynamically preferred heterodimer due to interactions at the C_H3. Finally, the bispecific product is re-oxidized to form disulfide-stabilized bsAb. The rate of re-oxidation shown is after reduction with 50 mM MEA but is expected to be faster if excess reductant is removed via dialysis.

This model was simulated and compared to FRET data from a cFAE reaction containing 222 nM of each parental Ab and 50 mM MEA (**Figure 4.18B**). The simulation provides the concentration of relevant species as cFAE proceeds. Strikingly, the simulated concentration of half-Ab heterodimer species accurately describes the experimental FRET data. The simulation also describes other relevant species that are more difficult to monitor experimentally, thus clarifying the maximum concentration and lifetime of intermediates. While significant levels of reduced half-Ab homodimers build up early in the reaction, the free half-Abs exist only transiently at this concentration. The energetic instability of the half-Ab intermediates is consistent with half-Ab dissociation as the rate-determining step of cFAE; after half-Abs dissociate, they rapidly re-combine to full Ab.

4.4 Discussion

While an understanding of the cFAE reaction is critically important for optimization of *in vitro* manufacturing, the precise chemical mechanism of bsAb formation using engineered IgG1 variants has not been established. Previously, a FRET assay was used to characterize the mechanism of FAE as it occurs naturally with human IgG4.[22] However, the kinetics of IgG1 cFAE presented here are substantially more complicated due to the exchange of two distinct half-Ab C_H3 domains and the resulting combination of heavy chain interactions including two homodimerization equilibria and one heterodimerization equilibrium. Among the similarities, both mechanisms have parental Ab dissociation as the rate-determining step.[22] Notably, Ab concentration did not affect the rate of cFAE, as there was no significant difference in rate at the bounds of concentrations used (16 nM to 4 μM) for either $IgG1_{WT}$ ($P = 0.173$) or $IgG1_{C\rightarrow S}$ ($P = 0.170$). In the case of bsAb formation, it is the dissociation of the K409R parental Ab, rather than the F405L Ab, that ultimately controls the rate of cFAE. The rate profiles for $IgG1_{WT}$ reduced with MEA or DTT are consistent with hinge reduction being a pre-equilibrium, rather than rate-limiting step, as was observed with IgG4.[22] Although higher concentrations of reductant resulted in faster reaction rates, the process was saturable. The $IgG1_{C\rightarrow S}$ mutants provide a clear upper limit for the rate of cFAE in the absence of hinge cysteines, and $IgG1_{WT}$ reaches this limit only under strongly reducing conditions.

The hinge mutants additionally provided information on the role of interchain disulfides and C_H3 interactions in each elementary step of cFAE. The C226S/C229S mutations have been used previously to prevent inter-heavy chain disulfide bond formation, but never in the context of the cFAE constructs or for mechanistic purposes.[40,41] By comparing the kinetics of cFAE for $IgG1_{WT}$ and $IgG1_{C\rightarrow S}$, it was determined that ionic strength affects the dissociation of half-Abs

based on C_H3 interactions while pH affects thiol redox chemistry as well as protein-protein interactions at the C_H3. The hinge mutants also facilitated the direct comparison of Ab dissociation rates and half-Ab K_Ds by removing the complexity associated with the hinge redox equilibrium.

SDS-PAGE experiments highlight the complexity of disulfide exchange at the hinge when MEA is used as the reducing agent. The fast hinge reduction was accompanied by an immediate, albeit slower, re-oxidation of free thiols. As a result, there was never a time when all hinge disulfides were in the reduced form. Kinetic FRET traces of bsAb formation for $IgG1_{WT}$ showed a lag phase associated with hinge reduction; but even when fits omitted this phase, the reaction was slower than for $IgG1_{C\rightarrow S}$. An explanation for these SDS-PAGE and FRET data is that inter-chain disulfides at the hinge are in a dynamic equilibrium between the oxidized and reduced states. Even after sufficient exposure to MEA, only a population of inter-chain disulfides are reduced at any given time. The ability of MEA to form stable mixed disulfides with protein cysteines, rather than reducing them immediately to the free thiol, likely contributes to this complexity.[42] Previously, hinge disulfides were shown not to undergo significant re-oxidation within the first four hours of cFAE after reduction with 50 mM MEA.[43] While the cause for this discrepancy has not been determined, it could be due to differences in reaction volume (5 mL versus 0.1 mL), temperature (18-22 ºC versus 25 ºC), or other experimental variables.

Both $IgG1_{WT}$ and $IgG1_{C\rightarrow S}$ underwent cFAE at an accelerated rate when DTT was present at concentrations above 25 mM, demonstrating that excess reducing agent can exhibit effects away from the hinge disulfides. This observation is not a result of light chain swapping because all inter-chain disulfide bonds of IgG1κ have been shown to have similar DTT reactivity[44], and the interaction between heavy chain and κ light chain is stable even when the inter-chain disulfides have been reduced and alkylated.[45] Rather, the high concentrations of DTT probably allow for

reduction of intrachain disulfide bonds, which causes an increased rate of half-Ab dissociation and thus of cFAE. It has been shown that the stability of immunoglobulin domains such as the C_H3 are weakened upon intrachain disulfide reduction, and it is not unreasonable that this destabilization could increase the rate of half-Ab dissociation.[46] Regardless of how this rate acceleration occurred, it did not affect other kinetic experiments performed under less reducing conditions.

Determination of binding affinity constants was hindered by their extremely tight affinity and the complication that any mixture of the two cFAE mutants can form half-Ab homodimers as well as heterodimers. To address these considerations, experiments were performed at subnanomolar concentrations and fit to a model accounting for each possible species. FCS was a suitable technique for monitoring fraction bound, as it is functional under the dilute conditions that were required to reach the monomeric state. However, at such concentrations, FCS is truly a single molecule technique. The resulting data are poorly sampled, which allows individual replicates to sometimes vary widely from the true mean. Increased sampling was achieved by lengthening the collection time, increasing the number of replicates, and performing each titration on multiple days. Although the data still appeared noisy, there were clear differences in affinity that were clarified by globally fitting the datasets with shared parameters. Half-Ab dissociation rates correlated strongly to affinities ($R^2 > 0.99$, **Figure 4.19**), indicating that the association rate is quite similar for each interaction and that dissociation rate is the primary determinant of differences in affinity.

The K_D values can also be used to calculate the equilibrium constant for the overall reaction and the theoretical yield of bsAb that would form for a fully reduced sample of cFAE mutants (see **Schemes 4.2** and **4.3** for derivations). Using experimentally derived K_Ds, the expected yield of bsAb is 93.9%, which is consistent with values of >90% that are observed experimentally with

methods such as hydrophobic interaction chromatography. Thus, there is a maximum achievable yield of bsAb defined by the relative affinities of parental and bispecific half-Ab dimerization. While this percentage may vary with experimental conditions, the point remains that even perfectly executed cFAE reactions are subject to these thermodynamic limitations of yield. This sets an important benchmark for the process of cFAE.

It has been reported that the IgG4 Fc domain can interact with other molecules of intact IgG1 and IgG4 Fc.[47-48] Thus, the possibility of whole Ab heterodimerization, heavy chain exchange, and dissociation to bsAb was considered as an alternative to half-Ab dissociation and re-association. If the mechanism involved initial dimerization of intact Abs, then this complexation would be the step monitored by FRET and the observed kinetics would be dependent on Ab concentration. Since association occurs first by this mechanism, the FRET-observed reaction would be concentration dependent even if the rate-determining step occurred after association. The observed concentration independence of cFAE therefore precludes this Ab complexation mechanism and unambiguously identifies half-Ab dissociation as the slow step of the reaction.

Because cFAE is used to create large batches of bsAbs, the mechanistic details obtained here have implications for therapeutic bsAb production. It is clear from FRET that the $IgG1_{WT}$ reaction with 50 mM MEA nears completion within three hours at 25 ºC, which is consistent with conditions cited in the protocol for large-scale cFAE incubations.[25] Reactions to form bsAb are often performed in buffers at neutral pH, which is fortuitously in the pH range at which cFAE approaches its maximum rate. The data demonstrate that even a small increase in pH from 7.0 to 7.5 can result in a 32% increase in reaction rate due to a combination of accelerated hinge reduction and accelerated Ab dissociation. Likewise, decreasing the ionic strength of the reaction buffer from 200 to 80 mM results in a 28% increase in cFAE rate due to faster dissociation into half-Ab.

Although high pH and low salt increase the rate of cFAE, there is no evidence to suggest that these conditions increase the final yield of bsAb. The reaction can also be accelerated using higher concentrations of reductant; however, the risk of intrachain disulfide reduction increases under extremely reducing conditions.

Comparison of experimental cFAE data and simulated data confirmed the validity of the mechanistic model and the accuracy of measured rates. The simulation itself incorporates data from three types of experiments to create a visual summary of cFAE that is both comprehensive and self-consistent. Furthermore, it highlights the remarkable efficiency of the cFAE reaction. Kinetically, a series of steps involving hinge reduction-oxidation and protein-protein interactions occurs at a rate determined by half-Ab dissociation and influenced by reduction conditions. Thermodynamically, the use of parental Abs with half-Ab dimerization affinities 5-fold to 180-fold weaker than that of the bispecific interaction ensures that cFAE will be driven toward the bsAb product. In the future, a similar experimental strategy could be used to characterize other processes involving multi-domain macromolecules.

SCHEMES

Scheme 4.1: Derivation of FCS fitting equations

The K_D for the heterodimerization of half-Fc A and half-Ab B depends on the relative amounts of free half-Fc, A_f, and free half-Ab, B_f, compared to the amount of the complex at equilibrium.

$$AB \overset{K_{AB}}{\longleftrightarrow} A_f + B_f \qquad\qquad K_{AB} = \frac{[A_f][B_f]}{[AB]}$$

However, A_f and B_f can also homodimerize to the corresponding full Fc, AA, and full Ab, BB.

$$AA \overset{K_{AA}}{\longleftrightarrow} 2A_f \qquad\qquad K_{AA} = \frac{[A_f]^2}{[AA]}$$

$$BB \overset{K_{BB}}{\longleftrightarrow} 2B_f \qquad\qquad K_{BB} = \frac{[B_f]^2}{[BB]}$$

The total half-Fc concentration A_t can be expressed in terms of the free half-Fc concentration, the concentration of the dimerized full Fc, and the concentration of the half-Fc/half-Ab heterodimer. The corresponding equation is true for B_t.

$$[A_t] = [A_f] + 2[AA] + [AB]$$

$$[B_t] = [B_f] + 2[BB] + [AB]$$

With five equations and five dependent variables (A_f, B_f, AA, BB, AB), it is then possible to solve for any dependent variable in terms of independent variables (A_T, B_T, K_{AA}, K_{BB}, K_{AB}). Thus, explicit equations were determined for A_f, AA, and AB using the Solve function of Mathematica 11.1. Since there were four solutions to each quartic function, ranges of values for K_{AA}, K_{BB}, and K_{AB} were tested for each solution to determine its viable domain. Solution 1 was valid when K_{AB} was less than both K_{AA} and K_{BB} while equation 3 was valid when K_{AB} was greater than or equal to either K_{AA} or K_{BB}. Thus, equation 1 was used for heterodimerization reactions while equation 3 was used for homodimerization reactions (when K_{AA}=K_{BB}=K_{AB}).

The observed diffusion time is equal to the diffusion time of each species multiplied by the relative amount of that species. Thus, the diffusion times observed during titrations can be modeled using the solved equations for A_f, AA, and AB.

$$\tau_{D,obs} = \frac{[A_f]}{[A_t]}\tau_{D,Af} + \frac{2[AA]}{[A_t]}\tau_{D,AA} + \frac{[AB]}{[A_t]}\tau_{D,AB}$$

Since individual species A_f, AA, and AB cannot be isolated, it is difficult to determine their precise diffusion times. However, the general relation between mass and diffusion time should hold such that

$$\frac{\tau_{D,bound}}{\tau_{D,unbound}} = \sqrt[3]{\frac{MW_{bound}}{MW_{unbound}}}$$

Therefore, the increase in diffusion time for AA and AB relative to A_f can be calculated based on the mass of each species. As a result, the observed diffusion time can be modeled to the equation below.

$$\tau_{D,obs} = \frac{[A_f]}{[A_t]}\tau_{D,Af} + \frac{2.52[AA]}{[A_t]}\tau_{D,Af} + \frac{1.59[AB]}{[A_t]}\tau_{D,Af}$$

As $[A_f]$, [AA], [AB] are equations in terms of A_T, B_T, K_{AA}, K_{BB}, and K_{AB}, the $\tau_{D,obs}$ equation was fit by fixing known values of A_T and B_T while letting K_{AA}, K_{BB}, K_{AB}, and $\tau_{D,Af}$ float. By fitting globally across datasets for each combination of half-Fc and half-Ab, it was possible to determine K_D values for F405L homodimerization, K409R homodimerization, and bsAb heterodimerization with higher confidence. The relevant K_Ds for each interaction are tabulated below. It was assumed that the affinity of a given half-Fc homodimer, half-Ab homodimer, and half-Fc/half-Ab heterodimer were equal since the interaction occurs predominantly in the C_H3 domain.

Half-Fc	**Half-Ab**	**K_{AA}**	**K_{BB}**	**K_{AB}**
F405L	F405L	F405L	F405L	F405L
F405L	K409R	F405L	K409R	bsAb
K409R	F405L	K409R	F405L	bsAb
K409R	K409R	K409R	K409R	K409R

Scheme 4.2: Derivation of the equilibrium constant for parental Abs and bsAb

Consider the following half-Ab homodimerization equilibria and corresponding K_D definitions, with half-Ab A containing F405L and half-Ab B containing K409R. AA and BB then represent full parental Abs containing two half-Abs with the respective mutations. Note that these equilibria are true only in the absence of hinge disulfide bonds (as occurs under reducing conditions and with $IgG1_{C\rightarrow S}$ or IgG1 Fc cleaved below the hinge).

$$AA \overset{K_{AA}}{\longleftrightarrow} 2A \qquad K_{AA} = \frac{[A]^2}{[AA]}$$

$$BB \overset{K_{BB}}{\longleftrightarrow} 2B \qquad K_{BB} = \frac{[B]^2}{[BB]}$$

In addition, A and B can heterodimerize to form bsAb AB.

$$AB \overset{K_{AB}}{\longleftrightarrow} A + B \qquad K_{AB} = \frac{[A][B]}{[AB]}$$

The cFAE reaction to form bsAb from two parental Abs containing cFAE mutations can then be considered in terms of the following net equilibrium, where the value of K_{eq} represents the preference for bsAb compared to parental Abs.

$$AA + BB \overset{K_{eq}}{\longleftrightarrow} 2AB \qquad K_{eq} = \frac{[AB]^2}{[AA][BB]}$$

To obtain K_{eq} in terms of individual K_D values, [AB], [AA], and [BB] can be substituted based on the individual K_D definitions.

$$K_{eq} = \frac{[AB]^2}{[AA][BB]} = \frac{\left(\frac{[A][B]}{K_{AB}}\right)^2}{\left(\frac{[A]^2}{K_{AA}}\right)\left(\frac{[B]^2}{K_{BB}}\right)} = \frac{K_{AA}K_{BB}}{K_{AB}^2}$$

Scheme 4.3: Calculation of %bsAb from K_{eq}

When cFAE is performed, AA are BB are incubated at equimolar concentrations in the presence of reducing agent, which allows AA, BB, and AB to reach equilibrium. Thus, [AA]=[BB] at the start of the reaction, and assuming concentrations are high enough to preclude significant [A] and [B] this is also true at equilibrium. This condition allows [AA], [BB], and [AB] to be rewritten in terms of [parental Ab] and [bsAb].

$$[AA] = [BB] = \frac{[Parental\ Ab]}{2}$$

$$[AB] = [bsAb]$$

These new definitions can be used in the previously derived equation for K_{eq}.

$$K_{eq} = \frac{[AB]^2}{[AA][BB]} = \frac{[bsAb]^2}{\left(\frac{[Parental\ Ab]}{2}\right)^2} = \frac{4[bsAb]^2}{[Parental\ Ab]^2}$$

Solving for [Parental Ab] yields

$$[Parental\ Ab] = \frac{2[bsAb]}{\sqrt{K_{eq}}}$$

Finally, the fraction of bsAb can be written in terms of [bsAb] and [Parental Ab].

$$Fraction\ bsAb = \frac{[bsAb]}{[bsAb] + [Parental\ Ab]}$$

Substituting for [Parental Ab] allows for expression of "fraction bsAb" in terms of K_{eq}.

$$Fraction\ bsAb = \frac{[bsAb]}{[bsAb] + \frac{2[bsAb]}{\sqrt{K_{eq}}}} = \frac{1}{1 + \frac{2}{\sqrt{K_{eq}}}}$$

FIGURES

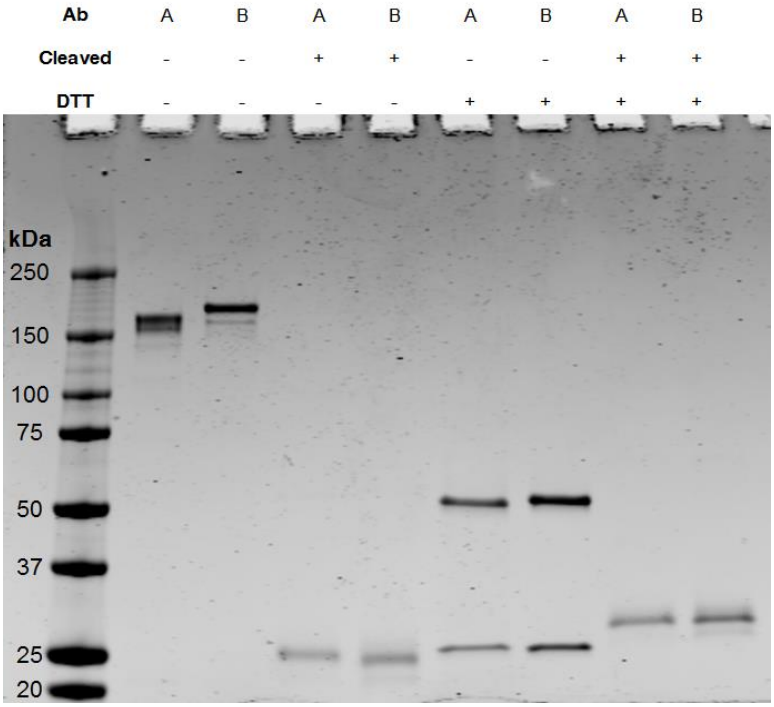

Figure 4.1: SDS-PAGE of parental Abs and purified Fc fragments. Ab A is α-RSV F405L and Ab B is α-gp120 K409R, both in IgG1. Samples were labeled with 10x Alexa 488 NHS ester and subsequently treated with IdeS enzyme (FabRICATOR, Genovis) per the manufacturer's instructions. After the reactions, Fc was purified by protein A chromatography and polished by SEC to remove uncleaved Ab. Experiment was performed by running a Mini-PROTEAN TGX 4-15% gel (Bio-Rad, 4561083) at 150 V using samples with or without 50 mM DTT.

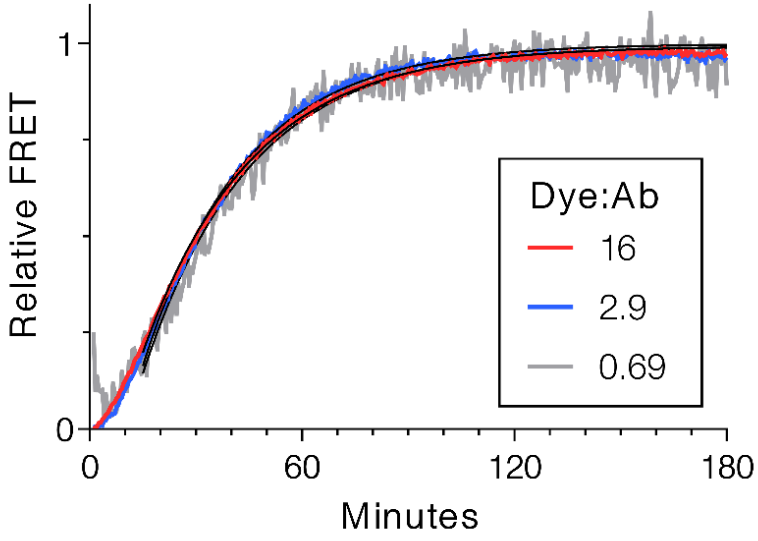

Figure 4.2: Kinetics of cFAE based on an increase in FRET for Abs containing different extents of labeling. Abs were labeled with a low, intermediate, or high concentration of dye to achieve varying ratios of dye:Ab and then cFAE was performed with IgG1 α-RSV F405L and α-gp120 K409R. Reactions contained 50 mM of 2-mercaptoethylamine and 500 nM of each Ab and were performed in duplicate at 25 ºC. The rate for the lowest labeled pair was 0.0253 ± 0.0001 min^{-1}, for the moderately labeled pair was 0.0294 ± 0.0026 min^{-1}, and for the heavily labeled pair was 0.0281 ± 0.0004 min^{-1}.

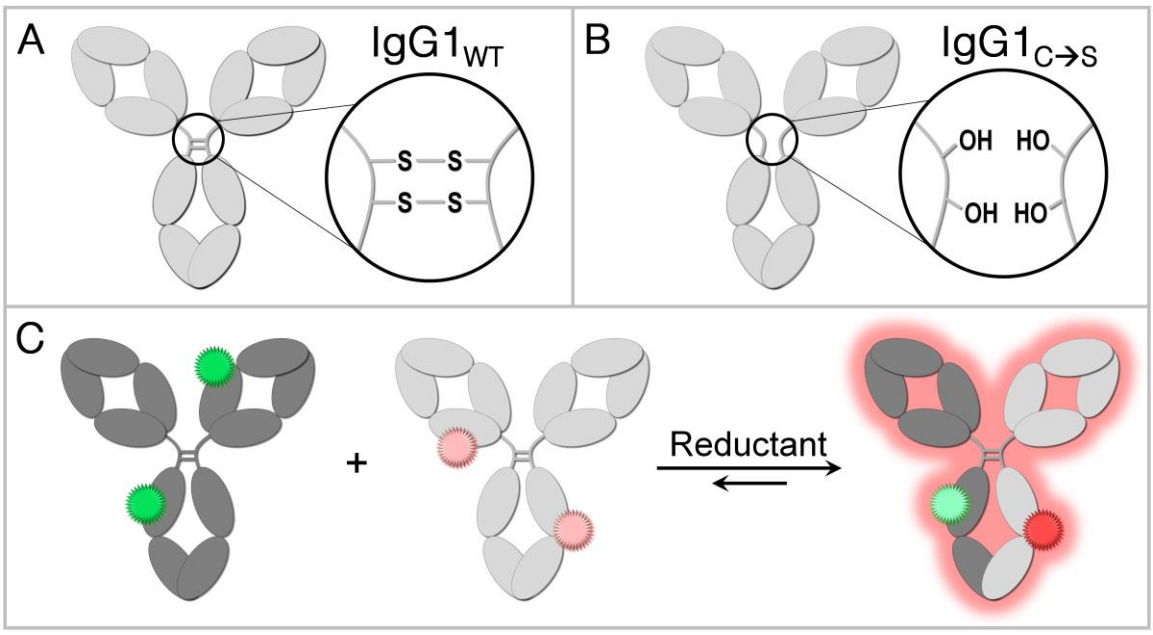

Figure 4.3: IgG1 with a wild-type hinge ($IgG1_{WT}$, A) contains two disulfide bonds connecting half-Abs via the heavy chain. Hinge mutants ($IgG1_{C\rightarrow S}$, B) contain serines in place of hinge cysteines, eliminating the covalent connection between half-Abs. The progress of cFAE is monitored using FRET (C), where each parental Ab is labeled with donor or acceptor fluorophore and fluorescence of the acceptor increases as bsAb is formed.

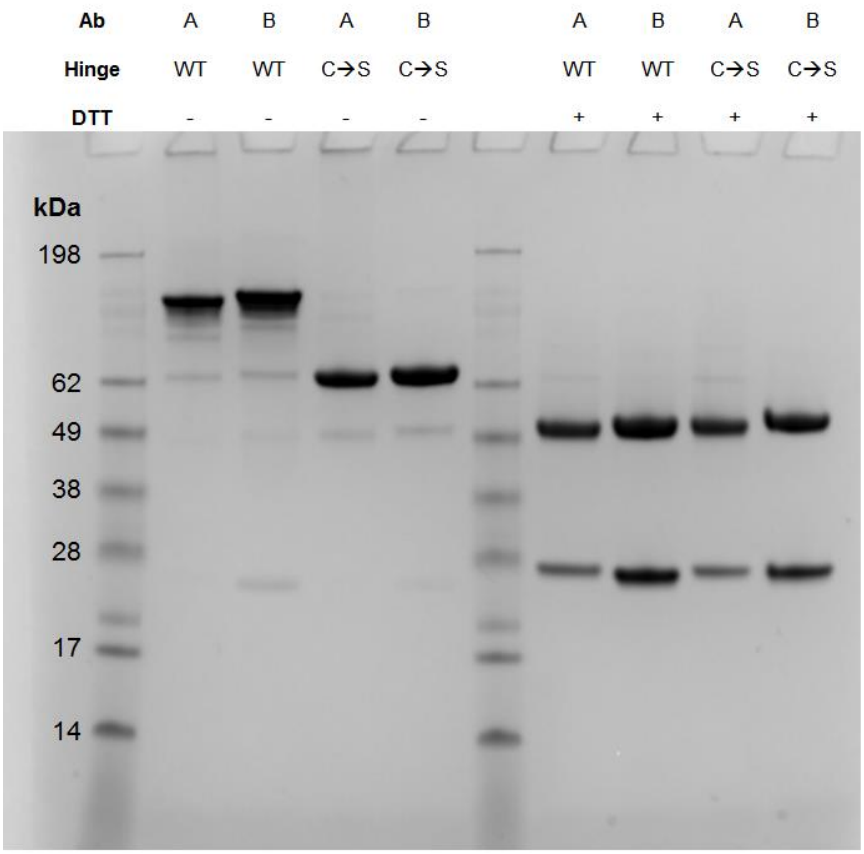

Figure 4.4: SDS-PAGE of Abs that were used to characterize cFAE kinetics. Ab A is α-RSV F405L and Ab B is α-gp120 K409R, both in huIgG1. Abs contained either a wild-type hinge region (WT), or contained C226S/C229S (C→S). Under non-reducing conditions (no DTT), Abs with a native hinge traveled as the expected 150 kDa species, while those containing hinge mutations appeared as a 75-kDa band indicative of half-Ab. When 50 mM DTT was added to samples, they were all shown to contain a 50-kDa heavy chain and a 25-kDa light chain. Experiment was performed by running a NuPAGE 4-12% gel (Thermo Fisher, NP0321BOX) at 150 V and loading 3 µg of protein per lane.

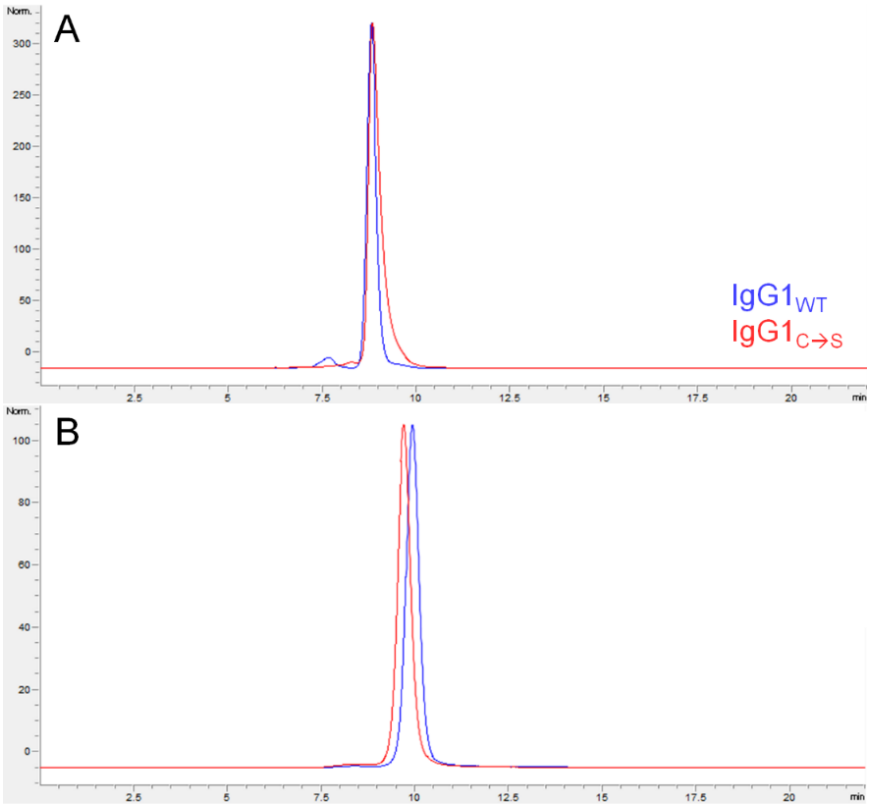

Figure 4.5: Size-exclusion chromatograms of α-RSV F405L (A) and α-gp120 K409R (B) demonstrate that wild-type ($IgG1_{WT}$) and C226S/C229S ($IgG1_{C\rightarrow S}$) behave similarly, with a single major peak at a retention time consistent with monomer. Twenty µg of each sample was run over a G3000SWxl column (Tosoh Bioscience, 08541) equilibrated in PBS at 1.0 mL/min, with plots showing relative absorbance at 280 nm versus retention time.

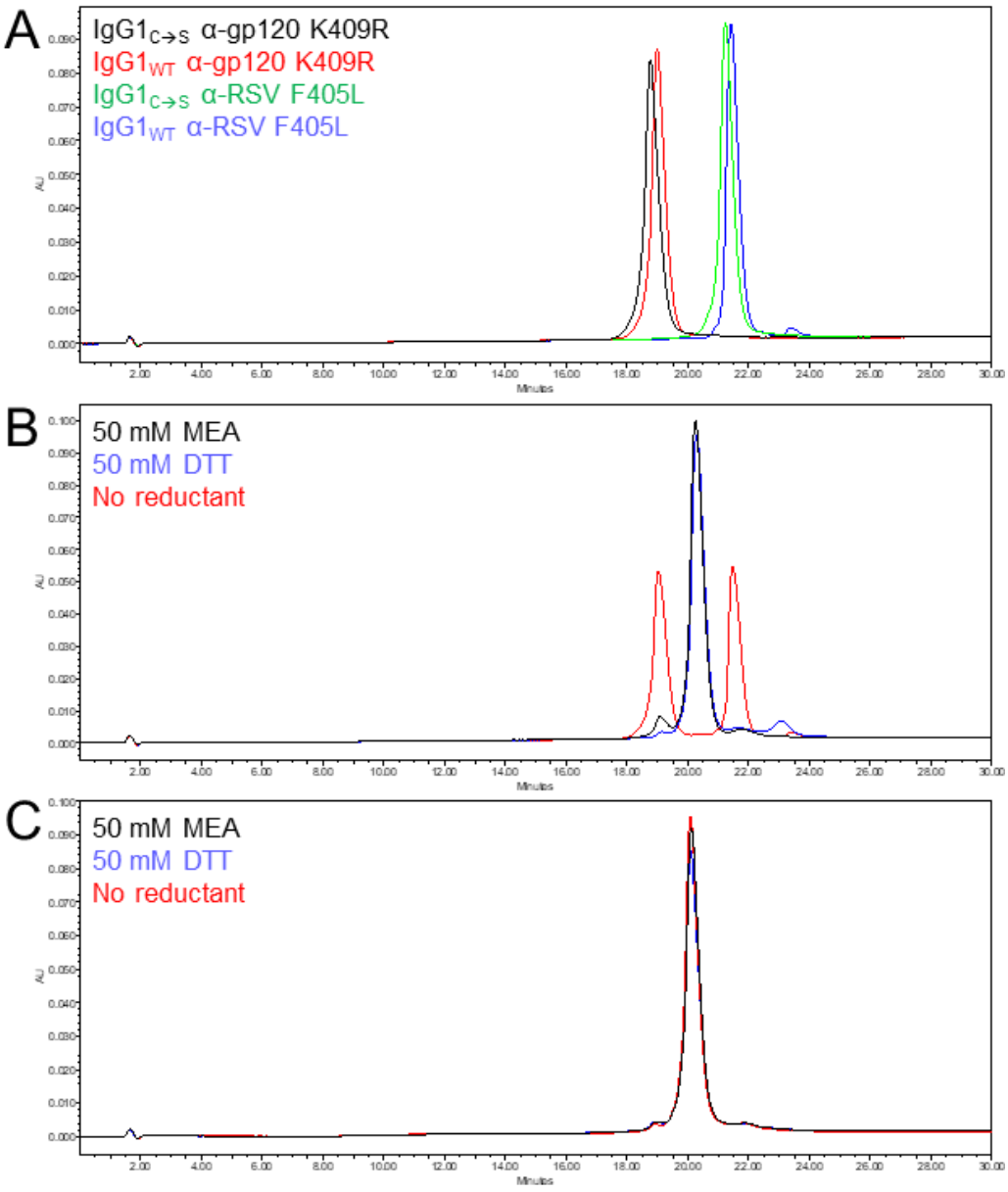

Figure 4.6: Hydrophobic interaction was used to separate parental Abs, with $IgG1_{WT}$ proteins at similar retention times as the corresponding $IgG1_{C\rightarrow S}$ proteins (A). When cFAE was performed with $IgG1_{WT}$ proteins in the presence of MEA or DTT, a peak corresponding to bsAb appeared at a retention time between those of parental Abs, but no bsAb was formed in the absence of reducing agent (B). When cFAE was performed with $IgG1_{C\rightarrow S}$ proteins, full formation of bsAb was observed with MEA or DTT, and in the absence of reducing agent (C). Absorbance at 280 nm is plotted versus retention time in minutes.

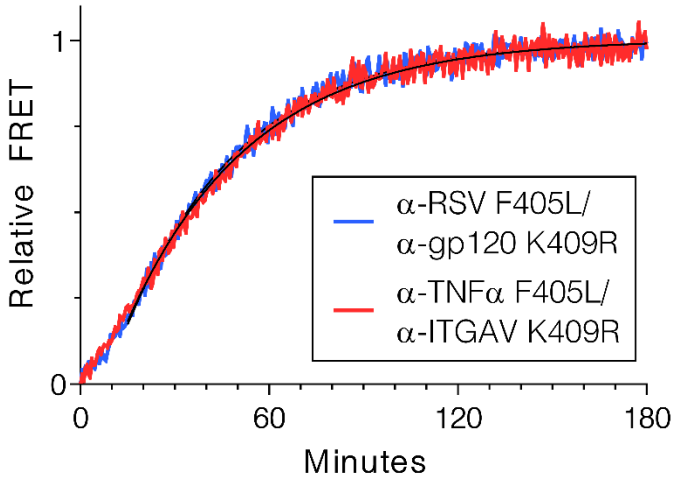

Figure 4.7: Kinetics of cFAE based on an increase in FRET for two pairs of IgG1 Abs targeting different antigens. Blue trace shows the cFAE reaction for Abs targeting respiratory syncytial virus (RSV) and HIV glycoprotein gp120, while red trace shows the same reaction for Abs targeting tumor necrosis factor α (TNFα) and integrin alpha-V (ITGAV). Both experiments contained 50 mM of 2-mercaptoethylamine and 100 nM of each Ab at 25 ºC, and traces show the average of both Ab-dye pairings (F405L Ab labeled with Alexa 488 and K409R Ab labeled with Alexa 594, or the opposite pairing of Ab and dye). The rate for α-RSV/α-gp120 (omitting the first 15 minutes containing reduction-related lag phase) was 0.0268 ± 0.0008 min^{-1} and for α-TNFα/α-gp120 was 0.0251 ± 0.0011 min^{-1}.

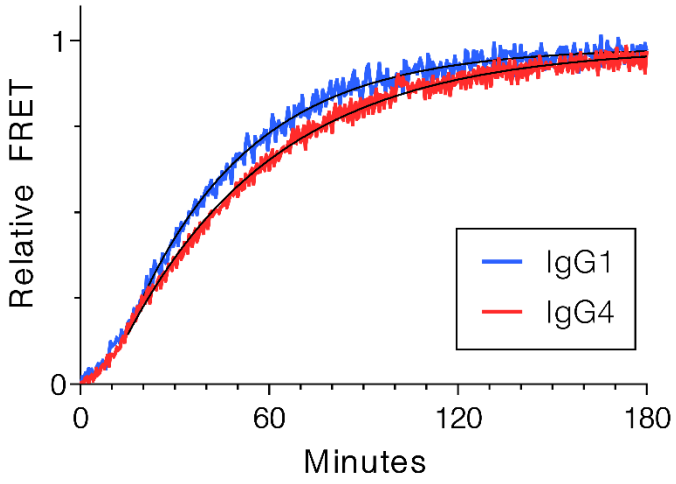

Figure 4.8: Kinetics of cFAE based on an increase in FRET for two sets of Abs having the same variable regions, but the framework of IgG1 or IgG4PAA (S228P/L234A/L235A). IgG1 Abs undergoing cFAE were α-RSV F405L and α-gp120 K409R, while IgG4 Abs were α-RSV F405L/R409K and α-gp120 (naturally having R409). Reactions contained 50 mM of 2-mercaptoethylamine and 100 nM of each Ab at 25 ºC, and traces show the average of both Ab-dye pairings. The rate (omitting the first 15 minutes containing reduction-related lag phase) for IgG1 was 0.0268 ± 0.0008 min^{-1} and for IgG4 was 0.0209 ± 0.0019 min^{-1}.

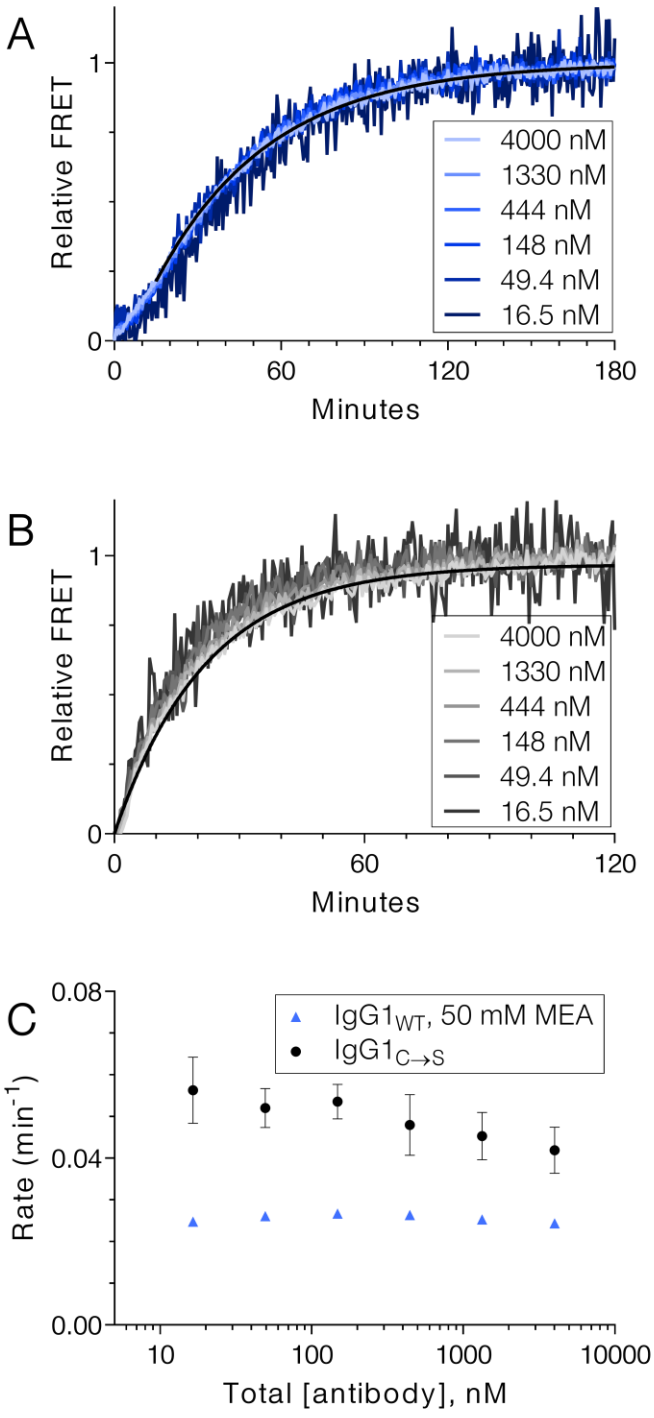

Figure 4.9: cFAE progress curves for the formation of bispecific $IgG1_{WT}$ (A) or $IgG1_{C\rightarrow S}$ (B) overlap when the reaction is performed with varying concentrations of Ab. The monoexponential fit is shown only for the 4 μM condition for the sake of clarity. The rate summary (C) indicates the fitted rate of cFAE as a function of total Ab concentration.

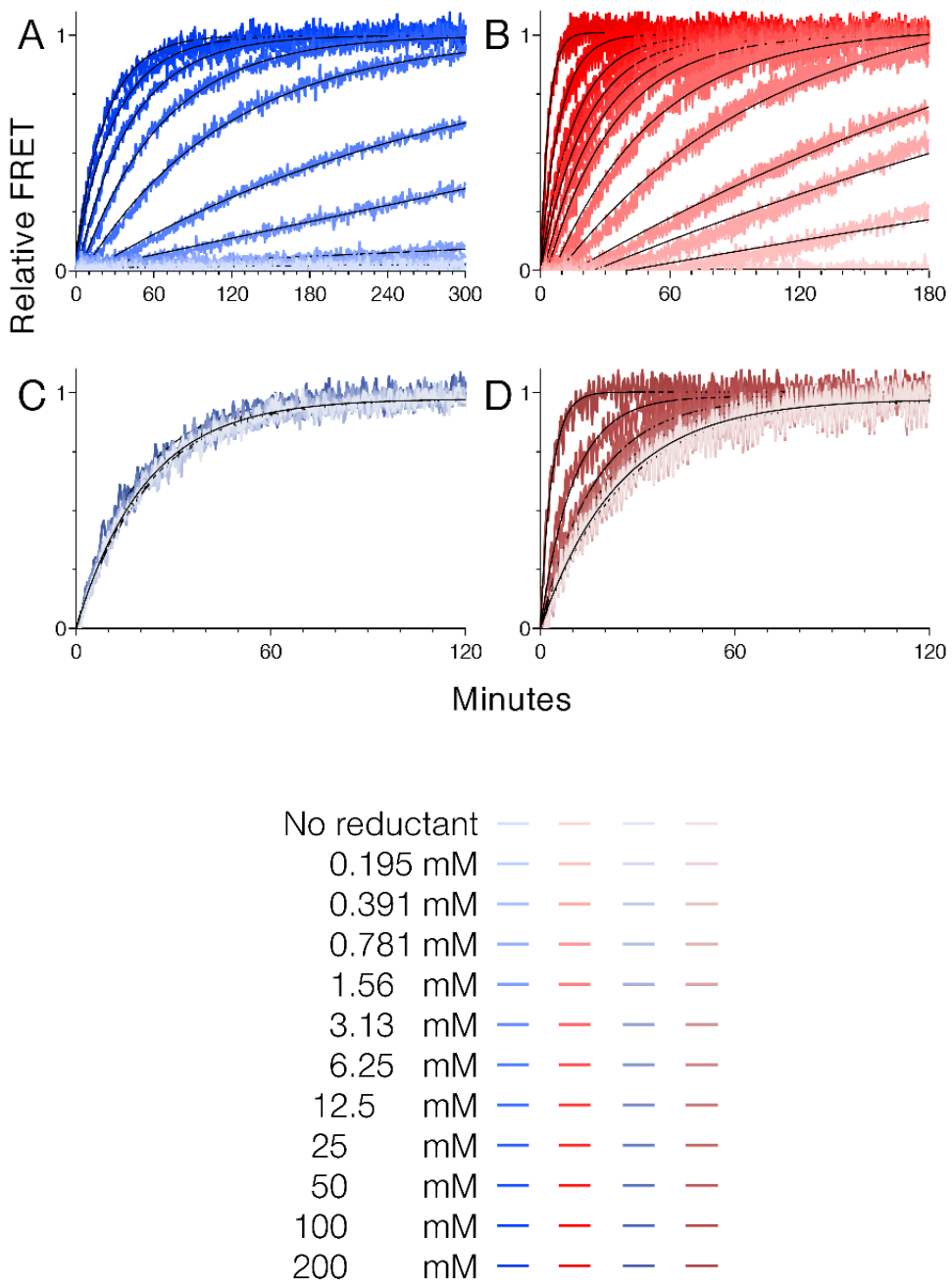

Figure 4.10: Kinetics of cFAE based on an increase in FRET for the formation of bispecific $IgG1_{WT}$ (A, B) or $IgG1_{C\rightarrow S}$ (C, D) in the presence of varying concentrations of MEA (A, C) or DTT (B, D) at 25 ºC. Concentration of reducing agent is denoted by the luminance of the trace, with the highest concentration of 200 mM as the darkest color, 1:2 dilutions in progressively lighter colors, and no reductant as the lightest colored trace.

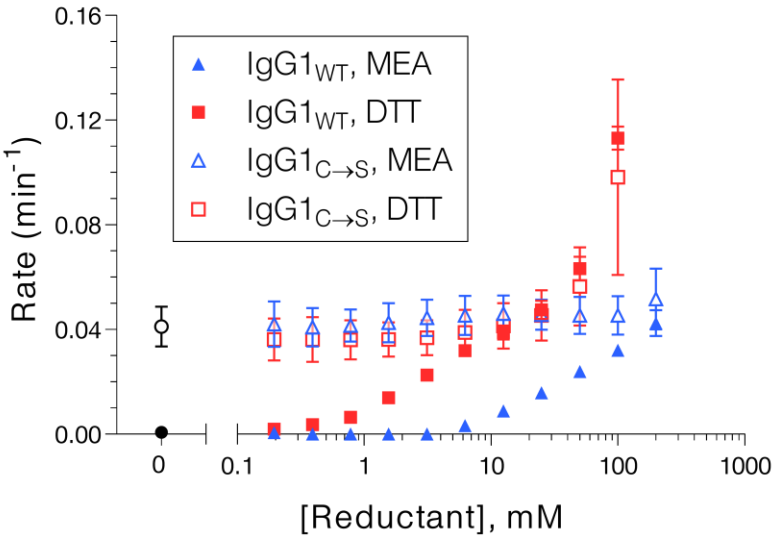

Figure 4.11: Rates of cFAE for $IgG1_{WT}$ and $IgG1_{C\rightarrow S}$ in the presence of various concentrations of MEA or DTT. Rates with no reductant are plotted as a closed black circle ($IgG1_{WT}$) or an open black circle ($IgG1_{C\rightarrow S}$). The reaction rate was faster than the plotted range in the presence of 200 mM DTT for both $IgG1_{WT}$ ($4.70\times10^{-3} \pm 0.28\times10^{-3}$ s^{-1}) and $IgG1_{C\rightarrow S}$ ($4.85\times10^{-3} \pm 1.27\times10^{-3}$ s^{-1}).

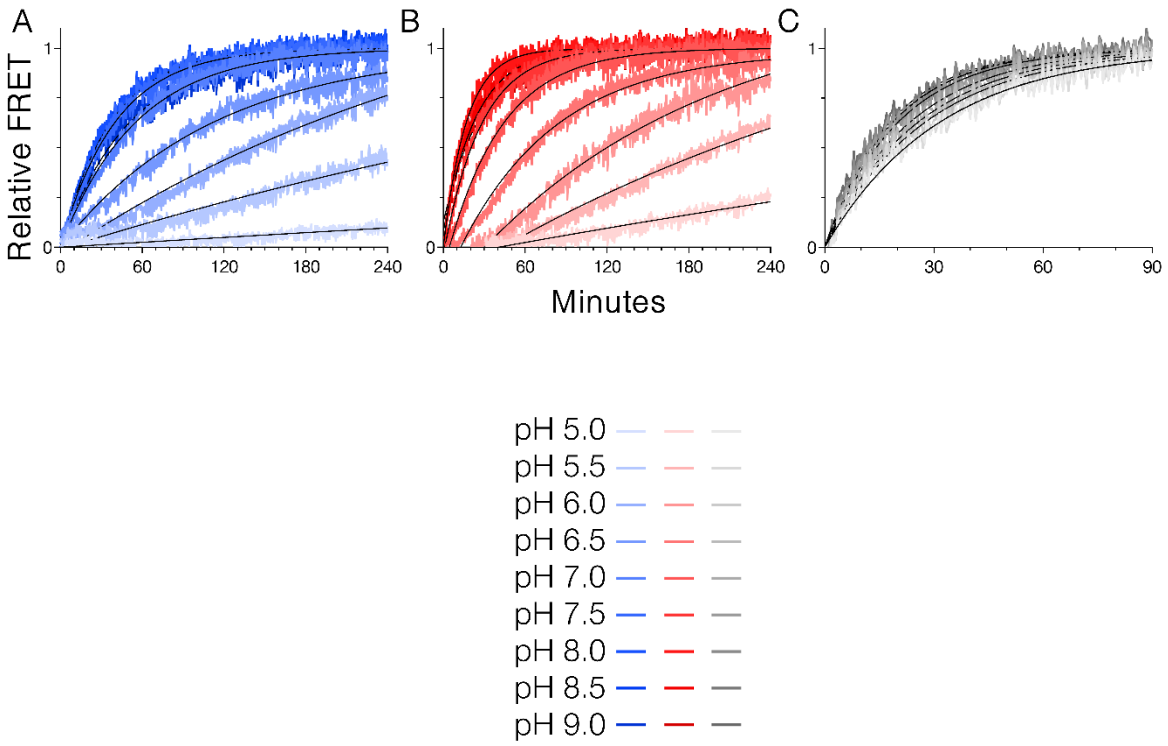

Figure 4.12: Kinetics of cFAE based on an increase in FRET for the formation of bispecific $IgG1_{WT}$ with 50 mM MEA (A), $IgG1_{WT}$ with 10 mM DTT (B), or $IgG1_{C\rightarrow S}$ (C) at varying pH. The cFAE reaction was performed in 100 mM potassium phosphate, 100 mM sodium chloride at pH 5 to 9 and at 25 ºC. As the pH is increased, kinetic traces are colored progressively darker.

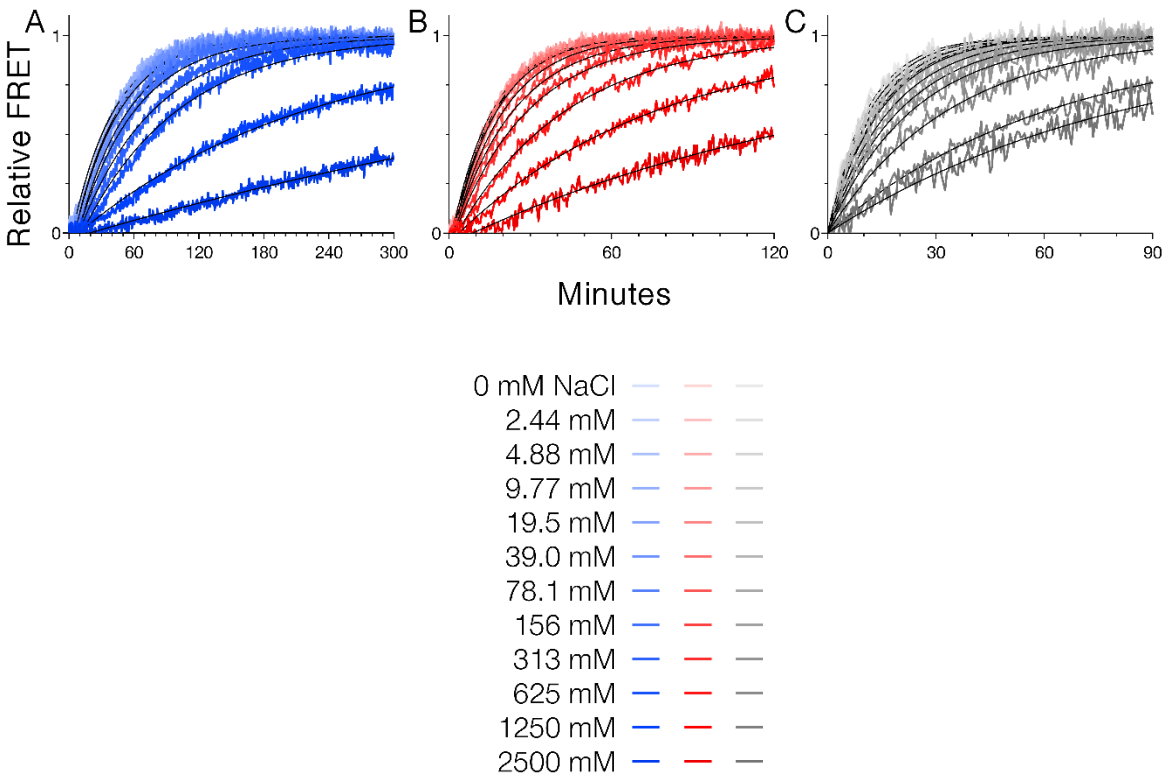

Figure 4.13: Kinetic FRET data showing progress of cFAE over time for the formation of bispecific $IgG1_{WT}$ with 50 mM MEA (A), $IgG1_{WT}$ with 10 mM DTT (B), or $IgG1_{C\rightarrow S}$ (C) at varying ionic strength. The cFAE reaction was performed in 20 mM potassium phosphate, pH 7.4 containing 0 to 2.5 M sodium chloride at 25 ºC. As the NaCl concentration is increased, kinetic traces are colored progressively darker.

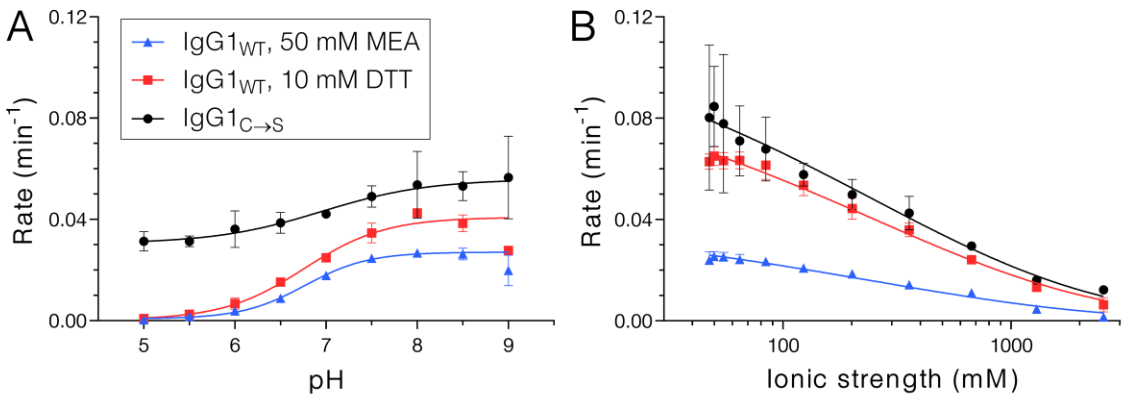

Figure 4.14: Rates of cFAE at varying pH (A) and ionic strength (B). The effect of pH was investigated by performing the reaction in 100 mM potassium phosphate, 100 mM sodium chloride at pH 5 to 9. The effect of ionic strength was investigated by performing the reaction in 20 mM potassium phosphate, pH 7.4 containing 0 to 2.5 M sodium chloride.

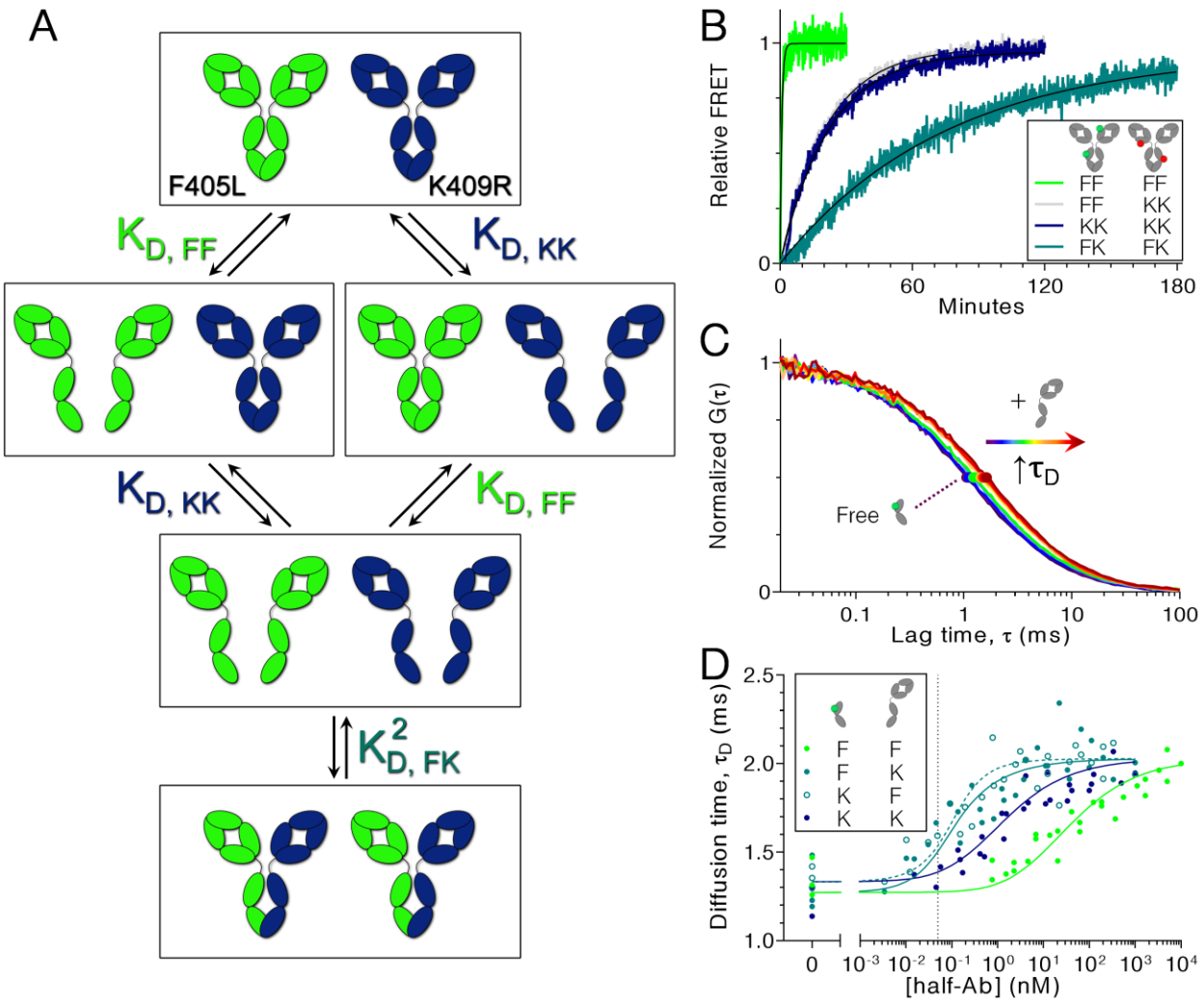

Figure 4.15: Rate of FAE for different pairs of Abs reveals relative half-Ab dissociation rates, which correlate with half-Ab dimerization affinities. The thermodynamics of bsAb formation (A) involve discrete energetic states with combinations of associated and dissociated half-Ab. Each transition is defined by an equilibrium dissociation constant, K_D, for either the F405L half-Ab homodimerization (FF), the K409R half-Ab homodimerization (KK), or the F405L/K409R half-Ab heterodimerization (FK). FAE progress curves for different combinations of labeled Abs (B) show the slowest half-Ab dissociation rate involved in the exchange reaction. Parental F405L $IgG1_{C\rightarrow S}$ (FF), K409R $IgG1_{C\rightarrow S}$ (KK), or pre-formed $IgG1_{C\rightarrow S}$ bsAb (FK) were labeled with FRET donor or acceptor and FAE was monitored by FRET. FCS binding titrations (C, D) were performed to determine K_D values shown in panel A. Panel C shows one dataset for Alexa 488-labeled K409R half-Fc binding to unlabeled K409R half-Ab ($IgG1_{C\rightarrow S}$) for determination of $K_{D,KK}$. The experiment was performed with a constant 50 pM of half-Fc and 1:3 serial dilutions of half-Ab (maximum 500 nM (red) decreasing to no half-Ab (purple)). Upon binding, there is an increase in the apparent size of the labeled Fc, resulting in a larger diffusion time (solid circles). Diffusion times from all FCS experiments (D) were globally fit to extract each of the three binding affinities (fitting described in supplemental material). Each data point shows the average of 3-10 replicates; standard deviation is omitted for clarity but was on average 9.54% of the measured value. Dotted line at 50 pM represents the fixed concentration of labeled half-Fc used in titrations.

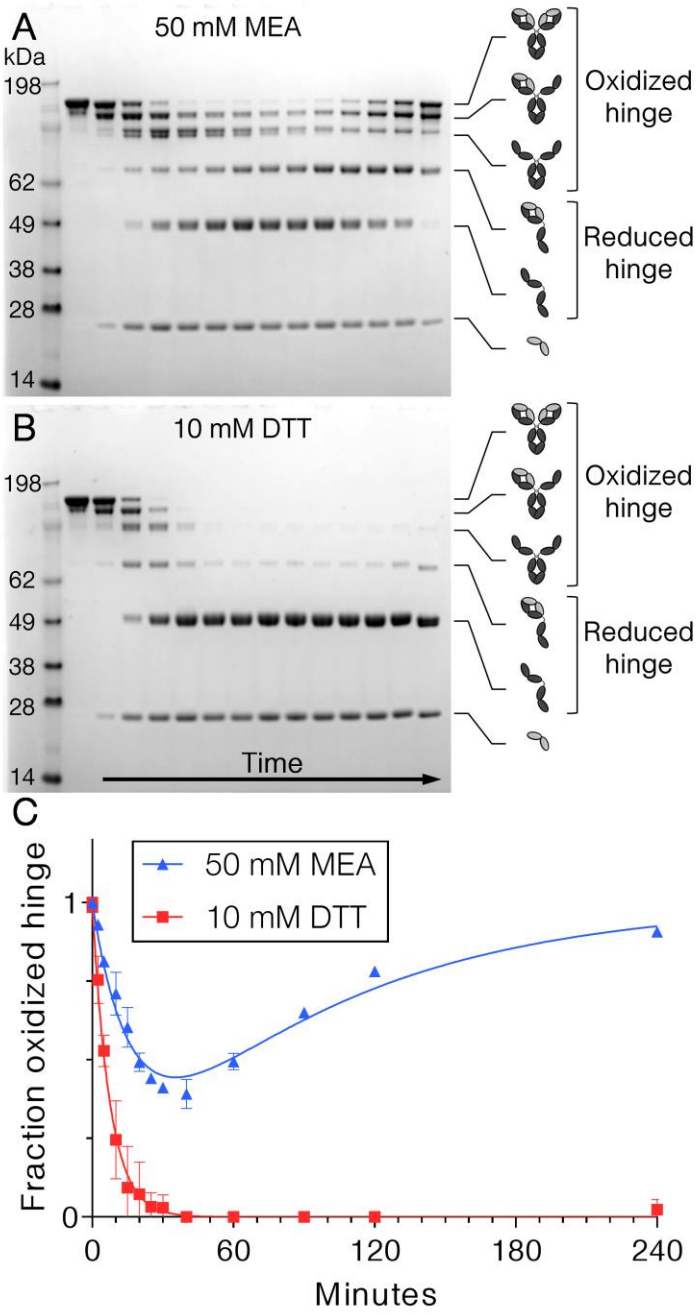

Figure 4.16: Non-reducing SDS-PAGE with iodoacetamide quenching was used to monitor the redox state of hinge disulfide bonds after 50 mM MEA (A) or 10 mM DTT (B) was added to initiate cFAE of $IgG1_{WT}$. Densitometry was then used to calculate the percentage of hinge disulfides that were oxidized at each time point using the densities of bands of oxidized heavy chains (150-, 125-, and 100-kDa) and reduced heavy chains (75- and 50-kDa). MEA data were fit to the sum of two exponentials to extract the fast rate of reduction and slower rate of re-oxidation. For DTT, the reduction rate alone was determined using a single exponential fit.

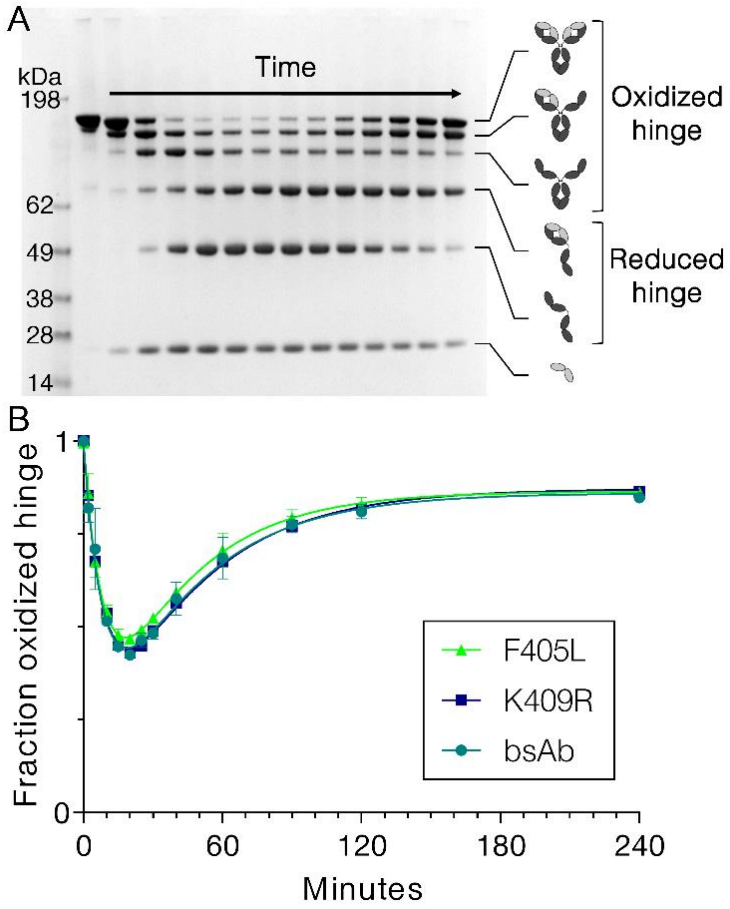

Figure 4.17: Kinetics of hinge reduction and re-oxidation by non-reducing SDS-PAGE. Two mg/mL of α-RSV F405L, 2 mg/mL of α-gp120 K409R, or 1 mg/mL of each were reduced with 50 mM MEA. The reaction was incubated at 300 rpm and 31 ºC, and time points were quenched by adding an excess of iodoacetamide. After performing SDS-PAGE densitometry to determine the fraction of oxidized hinge disulfides at each point and fitting the kinetics to the sum of two exponentials, rates of reduction were 0.0890 ± 0.0022 min^{-1} for F405L, 0.0894 ± 0.0041 min^{-1} for K409R, and 0.0924 ± 0.0038 min^{-1} for the mixture; and rates of oxidation were 0.0276 ± 0.0009 min^{-1} for F405L, 0.0240 ± 0.0016 min^{-1} for K409R, and 0.0252 ± 0.0015 for the mixture.

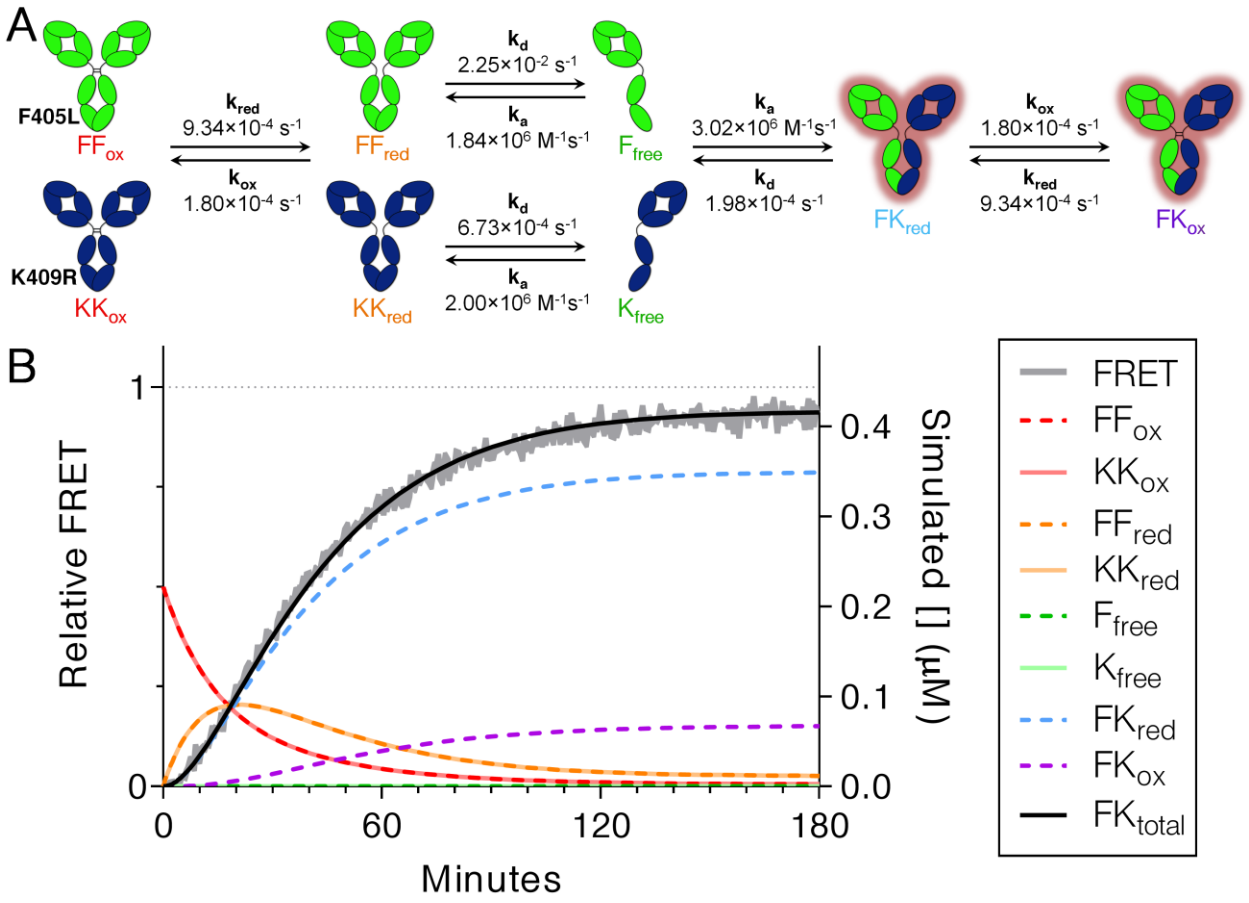

Figure 4.18: Kinetic scheme for the mechanism of cFAE including measured rates of each step at 25 ºC. Hinge disulfides of parental Abs must first be reduced (rate shown is with 50 mM MEA), followed by dissociation into half-Abs, re-association to form half-Ab heterodimer, and re-oxidation of hinge disulfides (again, rate shown is in the presence of 50 mM MEA) to stabilize the bispecific product. The kinetics of cFAE were simulated at an intermediate Ab concentration of 444 nM (B) to determine whether this model agrees with FRET data under these conditions. The simulated concentration of each species is shown along with kinetic FRET data, which aligns well with the total concentration of bispecific Ab present. A dotted line at relative FRET = 1 and [total bsAb] = 444 nM indicates the maximum yield of bsAb if all parental Ab were converted to bsAb product.

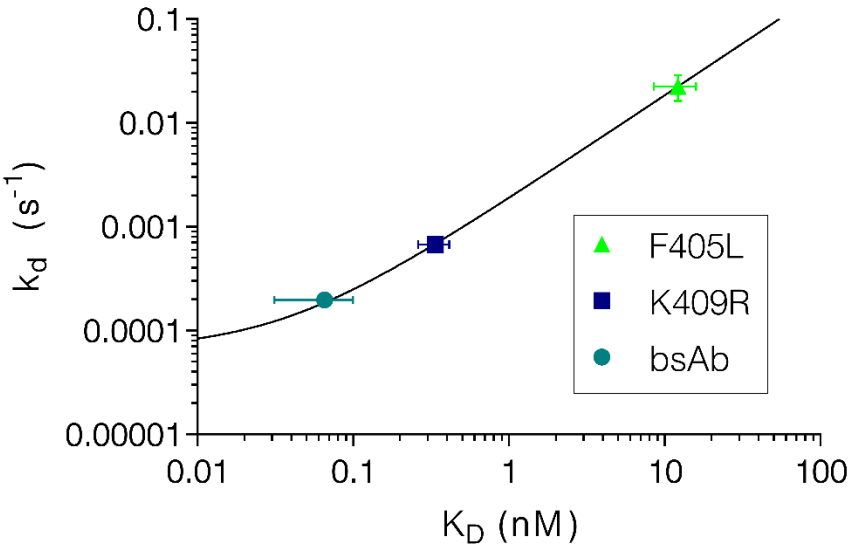

Figure 4.19: Comparison of half-Ab dissociation rates and half-Ab dimerization affinities. Y-axis is the half-Ab dissociation rate, measured by FRET with different pairs of Alexa 488- and Alexa 594-labeled $IgG1_{C\rightarrow S}$. X-axis is the half-Ab dimerization affinity, measured by FCS with Alexa 488-labeled half-Fc binding to unlabeled half-Ab. Values of k_d and K_D were tightly correlated with $R^2 > 0.99$. Note that the linear fit appears curved due to the log axes.

TABLES

Table 4.1: Experimental kinetic parameters of cFAE

Observation	Parameter	Method	Value ± SD
Reduction with 50 mM MEA	$k_{obs,red}$	SDS-PAGE	$9.34\times10^{-4} \pm 1.80\times10^{-4}$ s^{-1}
	$k_{obs,ox}$	SDS-PAGE	$1.80\times10^{-4} \pm 0.08\times10^{-4}$ s^{-1}
Reduction with 50 mM DTT	$k_{obs,red}$	SDS-PAGE	$2.23\times10^{-3} \pm 0.12\times10^{-3}$ s^{-1}
F405L homodimerization	$k_{d,FF}$	FRET	$2.25\times10^{-2} \pm 0.62\times10^{-2}$ s^{-1}
	$K_{D,FF}$	FCS	$1.22\times10^{-8} \pm 0.37\times10^{-8}$ M
	$k_{a,FF}$	k_d/K_D	$1.84\times10^{6} \pm 0.76\times10^{6}$ $M^{-1}s^{-1}$
K409R homodimerization	$k_{d,KK}$	FRET	$6.73\times10^{-4} \pm 0.22\times10^{-4}$ s^{-1}
	$K_{D,KK}$	FCS	$3.37\times10^{-10} \pm 0.76\times10^{-10}$ M
	$k_{a,KK}$	k_d/K_D	$2.00\times10^{6} \pm 0.46\times10^{6}$ $M^{-1}s^{-1}$
F405L/K409R heterodimerization	$k_{d,FK}$	FRET	$1.98\times10^{-4} \pm 0.05\times10^{-4}$ s^{-1}
	$K_{D,FK}$	FCS	$6.56\times10^{-11} \pm 3.43\times10^{-11}$ M
	$k_{a,FK}$	k_d/K_D	$3.02\times10^{6} \pm 1.58\times10^{6}$ $M^{-1}s^{-1}$

4.5 References

[1] Spiess, C.; Zhai, Q.; Carter, P. J. Alternative molecular formats and therapeutic applications for bispecific antibodies. *Mol. Immunol.* **2015**, *67*, 95-106.

[2] Kontermann, R. E.; Brinkmann, U. Bispecific antibodies. *Drug Discovery Today* **2015**, *20*, 838-847.

[3] Fan, G.; Wang, Z.; Hao, M.; Li, J. Bispecific antibodies and their applications. *J. Hematol. Oncol*. **2015**, *8*, 1-14.

[4] Thakur, A.; Lum, L. G.; "NextGen" biologics: bispecific antibodies and emerging clinical results. *Expert Opin. Biol. Ther*. **2016**, *16*, 675-688.

[5] Moores, S. L.; Chiu, M. L.; Bushey, B. S.; Chevalier, K.; Luistro, L.; Dorn, K.; Brezski, R. J.; Haytko, P.; Kelly, T.; Wu, S.; Martin, P. L.; Neijssen, J.; Parren, P. W. H. I.; Schuurman, J.; Attar, R. M.; Laquerre, S.; Lorenzi, M. V.; Anderson, G. M. A novel bispecific antibody targeting EGFR and cMet is effective against EGFR inhibitor-resistant lung tumors. *Cancer Res.* **2016**, *76*, 3942-3953.

[6] McDonagh, C. F.; Huhalov, A.; Harms, B. D.; Adams, S.; Paragas, V.; Oyama, S.; Zhang, B.; Luus, L.; Overland, R.; Nguyen, S.; Gu, J.; Kohli, N.; Wallace, M.; Feldhaus, M. J.; Kudla, A. J.; Schoeberl, B.; Nielsen, U. B. Antitumor activity of a novel bispecific antibody that targets the ErbB2/ErbB3 oncogenic unit and inhibits heregulin-induced activation of ErbB3. *Mol. Cancer Ther.* **2012**, *11*, 582-593.

[7] Kienast, Y.; Klein, C.; Scheuer, W.; Raemsch, R.; Lorenzon, E.; Bernicke, D.; Herting, F.; Yu, S.; The, H. H.; Martarello, L.; Gassner, C.; Stubenrauch, K. G.; Munro, K.; Augustin, H. G.; Thomas, M. Ang-2-VEGF-A CrossMab, a novel bispecific human IgG1 antibody blocking VEGF-A and Ang-2 functions simultaneously, mediates potent antitumor, antiangiogenic, and antimetastatic efficacy. *Clin. Cancer Res.* **2013**, *19*, 6730-6740.

[8] Zhukovsky, E. A.; Morse, R. J.; Maus, M. V. *Curr. Opin. Immunol.* **2016**, *40*, 24–35.

[9] Linke, R.; Klein, A.; Seimetz, D. Catumaxomab: clinical development and future directions. *mAbs* **2010**, *2*, 129-136.

[10] Lee, K. J.; Chow, V.; Weissman, A.; Tulpule, S.; Aldoss, I.; Akhtari, M. Clinical use of blinatumomab for B-cell acute lymphoblastic leukemia in adults. *Ther. Clin. Risk Manage*. **2016**, *12*, 1301-1310.

[11] Schuurman, J.; Parren, W. H. I. Editorial overview: Special section: New concepts in antibody therapeutics: What's in store for antibody therapy? *Curr. Opin. Immunol.* **2016**, *40*, vii-xiii.

[12] Nuñez-Prado, N.; Compte, M.; Harwood, S.; Álvarez-Méndez, A.; Lykkemark, S.; Sanz, L.; Álvarez-Vallina, L.; The coming of age of engineered multivalent antibodies. *Drug Discov. Today* **2015**, *20*, 588-594.

[13] Baeuerle, P. A.; Reinhardt, C. Bispecific T-cell engaging antibodies for cancer therapy. *Cancer Res.* **2009**, *69*, 4941-4944.

[14] Johnson, S.; Burke, S.; Huang, L.; Gorlatov, S.; Li, H.; Wang, W.; Zhang, W.; Tuaillon, N.; Rainey, J.; Barat, B.; Yang, Y.; Jin, L.; Ciccarone, V.; Moore, P. A.; Koenig, S.; Bonvini, E. Effector cell recruitment with novel Fv-based dual-affinity re-targeting protein leads to potent tumor cytolysis and in vivo B-cell depletion. *J. Mol. Biol*. **2010**, *399*, 436-449.

[15] Beckman, R. A.; Weiner, L. M.; Davis, H. M. Antibody constructs in cancer therapy: protein engineering strategies to improve exposure to solid tumors. *Cancer* **2007**, *109*, 170-179.

[16] Hanson, Q. M.; Barb, A. W. A perspective on the structure and receptor binding properties of immunoglobulin G Fc. *Biochemistry* **2015**, *54*, 2931-2942.

[17] Ridgway, J. B.; Presta, L. G.; Carter, P. 'Knobs-into-holes' engineering of antibody CH3 domains for heavy chain heterodimerization. *Protein Eng.* **1996**, *9*, 617-621.

[18] Liu, Z. Leng, E. C.; Gunasekaran, K.; Pentony, M.; Shen, M.; Howard, M.; Stoops, J.; Manchulenko, K.; Razinkov, V.; Liu, H.; Fanslow, W.; Hu, Z.; Sun, N.; Hasegawa, H.; Clark, R.; Foltz, I. N.; Yan, W. A novel antibody engineering strategy for making monovalent bispecific heterodimeric IgG antibodies by electrostatic steering mechanism. *J. Biol. Chem.* **2015**, *290*, 7535-7562.

[19] Labrijn, A. F.; Meesters, J. I.; de Goeij, B. E. C. G.; van den Bremer, E. T. J.; Neijssen, J.; van Kampen, M. D.; Strumane, K.; Verploegen, S.; Kundu, A.; Gramer, M. J.; van Berkel, P. H. C.; van de Winkel, J. G. J.; Schuurman, J.; Parren, P. W. H. I. Efficient generation of stable bispecific IgG1 by controlled Fab-arm exchange. *Proc. Natl. Acad. Sci. U.S.A.* **2013**, *110*, 5145-5150.

[20] Labrijn, A. F.; Buijsse, A.; van den Bremer, E. T. J.; Verwilligen, A. Y. W.; Bleeker, W. K.; Thorpe, S. J.; Killestein, J.; Polman, C. H.; Aalberse, R. C.; Schuurman, J.; van de Winkel, J. G. J.; Parren, P. W. H. I. Therapeutic IgG4 antibodies engage in Fab-arm exchange with endogenous human IgG4 in vivo. *Nat. Biotechnol*. **2009**, *27*, 767-773.

[21] Davies, A. M.; Rispens, T.; Ooijevaar-de Heer, P.; Gould, H. J.; Jefferis, R.; Aalberse, R. C.; Sutton, S. J. Structural determinants of unique properties of human IgG4-Fc. *J. Mol. Biol*. **2014**, *426*, 630-644.

[22] Rispens, T.; Ooijevaar-de Heer, P.; Bende, O.; Aalberse, R. C. Mechanism of immunoglobulin G4 Fab-arm exchange. *J. Am. Chem. Soc*. **2011**, *133*, 10302-10311.

[23] Angal, S.; King, D. J.; Bodmer, M. W.; Turner, A.; Lawson, A. D.; Roberts, G.; Pedley, B.; Adair, J.R. A single amino acid substitution abolishes the heterogeneity of chimeric mouse/human (IgG4) antibody. *Mol. Immunol.* **1993**, *30*, 105-108.

[24] Labrijn, A. F.; Rispens, T.; Meesters, J.; Rose, R. J.; den Bleker, T. H.; Loverix, S.; van den Bremer, E. T. J.; Neijssen, J.; Vink, T.; Lasters, I.; Aalberse, R. C.; Heck, A. J. R.; van de Winkel, J. G. J.; Schuurman, J.; Parren, P. W. H. I. Species-specific determinants in the IgG CH3 domain enable Fab-arm exchange by affecting the noncovalent CH3-CH3 interaction strength. *J. Immunol*. **2011**, *187*, 3238-3246.

[25] Labrijn, A. F.; Meesters, J. I. Priem, P.; de Jong, R. N.; van den Bremer, E. T. J.; van Kampen, M. D.; Gerritson, A. F.; Schuurman, J.; Parren, P. W. H. I. Controlled Fab-arm exchange for the generation of stable bispecific IgG1. *Nat. Protoc*. **2014**, *9*, 2450-2463.

[26] A study to evaluate safety and tolerability of JNJ-61178104 in healthy participants. In: ClinicalTrials.gov [Internet]. Bethesda (MD): National Library of Medicine (US). 2000-[cited 2016 Oct 31]. Available from: https://clinicaltrials.gov/ct2/show/NCT02758392 NML Identifier: NCT02758392.

[27] A dose escalation study of JNJ-61186372 in participants with advanced non-small cell lung cancer. In: ClinicalTrials.gov [Internet]. Bethesda (MD): National Library of Medicine (US). 2000-[cited 2016 Oct 31]. Available from: https://clinicaltrials.gov/ct2/show/NCT02609776 NML Identifier: NCT02609776.

[28] A dose escalation study of JNJ-63709178, a humanized CD123 x CD3 DuoBody in subjects with relapsed or refractory acute myeloid leukemia (AML). In: ClinicalTrials.gov [Internet]. Bethesda (MD): National Library of Medicine (US). 2000-[cited 2016 Oct 31]. Available from: https://clinicaltrials.gov/ct2/show/NCT02715011 NML Identifier: NCT02715011.

[29] Nunes, J. P.; Morais, M.; Vassileva, V.; Robinson, E.; Rajkuamr, V. S.; Smith, M. E.; Pedley, R. B.; Caddick, S.; Baker, J. R.; Chudasama, V. Functional native disulfide bridging enables delivery of a potent, stable and targeted antibody-drug conjugate (ADC). *Chem. Commun*. **2015**, *51*, 10624-10627.

[30] Canziani, G. A.; Melero, J. A.; Lacy, E. R. Characterization of neutralizing affinity-matured human respiratory syncytial virus F binding antibodies in the sub-picomolar affinity range. *J. Mol. Recognit*. **2012**, *25*, 136-146.

[31] Roben, P.; Moore, J. P.; Thali, M.; Sodroski, J.; Barbas, C. F., III; Burton, D. R. Recognition properties of a panel of human recombinant Fab fragments to the CD4 binding site of gp120 that show differing abilities to neutralize human immunodeficiency virus type 1. *J. Virol.* **1994**, *68*, 4821-4828.

[32] Sahoo, B.; Drombosky, K. W.; Wetzel, R. Fluorescence correlation spectroscopy: a tool to study protein oligomerization and aggregation in vitro and in vivo. *Methods Mol. Biol.* **2016**, *1345*, 67−87.

[33] *Molecular probes handbook: a guide to fluorescent probes and labeling technologies*, Thermo Fisher Scientific, 11th ed.; p. 39.
[34] Rispens, T.; Davies, A. M.; Ooijevaar-de Heer, P.; Absalah, S.; Bende, O.; Sutton, B. J.; Vidarsson, G.; Aalberse, R. C. Dynamics of inter-heavy chain interactions in human immunoglobulin G (IgG) subclasses studied by kinetic Fab arm exchange. *J. Biol. Chem.* **2014**, *289*, 6098-6109.
[35] Cleland, W. W. Dithiothreitol, a new protective reagent for SH groups. *Biochemistry* **1964**, *3*, 480-482.
[36] El-Hallag, I.; Al-Youbi, A. O.; Obaid, A. Y.; El-Mossalamy, E. H.; El-Daly, S. A.; Asiri, A. M. Electrochemical investigation of cysteamine at carbon fiber microdisk electrode. *J. Chil. Chem. Soc.* **2011**, *56*, 837-841.
[37] Creighton, T. E. Disulfide bond formation in proteins. *Methods Enzymol*. **1984**, *107*, 305-329.
[38] Shammas, S. L.; Travis, A. J.; Clarke, J. Remarkably fast coupled folding and binding of the intrinsically disordered transactivation domain of cMyb to CBP KIX. *J. Phys. Chem. B* **2013**, *117*, 13346-13356.
[39] Vijayakumar, M.; Wong, K. Y.; Schreiber, G.; Fersht, A. R.; Szabo, A.; Zhou, H. X. Electrostatic enhancement of diffusion-controlled protein-protein association: comparison of theory and experiment on barnase and barnstar. *J. Mol. Biol.* **1998**, *278*, 1015-1024.
[40] Durben, M.; Schmiedel, D.; Hofmann, M.; Vogt, F.; Nübling, T.; Pyz, E.; Bühring, H.; Rammensee, H.; Salih, H.; Große-Hovest, L.; Jung, G. Characterization of a bispecific FLT3 x CD3 antibody in an improved, recombinant format for the treatment of leukemia. *Mol. Ther.* **2015**, *23*, 648-655.
[41] Nalivaiko, K.; Hofmann, M.; Kober, K.; Teichweyde, N.; Krammer, P. H.; Rammensee, H.; Grosse-Hovest, L.; Jung, G. A recombinant bispecific CD20xCD95 antibody with superior activity against normal and malignant B-cells. *Mol. Ther.* **2016**, *24*, 298-305.
[42] Hermanson, G. T. *Bioconjugate Techniques*, 2nd ed.; Elsevier: San Diego, 2008.
[43] Gramer, M. J.; van den Bremer, E. T. J.; van Kampen, M. D.; Kundu, A.; Kopfmann, P.; Etter, E.; Stinehelfer, D.; Long, J.; Lannom, T.; Noordergraaf, E. H.; Gerritsen, J.; Labrijn, A. F.; Schuurman, J.; Van Berkel, P. H. C.; Parren, P. W. H. I. Production of stable bispecific IgG1 by controlled Fab-arm exchange: scalability from bench to large-scale manufacturing by application of standard approaches. *MAbs* **2013**, *5*, 962-973.
[44] Liu, H.; Chumsae, C.; Gaza-Bulseco, G.; Hurkmans, K.; Radziejewski, C. H. Ranking the susceptibility of disulfide bonds in human IgG1 antibodies by reduction, differential alkylation, and LC-MS analysis. *Anal. Chem.* **2010**, *82*, 5219-5226.
[45] Zimmerman, B.; Grey, H. M. Noncovalent interactions between immunoglobulin polypeptide chains. Stability to dissociation by denaturants. *Biochemistry* **1972**, *11*, 78-84.
[46] Thies, M. J. W.; Talamo, F.; Mayer, M.; Bell, S.; Ruoppolo, M.; Marino, G.; Buchner, J. Folding and oxidation of the antibody domain C(H)3. *J. Mol. Biol.* **2002**, *319*, 1267-1277.
[47] Rispens, T.; Ooievaar-De Heer, P.; Vermeulen, E.; Schuurman, J.; van der Neut Kolfschoten, M.; Aalberse, R. C. Human IgG4 binds to IgG4 and conformationally altered IgG1 via Fc-Fc interactions. *J. Immunol.* **2009**, *182*, 4275-7281.
[48] Rispens, T.; Meesters, J.; den Bleken, T. H.; Ooijevaar-De Heer, P.; Schuurman, J.; Parren, P. W.; Labrijn, A.; Aalberse, R. C. Fc-Fc interactions of human IgG4 require dissociation of heavy chains and are formed predominantly by the intra-chain hinge isomer. *Mol. Immunol*. **2013**, *53*, 35-42.

CHAPTER 5

Designing a Dual Fc Antibody with Enhanced Avidity for Fc Receptors

5.1 Introduction

Monoclonal antibody (mAb)-based, and in particular immunoglobulin G (IgG)-based, therapeutics have become an extremely successful class of drugs due to the potency, specificity, stability, and adaptability of the mAb framework.[1,2] Based on their role in adaptive immunity, Abs have an intrinsic ability to interact with other elements of the immune system. Thus, therapeutic mAbs can be used to elicit an anti-cancer immune response by directing leukocytes and other humoral factors to engage specific antigen-expressing cells.[3,4] Clinically, the most important IgG effector functions are complement-dependent cytotoxicity (CDC), antibody-dependent cellular phagocytosis (ADCP), and antibody-dependent cell-mediated cytotoxicity (ADCC), with each mechanism eliciting a distinct immune program for elimination of target cells.[5] Of these, CDC requires mAb binding via the crystallizable fragment (Fc) to C1q protein, which is the first component of the complement cascade. ADCP and ADCC rely on IgG Fc binding to Fcγ receptors (FcγRs) expressed on phagocytes and natural killer (NK) cells, respectively. Binding of mAbs to antigen-bearing target cells via their two antigen-binding fragments (Fabs) and to FcγRs via the Fc leads to cross-linking of FcγRs and downstream transcriptional changes associated with effector cell activation. Besides C1q and FcγRs, IgG mAbs also bind the neonatal Fc receptor (FcRn) at the acidic pH of the endosome, which rescues them from lysosomal degradation and confers them with their characteristically long serum half-lives.[6]

Numerous protein engineering efforts have focused on modulating effector function by altering Fc interactions with FcγRs.[7,8] Elimination of ADCP and ADCC can be achieved by abrogating Fc-FcγR binding and is desirable for mAbs whose intended therapeutic mechanism is

simple inhibition.[9,10] Conversely, enhancement of these effector functions can be beneficial for anti-cancer therapeutics and is achieved by amplifying IgG activation of effector cells. For example, amino acid substitutions of the Fc that cause tighter binding to FcγRIIIa result in enhanced ADCC. [11-13] However, incorporation of novel mutations has notable drawbacks including the possibility of decreased stability and increased immunogenicity.[14,15] The glycan profile of IgG mAbs has also been linked to their immune functions, with low fucose IgG glycoforms having improved binding to FcγRIIIa and more potent ADCC.[16]

A less established strategy for modulation of effector mechanisms is the duplication of the entire Fc domain. This Fc multimerization strategy has already proven effective for CDC, where Fc mutations favoring non-covalent IgG hexamerization result in more potent complement-mediated lysis of target cells.[17,18] Regarding ADCP and ADCC, incorporation of multiple Fc domains into each IgG molecule may amplify FcγR signaling by strengthening the avidity of the Fc-FcγR interaction or by facilitating FcγR cross-linking. In fact, studies with IgG variants containing two or three tandemly repeated Fc domains have shown enhanced FcγR-mediated effector function compared to the wild-type IgG.[19-21] Here, an alternative IgG scaffold with distinct structural geometry is presented. Fc and Fab domains were arranged into a 'tetrahedral' format to maximize bivalent binding to both antigens and FcγRs and therefore allow more efficient lymphocyte recruitment. Biochemical and structural characterization, detailed kinetic analysis of FcR binding mechanism, and investigation of effector cell activation demonstrate the potential utility of this framework for treatment of cancer or infection.

5.2 Experimental procedures

5.2.1 Proteins and other materials

Genes for anti-RSV (clone B21M) and anti-CD20 (clone 10F381, rituximab) HC, LC, and

LC-Fc fusion were synthesized and cloned into the pcDNA3.1 vector for bacterial replication and mammalian expression. The DNA sequence for the LC-Fc fusion used the entire light chain sequence immediately followed by the heavy chain sequence, beginning at the "DKTHTCPPCP" motif of the hinge and continuing to the end of the heavy chain. DNA was transformed into DH5α cells (Thermo Fisher, 18265017) for replication, purified (QIAGEN, 10023), and used for transfections.

Wild-type human IgG1 mAbs containing a single Fc domain were expressed transiently in HEK 293F cells (Thermo Fisher, R79007) using a 3:1 ratio of LC to HC DNA according to the manufacturer's instructions. For dual Fc variants, plasmids containing the LC-Fc fusion were used in place of normal LC plasmids. In this case, a 10:1 ratio of HC to LC-Fc fusion DNA was used in order to reduce formation of a contaminant with complexed LC-Fc chains. mAbs were purified using a MabSelect SuRe column (GE Life Sciences, 29049104) according to the manufacturer's protocol, followed immediately by SEC using a Superdex 200 10/300 GL column (GE Life Sciences, 17517501) in 1× phosphate-buffered saline (PBS; 2.67 mM KCl, 1.47 mM KH_2PO_4, 138 mM NaCl, 8.06 mM Na_2HPO_4), pH 7.2. Analytical SEC to characterize purified protein was run analogously, loading 20 μg of protein onto the column. SDS-PAGE was performed using a BioRad Protean TGX 4-15% acrylamide gel, Tris-glycine running buffer, and Laemmli sample buffer with or without 50 mM dithiothreitol (DTT). To eliminate $(LC\text{-}Fc)_4$ and $HC_1(LC\text{-}Fc)_3$ contaminants (roughly same size as desired $HC_2(LC\text{-}Fc)_2$ species) C_H1 affinity chromatography (Thermo Fisher, 5943462001) was performed by applying the protein A- and SEC-purified sample at neutral pH, washing with 25 mM sodium acetate, 1 M NaCl, pH 5.2 to remove contaminants, and eluting with 25 mM sodium acetate, pH 3.6. Buffer exchange was immediately performed back into 1×PBS, pH 7.2.

5.2.2 Fc receptor binding kinetics to mono- and dual-Fc antibodies

Anti-6x-His Fab was generated from the full-length mAb using a Pierce™ Fab Micro Preparation Kit (Thermo Fisher, 44685) according to the manufacturer's instructions. A Biacore T200 instrument and CM5 chip containing anti-6x-His Fab were used for binding analysis. In separate experiments, 3 nM FcγRI, 10 nM FcγRIIIa, or 200 nM FcRn was captured onto the chip surface for 60 seconds, resulting in a capture level of 40 RU, 50 RU, and 100 RU, respectively. For FcγRI, association was performed using 1:3 serial dilutions of anti-RSV 1Fc or 2Fc (2-162 nM) for 90 seconds, followed by a 300-second dissociation. For FcγRIIIa, association was performed using 1:3 serial dilutions of anti-RSV 1Fc or 2Fc (12-3000 nM) for 60 seconds, followed by a 300-second dissociation. For FcRn, association was performed using 1:3 serial dilutions of anti-RSV 1Fc or 2Fc (1.2-300 nM) for 60 seconds, followed by a 180-second dissociation. Flow rate was 50 µL/min and running buffer was 1× PBS, 0.05% Tween 20 (pH 7.2 for FcγRI and FcγRIIIa and pH adjusted to 6.0 using HCl for FcRn). Regeneration was achieved with a 10-second pulse of 10 mM glycine, pH 1.5 at 20 µL/min, followed by a 180-second stabilization period. For consistency, each double-referenced dataset containing duplicates of each concentration was globally fit using the bivalent analyte model, with reported rates as the first set of kinetic parameters, k_{a1} and k_{d1}.

5.2.3 Effect of Fc receptor density on complex dissociation rate

3,000 RU of anti-6x-His Fab in 10 mM citrate, pH 4.0 was covalently immobilized onto each of two flow cells of a CM5 sensor chip (GE Life Sciences, 29104988) using Biacore T200. At a flow rate of 50 µL/min, 1, 3, 10, 30, or 100 nM of His-tagged Fc receptor (FcγRI or FcRn) was captured to the surface for 60 seconds, followed by a 60-second association step with 10 nM anti-RSV 1Fc or 2Fc and a 300-second dissociation step. Each capture level (concentration of

receptor) was performed in duplicate with double reference subtraction. Running buffer was 1× PBS, 0.05% Tween 20 (pH 7.2 for FcγRI and pH adjusted to 6.0 using HCl for FcRn). Regeneration was performed using a 10-second pulse of 10 mM glycine, pH 1.5 at 20 µL/min, followed by a 180-second stabilization period. As some of the dissociation data did not fit well to a single exponential, two-point dissociation rates were calculated using the response at the beginning of the disassociation phase and after 300 seconds (FcγRI) or 60 seconds (FcRn).

5.2.4 Stoichiometry of Fc receptor binding

CNTO 6559 (anti-B21M idiotype) Fab was generated from the full-length mAb using a Pierce™ Fab Micro Preparation Kit (Thermo Fisher, 44685) according to the manufacturer's instructions. 1,500 RU of CNTO 6559 Fab in 10 mM citrate, pH 4.0 was covalently immobilized onto each of two flow cells of a CM5 sensor chip (GE Life Sciences, 29104988) using Biacore T200. For FcγRI, 5 nM of anti-RSV 1Fc or 2Fc was captured via the Fab for 40 seconds in 1× PBS, 0.05% Tween 20, pH 7.2, followed by a 180-second association to 1:3 serial dilutions of FcγRI (0.12-30 nM) and a 300-second dissociation. For FcRn, 5 nM of anti-RSV 1Fc or 2Fc was captured via the Fab for 30 seconds in 1× PBS, 0.05% Tween 20 (pH adjusted to 6.0 using HCl), followed by a 180-second association to 1:3 serial dilutions of FcRn (4.1-1000 nM) and a 300-second dissociation. Each concentration of receptor was examined in duplicate at 50 µL/min with double reference subtraction. Regeneration was performed using a 10-second pulse of 10 mM glycine, pH 1.5 at 20 µL/min, followed by a 180-second stabilization period. The response values were used to calculate the ratio of bound receptor to mAb at each concentration using the following equation:

$$\frac{FcR}{mAb} = \frac{Response}{Capture\ level} \div \frac{MW_{FcR}}{MW_{mAb}}$$

where Response is the binding response in RU achieved during the 180-second association,

Capture level is the amount of mAb captured in RU, and MW is the molecular weight of the appropriate protein. Molecular weights were 146,691 Da for 1Fc, 197,751 Da for 2Fc, 40,096 Da for FcγRI, and 43,282 Da for FcRn. Note that the protein-only MW of FcγRI (30,843 Da) was multiplied by 1.3 to account for its high level of glycosylation.[22] The FcR:mAb ratio was then plotted as a function of [FcR] and fit to the hyperbolic binding equation,

$$\frac{FcR}{mAb} = \frac{B_{max} \cdot [FcR]}{K_D + [FcR]}$$

where B_{max} is the maximal FcR:mAb stoichiometry and K_D is the equilibrium dissociation constant.

5.2.5 ADCC reporter bioassay

ADCC was measured using a reporter bioassay kit (Promega, G7015) and following the manufacturer's instructions. Briefly, 200 µL each of anti-RSV 1Fc, anti-RSV 2Fc, anti-CD20 1Fc, and anti-CD20 2Fc were prepared at 15 µg/mL in the provided ADCC assay buffer and transferred to four wells of a 96-well plate. Serial 1:3 dilutions in ADCC assay buffer were performed to generate nine concentrations of each mAb as well as Ab-less controls. Raji target cells, which express CD20, were thawed and diluted into assay buffer as instructed. 25 µL of Raji cells was transferred to the inner 60 wells of two new 96-well plates. To these plates was added 25 µL of the mAb dilutions in order to have triplicates of each mAb concentration. Effector cells were thawed, diluted in assay buffer as instructed, and 25 µL was added to each well. Target cells, effector cells, and mAbs were incubated for six hours at 37 °C. After six hours, the plates were equilibrated to room temperature for 15 minutes, and then 75 µL of pre-mixed Bio-Glo assay reagent was added to the inner 60 wells of each plate, and also to three outer control wells. After 10 minutes, luminescence was measured using an integration time of 0.5 seconds/well. Data were plotted as luminescence intensity versus mAb concentration and fit with a dose response curve.

5.3 Results

5.3.1 Design of dual Fc antibody

In order to test whether a novel mAb scaffold containing two Fab and two Fc domains would have functional advantages compared to a wild-type mAb containing two Fabs and a single Fc domain, we designed the 1Fc (wild-type) and 2Fc mAbs depicted in **Figure 5.1** using the human IgG1 framework. Whereas 1Fc mAbs are composed of heavy chains (HCs) and light chains (LCs), 2Fc mAbs can be generated by co-expression of a normal HC and a LC-Fc fusion. The DNA sequence of this fusion was designed by appending the hinge and Fc sequence from a normal HC to the C-terminus of the LC. Thus, rather than terminating at the end of the Fab domain, the LC sequence continues for the formation of a second Fc domain. These constructs were expressed using the variable sequences of an anti-respiratory syncytial virus (RSV) mAb to create anti-RSV 1Fc and 2Fc mAbs.

5.3.2 Purification and biochemical characterization

As expected, multiple protein products were obtained resulting from self-assembly of different combinations of the 2Fc mAb gene products in human embryonic kidney (HEK) cells. After the initial protein A affinity chromatography step to purify Fc-containing proteins, it was evident that the desired 2Fc mAb had been formed along with undesired products. Size-exclusion chromatography (SEC) revealed a 200-kDa protein consistent with the expected mass of the 2Fc mAb, as well as an abundance of 100-kDa protein (likely the monomeric version of 2Fc mAb containing one Fc and one Fab domain) and some larger species representative of higher oligomers (**Figure 5.2a**). Nevertheless, size-exclusion chromatography was used to purify the 200-kDa product for further characterization.

In addition to analytical SEC, SDS-PAGE was used to verify the composition of the 200-

kDa product. Consistent with the structure of 2Fc mAb, this species produced bands at 200 kDa under non-reducing conditions (size of assembled complex) and at 50 kDa under reducing conditions (size of HC and LC-Fc) (**Figure 5.2b**). The lack of intense bands below 200 kDa under non-reducing conditions indicates that disulfide bonds were primarily in the native, oxidized state. As expected, the 1Fc mAb showed bands at 150 kDa for the non-reduced complex, and at 25 and 50 kDa for the reduced LC and HC. Electron microscopy data collected and analyzed by James Williams in the lab of Kelly Lee verified the presence of the predicted four-lobed protein structure (**Figure 5.2c**).

5.3.3 Functional characterization

Because the geometry of the 2Fc Ab is distinct from that of standard IgGs, it was necessary to determine whether the function of the Fab domains was maintained. Therefore, an anti-idiotype mAb that targets the variable region of the anti-RSV mAbs was used to demonstrate that the 1Fc and 2Fc mAbs have similar binding via their Fab domains (**Figure 5.2d**). These data, combined with subsequent Fc binding experiments, support the predicted composition of the designed 2Fc mAb.

5.3.4 Affinity for Fc receptors

To determine accurate affinity values of 1Fc and 2Fc mAbs to Fc receptors, an intermediate amount of receptor was captured and a full titration of varying mAb concentrations was performed. In addition to FcγRI and FcRn, FcγRIIIa V158 (high affinity variant) was analyzed due to its importance for ADCC. As some of these interactions contained multivalent molecules in solution, each dataset was fit with the bivalent analyte model for ease of comparison. Although both 1Fc and 2Fc mAbs bound with high affinity to FcγRI, the dissociation rate was noticeably slower with 2Fc (**Figure 5.3a,b**). For FcγRIIIa, the 2Fc mAb displayed a significant increase in binding affinity

over the 1Fc mAb, which was mediated in large part by its slower off rate (**Figure 5.3c,d**). FcRn binding at pH 6.0 was characterized by the same decrease in dissociation rate for the 2Fc mAb (**Figure 5.3e,f**). These data are summarized in **Table 5.1**, and demonstrate that the 2Fc mAb has a higher affinity for each surface-bound receptor, driven primarily by slower dissociation kinetics.

5.3.5 Confirmation of bivalent binding

mAbs achieve their high avidity for antigen, in part, due to bivalent binding of their two Fab domains to immobilized antigens, which allows for slow dissociation when both Fab arms are bound. Similarly, the 2Fc mAb was expected to dissociate from Fc receptors at a rate that is dependent upon receptor density; high levels of immobilized receptor allow for enhanced avidity due to bivalent binding and slower off rates. Thus, varying levels of FcR were captured onto a Biacore sensor chip surface and binding parameters for their interaction with 1Fc and 2Fc mAbs were measured (**Figure 5.4**). The high affinity Fcγ receptor I (FcγRI) was chosen to represent Fcγ receptors that bind IgG mAbs at the upper Fc region, and the neonatal Fc receptor (FcRn) was used to examine binding at its distal binding site at the C_H2-C_H3 interface of the Fc domain. For the 1Fc mAb, which was expected to bind FcγRs with the 1:1 stoichiometry typical of IgG mAbs[23,24], there was no dependence of dissociation rate (k_d) on FcγRI capture density (**Figure 5.5a**). However, the k_d value for FcγRI-2Fc binding was strongly dependent on receptor capture level, with higher receptor density causing slower dissociation. For FcRn, both 1Fc and 2Fc mAbs showed k_d values that were dependent on receptor density; however, the 2Fc mAb demonstrated consistently slower off rates (**Figure 5.5b**). Because each IgG heavy chain contains an independent FcRn binding site[25,26], multivalent binding and varying k_d values were expected for both 1Fc and 2Fc mAbs. The stronger dependence on receptor density for 2Fc indicates a higher-avidity interaction.

5.3.6 Stoichiometry of Fc receptor binding

As a final verification that the tighter Fc receptor binding of 2Fc was driven by its additional Fc domain, experiments were devised to calculate the binding stoichiometry of 1Fc and 2Fc mAbs for FcRs. The 2Fc mAb was expected to bind twice the number of FcRs as the 1Fc mAb. Each mAb was captured to the surface of a Biacore chip via its Fab domains, and then the ratio of bound receptor to mAb was calculated when varying concentrations of FcRs were analyzed (**Figure 5.6**). The resulting hyperbolic fits provide the K_D value for mAbs binding to soluble Fc receptor, and the capacity of receptor binding to captured mAb (**Figure 5.7**). As expected based on previous studies of IgG1 mAbs, the stoichiometry of the 1Fc mAb for Fc receptors was approximately 1:1 mAb:FcγRI and 1:2 mAb:FcRn.[23-26] The 2Fc mAb bound with double the stoichiometry to both FcγRI and FcRn, indicating that each Fc domain within the molecule is competent for receptor binding (**Table 5.2**). In terms of affinity, the 1Fc and 2Fc mAbs had very similar K_D values for soluble FcγRI and FcRn. Thus, the enhancement in affinity of 2Fc for FcRs noted previously requires receptor immobilization for the avidity effect to occur.

5.3.7 Antibody-dependent cellular cytotoxicity

To determine whether the increased FcγRIIIa avidity of 2Fc translates to enhanced ADCC, 1Fc and 2Fc mAbs were generated using the design strategy described above, but with variable regions of anti-CD20 (rituximab). Raji cells expressing CD20 are a widely used model for B cell malignancies, and were used as target cells for ADCC. Anti-CD20 1Fc or 2Fc mAbs were co-incubated with Raji target cells and a Jurkat effector cell line that stably expresses human FcγRIIIa V158. When effector cells are activated by FcγR-mediated signaling, they upregulate the NFAT pathway, which is coupled to expression of firefly luciferase. Thus, activation of the NK cell surrogates leads to an increase in luminescence in this ADCC reporter bioassay.

ADCC results using this reporter bioassay showed that rituximab 1Fc and 2Fc had similar activation of effector cells based on a similar EC50 in the luminescence assay (**Figure 5.8**). EC50 values were 460 pM (95% CI: 312-700 pM) and 548 pM (95% CI: 358-1080) for the 1Fc and 2Fc mAbs, respectively. The dual Fc version of rituximab reached a smaller maximum luminescence, plateauing at $8.26\times10^5 \pm 0.48\times10^5$ RLU rather than the $1.04\times10^6 \pm 0.04\times10^6$ RLU observed for the wild-type mAb. Because 2Fc is expected to have enhanced avidity for FcγRs only at high enough receptor densities, we asked whether the Jurkat-derived effector cells express enough FcγRIIIa to allow for bivalent binding to 2Fc. In fact, an assay development scientist at Promega stated that these effector cells are specifically engineered to express low densities of the receptor, which allows for a low level of background. Thus, although a difference in effector cell activation was not observed with this assay, it is likely that the low density of FcγRIIIa on the artificial cell line prevented bivalent interactions from occurring.

To determine whether 2Fc elicits enhanced ADCC, it was therefore necessary to explore other assays with effector cells that display a physiologically relevant density of FcγR. Traditional ADCC assays use peripheral blood mononuclear cells as effector cells (PBMCs), since this blood fraction contains the FcγRIIIa-expressing natural killer cells. To test whether such an assay could reveal functional differences between 1Fc and 2Fc, CD20-expressing RPMI8866 cells were used as target cells and PBMCs as effector cells. Cell lysis was measured based on release of the normally intracellular enzyme lactate dehydrogenase (LDH). After an induction period of in which target cells, effector cells, and mAb were incubated for several hours, an LDH substrate was added to quantify lysis based on generation of its product, which absorbs at 490 nm.

The LDH release assay was optimized and performed by David Plotnik in the lab of Shiu-Lok Hu. The ADCC data (**Figure 5.9**) show differences between rituximab 1Fc and 2Fc, and

between PBMCs derived from different donors. The donor-associated variability in ADCC is commonly observed, and can be explained by differences in NK cell number, FcγR expression (receptor density), and FcγR polymorphism.[27] Dose-response curves were fit to extract EC50 and max lysis values (**Table 5.3**). Most notably, the assays with PBMCs from donors 1 and 3 showed a significantly higher level of maximum lysis for 2Fc rituximab. The assay with donor 2 PBMCs, however, showed lower max lysis for 2Fc. This discrepancy could be explained by the low dynamic range of the donor 2 data, which is quite noisy relative to background lysis. Data for all three batches of PBMCs indicate that 2Fc may have more potent NK-mediated lysis of tumor cells. However, more work is required to show a definitive functional difference between the 1Fc and 2Fc mAbs.

5.3.8 Mouse pharmacokinetics

The pharmacokinetics (PK) of the 2Fc mAb were tested to ensure that enhancement of FcRn binding avidity did not negatively impact mAb clearance. This work was performed by Susan Tam at Janssen Biologics Research. Human FcRn transgenic mice were intravenously-injected once with 2 mg/kg doses of anti-RSV human IgG1 wild-type (1Fc) or 2Fc. Human IgG serum concentrations over time for the mice are shown in **Figure 5.10**. PK profiles displayed a linear and similar decrease in IgG levels from Day 2 through 36. The calculated terminal half-life values were 12.1 ± 1.2 d for the 1Fc mAb, and 12.8 ± 3.1 d for the 2 Fc mAb. This result demonstrates that the 2 Fc framework does not alter the PK compared to a wild-type IgG.

5.4 Discussion

Here, we designed a novel mAb framework using the human IgG1 scaffold, which contains two functional Fc domains in addition to its two Fabs. These 2Fc mAbs were straightforward to produce, with just one additional SEC purification step compared to normal IgG1 mAbs. After

purification, 2Fc mAbs had the expected structural properties, including a mass of ~200 kDa and the presence of four discrete domains. Functionally, these 2Fc mAbs retained binding activity via their Fab domains and had greatly enhanced avidity to immobilized Fc receptors.

Other mAb frameworks utilizing Fc multimerization strategies have shown augmented effector functions including ADCP, ADCC, and opsonophagocytic killing.[19-21] These tandem Fc proteins are similar to our 2Fc mAb in terms of size, biochemical properties, and improvement of FcγR binding. However, tandem 2Fc and 3Fc mAb had significantly accelerated clearance relative to the control 1Fc mAb, whereas our tetrahedral 2Fc mAb had normal PK properties in mice.[21] Clearly the number of Fc domains is not the sole determinant of FcR interactions and biological properties. Rather, the molecular geometry likely contributes to this difference in pharmacokinetics by altering the relative preference for different FcRs and possibly the pH dependence of FcRn binding.

Roche's DuoMAbs, distinct 2Fc mAbs prepared using CrossMAb technology, have striking structural similarity to the 2Fc mAbs investigated here.[28] Although this framework is briefly described in a review, we did not find any primary literature other than a public patent application.[28,29] It appears that DuoMAbs share many functional features of the 2Fc mAbs presented here, including enhanced ADCC activity. Despite the similarities, DuoMAbs are distinct in primary sequence since they have the C_H1-C_L domain swap typical of CrossMAb Abs. This change could possibly facilitate protein purification by preventing light chain dimerization, but it makes the sequence slightly less native and therefore necessitates additional cloning efforts.

Although the 2Fc mAb showed a clear increase in FcR binding avidity compared to 1Fc, it was more difficult to demonstrate a difference in function. The ADCC reporter bioassay showed similar EC50 values for 1Fc and 2Fc, but this lack of effect could be due to low receptor expression

and the resulting inability of 2Fc to bind bivalently. Additionally, this type of assay reports on effector cell activation, which is one step removed from target cell killing. The LDH release assay, while using effector cells with relevant FcγR expression levels and reporting on cell lysis, was also complicated by experimental factors. For example, the variability in specific lysis was highly variable between PBMC donors. Since the assay was optimized using a batch of highly active PBMCs, the other datasets show a low amount of lysis that complicates quantitative comparison of mAb formats. The LDH release assay could be repeated with optimized conditions including effector:target ratio, which would increase the dynamic range of the data. Additionally, lower mAb concentrations could be included in an attempt to reach a similar baseline level for the different mAb constructs. In the future, other assay formats that quantify ADCC or ADCP could also be explored to determine whether the 2Fc mAb enhances immune recruitment.

If the 2Fc format is found more conclusively to enhance effector functions using *in vitro* assays, experiments in animal models would demonstrate whether these effects also occur *in vivo*. While functional activity so far has been investigated only for anti-CD20 mAbs, Abs targeting other cancer antigens could also be studied for their tumor-ablating activity. Additionally, the 2Fc framework could be easily modified to allow for generation of bispecific 2Fc molecules using established HC-HC and HC-LC pairing strategies.[30] These same methods may also help to improve the yield of the 2Fc protein relative to the 100-kDa side product. Finally, mAbs containing two distinct Fc domains (such as IgG1 and IgG3, or IgG and other Ig classes) could be prepared, allowing for mixing and matching of desired effector functions.

FIGURES

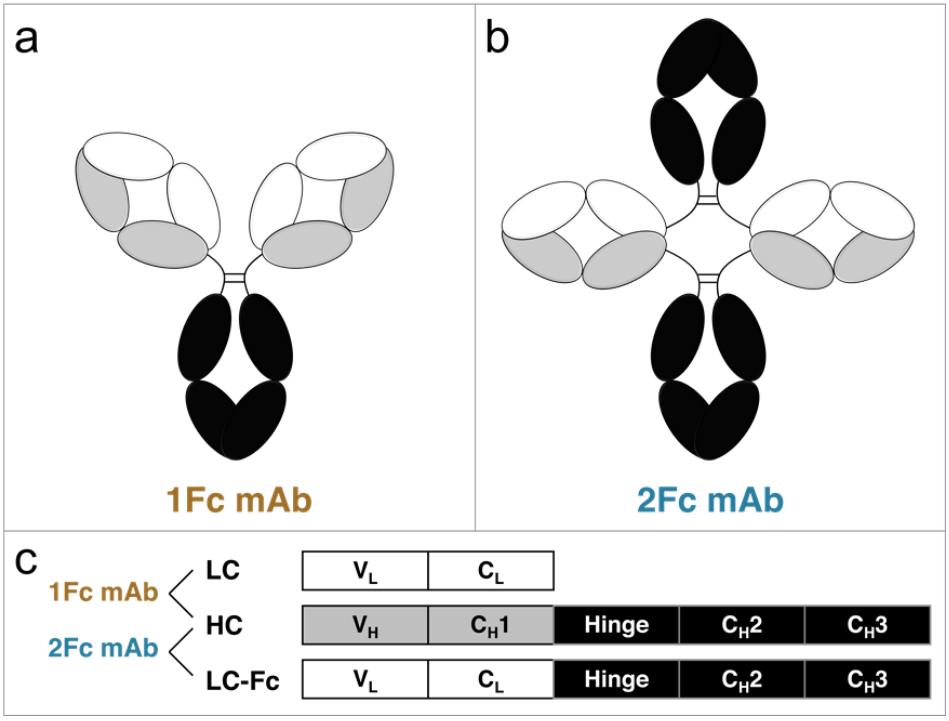

Figure 5.1: Design of 1Fc and 2Fc antibodies. Wild-type 1Fc antibodies (a) contain a normal γ1 heavy chain and κ light chain, while engineered 2Fc antibodies (b) contain the normal γ1 heavy chain combined with a κ-Fc fusion chain. Panel (c) shows the chain and domain composition of 1Fc and 2Fc genes.

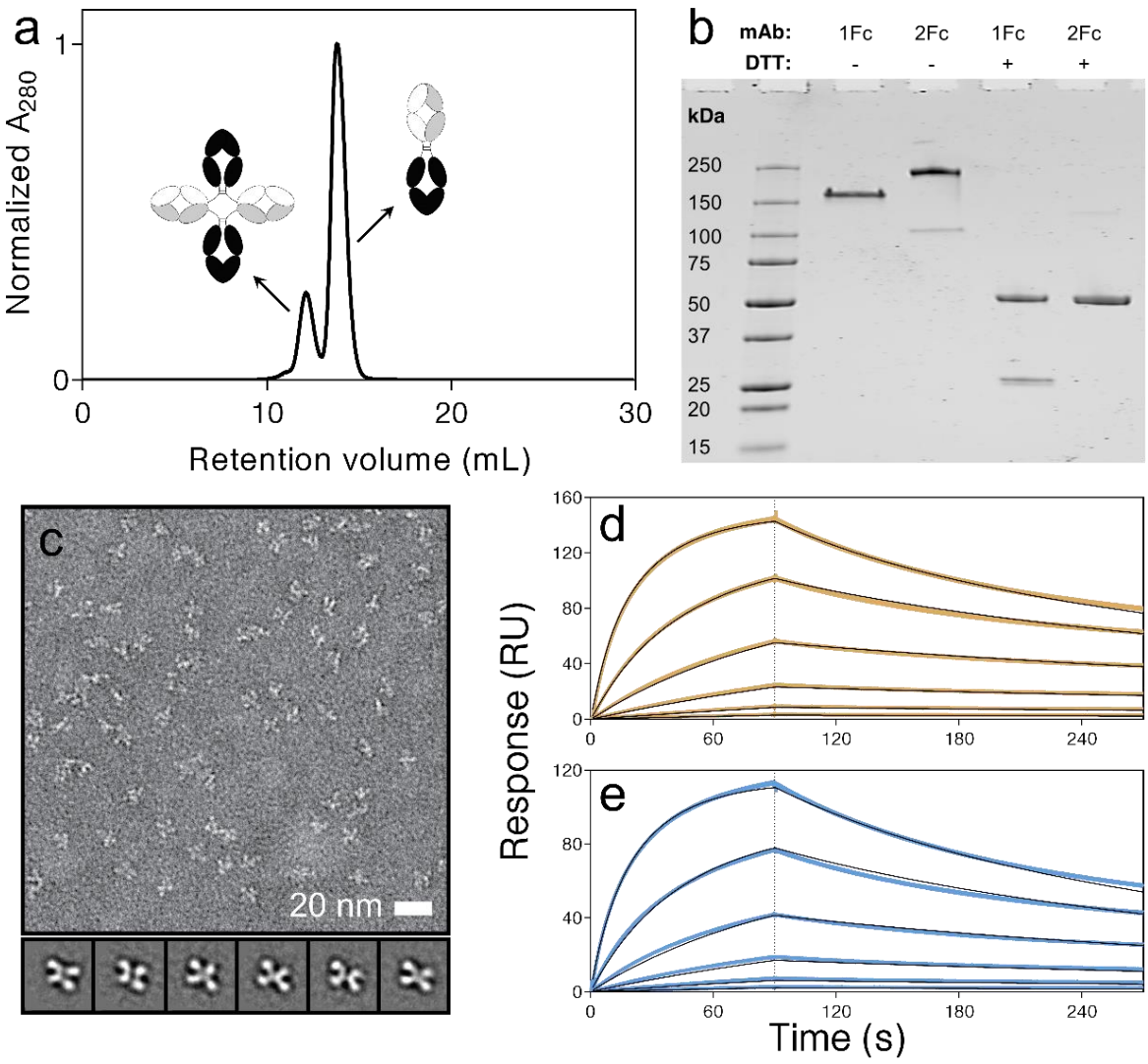

Figure 5.2: Biochemical, structural, and functional characterization of anti-RSV 1Fc and 2Fc antibodies. After protein A purification, the 2Fc antibody was further purified by size-exclusion chromatography (a), where a small peak on the left corresponded to the desired 200-kDa species and a larger peak on the right corresponded to a 100-kDa contaminant. SDS-PAGE of the 1Fc and 2Fc antibodies (b) was performed under non-reducing and reducing conditions to conform the full size and chain composition of each protein. Negative stain electron microscopy (c) was used to visualize the 2Fc antibody, where selected classifications shown on the bottom confirm a four-lobed structure. Negative stain data were collected and analyzed by James Williams in the lab of Kelly Lee. Surface plasmon resonance of 1Fc (d) and 2Fc (e) antibodies binding to an immobilized anti-RSV idiotype antibody was used to confirm the formation of functional antigen-binding domains.

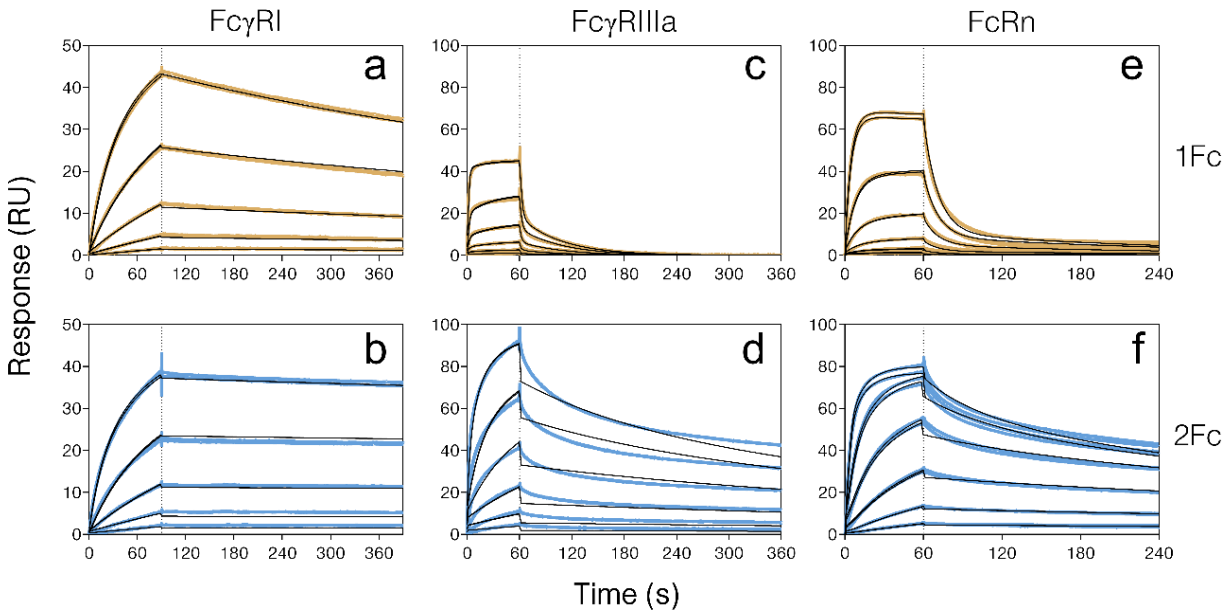

Figure 5.3: Binding sensorgrams for anti-RSV 1Fc (a, c, e) and 2 Fc (b, d, f) antibodies binding to surface-captured FcγRI (a, b), FcγRIIIa (c, d), and FcRn (e, f). For FcγRI, 3 nM of soluble receptor was captured via its C-terminal His tag for 60 seconds before a 90-second association phase with 1:3 serial dilutions of maximum 162 nM 1Fc or 2Fc antibody followed by a 300-second dissociation phase. For FcγRIIIa, 10 nM of soluble receptor was captured via its C-terminal His tag for 60 seconds before a 60-second association phase with 1:3 serial dilutions of maximum 3 μM 1Fc or 2Fc antibody followed by a 300-second dissociation phase. For FcRn, 200 nM of soluble receptor was captured via its C-terminal His tag for 60 seconds before a 60-second association phase with 1:3 serial dilutions of maximum 300 nM 1Fc or 2Fc antibody followed by a 300-second dissociation phase. Each dataset was globally fit to a bivalent analyte model to extract kinetic parameters.

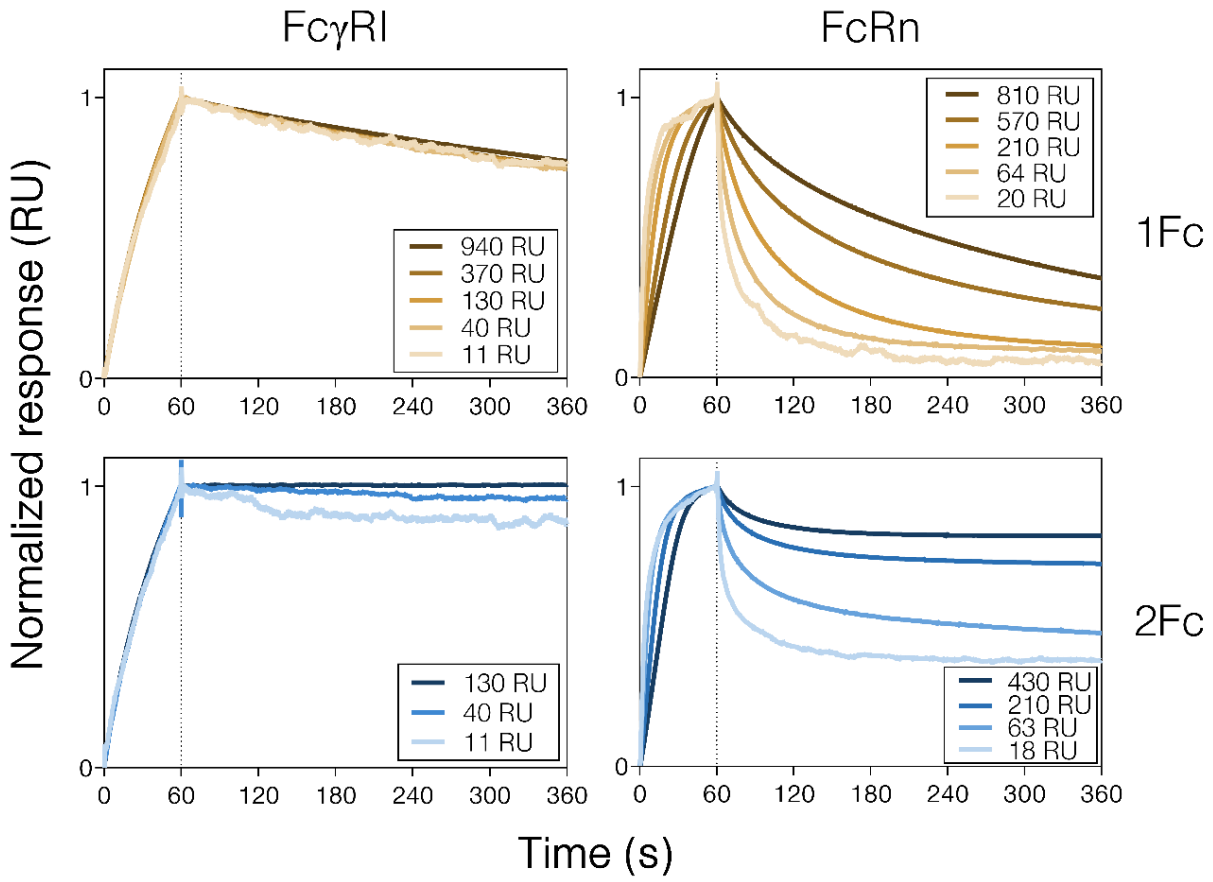

Figure 5.4: Effect of FcγI and FcRn capture density on FcR:Ab dissociation rate of anti-RSV 1Fc and 2Fc antibodies. Variable amounts of C-terminally His-tagged FcγRI or FcRn were captured to the surface of a CM5 chip containing immobilized anti-His Fab, and 1Fc or 2Fc were subsequently allowed to associate for 60 seconds and dissociate for 300 seconds. Data were normalized by maximum response at each concentration to facilitate comparison of dissociation rates.

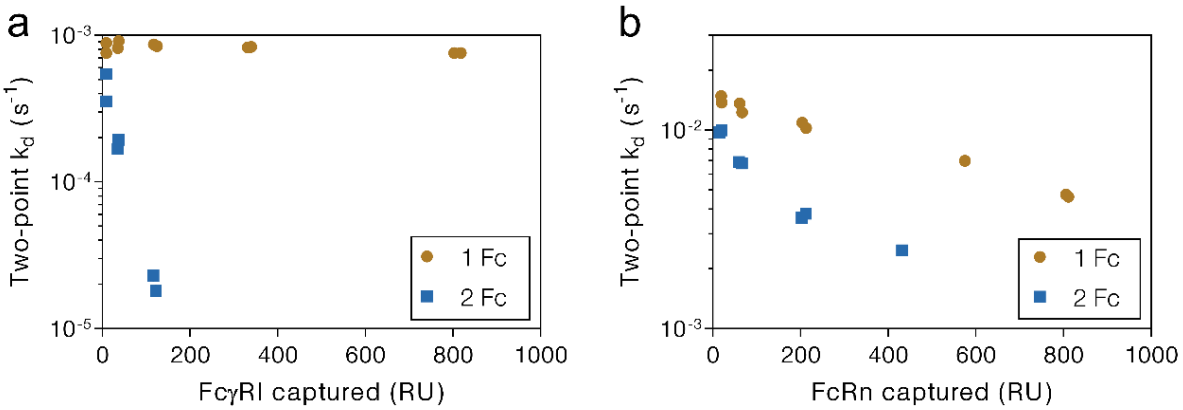

Figure 5.5: Effect of FcR capture density on FcR:Ab dissociation rate of anti-RSV 1Fc and 2Fc antibodies. Variable amounts of C-terminally His-tagged FcγRI (a) or FcRn (b) were captured to the surface of a CM5 chip containing immobilized anti-His Fab, and 1Fc or 2Fc were subsequently allowed to associate for 60 seconds and dissociate for 300 seconds. Two-point dissociation rates were calculated based on the first 300 seconds (FcγRI) or 60 seconds (FcRn) of dissociation data.

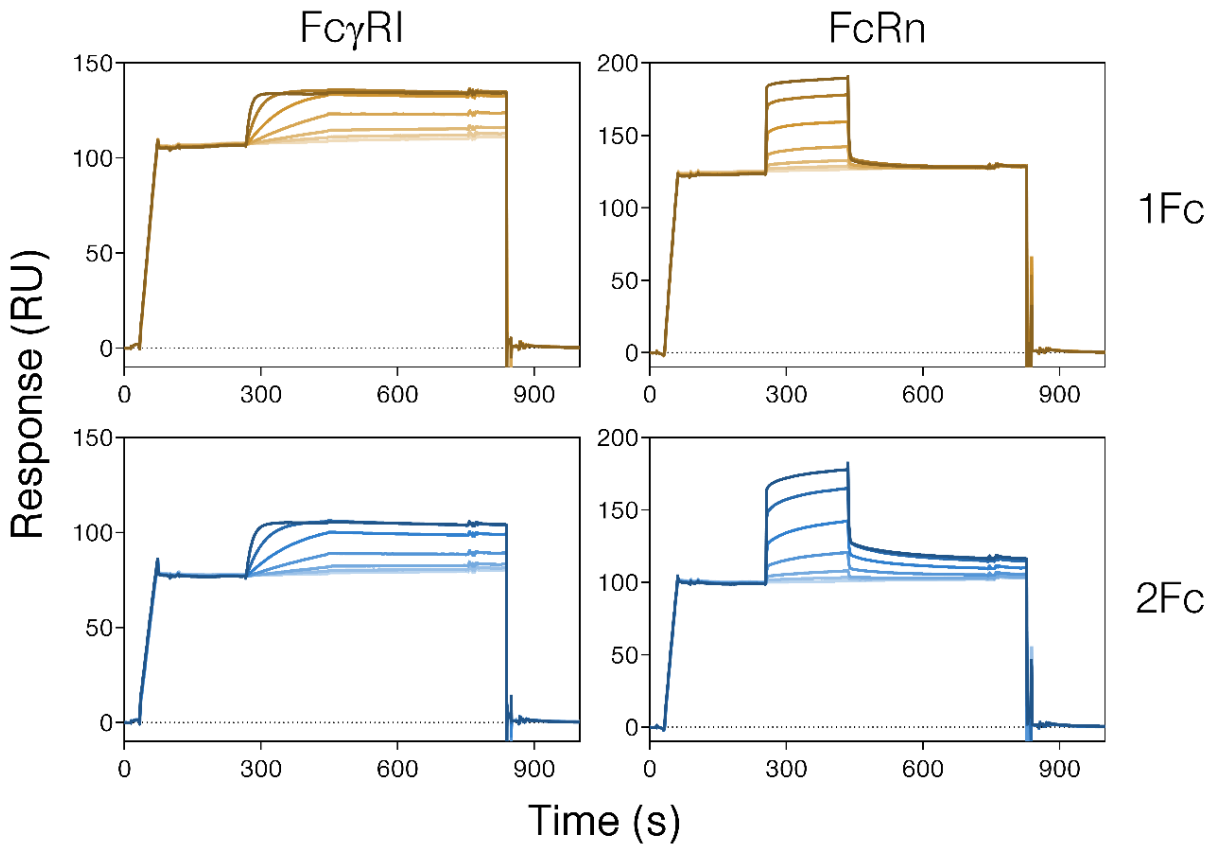

Figure 5.6: Surface plasmon resonance to determine stoichiometry of FcR binding to anti-RSV 1Fc and 2Fc antibodies. Antibodies were captured to the surface using anti-B21M idiotype Fabs, and subsequently associated with 1:3 serial dilutions of 30 nM FcγRI or 1 μM FcRn for 180 seconds, followed by a 300-second dissociation phase. The binding response achieved during capture and association phases was used, along with protein molecular weights, to determine the ratio of FcR to IgG at each FcR concentration.

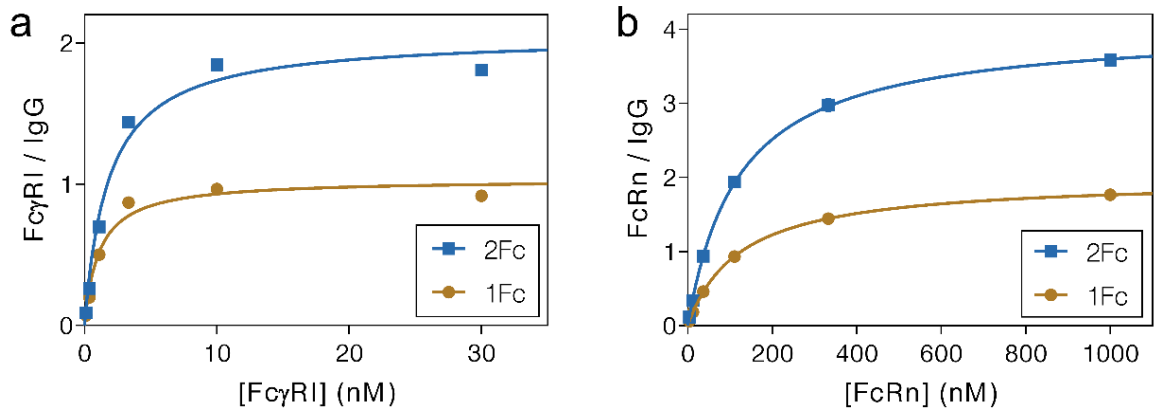

Figure 5.7: Surface plasmon resonance to determine stoichiometry of FcR binding to anti-RSV 1Fc and 2Fc antibodies. The binding response achieved during capture and association phases was used, along with protein molecular weights, to determine the ratio of FcR to IgG at each FcR concentration. These ratios were plotted as a function of receptor concentration and fit to a hyperbolic equation to determine plateaus that correspond to the maximum stoichiometry of binding.

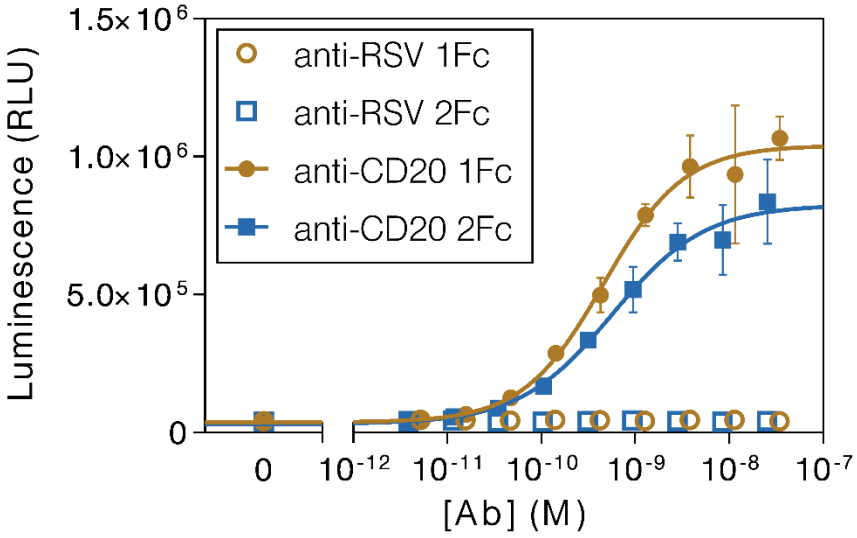

Figure 5.8: Antibody-dependent cellular cytotoxicity based on an effector cell activation reporter bioassay. Target Raji cells, effector cells, and varying concentration of rituximab or anti-RSV 1Fc or 2Fc antibodies were co-incubated for six hours before reading luminescence, which is a reporter of FcγRIIIa-mediated induction of the NFAT pathway.

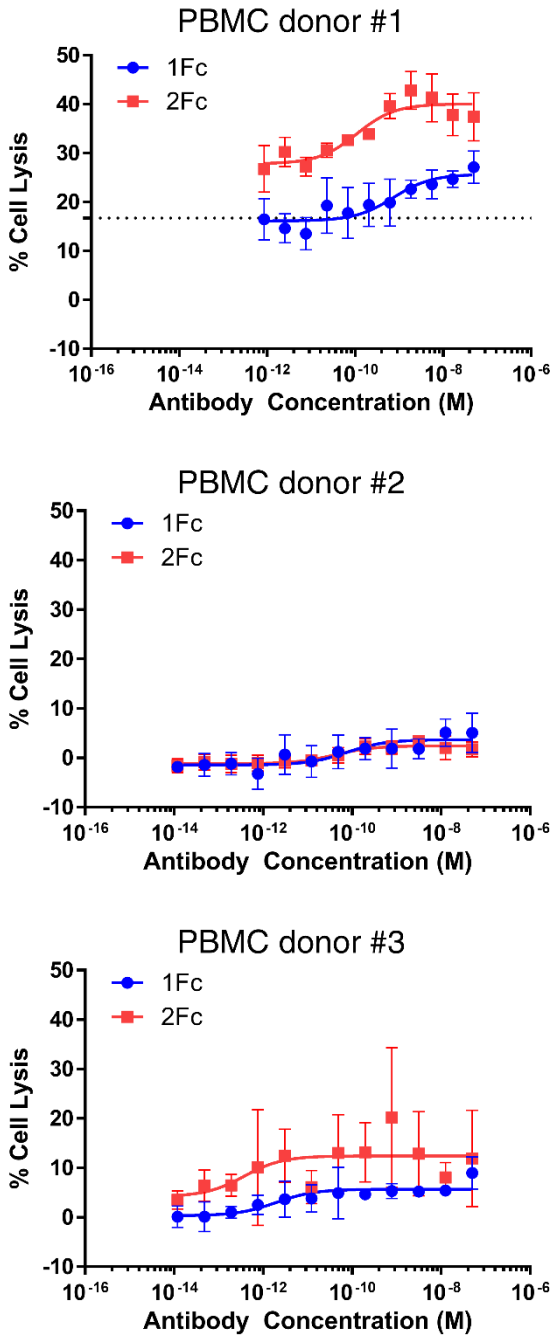

Figure 5.9: ADCC assay based on release of lactate dehydrogenase from lysed cells. RPMI8866 cells, which express CD20, were used as target cells along with the peripheral mononuclear blood cells (PBMCs) from three donors as effector cells. Cells were incubated with varying concentrations of 1Fc or 2Fc antibody for six hours before adding LDH substrate and measuring absorbance at 490 nm. The dotted line for donor #1 indicates the background level (no antibody). These data were collected and analyzed by David Plotnik in the lab of Shiu-Lok Hu.

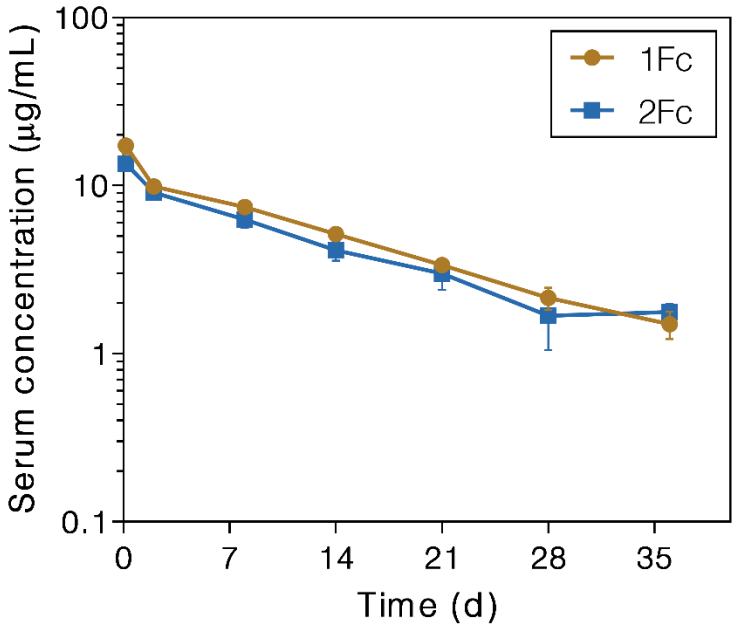

Figure 5.10: PK profiles of 1Fc and 2 Fc mAbs. Tg32 human FcRn transgenic mice were IV-injected with 2 mg/kg doses of human IgG1 anti-RSV mAbs. Blood samples from 5 mice per group were taken at 4 h to day 36 post-dose. Serum concentration of mice determined over time are shown. Data points represent the mean serum concentration ± standard error of the mean (SEM). These data were collected and analyzed by Susan Tam at Janssen Biologics Research.

TABLES

Table 5.1: Kinetic parameters for 1Fc and 2Fc mAbs binding to captured Fc receptors

Receptor	Antibody	*k_a ($M^{-1}s^{-1}$)	1Fc/2Fc	*k_d (s^{-1})	1Fc/2Fc	K_D (nM)	1Fc/2Fc
FcγRI	1Fc	76,600 ± 200	0.87	0.00128 ± 0.00001	6.2	16.7 ± 0.1	7.1
	2Fc	87,800 ± 300		0.000207 ± 0.000002		2.36 ± 0.02	
FcγRIIIa	1Fc	51,300 ± 200	3.2	0.4682 ± 0.002	130	9,130 ± 50	42
	2Fc	15,900 ± 100		0.00349 ± 0.00002		219 ± 2	
FcRn	1Fc	218,000 ± 1,000	0.25	0.0872 ± 0.0003	8.9	400 ± 2	35
	2Fc	860,000 ± 1,000		0.00980 ± 0.00008		11.4 ± 0.1	

*k_a and k_d values shown are the first set of kinetic parameters from bivalent analyte fits.

Table 5.2: Stoichiometry and affinity of 1Fc and 2Fc mAbs binding to soluble Fc receptors

Receptor	Antibody	N	2Fc/1Fc N	K_D (nM)	1Fc/2Fc K_D
FcγRI	1Fc	1.03 ± 0.04	2.0	1.11 ± 0.18	1.6
	2Fc	2.05 ± 0.07		1.82 ± 0.25	
FcRn	1Fc	1.98 ± 0.02	2.0	124 ± 4	1.0
	2Fc	4.03 ± 0.04		121 ± 4	

Table 5.3: Parameters from ADCC assay measured by LDH release (data from David Plotnik)

Donor	Antibody	EC50, pM (95% CI)	Change	Max lysis ± SE (%)	Change
1	1Fc	739 (138-3940)	**↓6.8x**	25.7 ± 1.5	**↑1.6x**
	2Fc	109 (32-371)		40.0 ± 1.0	
2	1Fc	76.1 (7.2-807)	**↓1.9x**	3.7 ± 0.9	**↓1.5x**
	2Fc	40.1 (8.0-205)		2.4 ± 0.4	
3	1Fc	1.96 (0.25-15.3)	**↓5.3x**	5.7 ± 0.6	**↑2.2x**
	2Fc	0.37 (0.005-25.5)		12.4 ± 1.6	

5.5 References

[1] Ecker, D. M., Jones, S. D., and Levine, H. L. (2015) The therapeutic monoclonal antibody market. *MAbs*. **7**, 9–14

[2] Kaplon, H., and Reichert, J. M. (2018) Antibodies to watch in 2018. *MAbs*. **10**, 183–203.

[3] Weiner, G. J. (2015) Building better monoclonal antibody-based therapeutics. *Nat. Rev. Cancer*. **15**, 361–370.

[4] Redman, J. M., Hill, E. M., AlDeghaither, D., and Weiner, L. M. (2015) Mechanisms of action of therapeutic antibodies for cancer. *Mol. Immunol.* **67**, 28–45.

[5] Vidarsson, G., Dekkers, G., and Rispens, T. (2014) IgG subclasses and allotypes: From structure to effector functions. *Front. Immunol.* **5**, 1–17.

[6] Roopenian, D. C., and Akilesh, S. (2007) FcRn: the neonatal Fc receptor comes of age. *Nat. Rev. Immunol.* **7**, 715–725.

[7] Kellner, C., Otte, A., Cappuzzello, E., Klausz, K., and Peipp, M. (2017) Modulating cytotoxic effector functions by Fc engineering to improve cancer therapy. *Transfus. Med. Hemotherapy*. **44**, 327–336.

[8] Wang, X., Mathieu, M., and Brezski, R. J. (2017) IgG Fc engineering to modulate antibody effector functions. *Protein Cell*. **9**, 1–11.

[9] Alegre, M. L., Collins, A. M., Pulito, V. L., Brosius, R. A., Olson, W. C., Zivin, R. A., Knowles, R., Thistlethwaite, J. R., Jolliffe, L. K., and Bluestone, J. A. (1992) Effect of a single amino acid mutation on the activating and immunosuppressive properties of a "humanized" OKT3 monoclonal antibody. *J. Immunol.* **148**, 3461–3468.

[10] Vafa, O., Gilliland, G. L., Brezski, R. J., Strake, B., Wilkinson, T., Lacy, E. R., Scallon, B., Teplyakov, A., Malia, T. J., and Strohl, W. R. (2014) An engineered Fc variant of an IgG eliminates all immune effector functions via structural perturbations. *Methods*. **65**, 114–126.

[11] Richards, J. O., Karki, S., Lazar, G. A., Chen, H., Dang, W., and Desjarlais, J. R. (2008) Optimization of antibody binding to Fc RIIa enhances macrophage phagocytosis of tumor cells. *Mol. Cancer Ther.* **7**, 2517–2527.

[12] Shields, R. L., Namenuk, A. K., Hong, K., Meng, Y. G., Rae, J., Briggs, J., Xie, D., Lai, J., Stadlen, A., Li, B., Fox, J. A., and Presta, L. G. (2001) High resolution mapping of the binding site on human IgG1 for FcγRI, FcγRII, FcγRIII, and FcRn and design of IgG1 variants with improved binding to the FcγR. *J. Biol. Chem.* **276**, 6591–6604.

[13] Lazar, G. A., Dang, W., Karki, S., Vafa, O., Peng, J. S., Hyun, L., Chan, C., Chung, H. S., Eivazi, A., Yoder, S. C., Vielmetter, J., Carmichael, D. F., Hayes, R. J., and Dahiyat, B. I. (2006) Engineered antibody Fc variants with enhanced effector function. *Proc. Natl. Acad. Sci.* **103**, 4005–4010.

[14] Liu, Z., Gunasekaran, K., Wang, W., Razinkov, V., Sekirov, L., Leng, E., Sweet, H., Foltz, I., Howard, M., Rousseau, A. M., Kozlosky, C., Fanslow, W., and Yan, W. (2014) Asymmetrical Fc engineering greatly enhances antibody-dependent cellular cytotoxicity (ADCC) effector function and stability of the modified antibodies. *J. Biol. Chem.* **289**, 3571–3590.

[15] Tam, S. H., Mccarthy, S. G., Armstrong, A. A., Somani, S., Wu, S.-J., Liu, X., Gervais, A., Ernst, R., Saro, D., Decker, R., Luo, J., Gilliland, G. L., Chiu, M. L., and Scallon, B. J. (2017) Functional, biophysical, and structural characterization of human IgG1 and IgG4 Fc variants with ablated immune functionality. *Antibodies*. **6**, 12.

[16] Shields, R. L., Lai, J., Keck, R., O'Connell, L. Y., Hong, K., Gloria Meng, Y., Weikert, S. H. A., and Presta, L. G. (2002) Lack of fucose on human IgG1 N-linked oligosaccharide improves binding to human FcγRIII and antibody-dependent cellular toxicity. *J. Biol. Chem.* **277**, 26733–26740.

[17] Diebolder, C. A., Beurskens, F. J., de Jong, R. N., Koning, R. I., Strumane, K., Lindorfer, M. A., Voorhorst, M., Ugurlar, D., Rosati, S., Heck, A. J. R., van de Winkel, J. G. J., Wilson, I. A., Koster, A. J., Taylor, R. P., Saphire, E. O., Burton, D. R., Schuurman, J., Gros, P., and Parren, P. W. H. I. (2014) Complement is activated by IgG hexamers assembled at the cell surface. *Science.* **343**, 1260–1263.

[18] Cook, E. M., Lindorfer, M. A., van der Horst, H., Oostindie, S., Beurskens, F. J., Schuurman, J., Zent, C. S., Burack, R., Parren, P. W. H. I., and Taylor, R. P. (2016) Antibodies that efficiently form hexamers upon antigen binding can induce complement-dependent cytotoxicity under complement-limiting conditions. *J. Immunol.* **197**, 1762–1775.

[19] Nagashima, H., Tezuka, T., Tsuchida, W., Maeda, H., Kohroki, J., and Masuho, Y. (2008) Tandemly repeated Fc domain augments binding avidities of antibodies for Fcγ receptors, resulting in enhanced antibody-dependent cellular cytotoxicity. *Mol. Immunol.* **45**, 2752–2763.

[20] Nagashima, H., Ootsubo, M., Fukazawa, M., Motoi, S., Konakahara, S., and Masuho, Y. (2011) Enhanced antibody-dependent cellular phagocytosis by chimeric monoclonal antibodies with tandemly repeated Fc domains. *J. Biosci. Bioeng.* **111**, 391–396.

[21] Wang, Q., Chen, Y., Pelletier, M., Cvitkovic, R., Bonnell, J., Chang, C. Y., Koksal, A. C., O'Connor, E., Gao, X., Yu, X. Q., Wu, H., Stover, C. K., Dall'Acqua, W. F., and Xiao, X. (2017) Enhancement of antibody functions through Fc multiplications. *MAbs*. **9**, 393–403.

[22] Hayes, J. M., Cosgrave, E. F. J., Struwe, W. B., Wormald, M., Davey, G. P., Jefferis, R., and Rudd, P. M. (2014) Glycosylation and Fc receptors. *Curr. Top. Microbiol. Immunol.* **382**, 165–199.

[23] Kiyoshi, M., Caaveiro, J. M. M., Kawai, T., Tashiro, S., Ide, T., Asaoka, Y., Hatayama, K., and Tsumoto, K. (2015) Structural basis for binding of human IgG1 to its high-affinity human receptor FcγRI. *Nat. Commun.* **6**, 1–11.

[24] Radaev, S., and Sun, P. (2001) Recognition of immunoglobulins by Fcγ receptors. *Mol. Immunol.* **38**, 1073–1083.

[25] Sánchez, L. M., Penny, D. M., and Bjorkman, P. J. (1999) Stoichiometry of the interaction between the major histocompatibility- complex-related Fc receptor and its Fc ligand. *Biochemistry*. **38**, 9471–9476.

[26] Abdiche, Y. N., Yeung, Y. A., Chaparro-Riggers, J., Barman, I., Strop, P., Chin, S. M., Pham, A., Bolton, G., Mcdonough, D., Lindquist, K., Pons, J., and Rajpal, A. (2015) The neonatal Fc receptor (FcRn) binds independently to both sites of the IgG homodimer with identical affinity. *MAbs*. **7**, 331–343.

[27] Parekh, B. S., Berger, E., Sibley, S., Cahya, S., Xiao, L., LaCerte, M. A., Vaillancourt, P., Wooden, S., and Gately, D. (2012) Development and validation of an antibody-dependent cell-mediated cytotoxicity-reporter gene assay. *MAbs*. **4**, 310–318.

[28] Klein, C., Schaefer, W., and Regula, J. T. (2016) The use of CrossMAb technology for the generation of bi- and multispecific antibodies. *MAbs*. **8**, 1010–1020.

[29] Bossenmaier, B., Kettenberger, H., Klein, C., Kuenkele, K.-P., Regula, J.-T., Schaefer, W., Schwaiger, M., and Sustmann, C. (2012) Wo2012116926a1: Antigen Binding Proteins.

[30] Brinkmann, U., and Kontermann, R. E. (2017) The making of bispecific antibodies. *MAbs*. **9**, 182–212.